2013

Design of Engineered Biomaterial Architectures Through Natural Silk Proteins

Nicholas Kurland
Virginia Commonwealth University

Design of Engineered Biomaterial Architectures Through Natural Silk Proteins

A dissertation submitted in partial fulfillment of the requirements for the degree of Doctor of Philosophy at Virginia Commonwealth University

by

Nicholas E. Kurland

Master of Science in Chemical and Life Science Engineering – Virginia Commonwealth University, 2011

Bachelor of Science in Chemical and Life Science Engineering – Virginia Commonwealth University, 2009

Advisor: Vamsi K. Yadavalli, Ph.D.

Associate Professor of Chemical and Life Science Engineering

Virginia Commonwealth University

Richmond, Virginia

November 2013

Acknowledgements

The work described in this dissertation would not have been possible without the contributions of numerous colleagues and mentors involved in all stages of research planning and implementation. To my friends and family, I am extremely appreciative of the constant support throughout the duration of my graduate work at VCU.

Central to this research were a number of collaborations that helped to shape fundamental studies through the exchange of ideas and research assistance. I am very grateful to Subhas Kundu, Ph.D. (Department of Biotechnology, Indian Institute of Technology, Kharagpur) for the influx of materials and ability to advance my work into the regime of biotechnology, and Tuli Dey, Ph.D. for helping to conduct cellular studies. Later stages of this work would not have been possible without Xuejun Wen, M.D., Ph.D. (Department of Chemical and Life Science Engineering, Virginia Commonwealth University, Richmond, Virginia), for opening access to his laboratory, and Ben Whatley, Ph.D., for offering endless assistance with biological work and imaging.

My committee members have inspired the outcome of my research with an influx of ideas and guidance throughout planning and experimentation phases of work. I would also like to thank the numerous individuals assisting in fundamental studies that furthered the impact of this research. Dmitry Pestov, Ph.D., thanks for the immense assistance with surface characterization techniques and use of the VCU Nanomaterials Core Characterization facility for conducting integral analyses. Darrell Peterson, Ph.D. and Ali Siamaki, Ph.D. further provided much needed assistance with spectroscopic analyses.

All of my colleagues have fostered a friendly, collaborative atmosphere that has motivated forward progress in my research. In particular, I am grateful for the camaraderie of three individuals that have been influential in this work. Congzhou, thank you for the engaging conversation and exchange of ideas throughout my last year of work. Eric, thanks for helping to get through the rigor of scientific research with constant intellectual conversations. Xiaojuan, thank you for the immense assistance provided at the start of my research.

Perhaps most important to the success of this research was my research advisor, Vamsi Yadavalli, Ph.D., who provided me with the opportunity to initiate research projects in his laboratory, and helped to direct the outcome of this work. He lent support through his scientific expertise, allowing me to enhance my scientific writing skills and overcome obstacles while engaging in the rigors of research.

Table of Contents

List of Tables

List of Figures

List of Abbreviations

Nomenclature

α-helix Alpha helix

β-sheet Beta sheet

D_f Fractal dimension

L Path length

A Absorbance

A_{280} Absorbance (280 nm)

Acronyms

AFM Atomic Force Microscopy

BSA Bovine Serum Albumin

CD Circular Dichroism

DMSO Dimethyl Sulfoxide

DLS Dynamic Light Scattering

EtOH Ethanol

GPa Gigapascal (10^9 Pa)

H_2O Water

HFIP 1,1,1,3,3,3-Hexafluoro-2-propanol

kDa Kilodalton (10^3 Da)

LiBr Lithium Bromide

LiCl Lithium Chloride

MeOH Methanol

N_2 Nitrogen (gas)

$NaHCO_3$ Sodium Bicarbonate

NaOH Sodium Hydroxide

OD Optical Density

SEM Scanning Electron Microscopy

SLS Static Light Scattering

SPL Silk Photolithography Platform

TFE 2,2,2-Trifluoroethanol

Abstract

DEVELOPMENT OF SMART BIOMATERIAL ARCHITECTURES THROUGH NATURAL AND ENGINEERED SILK

By Nicholas E. Kurland, Ph.D.

A dissertation submitted in partial fulfillment of the requirements of the degree of Doctor of Philosophy at Virginia Commonwealth University.

Virginia Commonwealth University, 2013

Major Director: Vamsi K. Yadavalli, Ph.D., Associate Professor of Chemical and Life Science Engineering

Silk proteins have provided a source of unique and versatile building blocks in the fabrication of biomedical devices for addressing a range of applications. Critical to advancing this field is the ability to establish an understanding of these proteins in their native and engineered states as well as in developing scalable processing strategies, which can fully exploit or enhance the stability, structure, and functionality of the two constituent proteins, silk fibroin and sericin. The research outlined in this dissertation

focuses on the evolution in architecture and capability of silks, to effectively position a functionally-diverse, renewable class of silk materials within the rapidly expanding field of smart biomaterials.

Study of the process of building macroscopic silk fibers provides insight into the initial steps in the broader picture of silk assembly, yielding biomaterials with greatly improved attributes in the assembled state over those of protein precursors alone. Self-organization processes in silk proteins enable their aggregation into highly organized architectures through simple, physical association processes. In this work, a model is developed for the process of aqueous behavior and aggregation, and subsequent two-dimensional behavior of natural silk sericin, to enable formation of a range of distinct, complex architectures. This model is then translated to an engineered system of fibroin microparticles, demonstrating the role of similar phenomena in creating autonomously-organized structures, providing key insight into future "bottom up" assembly strategies.

The aqueous behavior of the water-soluble silk sericin protein was then exploited to create biocomposites capable of enhanced response and biocompatibility, through a novel protein-template strategy. In this work, sericin was added to the biocompatible and biodegradable poly(amino acid), poly(aspartic acid), to improve its pH-dependent swelling response. This work demonstrated the production of a range of porous scaffolds capable providing meaningful response to environmental stimuli, with application in tissue engineering scaffolds and biosensing technologies.

Finally, to expand the capabilities of silk proteins beyond process-driven parameters to directly fabricate engineered architectures, a method for silk

photopatterning was explored, enabling the direct fabrication of biologically-relevant structures at the micro and nanoscales. Using a facile bioconjugation strategy, native silk proteins could be transformed into proteins with a photoactive capacity. The well-established platform of photolithography could then be incorporated into fabrication strategies to produce a range of architectures capable of addressing spatially-directed material requirements in cell culture and further applications in the use of non-toxic, renewable biological materials.

CHAPTER 1

INTRODUCTION

1.1 Introduction

Biomaterials constitute a diverse subset of materials that can interact with biological systems, in order to augment, repair or replace the structure and function of tissues and organs.[1] These materials have been incorporated into applications ranging from matrices for cell culture in tissue engineering, to vehicles for drug delivery, and further, to biologically-integrated arrays and bioactive devices for conducting fundamental biological studies.[2, 3] Desired specifications for biomaterials include a high degree of biocompatibility with minimal immune response, and, in the case of implantation, either *in vivo* stability or controlled biodegradability. These requirements have been fulfilled by a range of synthetic and natural materials, from poly(lactic acid) and poly(ethylene glycol) to collagen and silk.[4-7] The building blocks as components of various biomedical devices often balance a range of functionalities in order to address application-specific needs. While synthetic materials are associated with facile processing strategies and the development of mechanically-robust architectures with tailored structure and mechanics, naturally-derived biomaterials offer a renewable source of abundant materials displaying fundamental compatibility with established *in vivo*

pathways in the host's complex biological systems.[8, 9] Often, the choice has to be made between these conflicting parameters to best select the material of choice for a specific application.

Considerable effort has been directed at matching biomaterial structure to desired functionality through diverse processing strategies in order to address a range of material applications, including tissue engineering, biosensing, and other biologically-integrated devices.[5, 10-12] Despite the many mechanical, biological and chemical advantages of natural materials, their employment as biomaterials has been hindered by limited fabrication strategies, uneven stability, loss of function, and lack of versatility in use.[13, 14] Thus, the rational design of biocompatible and biofunctional materials that can be precisely engineered and tailored to address diverse applications remains a critical technological challenge.

Amongst natural materials, silk provides a renewable source of abundant, protein-based materials that has gained considerable interest for addressing varied biological applications. Chemical stability, high biocompatibility, and remarkable mechanical strength all contribute to silk's role as an ideal biomaterial. Silk exists in nature as a biopolymer consisting primarily of the fibrous protein fibroin, and glue protein sericin (Figure 1.1).[15] The ability to tune protein surface chemistry and functionality is desired in order to precisely control the bulk physical attributes and interactions between silk materials and living systems.[16] When isolated, these proteins can be translated into simple architectures, or blended with other, often synthetic, materials to form composites for enhancing silk functionality. These strategies enable the creation of specialized silk-based films, electrospun fibers, aqueous sponges, and hydrogels for drug delivery and

tissue engineering.[15, 17-21] While composite architectures may improve silk performance in specific areas, they may be limited in their ability to preserve the fundamental properties of silk—biodegradability, biocompatibility and mechanical strength, which are easily degraded due to processing steps.[22, 23] Therefore, in order to position silk as a renewable, natural alternative to the use of synthetic biomaterials, a challenge lies in tailoring the structure and function of silk to directly address a broader range of biomedical applications, without negatively impacting the biologically favorable aspects of constituent silk proteins.

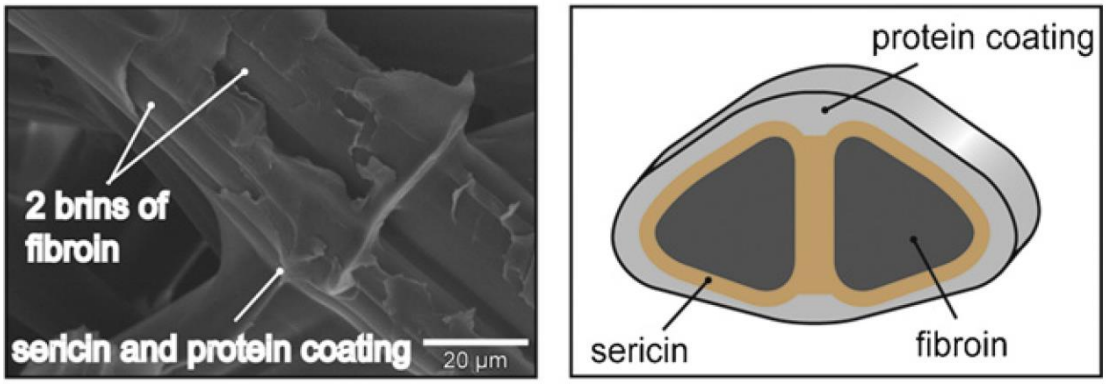

Figure 1.1. SEM and schematic of a silk fiber, depicting the self-assembled configuration, in which sericin and a protein coat envelop a fibroin 'core'.

The ability to tune protein surface chemistry and functionality is desired in order to precisely control the bulk physical attributes and interactions between silk materials and living systems.[16] In recent years, the use of surface immobilization and chemical modification strategies for proteins has effectively demonstrated the widespread reactions available for protein chemistry.[24-26] The incorporation of these techniques for

conducting silk modification enables enhancement of the limited properties of silk, or diversifying the bioactive functionalities of silk proteins, which would otherwise require blended biomaterials.[15] To date, numerous silk bioconjugation reactions have been established that enhance silk biocompatibility in tissue engineering, or extend new functionality to silk, such as anticoagulant activity.[27, 28] Engineered approaches to silk modification provide advantages of relatively mild processing conditions when compared to synthetic routes, as well as the ability to produce structured architectures preserving the fundamental properties of silk.[21]

Increasingly, the incorporation of sustainable processing strategies to biomaterial synthesis and processing has demonstrated the potential for effectively producing biofriendly, renewable materials.[29] An advantage to this philosophy of "green chemistry" based biomaterial synthesis is the enhanced biocompatibility and decreased toxicity of resulting materials as a result of altered processing strategies.[30-32] A critical challenge in combining these approaches lies in the formation of concerted, 'green' strategy for conducting bioconjugation and subsequent processing in order to produce complex, biologically-relevant architectures, which has not been demonstrated in a consolidated platform to-date. Furthermore, the relative structural impact of covalently-linked functionalities has not been established.

Biochemical modification of silk thus provides an avenue to forming a new class of materials with greater chemical and mechanical versatility, and tunable parameters—including stability, biodegradability and biocompatibility. This opens up possibilities in applying silk in hitherto difficult or impossible ways, while retaining its unique properties and not requiring composite formation with synthetic materials. Possibilities range from

spatial patterning of protein to enable controlled cellular patterning for tissue engineering applications, to the creation of a new class of natural materials with the ability to actively respond to their environment with dynamic changes in morphology. This ultimately allows the creation of a class of tailorable silk materials able to better address the growing requirements within the biomedical field, and further positions silk as sustainable, green alternative to existing synthetic materials. This research is intended to explore the implications and pathways to diversifying silk structure and functionality.

1.1.1 Research Objective

The primary objective of this research was to investigate natural architectures produced by silk proteins and evaluate the impact of physical and chemical modification strategies, and their ability to form complex silk-based biomaterials. In this work, it was desired to explore a hierarchy of natural and engineered assembly strategies in order to facilitate the production of smart silk architectures capable of demonstrating application-specific response to environmental parameters. Initially, the study of the isolated silk protein, sericin, established a general mechanism for silk self-assembly, which was translated to a system of engineered fibroin microparticles. The aqueous self-aggregation behavior of water-soluble sericin was then expanded upon and exploited in order to fabricate protein-based pH-responsive biomaterials capable of enhanced swelling response. Based on fundamental limitations governing the use of water-soluble silk proteins in complex architectures, a bioconjugation technique was developed to improve the physical properties of silk fibroin and sericin, and enable a light-based stimuli-

response. From these conjugates, the incorporation of a modified photolithography strategy allowed the production of precisely-patterned arrays of micrometer-scale protein features. Micropatterned silk architectures were characterized for their guidance of cell-adhesive and proliferative properties, establishing the bioactive aspects of engineered silk species. Overall, these engineering approaches provide valuable insight into the production of modular biomaterials from abundant natural precursors, adding value and expanding the repertoire of potential applications through the use of natural site-specific additions and engineered assembly techniques.

1.2 Specific Aims

The relative lack of knowledge and intrinsic limitations in translating the simple properties of silk materials into complex architectures and functionalities has hindered the use of silk across diverse applications. Fundamental and applied research into silk fibroin and sericin proteins can enable the effective integration of physical and chemical modification strategies in order to develop biologically-relevant and compatible architectures. This research project is directed along two key specific aims:

1. **Elucidating the fundamental self-assembly properties of silk peptides to enable bottom-up fabrication.** This is achieved through the development of models to understand self-assembly of silk proteins.

2. **Development of strategies for producing stimuli-responsive silk conjugates to enable versatile fabrication across length scales.** The formation of sustainable protein composites and biochemical modifications of silk proteins to form responsive architectures provides a framework for satisfying this aim.

1.2.1 Investigation of the intrinsic self-assembly of silk proteins

Silk proteins are unique biopolymers due to their ability to undergo independent and autonomous self-organization processes, which drive the transition of precursors into macroscopic fibers. These processes prove insightful in order to generate highly-ordered structures at the nano- and microscales relevant to materials fabrication approaches. The aim of the initial portion of this research will be to elucidate these self-assembly processes in order to develop a coherent model for silk peptide self-assembly—effectively demonstrating the formation of bottom-up architectures through control of environmental parameters.

1.2.2 Development of engineered, stimuli-responsive silk biomaterials

To overcome limitations in self-assembly processes, the development of processing strategies allows the production of versatile silk architectures, exhibiting stimuli-responsive properties. Strategies of biocomposite formation and chemical bioconjugation provide a route to the sustainable production of engineered silk materials, capable of exhibiting environmentally-dependent properties. The aim of this work is to

expand the repertoire of potential silk functionalities, effectively enhancing silk protein stability and mechanics, while preserving the intrinsic properties of silk critical to its use in materials research.

1.2.3 Fabrication of novel silk architectures at multiple length scales

Expanding on the previous aim, the incorporation of engineered silk materials into a range of biologically-relevant architectures, such as hydrogels, films, and scaffolds, is desired for harnessing the bioactive functionalities of silk proteins. In order to produce architectures across a range of length scales, stimuli-responsive properties are taken advantage of to conduct bottom-up assembly into a range of microscale architectures. Conversely, architectures may be formed initially, that are capable of presenting stimuli-response in the assembled configuration. The aim of this work is to establish the potential for silk proteins to undergo assembly through environmental modification and controlled assembly techniques. From this work, a versatile platform for the production of 'green' biocompatible silk architectures across diverse length scales will be established.

1.3 Background and Significance

The research outlined in this dissertation is focused on the fabrication of stimuli-responsive silk architectures, capable of addressing biologically-relevant structure and

function requirements. In order to produce such materials, initially, fundamental and applied studies were conducted on natural and engineered silk proteins using a multidisciplinary approach of physical and chemical techniques. This section will define the background and significance of this research, first introducing the intrinsic capabilities and limitations of silk proteins, and expanding into proposed approaches to yield engineered silk architectures.

1.3.1 The influence of molecular assembly in biological processes

Spontaneous assembly is responsible for the organization of molecular subunits into highly-ordered functional assemblies in nature.[33] This process arises from weak molecular interactions which act to direct self-assembly into supramolecular complexes. As a result, biomolecules combine through self-organization to yield specialized structures including phospholipid bilayers, protein assemblies such as collagen fibers and β amyloid fibrils, and even engineered DNA nanostructures.[34, 35] Understanding the underlying mechanisms is therefore of interest, to establish how bulk architectures arise out of nanoscale subunits. This ultimately can provide routes to exploit intrinsic self-assembly and form specialized architectures, with user-specified properties.

Silk is a prominent example of an extensively-characterized, self-assembled system with diverse biomedical and renewable materials applications. The *in vivo* silk assembly process in silkworms and spiders consists of protein subunit folding and self-organization to produce macroscopic silk fibers. Functional silk fibers are formed as a result of a number of precisely-controlled steps, during which shear forces, pH and ionic

strength play a key role in the liquid crystalline spinning of these fibers.[36] This autonomous assembly is exhibited by constituent peptides when isolated from each other.[37-39] As a result, the macroscale self-assembly process is a function of assembly at smaller length scales, down to individual silk peptides. The *in vivo* environment merely directs otherwise intrinsic self-assembly of constituent silk proteins to produce mechanically robust, macroscale silk fibers.

Specifically, this research focuses on silk and its constituent proteins, due to their intrinsic self-assembly potential and diverse range of chemical and mechanical properties. Silk-based materials are widely studied as biomaterials, due to mechanical robustness and a high degree of biocompatibility.[5] Silk provides a natural, renewable material gaining an increasing focus for diverse applications in biomaterials research. Silk proteins thus present a unique platform of materials to yield insight into intrinsic assembly, and enable the exploitation of their remarkable properties for use in developing novel, functional biomaterials.

1.3.2 Silkworm silk

Silk has played an integral role in history, with the earliest known use dating back 6,000 years to the Yangshao culture in China.[40] This early use has predominantly exploited the fibrous state of silk, which has proved ideal for the production of textiles—owing to the significant mechanical robustness and durability of silk. These properties have profound implications in the use of silk as a century-old biomaterial, enabling silk to act as a key material in the clinical setting.[41] In recent years, silk has experienced a

resurgence in the research and biomedical communities due to a high relative abundance, relatively low-cost, facile processing strategies, and attractive mechanical and biological properties.[5, 42]

The most widely-available silk originates from the domesticated mulberry silkworm, *Bombyx mori*. Silk from this species has been extensively characterized through a range of physical, biochemical, and functional studies, establishing a solid framework of properties and potential applications.[43-46] In contrast, spider silk, which possesses far superior mechanics to that of silkworms, is of greater difficulty to source due to comparatively lower yields and the territorial nature of some spider species.[47] Silkworm silk is produced through *in vivo* self-assembly of the fibroin and sericin proteins, and extruded as a self-assembled biopolymer. Silk fibers primarily consist of the mechanically-robust protein fibroin (~70% of fiber), which composes the core of the silk fiber, and a glue glycoprotein sericin (~30% of fiber) surrounds this core, adhering multiple two fibroin fibrils into an adhesive, microscale silk fibrous subunit.[48] This unique configuration results from distinct amino acid compositions—the relative strength of fibroin is derived from an abundance of Gly-Ala-rich repeats arranging into β-sheet rich regions, while sericin presents a significant quantity of hydrophilic amino acids, enabling the formation of a soluble protein coat (Table 1.1).[49] This makes it possible to yield a single high tensile strength (> 0.5 GPa), high elasticity (5 – 12 GPa) fiber from the additive contributions of multiple single fibroin subunits.[50]

Table 1.1. The relative abundance of common amino acids in silk fibroin and sericin proteins. Cysteine, tryptophan, methionine, and proline occur in trace amounts < 0.5%.

Amino Acid	Fibroin	Sericin
Alanine	29.4	5.0
Arginine	0.5	3.2
Aspartic acid	1.3	18.5
Glutamic acid	1.0	4.3
Glycine	44.6	16.8
Histidine	1.4	0.9
Isoleucine	0.7	0.6
Leucine	0.5	1.0
Lysine	0.3	2.6
Phenylalanine	0.6	0.4
Serine	12.1	28.6
Threonine	0.9	9.9
Tyrosine	5.2	3.3
Valine	2.2	2.8

In native silk, self-assembly mechanisms are responsible for the process in which β-sheet interactions drive hierarchical organization of fibroin into macroscopic fibrils. The concurrent self-assembly of sericin then provides an adhesive outer layer to fibrils, which enables sticky fibrils to adhere, and produce macroscopic, mechanically stable fibers.[51] Self-assembling biomaterials are not a novel concept, however self-assembly

often arises from highly-modified biomolecules and engineered synthetic materials.[52, 53] Silk stands apart from other biomaterials due to this remarkable *in vivo* assembly process, which offers potential for utilization in complex architectures and applications.

Silk has demonstrated effectiveness across a range of clinical applications in the purified state. However, in the native assembled configuration, the use of silk has been contraindicated in biomedical settings due to a high degree of immunogenicity in the form of a macrophage response and the formation of IgE and IgG antibodies to silk peptides.[54] For many decades, this immunogenicity has been attributed to the presence of the sericin protein coat, allowing the use of purified fibroin as a suture material.[55] However, recent studies on the relative immunogenicity of isolated silk proteins have demonstrated that sericin alone is immunologically inert, possessing a low inflammatory potential.[56] When separated, silk provides two new materials with a vast array of properties including: biocompatibility, antibacterial activity, oxidation resistance, and controllable degradation, in addition to facile processability and mechanical strength exceeding comparable synthetic materials.[5]

Silk fibroin

The silk fibroin protein composes the bulk of modern biomaterials research, largely due to an impressive set of properties: high tensile strength and elasticity, in addition to native biocompatibility.[5, 42] In order to understand how these properties arise, it is necessary to consider the structure and chemistry of fibroin. Silk fibroin fibers from the domesticated silkworm, *B. mori*, are composed of a light chain (MW = 26 kDa)

and a heavy chain (MW = 390,000 kDa) linked by a single disulfide bridge.[57] Silk fibroin is essentially a block copolymer consisting of hydrophobic β-sheet blocks, interspersed with small non-repetitive hydrophilic linker sequences.[42] These crystalline domains are predominantly composed of glycine-X repeats, where X is alanine, serine, threonine, or valine.[58] Within these domains are subdomain hexapeptides (e.g. GAGAGS, GAGAGY, GAGAGA, and GAGYGA), which incorporate the abundant amino acids glycine (43%), alanine (30%) and serine (12%). Self-assembly of core sequences enables the formation of a hydrophobic protein that is structurally and mechanically stable.

The high abundance of β-sheet crystalline domains within the fibroin imparts the protein with high tensile strength, elasticity, and overall toughness.[59] The toughness and extensibility of silk greatly exceeds that of some of the strongest synthetic materials available, including Kevlar, carbon fiber, and high-tensile steel.[60] Furthermore, the strength and elasticity of silk exceeds that of many biodegradable polymers commonly employed in biomedical applications, such as collagen and poly(L-lactic acid), and even chemically-crosslinked collagen.[61, 62] *B. mori* silk demonstrates an ultimate tensile strength of 500 MPa and an elastic modulus of 5 – 12 GPa.[42, 46] After degumming, an enhancement in these mechanical properties is demonstrated in comparison to native silk.[63] For these reasons, fibroin provides an excellent source of a mechanically-robust biopolymer for biomedical applications.

B. mori silk fibroin is an intrinsically biodegradable and biocompatible polymer, which provides marked benefits to its use as a biomaterial. The rate of biodegradation is primarily a function of β-sheet crystallinity, which is controlled through silk processing

and material fabrication steps, however environmental and mechanical parameters of implantation also influence degradation.[64, 65] Degradation of fibroin is mediated by proteases, which hydrolyze peptide bonds to allow for metabolism of resulting peptide fragments. Proteolytic degradation of *B. mori* fibroin via Protease XIV demonstrates predictable degradation due to surface erosion, which corresponds to a loss of mechanical integrity protein molecular weight over periods up to 12 weeks.[43] This degradation occurs for many species of fibroin-producing silkworms.[66] However, the rate of fibroin degradation may also have biological impacts on cells cultured or in contact with the material, leading to altered metabolism and osteogenesis for human mesenchymal stem cells.[67] Therefore, elucidation of silk biodegradation and impacts on mechanics and biological activity makes fibroin ideal for use in regenerative biomedical applications.

Silk fibroin demonstrates minimal inflammatory potential and low overall immunogenicity when utilized in the purified state.[56, 68] Immune response to silk fibers is largely attributed to the presence of the sericin protein, which when removed, results in favorable immunological properties.[54, 55] For this reason, silk fibroin must necessarily be utilized in the purified state in order to ensure biocompatibility. The i*n vitro* culture of macrophages in the presence of silk fibroin demonstrates pro-inflammatory cytokine levels comparable to that of a tissue culture plate.[56] Furthermore, *in vivo* culture of mesenchymal stem cells on fibroin films demonstrates a lower inflammatory tissue reaction than that of implanted collagen and poly(L-lactic acid).[69] Silk fibroin thus provides an ideal candidate material for the fabrication of biocompatible, mechanically robust biomaterials that may be tuned to the structural properties of the host tissue, yet are able undergo predictable biodegradation. However,

despite the excellent biomaterial capabilities of fibroin, its processing leaves behind sericin as a waste product, for which properties and potential applications have been largely overlooked in past biomaterials research.

Silk sericin

The processing of natural silk to isolate fibroin for both textile and research use results in the extraction of sericin, typically as an undesired waste product. Despite the natural existence of silk as a biocomposite of two proteins, silk sericin is both chemically and structurally distinct from silk fibroin. Silk sericin is a natively water-soluble glycoprotein, composed primarily of polar amino acids serine (33%) and aspartic acid (17%). This serine-rich protein is organized into the highly conserved 38-mer repetitive sequence, SSTGSSSNTDSNSNSVGSSTSGGSSTYGYSSNSRDGSV.[70] Sericin from the common *B. mori* silkworm consists primarily of three polypeptide chains, at 400, 250, and 150 kDa molecular weights, with the extreme chains having similar amino acid sequences.[71] Structurally, sericin is dominated by amorphous random coil regions, with little or no α-helical content.[72] Thus, sericin displays a high degree of water-solubility, which is determined by the ratio of random coil to β-sheet structure—an environmentally dependent parameter.[73]

Studies on sericin behavior in *in vivo* and *in vitro* settings are far limited in comparison to that of fibroin. In the past decade, studies have begun to illuminate the biological activity of sericin, which is largely attributed to the 38-amino repetitive domain.[70] Work from Panilaitis *et al.* (2003) on the inflammatory potential of silk

fibroin has demonstrated sericin alone is not inherently immunogenic, a finding which has upended decades of research aversion to sericin due to assumed biological incompatibility.[56] Despite this, sericin has extensively demonstrated native cytocompatibility, effectively promoting cellular adhesion and proliferation, as a result of the 400 kDa fraction and the serine-rich regions.[74] This is demonstrated for fibroblasts, and osteoblasts, for which culture on sericin is associated with increased alkaline phosphatase activity.[75] In contrast, smaller sericin fractions serve as effective mitogenic factors, demonstrating an enhancement in mammalian cell proliferation over that of larger fractions.[76] Therefore, preliminary silk sericin cytocompatibility has been established, providing a foundation for further work involving sericin biomaterials.[77]

A recent finding has demonstrated the conservation of self-assembly in isolated silk sericin, providing fundamental insight into a key process of silk assembly.[37] Combined with simple processing, the biomedically-relevant attributes of sericin place a focus on characterizing how sericin self-assembly may add yet another unique property to the repertoire of silk functionalities. However, limited research on silk sericin to date in comparison to the well-studied fibroin, provides an incomplete foundation of fundamental knowledge and properties on which to build. For this reason, further evaluation of the self-assembly capacity of silk proteins, which have only been lightly studied, enables the combining of biologically-relevant properties with self-assembly for the formation of biologically-active silk architectures. A number of potential applications in biomaterials such as hydrogels and membranes have already been demonstrated, due to the ease of sericin processing and favorable mixing with other water-soluble biomaterial precursors.[78] In this work, strategies are explored for producing complex sericin

architectures with biomedical relevance—that is, it is desired to establish sericin as a structurally-stable and versatile biomaterial with comparable utility to fibroin. However, as will be expanded upon in the following section, fabrication strategies are limited in their capacity to produce stable, biologically-active architectures.

1.3.3 Architectures of silk proteins

Native architecture and applications

Including the self-assembly highlighted in previous sections, silk proteins are capable of forming structurally-diverse architectures for tissue engineering, biologically-integrated devices, and drug delivery applications, without the need to introduce additional materials or chemical modification steps.[21] After degumming and regeneration, water-soluble fibroin is easily transformed into films, membranes, and hydrogels through casting fibroin onto a substrate or patterned 'master' for reproduction of nano- and microscale surface and bulk features.[79-82] Patterning of optically-transparent fibroin introduces potential applications in biomedically-related diffractive optics, microfluidics, and spatially-organized substrata for cellular culture.[83] Using a variation on these techniques, patterning topographies are introduced via nanoimprinting of thin fibroin films, which enables self-sensing optofluidics for conducting bioanalytic studies.[84] Techniques are often combined with treatments to improve β-sheet crystallinity, in order to increase mechanics, decrease aqueous solubility, and decrease the rate of biodegradation.[64, 65] When water-soluble attributes are desired, the native degradability and flexibility possessed by silk fibroin is advantageous in acting as a

temporary or permanent ‘supporting substrate’ for applications such as biodegradable and conformal bio-electronics.[85-87] Dissolution of purified fibroin in fluorinated solvents allows electrospinning into nanofibers and nonwoven mats; however, considerable mechanics are lost as a result of this process.[88, 89] Despite the range of architectures available, fibroin has been limited to a finite set of attributes following materials processing steps which have often exchanged solubility and flexibility for stability and stiffness, which can lead to degradation of fibroin characteristics.

The same tendency is observed for the silk sericin protein—the high degree of water solubility exhibited by sericin hinders fabrication into materials that provide sufficient strength and environmental stability.[78] The formation of simple architectures, such as films and hydrogels therefore demonstrate inadequate mechanics for employment in many relevant applications.[72, 90] Similar β-sheet crystallinity-inducing treatments to those of fibroin offer a means of decreasing solubility of the sericin architecture. However, sericin gel films fabricated out of ethanol-precipitated sericin demonstrate that while improving aqueous stability is possible, this occurs at the expense of diminished cellular adhesion capacity both in the presence and absence of serum.[77] This effectively demonstrates that non-chemical techniques to stabilize sericin for uses in an aqueous environment also reduce potentially desired cellular adhesive and mechanical properties. Limitations in architecture stability, the finite range of silk protein functionalities, and complex fabrication strategies have provided an impetus to look to advanced processing strategies, involving the formation of silk protein composite biomaterials instead.

The initial effort of this research is to study the assembly mechanisms of silk proteins at multiple length scales. The study of fundamental silk assembly is intended to provide a framework establishing the capabilities of natural silk proteins, which may produce higher-ordered architectures. To expand the repertoire of silk, structural modification can lead to enhanced function, or the presentation of non-native functionalities, such as the ability to photocrosslink, and stimuli-responsive capabilities, such as temperature or pH-responsive properties.[15, 16] By focusing on the addition of well-characterized systems to silk, silk proteins may retain their remarkable chemical and mechanical properties, yet yield functionalities better suited to use in biomaterials. Thus, the intrinsic self-assembly of silk coupled with engineered assembly approaches leads to the ability to form new biological materials with application in a variety of higher-order architectures.

Enhanced Functionality Through Composite Architectures

Based on the discussion above, it is evident that the evaluation of advanced processing techniques to address shortcomings of silk protein performance across a range of applications is needed. An alternative and more widespread approach is the creation of physical blends of silk proteins with other materials to incorporate multiple properties into a single composite biomaterial. These composites are created by techniques such as self-assembly, copolymerization of interpenetrating networks, co-fabrication and direct inclusion. The formation of silk-based composite materials allows silk to act as a protein building block for producing new materials with improved performance and functionality

over that of silk alone.[15] In fact, the existence of natural silk as a biocomposite greatly enhances elastic modulus over that of the isolated proteins.[63] Conversely, the addition of silk proteins to existing systems provides enhanced properties as well. These approaches provide an avenue to augmenting silk functionality, while preserving the native attributes of silk alone.

Silk is able to form composites that are electrically conductive, demonstrate improved water permeability, possess enhanced biocompatibility and novel anticoagulant properties, and display improved cellular adhesion.[20, 91-93] Enhancement of mechanics and biocompatibility has been demonstrated via self-assembly of nanostructured silk with polycaprolactone to produce durable, composite scaffolds for bone regeneration.[94] Silk fibroin improves cellular attachment and differentiation over that of polycaprolactone alone, and conversely, the compressive strength of fibroin is improved. The addition of other materials, such as chitosan, has the ability to form water-stable, porous scaffolds with improved tensile strength and cell adherent behavior.[95, 96] *In situ* polymerization of conductive monomers enables enable the coating of silks with electrically-conductive layers, leading to potential use in nerve regeneration applications.[97] The concept of producing biocompatible blends of silk and other well-established biomaterials provides valuable options for integrating sericin into a functional architecture without structural degradation.

This concept of silk composite formation is harnessed in conjunction with a number of other critical design philosophies: the need for generating fundamentally biocompatible and biodegradable materials, and the incorporation of naturally-sustainable materials into such designs to improve function. This can be achieved by the composite

fabrication of silk with naturally-occurring species, such as collagen, chitosan, hydroxyapatite, cellulose, and polylactic acid.[95, 98-101] These chemical species offer a class of naturally-sourced materials displaying native biocompatibility, tunable or predictable rates of biodegradation, diverse mechanics including elasticity and tensile strength, and assorted bioactive functionalities.[102] Processing strategies to develop composites into complex two- and three-dimensional architectures with satisfactory stability and mechanical properties are lacking, however.[22, 103] In recent years, natural poly(amino acids), such as poly(ε-L-lysine) and poly(glutamic acid), have been embraced due their natural existence *in vivo* and ability to undergo naturally-controlled proteolytic degradation processes.[69, 102, 104] The benefit of utilizing additional peptides for silk composites extends beyond physical properties—processing strategies of natural, water-soluble amino acids, in addition to unique side chain chemistry, facilitates the development of complex architectures. Previously, fibroin has been demonstrated in conjunction with poly(aspartic acid), enabling the formation of highly-porous scaffold.[19, 105, 106] The broad class of polyelectrolytic poly(amino acids), such as poly(aspartic acid) and propylated-poly(glutamic acid), possess intrinsic pH- and thermo-sensitivity, demonstrating stimuli-dependent hydration behavior.[107] To date, these attributes in conjunction with silk have not been investigated. A goal of this research was to take advantage of the relatively similar water solubility between poly(amino acids) and hydrophilic sericin in order to achieve a complex, 3D architecture. Through the investigation of stimuli-response in this complex, a route to augmenting silk functionality to add the nascent ability to respond to environmental influences is achievable.

Stimuli-responsive materials are defined as those which exhibit a meaningful mechanical change in response to specific physical and chemical stimuli.[108] The advanced capabilities of stimuli-responsive polymer-based materials provide significant potential in materials science and biosensing applications. These materials are produced in such a way that structural changes or 'output' is proportional to the amount of material present. As such, macroscale architectures provide a maximal signal to certain stimuli, such as temperature, pH, light, or chemical composition.[109, 110] These "smart" architectures rely on engineered assembly between stimuli-responsive molecular subunits. This provides a means of directing sensitivity of response, as well as other material properties, as necessary to ensure compatibility in a given application.

Investigation of biopolymer composite-formation methods provides an avenue for adding non-natural functionalities (e.g. pH-dependent swelling, temperature-responsive morphological changes, and fluorescent signaling). Silk-based materials have been characterized in arrangements such as hydrogels responsive to molecular binding. However extensive work on physical response to chemical cues is not well characterized.[111] One of the stimuli investigated in this research is pH and attempting to fabricate porous protein hydrogels for utilization in pH response. In order to achieve this, hydrophilic silk sericin is incorporated into a protein-based, pH-sensitive network polypeptide, producing a hydrogel network capable of response to environmental changes.

Chemically-Modified Silk Architectures

A new class of functional silk materials is realized when the desired properties to be imparted unto silk as a result of composite formation are instead added to silk directly. Chemical functionalization can be employed to yield an improvement of existing properties (physical or biochemical), or to expand the library of potential functionalities. These can range from chemical modification of amino acid residues to functionalization via insertion of chemical species into silk. Chemical modification strategies such as covalent grafting and chemical crosslinking, provide an avenue to the site-specific grafting of functional moieties onto structurally-diverse amino acids. Residue-specific bioconjugation enables the preservation of fundamental attributes of silk fibroin and sericin proteins, while improving stability, mechanics, and overall functionality.[78] For example, the covalent decoration of silk fibroin fibers with the integrin-recognition sequence Arg-Gly-Asp (RGD) improves the cytocompatibility of silk.[12] Interestingly, the RGD motif is naturally present in non-mulberry silk fibroins, making this modification applicable only to mulberry silks, i.e. *B. mori*.

In the interest of developing biologically-relevant architectures, stimuli-responsive parameters, in conjunction with bioconjugation approaches, can be exploited to yield improvements in silk structure and function. There is a considerable gap to fill in existing research into silk protein applications using engineered assembly methods. Fabrication processes have traditionally been conducted in a non-specific manner, using chemical crosslinking or physical processing approaches.[112, 113] Of available stimuli-responsive moieties, the addition of moieties capable of response to a stimulus input with an ‘assembly’ or stability-enhancing output, enable the generation of highly-ordered

patterns. By taking advantage of the fundamental biocompatibility and biodegradability of silk proteins, their potential utility is expanded through the investigation of further conjugation techniques. Due to the importance of this area, the next section is dedicated in its entirety to the consideration of proteins in microfabrication strategies by means of chemical conjugation.

1.3.4 Development of a Platform for Protein Microfabrication

A critical step in the development of biologically-integrated silk-based materials is the ability to spatially organize silk proteins over large areas with micrometer-resolution. While induced self-assembly of silk and other biomolecules provides a route to the fabrication of 2D architectures, fundamental limitations exist in the generation of large-scale patterns with defined size and geometries. These limitations make self-assembled architectures impractical for applications utilizing protein micropatterns, including tissue engineering, fundamental research studies in cellular biology, and bioelectronics.[114, 115] For tissue engineering in particular, the presence of substrate microstructure is crucial to directing cellular spatial orientation and behavior of cells, in order to encourage cellular adhesion and proliferation along preferential gradients.[116] In addressing silk's contribution to areas of tissue engineering and cell culture, these fields demand biocompatible and biodegradable materials with precisely micropatterned architectures.[117, 118] In order to produce higher-ordered features at length scales greater than those exhibited by self-assembly processes alone, directed assembly techniques can provide a versatile avenue to yielding such architectures. This offers silk

the opportunity to not only replace existing biomaterials, but importantly, offer their fundamental properties of biocompatibility and low immunogenicity to existing biomaterials.[118, 119]

Conventional Approaches to Protein Patterning

A number of approaches have been extensively demonstrated for the fabrication of general protein architectures, including soft lithography and the generation of patterned self-assembled monolayers.[117] For silk fibroin in particular, soft lithographic casting and nanoimprinting have enabled the creation of architectures down to 200 nm resolutions.[80, 84] For these soft lithographic approaches, the physical (i.e. mechanical properties) and chemical (i.e. solubility) properties of silk proteins remain unchanged as a result of soft lithographic steps, which may leave architectures unstable and subject to degradation, potentially limiting applications.

Protein crosslinking agents, such as NHS esters, diisocyanates, carbodiimides, and naturally-derived genipin, offer a route to increased stability through the induction of bulk crosslinks in protein architectures.[120-122] Crosslinking of silk proteins has previously been successful in stabilizing architectures, for example: sericin-poly(vinyl alcohol) hydrogel crosslinking via glutaraldehyde, fibroin-collagen hydrogel crosslinking via EDC (a carbodiimide), and fibroin-sericin film crosslinking via PEG/genipin.[98, 112, 123] The crosslinkers employed for silk protein crosslinking are primarily aimed at decreasing solvation and improving mechanic, rather than stabilizing the 3-dimensional configuration silk-based biomaterials. However, as chemical crosslinking occurs during

the addition of the crosslinker, this essentially leads to the kinetics of crosslinking occurring in competition with the process of mixing, preventing homogeneity in crosslinking and bulk material properties. Furthermore, employment of these crosslinkers in biomaterials is limited by toxicity of the crosslinker and reaction byproducts.

Photocrosslinking offers a viable alternative for overcoming the limitations of bulk crosslinking strategies during polymeric biomaterials fabrication.[124] This strategy achieves the same crosslinking as chemical crosslinkers, yet presents the requirement of a light stimulus prior to the initiation of crosslinking. Ease of processing and the rapid reaction of photocrosslinkers enable the patterning of polymers into various architectures.[125, 126] Furthermore, through focused light and photolithographic approaches, selective crosslinking can be achieved with high spatial resolution, allowing light-directed syntheses and fabrication of micro and nanometer-scale patterns.[127-129] Synthetic photocrosslinkers and photoinitiators have been used for developing biologically-interacting materials without cytotoxic effects.[130-132] Despite the use of photocrosslinking in synthetic polymers, the lack of intrinsic photoactive functionality in proteins limits their employment in light-based processing methods.

Common silk microfabrication approaches fundamentally depend on conventional photolithography, to either generate a ‘master’ stamp for soft lithography of silk, or to enable selective patterning of protein-adherent ligands, often based on silane chemistry.[114, 133] For example, biomolecule patterning may be achieved through a lift-off strategy, in which a biocompatible photoresist is used to generate patterned, non-adherent regions of a substrate, selectively limiting biomolecule localization.[134] Sequential photoexposure and biomolecule immobilization steps enable the creation of

multifunctional, complex biomolecule arrays.[135] This bio-lithographic technique enables the incorporation of conductive substrates, effectively imparting biomolecular arrays with diverse electrochemical functionalities for potential use in biosensing. For self-assembled monolayer (SAM)-based approaches, photolithography is incorporated to generate biomolecule patterning indirectly—a reactive SAM layer (e.g., n-octadecyltrimethoxysilane) is deposited, and through light exposure the SAM is selectively removed to create high contrast patterns for directing protein adhesion.[133] These techniques often incorporate non-covalent bonding—molecular adsorption is demonstrated for inducing protein adhesion, and furthermore bulk, mechanically-resilient architectures of adhered protein are not possible due to reliance on monolayer adhesion.

Harnessing conventional photolithography in conjunction with a silk 'photoresist' would enable the direct fabrication of microstructures of silk, and have implications for the broad class of proteins and other biomolecules. Photolithographic patterning of proteins numerous benefits over soft lithography, allowing the generation of static patterns of silk proteins, which are covalently bonded to improve chemical stability, and further enables greatly improved mechanics. Furthermore, the fabrication of tethered and independent shapes directly formed at micrometer scales without mold fabrication or transfer steps has not been previously demonstrated for silk. In order for this approach to be viable, the development of a facile process for photoactive modification, and translation of biomolecules into a multi-step platform is necessary.

Strategies for Photoactive Modification

The development of an intrinsically photoactive silk protein is dependent on the attachment of a stable, covalently-bonded photo-reactive ligand. A number of methods are available for biomolecular functionalization, ranging from bioconjugation techniques to recombinant synthesis.[136, 137] The addition of a photo-reactive amino acid, p-benzoyl-L-phenylalanine, to the genetic code of *E. coli* has been demonstrated via the orthogonal synthesis of an aminoacyl-tRNA synthetase/tRNA pair.[138] Recombinant synthesis in an *E. coli* host has provided a modular route to creating photo-reactive proteins, via the orthogonal addition of non-canonical photoactive peptides.[139, 140] The complexity of recombinant gene expression, involving numerous steps of sequence cloning, plasmid design and purification in combination with low yield, has made bioconjugation techniques a more suitable alternative for generating photoactive proteins. For example, residue-specific modifications may be achieved through thiol to cysteine functionalization, NHS ester to primary amide conjugation, or EDC-based conversion of carboxyl-containing residues into reactive moieties.[120, 141] Lower specificity reagents such as isocyanates are capable of undergoing promiscuous conjugation to nucleophilic amino acids.[142] To date, bioconjugation techniques are comparatively limited in their production of photoactive protein conjugates—a prominently reported exception is the conjugation of recombinantly expressed proteins via NHS ester–diazirine.[143] Among all reagents available for conjugation, the diverse reactions possible through isocyanates provide an ideal route to demonstrating bioconjugation in structurally-diverse silk proteins. The proteins fibroin and sericin are therefore, ideal biomolecular pairs in

conjunction with an isocyanate-based photoactive group, for the demonstration of a versatile photolithography process.

General Approaches and Limitations to Conventional Photolithography

Photolithography holds a prominent position in the microelectronics field for the large-scale, high-throughput fabrication of micro- and nanoscale architectures. Recently, photolithography has undergone a translation to applications including biologically-integrated devices, light-directed synthesis and Bio-MEMS fabrication.[128, 144] In this process, light-sensitive 'photoresists' are employed, providing a response to light in the form of chemical crosslinking (negative photoresist). In conjunction with a selectively light-permeable photomask, employing patterned light-absorbing chrome on a glass substrate, reproducible patterning is achieved via UV/optical light exposure. The epoxy-based photoresist, SU-8, has been extensively utilized for the formation of biocompatible architectures, and more recently has shown applicability in biomolecule patterning and Bio-MEMS.[145, 146] Despite its favorable biocompatibility *in vivo*, the use of toxic solvents in processing (e.g.,γ-butyrolactone and 1-methoxy-2-propyl acetate) and limited data on *in vivo* stability and biodegradation, limits potential biological applications.

The general process of photolithography employs multiple steps: 1) substrate preparation to improve photoresist adhesion, 2) spin-coating to form a thin, homogenous layer of photoresist, 3) soft baking removes excess photoresist solvent, 4) exposure (UV or optical) induces photoresist crosslinking, 5) a post-exposure bake removes exposure

artifacts, and finally, 6) development enables the removal of unexposed photoresist, revealing micropatterns (Figure 1.2).

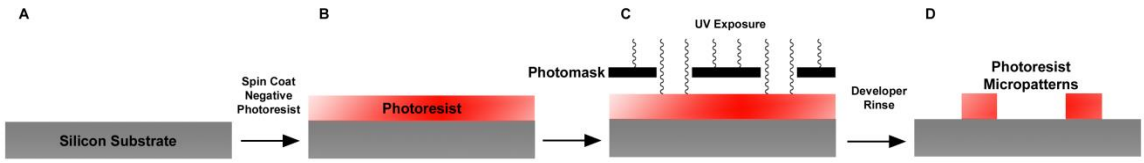

Figure 1.2. Conventional UV lithography, demonstrating application and UV exposure of photoresist to produce micropatterns.

Contact and proximity lithography comprise two simple and inexpensive photolithographic exposure techniques capable of 1:1 reproduction of micrometer-scale features from a patterned photomask.[147] Both techniques can be conducted at the bench-scale with a UV light source and chrome photomask, in contrast to the more complex projection lithography technique, which employs an expensive stepper system—containing a reduction projection lens system.[148] Contact photolithography employs the photomask in contact with the underlying photoresist, effectively minimizing diffraction effects to ensure high resolution of reproduction. However, this technique degrades the photomask chrome layer due to mechanical contact, while trapped dust and particulates produce altered patterns in the photoresist. Proximity photolithography offers an alternative, in which the photomask is separated from the photoresist by a small gap, however, diffraction effects limit the resolution attainable through this method.[149]

Feature resolution is largely a function of the wavelength of light used in optical lithography, which for monochromatic light, Rayleigh's scaling laws of resolution produce an approximate minimum resolution of ~ 0.5 μm. Fresnel (near-field) diffraction effects occur as light travels through an aperture (i.e. optically transparent portions of the photomask), expanding outwards as distance from the aperture increases. For photolithography techniques in which: 1) the aperture is in close proximity to the area of photoresist exposure, and 2) the gap between aperture and photoresist is greater than the aperture size and/or the wavelength of light, Fresnel diffraction effects are significant. Taking this diffraction limit into consideration, the minimum resolvable feature size achieved through photolithography is determined by the equation [150]:

$$R = \frac{3}{2}\sqrt{\lambda(s + \frac{z}{2})}$$

λ is the wavelength of exposing radiation, s is the gap between the mask and photoresist surface (μm), and z is the photoresist thickness (μm).

Depending on the mode of photolithography utilized, the minimum resolution ranges from 0.6 μm (s = 0), largely limited due to the diffraction of light, to 3 μm (s = 10 μm) in proximity mode. Together, these modes offer two approaches to conducting photolithography down to the resolutions into the single-digit micrometer scale, while providing the option to preserve the integrity of the photomask during photolithography.

Design Considerations of Protein Photolithography

The investigation of silk protein bioconjugation and photolithography provides a platform for the generation of high-resolution silk microstructures using light-based patterning. However, a number of important design considerations must be addressed to effectively demonstrate silk modification and photolithographic processing:

1) Chemical modification of silk proteins has the potential to impact physical, biological properties via blocking the interactions of critical amino acids. For example, polar amino acids in sericin (e.g. serine) are integral to polar zipper interactions in β-sheet-rich regions.[151] Serine-rich regions are simultaneously responsible for biologically favorable interactions.[70] In fibroin, structural concerns arise as well—the hexapeptide GAGAGS dominates the crystalline β-sheet-rich regions responsible for structural integrity.[58] Modification of key sequences silk proteins could thus prove disastrous for preserving the properties that make silk proteins biologically-relevant.

2) The introduction of a non-native chemical group onto silk has the potential to alter protein surface chemistry, and negatively impact solubility. It has long since been established that even the introduction of fluorescent labels has pronounced effects on solubility.[152] The surface hydrophobicity presented by a protein directly influences aggregation potential, thus determining relative solubility.[153] Common photoactive moieties such as acrylates possess a partially hydrophobic character due to the vinyl functional group.[154] This hydrophobic character has the potential to destabilize the silk conjugates,

inducing aggregation or insolubility in common solvents.

3) In conventional photolithography, the development of negative photoresist is achieved through solvents capable of solvating only unexposed photoresist. In translating this process to silk proteins, it is necessary to consider the use of a novel solvent system for achieving film casting, and subsequently, development without markedly degrading the proteins. For sericin, certain dissolution processes have been associated with significant protein degradation, negatively influencing biological properties.[155] These dissolution steps may also have an impact on mechanics and other properties, as is observed with fibroin.[156]

Potential challenges further exist due to the chemical and structural diversity possessed by constituent silk proteins, which necessitates the fabrication of a broadly accommodating platform for silk protein photolithography. The design of a platform applicable to both sericin and fibroin has a wider applicability to proteins of variable sequence and structure, allowing potential use for proteins in general. However, preserving the functional attributes of silk proteins is key in this approach, as any loss of function is detrimental to the concept of protein patterning. This platform offers the potential to address deficiencies implicit to current patterning methods, to yield large-scale patterning and the creation of features down to the microscale. This provides an opportunity to greatly simplify and improve upon currently existing methods for producing accurately-patterned silk for use in protein arrays, cellular scaffolds and other biomaterials applications.

Fabrication of "Smart" Silk Architectures

The extensive field of silk materials research has been steadily evolving alongside research into biomaterials design, with increasing overlap as the capabilities of silk are slowly expanded upon. An extraordinary amount of work has been invested into the study of silk in the design of novel architectures, for their unique mechanics, ease of processing, and position as renewable, natural materials. Currently, there is an untapped potential in expanding on the valuable properties of silk proteins by actively augmenting function to create a new library of silk-based biomaterials.[16] While silk fibroin has been thoroughly characterized and transformed into an array of architectures, concerns of biocompatibility have delayed similar studies on sericin.[5] For this reason, sericin is of particular interest in order to expand potential capabilities and function in the role of a new class of materials capable of eliciting stimuli-responsive attributes. Recent research has highlighted the role of sericin in producing enhanced biological function in terms of cellular attachment and proliferation.[74, 75] This has provided a push to evaluate new assembly techniques for the formation of protein architectures, in order to place sericin into biologically-relevant architectures capable of presenting the unique properties presented by sericin. These studies may be further translated to fibroin to demonstrate equivalent properties and versatility of the platforms established.

The primary objective was to demonstrate the development of a scalable and versatile silk protein photolithography system capable of producing functional, biologically-relevant silk protein structures. Recent techniques in creating cell-adherent, photoactive proteins through recombinant engineering have provided an incentive to designing an equivalent, yet modular biochemical approach applicable to silk

proteins.[139] Optimizing this process to enable large-scale patterning and the creation of features down to the microscale provides a method to form high-resolution patterns ideal for use in tissue engineering scaffolds, biosensing and other bioengineering applications.[115, 157] Silk fibroin was initially investigated in this platform, due to the wealth of chemical knowledge available and superior mechanics, and this technique was then translated to producing sericin through a biofriendly, water-based processing approach. In this research, strategies are developed that take advantage of the fundamental properties of silk proteins to yield non-toxic, naturally-derived silk materials of enhanced structure and function, capable of spatially directing cellular behavior.

1.3.5 The Scope of Attainable Silk Protein Structure and Function

The research presented in this dissertation sought to demonstrate the role of silk in establishing "smart" architectures by capitalizing on the fundamental attributes of silk proteins. This was achieved through establishing the role of silk proteins in a hierarchy of configurations and length scales: 1) from elucidating the intrinsic properties of individual silk proteins, to 2) the design of silk biocomposites for allowing the evolution of novel stimuli-responsive properties, and 3) lastly, to the millimeter-scale and beyond, by evaluating the application of chemically-versatile bioconjugation and lithographic approaches to producing precisely tailored, biologically-relevant silk architectures.

To date, the deficiency of fundamental characterization data on the properties and function of sericin have significantly limited its incorporation into biomedical microdevices. As a means of assembly, self-organization is an attractive attribute to

potentially harness for biomaterials development at the nano- and microscales.[37] Taking advantage the self-assembled, aggregated state of this protein allows enhancement of the biologically-favorable, yet functionally-inert, sericin with the ability to provide a meaningful response to external environments at the range of micro-to-centimeter scales. Finally, the necessary evolution of this approach incorporates moieties directly responsible for activity in bioconjugates, to modify silk protein directly. The hitherto unexplored strategy of inserting a naturally-derived, biocompatible material into photolithographic techniques provides immense benefits over the use of synthetic materials, and as a technique for enabling facile processing of silk, greatly expanding the repertoire of potential applications.

CHAPTER 2

SELF-ASSEMBLY OF NATURAL AND ENGINEERED SILK PROTEINS

2.1 Introduction

Spontaneous organization at various length scales to form larger, functional complexes via molecular self-assembly is common in diverse natural systems.[33] Multiple weak, non-covalent interactions mediate this process, allowing the assembly of supramolecular structures from smaller building blocks.[158] Understanding this aggregation or agglutination of small particles to form larger assemblies and clusters has widespread applications. These include colloid and gel formation, as well as beneficial and detrimental biomolecular aggregation processes.[34, 159] Self-assembly of natural precursors demonstrates potential applications in materials engineering, whereby autonomous assembly from components with an apparent lack of order into well-structured complexes, can be used to create novel biomaterials.[53, 160] The identification of natural and synthetic systems that can enable the study of self-assembly processes is therefore of great benefit to such fundamental and applied investigations, enabling the incorporation of biomolecules in new classes self-assembling materials.

Self-assembly and organization processes are generally modeled on the basis of architecture, dimensionality, and kinetic regimes–fast, diffusion-limited cluster aggregation (DLA), ballistic aggregation, and a slower, reaction-limited aggregation (RLA).[161, 162] The process of substrate deposition and aggregation from protein solutions occurs as the solvent evaporates, eventually allowing precipitation of the soluble species, resulting in structures having a smaller fractal dimensionality than that of the embedding space or lattice.[163, 164] In two dimensional models on simple planar or curved substrates, these mechanisms result in complex architectures, classified by physical properties, including fractal dimension, density, and texture.[165, 166]

Currently, studying such 2D self-assembly processes and aggregation processes is achieved primarily via theoretical models and computer simulations.[164, 167] It has been hypothesized that these limiting cases of aggregation are universal and independent of the chemical nature of the systems.[168] While this has been shown using various colloids, to date, there have been limited demonstrations in natural protein systems, particularly in the absence of salt or other chemicals such as stabilizing agents.[168, 169] With notable exceptions, most models deal with "ideal" particles of a single size, an approximation that rarely holds true in nature.[170] A small set of natural species including engineered polypeptides, lysozyme, gelatin and polyelectrolyte complexes have been reported.[163, 171-173] Identification and characterization of real systems as models for the characterization of DLA and hierarchical self-assembly would greatly enhance the global understanding of self-assembly, as well as allow exploiting this behavior in the development of functional, self-assembling materials that are self-similar across length scales.

The silk biopolymer, originating from a wide range of silkworm and spider species, is a unique example of a self-assembling material, providing evidence for the phenomenon whereby the whole (i.e. macroscale silk fiber) is greater than the sum of the parts (i.e. constituent silk proteins). An early reported on the assembly of a silk protein, sericin that spontaneously associates to form micro-scale structures.[37] Silks are widely-studied examples of hierarchical assembly, forming chemically and mechanically stable, β-sheet-rich composites, exhibiting superior biocompatibility in the purified state, and favorable biomechanics.[5, 174, 175] Sericin has the ability to form various fractal architectures in the absence of salt or electrolytes that can shield charge or encourage attraction between particles. This novel observation is elaborated on in order to model and study self-assembly phenomena in natural systems. To enable the modeling of fractal architectures as a two-dimensional process, the behavior of sericin from different sources leading to a diversity of cluster aggregation morphologies is discussed. Self-assembly with distinct patterns on hydroxylated silicon substrates is characterized across multiple length scales. Atomic force microscopy (AFM) and scanning electron microscopy (SEM) are used to provide topographic and morphological data on aggregates. These different mechanisms leading to DLA formation can be explained by considering differences in the physical properties of protein particles, measured via particle size estimation and zeta potential.

The core fibroin protein has been thoroughly studied in research, largely due to the implications of a mechanically-robust material in biomaterials design. In order to translate the aforementioned model of protein self-assembly to a structurally and chemically-distinct species, engineering strategies are explored for producing sericin-like

architectures of fibroin. The exploration of β-crystalline-inducing desolvation strategies enable the translation of a hydrophobic, fibrous silk protein into a relatively monodisperse range of microparticles, the properties of which are dependent on a number of treatment strategies.[176] Investigation of monodisperse particle fractions demonstrates the applicability of a similar model of diffusion-limited aggregation to a protein that shares little in common with sericin, aside from its co-production in silkworm species. This observation helps to demonstrate the ease of translation of diffusion-limited aggregation models to distinct protein systems, in producing diverse architectures through autonomous assembly processes alone.

The observed self-assembly may potentially be harnessed in the formation of novel, composite bio- and nanomaterials with self-similarity at different length scales. It is demonstrated that self-assembly in protein systems can be modeled as a purely physical phenomenon depending on properties such as particle size, dispersity and charge that causes differences in architectures from proteins that may share the same chemical function. These findings thus have profound implications in the formation of future classes of mechanically-robust, and structurally-stable materials through self-assembly alone.

2.2 Experimental Section

2.2.1 Materials

Silk samples were obtained from cocoons of: *Bombyx mori* (Jhargram Tropical Tasar Farms, West Midnapore, West Bengal, India), *Antheraea mylitta* (Debra Sericulture Farm, West Midnapore, West Bengal, India), *Antheraea assamensis* (Central Silkboard Farm, Coochbehar, West Bengal, India), and also used in the form of commercially-available pure sericin (subsequently referred to as Wako sericin in this work). *Note: Wako sericin is considered a commercial source of Bombyx mori silkworm sericin, due to the high relative abundance and widespread commercial use of this species.* Molecular biology grade water (0.1 µm filtered, < 2 µS/cm, Fisher Scientific, Fair Lawn, NJ) was used for solubilizing sericin powders. Sodium carbonate (Na_2CO_3) and lithium bromide (LiBr) were employed for fibroin purification from Fisher Scientific (Fair Lawn, NJ). Phosphate buffered saline (PBS, Fisher Scientific, Fair Lawn, NJ) was employed after 0.22 µm filtration at pH 7.4.

2.2.2 Sericin Extraction and Purification

The former three samples were utilized in the purified form, after extraction from silkworm silk by using a hot boil method under pressure (via autoclaving).[177] In this method, 50 mL of deionized water was added to 1 g of silkworm cocoons, which were then heated at 110 - 120 °C for 120 minutes. The resulting solution, containing solubilized sericin, is then filtered through a glass microfiber filter to remove insoluble

fibroin, and then dialyzed and lyophilized to yield a dried protein powder. Wako sericin was used as received, without further treatment. Sericin was reconstituted by dissolving the protein powder in molecular biology grade water to create 2 mg/ml stock solutions. Samples were vortex mixed at low-speed for 30 minutes to ensure complete dissolution. Finally, filtration with 0.22 μm nylon syringe filters removed large insoluble particulates, and the resulting solutions were stored at 2 °C.

2.2.3 Fibroin Extraction and Purification

Fibroin was extracted and purified from *B. mori* silkworm cocoons. Hot boil degumming was first conducted in order to remove the sericin glue protein.[21] Silk cocoons (1 g) were cut into small, 1 cm^2 fragments and a solution (400 mL) of 0.02M Na_2SO_3 was prepared and heated until boiling. The silk cocoon fragments were added to the boiling solution of sodium carbonate and intermittently stirred for a period of 30 minutes. The degummed fiber mass was removed from the solution, and immersed for 30 minutes in a stirred solution of cold deionized water, for a total of three rinses. The degummed fiber was then dried overnight at ambient temperature. Regeneration of silk fibroin was achieved via a solution of 9.3M LiBr. The degummed fiber was packed into a small beaker with 9.3M LiBr added to form a 20% (wt/vol) solution, and dissolved in an oven at 60 °C for 4 hours. The resulting solution was optically transparent, with a dull yellow coloration. This solution was then transferred to 3500 molecular weight cut-off (MWCO) dialysis tubing, and dialyzed against deionized water for 48 hours, with buffer changes at 1 and 2 hours, and subsequently every 8 hours. The regenerated fibroin

solution was then recovered, and centrifuged at 4500 rpm and 4 °C for 20 minutes to remove insoluble particles. This process was repeated following recovery of the supernatant for a total of three times. The resulting solution (7 – 8 % (wt/vol)) was then stored at 4 °C until ready to use.

2.2.4 Preparation of silk fibroin particles

Microparticles of fibroin were prepared according to established methods.[176] The concentrated fibroin solution was diluted down to 3.0% (wt/vol) in preparation for microparticle formation. Variable amounts of ethanol (V_{EtOH}/V_{SF} of 6:20, 8:20, and 9:20) were slowly added over a period of 2 minutes to a volume of fibroin (200 µL) while undergoing low-speed vortex mixing. The sample was then incubated at -20 °C for a period of 24 hours. The sample is noted to be milky white in appearance after defrosting. A subsequent 10x dilution enabled storage at 4 °C without gelation of the fibroin solution. Subsequent isolation of particles with a particular size range was conducted via filtration using a 0.22 µm syringe filter, on samples diluted to 50x to prevent clogging of the filter.

2.2.5 Dynamic Light Scattering (DLS) and Zeta Potential Analysis

To evaluate particle size and distribution, dynamic light scattering (DLS) was conducted using a Malvern Zetasizer Nano ZS90 (Malvern Instruments Ltd., Worcestershire, UK) at 20.0 °C, repeated three times. Zeta potential analysis was

performed as a measure of protein aqueous stability, via a zeta potential aqueous dip cell, following analysis of particle size.

2.2.3 Polyacrylamide Gel Electrophoresis

Sodium dodecyl sulfate polyacrylamide gel electrophoresis (SDS-PAGE) was used to determine species molecular weight. Along with 10 µL of SeeBlue protein standard, 10 µL mixtures of 5 µg of sericin, mixed with 5 µL 2x Novex Tricine SDS sample buffer (Invitrogen, Carlsbad, CA) were loaded into wells of a 5% stacking gel cast on top of a 8% polyacrylamide gel. The gel was run at 150 V for approximately 90 minutes and stained with MagicBlue rapid protein stain to enable band visualization.

2.2.4 UV-Visible Spectroscopy

Sericin was spectroscopically analyzed to ensure consistency between samples (at 1 mg/ml), and to verify accurate protein concentration in serial dilutions of the stock solutions. A Shimadzu BioSpec-mini UV-Vis Spectrophotometer was used to determine relative absorbance (A_{280}) at 280 nm for each solution. Analyses were conducted on 200 µL volumes in a quartz cuvette. A deionized water-filled blank was utilized as a reference sample, to which the A_{280} value was set to zero.

2.2.5 Substrate Preparation

Protein self-assembly was observed on hydroxylated p-type <111> silicon (Si) substrates. Si substrates were cut to sizes of 1 cm^2, and rinsed thoroughly with deionized water and ethanol to remove Si dust and surface contaminants. Substrates were then treated with a Piranha solution of 3:1 98% H_2SO_4:30% H_2O_2, for a period of 30 minutes, to remove organic contaminants and render the substrate hydrophilic (Caution: Piranha solution reacts violently with organic materials and must be handled with extreme care). The surface was repeatedly washed with deionized water and ethanol and dried at 150 °C. Small volumes (5 µL droplets) of solubilized sericin protein were placed on the clean substrates, and allowed to air-dry overnight at ambient temperature (22 °C).

2.2.6 Optical Microscopy

Optical imaging of dried samples (Nikon Eclipse LV100 optical microscope, Nikon, Japan) was used to analyze microscale self-assembly of sericin architectures. Samples were observed under brightfield illumination, using LU Plan Fluor lenses at 10x and 50x magnifications. In addition to providing low-magnification representations of dried protein architecture, images acted as a reference for locating regions of interest for further investigation.

2.2.7 Atomic Force Microscopy (AFM)

AFM images of the self-assembled architectures were obtained on an Asylum Research MFP-3D AFM (Asylum Research, Santa Barbara, CA). Imaging was performed in tapping (AC) mode using an AC240TS AFM probe (nominal spring constant k ~2 nN/nm, Olympus, Japan). The tip was operated at an optimal driving frequency of ~73 kHz, at a scan rate of 0.80 Hz to minimize imaging noise. Images were collected over a decreasing range of scan sizes (90 µm down to 1 µm), at a resolution of 512 x 512 points. Selected areas of the samples were examined further using scanning electron microscopy.

2.2.8 Scanning Electron Microscopy (SEM)

SEM imaging was conducted on a Hitachi SU-70 high-resolution field emission microscope, (3 nm resolution via secondary electron detection). Due to the relatively non-conducting nature of proteins, among many other biological samples, it was necessary to coat samples with a thin layer of metal to allow for electron conduction, and to minimize charging during imaging. Samples were sputter coated with palladium to a thickness of 4.0 nm using a Denton Vacuum Desk V cold sputtering system (Denton Vacuum, Moorestown, NJ). To further prevent protein degradation due to electron bombardment, the accelerating voltage was run significantly lower than the default of 20 kV: image quality was found to be optimal at 5.0 kV accelerating voltage and a working distance of 10 mm. At high magnification (> 100,000x), image collection was limited due to visible sample degradation when focused on a single area over an extended period of time. Magnification otherwise varied from 1,000x for single aggregates up to 100,000x for

discrete particles.

2.2.9 Fractal Dimension Calculations

Fractal dimensions were determined for both AFM and SEM images of sericin using the ImageJ image processing program.[178] Images were converted into a 2-dimensional binary form (B&W) to enable accurate analysis in ImageJ. The box-counting algorithm was used to estimate the fractal dimension (D_f) as previously described.[179]

2.2.10 Circular Dichroism (CD)

α-Helix and β-sheet content for the sericin samples were measured using a Olis DSM 1000 Circular Dichroism Spectrophotometer (Olis Inc, Bogart, GA). Analysis of the CD spectra was performed using DichroWeb Online Circular Dichroism Analysis via the SELCON3 secondary structure reference database at 178–260 nm.[180, 181]

2.2.11 Salt-Mediated Protein Assembly

Investigation of the influence of physiological buffers on sericin self-assembly was conducted via a 1x PBS solution, at pH 7.4. The PBS was filtered prior to use, to remove precipitated salts and other contaminants. Solutions of Wako sericin at 1 mg/ml in deionized water and PBS buffer were formulated, and 20 µL volumes were cast onto Piranha-treated silicon to study self-assembly effects. A solution of 1x PBS in the

absence of protein, acted as a control.

2.3 Results and Discussion

Models for aggregation have shown that structures formed have a characteristic fractal dimension (D_f) that is smaller than the embedding space or the lattice.[163, 164] Two-dimensional (2D) aggregates differ from higher dimensional assemblies in their substrate-dependence, a phenomenon absent in bulk solution. This aggregation can occur on hydrophilic substrates, or be stimulated by substrate modifications, where the addition of charge can allow for the favorable assembly of an oppositely charged biomolecular species.[173, 182] Here, the individual characterizations of the self-assembly of sericin from different species are presented as models for investigating diffusion limited aggregation behavior in 2D. On a surface, this protein would therefore assemble with a $D_f < 2$. This assembly by a pure protein in the absence of any charge shielding or modulation represents a novel system for fundamental and applied studies. In particular, the ability to control self-assembly at the molecular scale on surfaces by non-covalent forces can serve as a powerful model and tool in developing nanoscale biomaterials.

While the structural and functional role of sericin is conserved between silkworm species, its physical and chemical properties may vary greatly. Sericins from 3 different species of silkworms are characterized: *Bombyx mori, Antheraea mylitta* and *Antheraea assamensis*. The cocoon sericin from *B. mori* is the most extensively characterized for

sequence, molecular weight distribution, and chemical properties of all silkworm species.[5] *B. mori* sericin is comprised of a group of proteins ranging from 20 to 400 kDa with three major fractions at 150, 250 and 400 kDa.[71] Another characterized non-mulberry silkworm species, *A. mylitta* has higher molecular weight sericins with a light chain at 70 kDa, and heavy chains at 200 kDa, and > 200 kDa.[183, 184] *A. assamensis* has not been characterized to the extent of other sericin sources, though it is known to consist of a single 66 kDa chain.[185] Little information exists on the properties and origin of commercially-available Wako sericin, though it appears to have been purified from the common *B. mori* silkworm. Following autoclave-based extraction, these dominant fractions are degraded from their native state, yielding bands across a range of molecular weights and the presence of high molecular weight fractions for *B. mori* and *A. mylitta* (Figure 2.1).

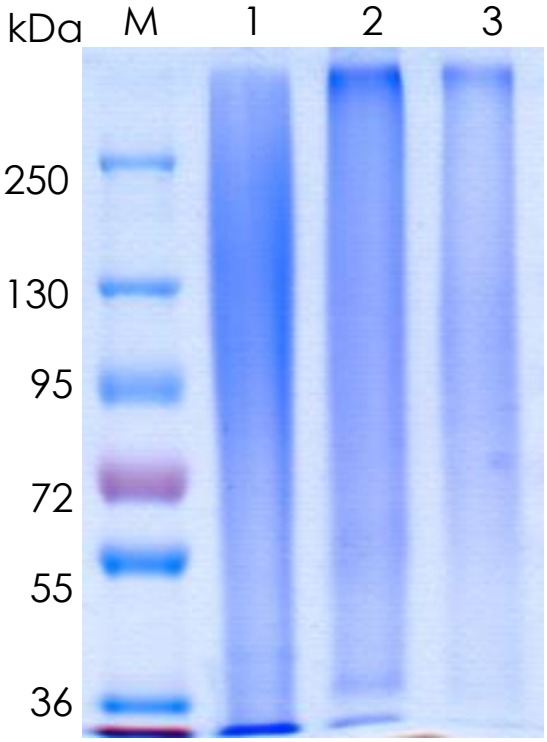

Figure 2.1. SDS PAGE (8%) gel pictures of 0.1% sericin solutions isolated from cocoons of different species: M - Molecular weight marker, 1 - *B. mori* sericin, 2 - *A. mylitta* sericin, 3 - *A. assamensis* sericin.

Incomplete and/or unknown sequence data, molecular weight distribution, amino acid compositions, and crystal structures preclude making a direct comparison between sericin proteins from the various silkworm species. However, it is possible to use a morphological and mechanistic evaluation of these systems to determine models for protein self-assembly via diffusion-limited aggregation.

The secondary structural content of sericin, predominantly β-sheets, with minimal α-helical content, may play a role in the observed hierarchical self-assembly described

below.[72] This was confirmed by circular dichroism measurements (Table 2.1). Aqueous solutions of sericin were further analyzed by UV-Vis spectroscopy to obtain absorbance values at 280 nm (A_{280}) for each protein (Table 2.2).

Table 2.1. Tabulated results from DichroWeb's SELCON3 secondary structure analysis at 178-260 nm, demonstrating relative similarity in structural content of various sericins.

Sericin	α-Helix (%)	β-Sheet (%)	β-Turn (%)	Random Coil (%)
B. mori	**2.3**	**43.6**	**22.3**	**32.4**
Wako sericin	**0.0**	**48.1**	**23.6**	**31.2**
A. mylitta	**1.9**	**48.8**	**23.9**	**29.3**
A. assamensis	**1.7**	**44.7**	**22.3**	**33.3**

Table 2.2. UV-Vis spectroscopy data for sericin samples, determined at 1 mg/ml concentrations. Variations in A_{280} values are attributed to relative differences in the abundance of tryptophan, tyrosine and phenylalanine (in order of descending molar absorption coefficient) in that respective sericin sample.

Sericin	Absorbance, 280 nm (A_{280})
B. mori	**0.273**
Wako sericin	**0.380**
A. mylitta	**1.071**
A. assamensis	**1.356**

From variation in A_{280} data for sericin, it can be inferred that there exist relative differences in the abundance of 280 nm absorbing residues—trytophan, tyrosine and phenylalanine. This observation suggests that the variation in secondary structural content is tied to species-dependent amino acid compositions of sericin. Overall, the driving forces present in these sericin species may be quantified by considering the tendency to spontaneously aggregate in solution, through electrokinetic measurements, summarized in Table 2.3. The zeta potentials for sericin species are similar in distribution ranging from -10.0 to -30.0 mV. *B. mori*, at -14.5 mV, is comparable to an earlier reported value of -20.7 mV for heat-degraded sericin, where the extraction method may account for the difference.[155] The low zeta potential values are all in the incipient instability regime, indicating that sericin possesses intrinsic instability in solution. This relationship between low zeta potential and tendency for DLA has also been previously observed in colloidal systems.[186] DLVO theory supports this colloidal instability as a function of both van der Waal's and electrostatic interactions between discrete particles undergoing Brownian motion. It is hypothesized that the presence of sufficiently weak or negligible energetic barriers due to weak surface charges between particles, favors the DLA process for proteins as well.[187]

The drying induced self-assembly of sericin was observed on silicon substrates. This process can be studied across multiple length scales using optical microscopy (millimeter), atomic force microscopy (AFM) and scanning electron microscopy (SEM) (micrometer and nanometer). Three discrete modes of self-assembly are present based on the general structural features and characteristics of the studied species, as seen in optical microscope images (Figure 2.2).

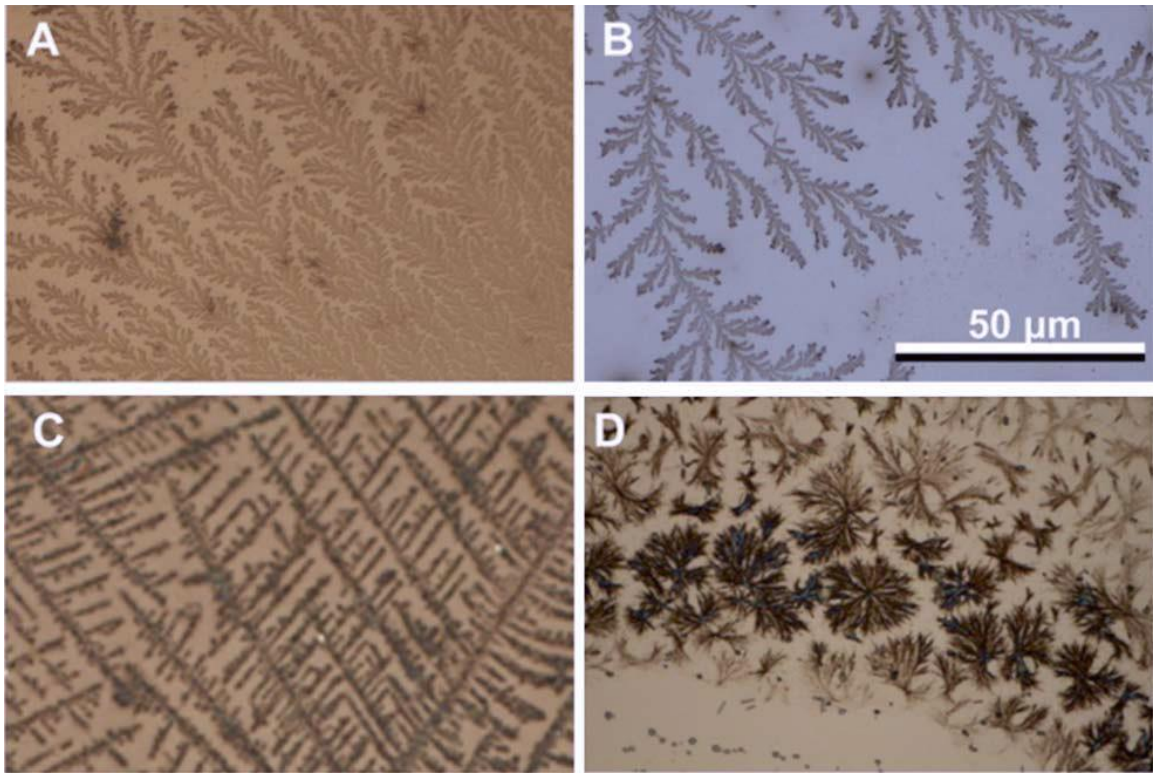

Figure 2.2. Optical images of (A) 1 mg/ml Bombyx mori, (B) 1 mg/ml Wako sericin, (C) 2 mg/ml Antheraea mylitta; (D) 1 mg/ml Antheraea assamensis. Scale bar = 50 µm.

B. mori and Wako sericin form irregular, dense dendritic aggregates, which are different in structure and dimension to *A. mylitta*, which also possesses an outward-branching regular, orthogonal architecture. Interestingly, *A. assamensis* falls outside of the outward-branching tendency exhibited by other species, and appears to aggregate into spherulitic form of DLA. Using the size distributions and the observed architectures, a hypothesis is presented for the possible mechanisms for the DLA based on the self-assembly of sericin nanoparticles and nanorods. The application of colloidal aggregation mechanisms to a coalescing protein is simplified by the assumption that the size difference between

protein molecules and the solvent allows treating globular protein particles in solution as colloids.[188] For the sake of simplifying the explanation of self-assembly, the mechanisms can be separated by architecture and species, and analyzed independently.

2.3.1 Mechanisms for assembly of mulberry silk sericin

The radially-branched, dendritic architectures of the mulberry silkworm sericins, *B. mori* and Wako sericin (Figure 2.2A, B) are best described by theoretical models on the random aggregation of solid particles into branched structures.[189] The classical diffusion-limited aggregation (DLA) model is described using the irreversible coalescence of colloidal particles into an outward-branching aggregate. For this protein, this process occurs during solvent evaporation, leaving a two-dimensional, fractal structure on the substrate, seen in AFM images (Figure 2.3A, B).

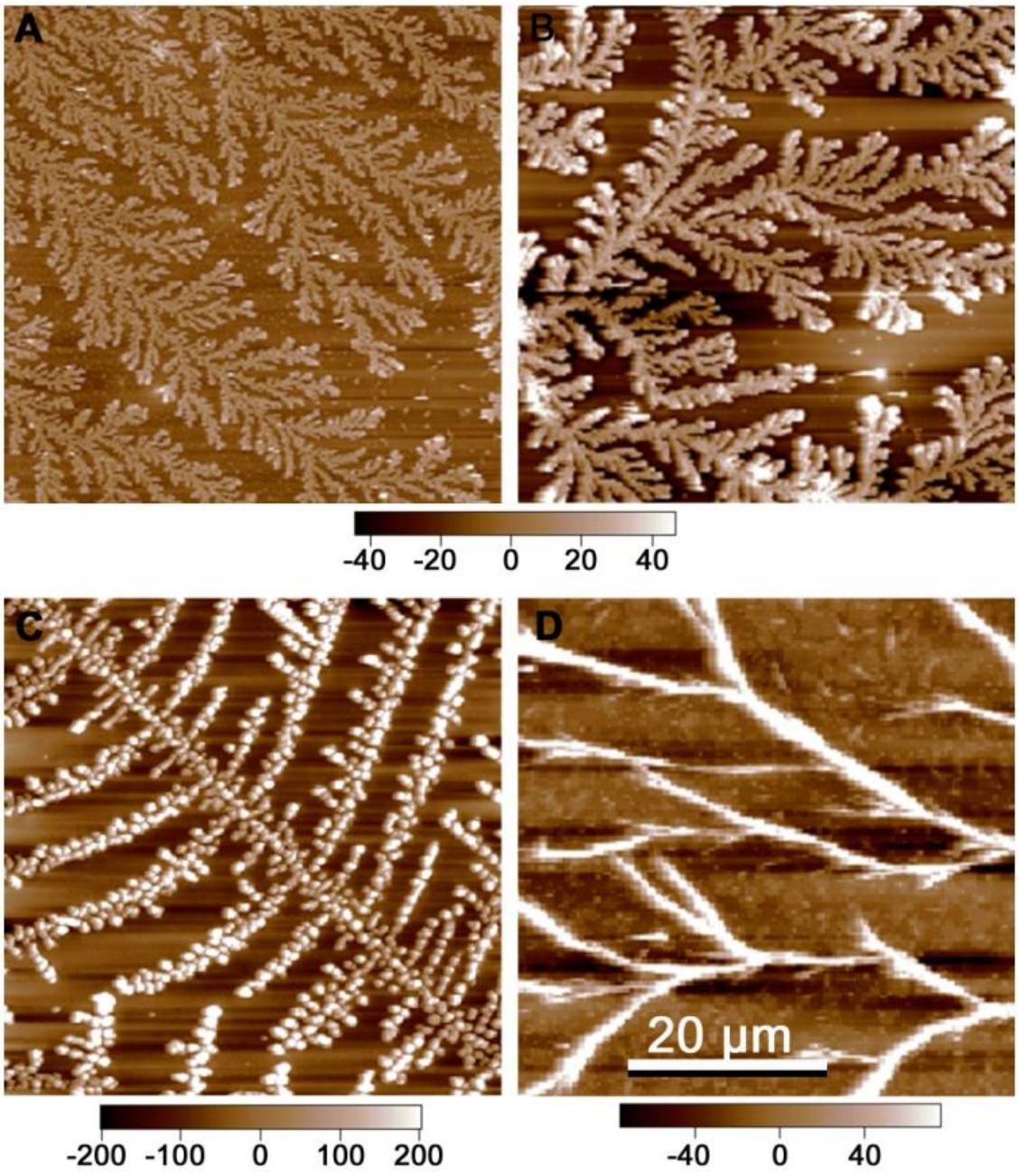

Figure 2.3. AFM images of (A) 1 mg/ml Bombyx mori, (B) 1 mg/ml Wako sericin, (C) 2 mg/ml Antheraea mylitta, and (D) 1 mg/ml Antheraea assamensis. Scale bar = 20 µm.

Self-similarity in fractal architectures is observed in SEM for *B. mori* and Wako (Figure 2.4A, C). Importantly, these images confirm the absence of microscale salt crystals or aggregates that may integrate and guide architectures.

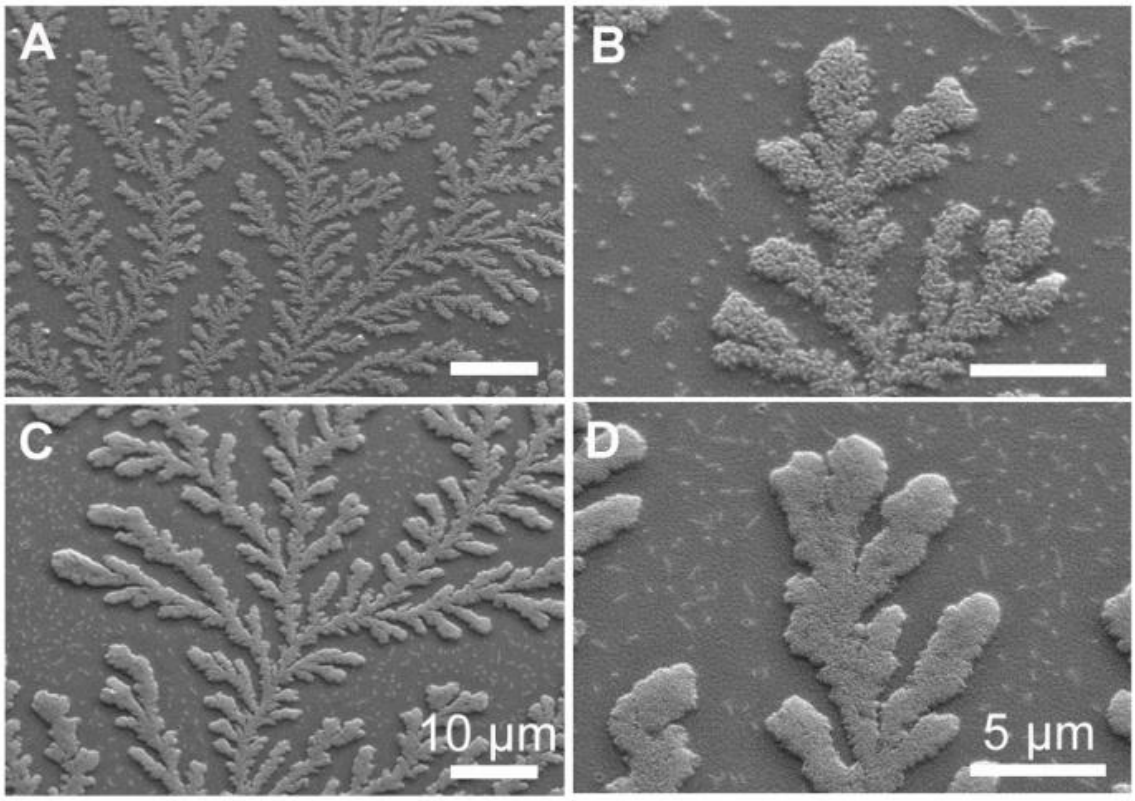

Figure 2.4. SEM images of (A and B) 1mg/ml Bombyx mori (C and D) 1 mg/ml Wako sericin. Panels B and D are higher magnification images highlighting similar dendritic architecture and scale for single branches.

In this model, the diffusion of colloidal particles into a growing cluster acts as the rate-limiting step of aggregate formation, to form intricate branched structures from dendrites to other random patterns.[190] DLA starts with a seed particle acting as the nucleation center of the cluster. Subsequent particles at a random position and infinite

distance undergo a ‘random walk’, or Brownian motion, to encounter and irreversibly integrate with the growing cluster. The diffusion rate-limiting step occurs with a negligible repulsive force between adjacent particles, thus the aggregation process is entirely under the influence of Brownian motion. The net gain of protein particles resulting from this randomness possessed by the diffusion field yields a highly branched dendritic aggregate, or Brownian cluster.

The presence of a polydisperse particle size distribution found from dynamic light scattering (DLS) (radii of 10.8 ± 0.8, 132.8 ± 19.8 nm for *B. mori*, and 8.2 ± 0.6, 123.0 ± 18.5 nm for Wako sericin) implies that this system deviates from the aggregation of same-size particles in previously described computational DLA models (Figure 2.5).

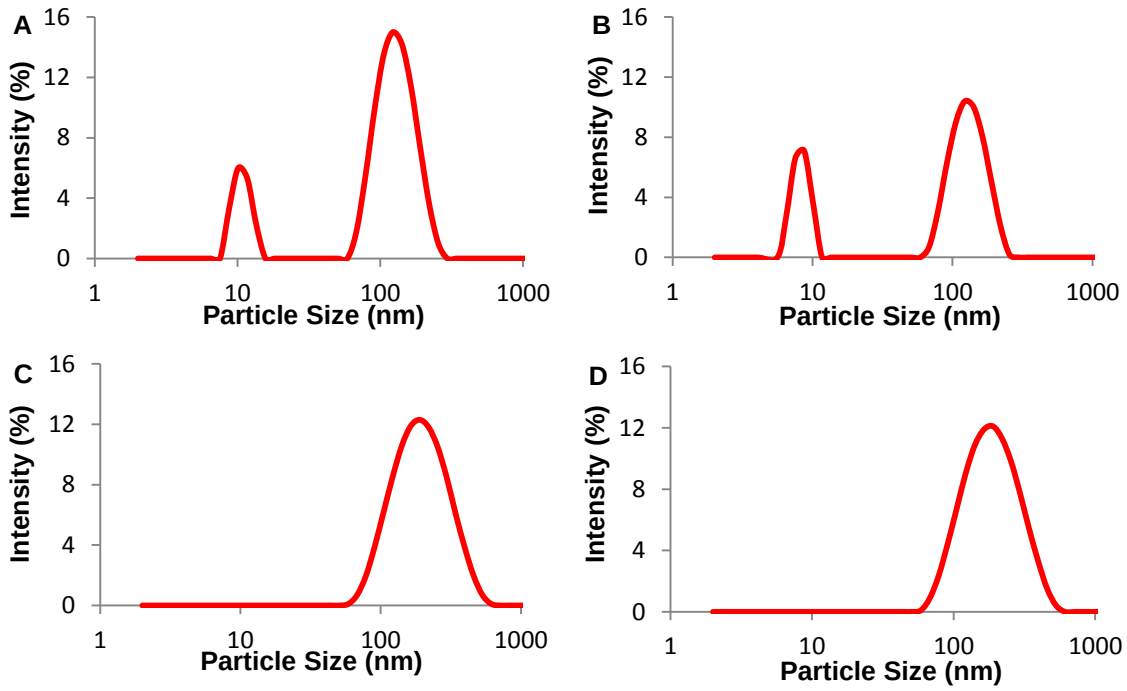

Figure 2.5. Sericin particle size analysis via DLS: (A) *B. mori*. (B) Wako sericin (*B. mori* commercial source). (C) *A. mylitta*. (D) *A. assamensis*. DLS data indicates both *B. mori* and Wako sericin possess two predominant particle sizes, while *A. mylitta* and *A. assamensis* have single, broad particle size distributions.

The presence of smaller molecular weight fractions results in smaller particles that play a key role in the dense architectures observed. A dynamic interplay between aggregation of small and large particles is likely whereby larger particles act as new nucleation sites for smaller particles.[191] Higher magnification SEM imaging of *B. mori* (~30,000 x) (Figure 2.4 B) presents a topography for which protein particles in branches are visible, incorporated into a tightly packed configuration. This rough microscale topography is shared by Wako sericin (Figure 2.4 D). The particle-cluster variant of DLA, where particles sequentially collide with and further the growth process of single

aggregates, is thus supported by the presence of aggregates consisting of a single nucleation site.[164] The lack of resolvable single particles commonly present in DLA models highlights the role of the smaller fraction of particles in competing for incorporation into the cluster. Particle analysis from SEM images (Figure 2.6 A-B), indicates a disparity between DLS data and particle dimensions in aggregates.

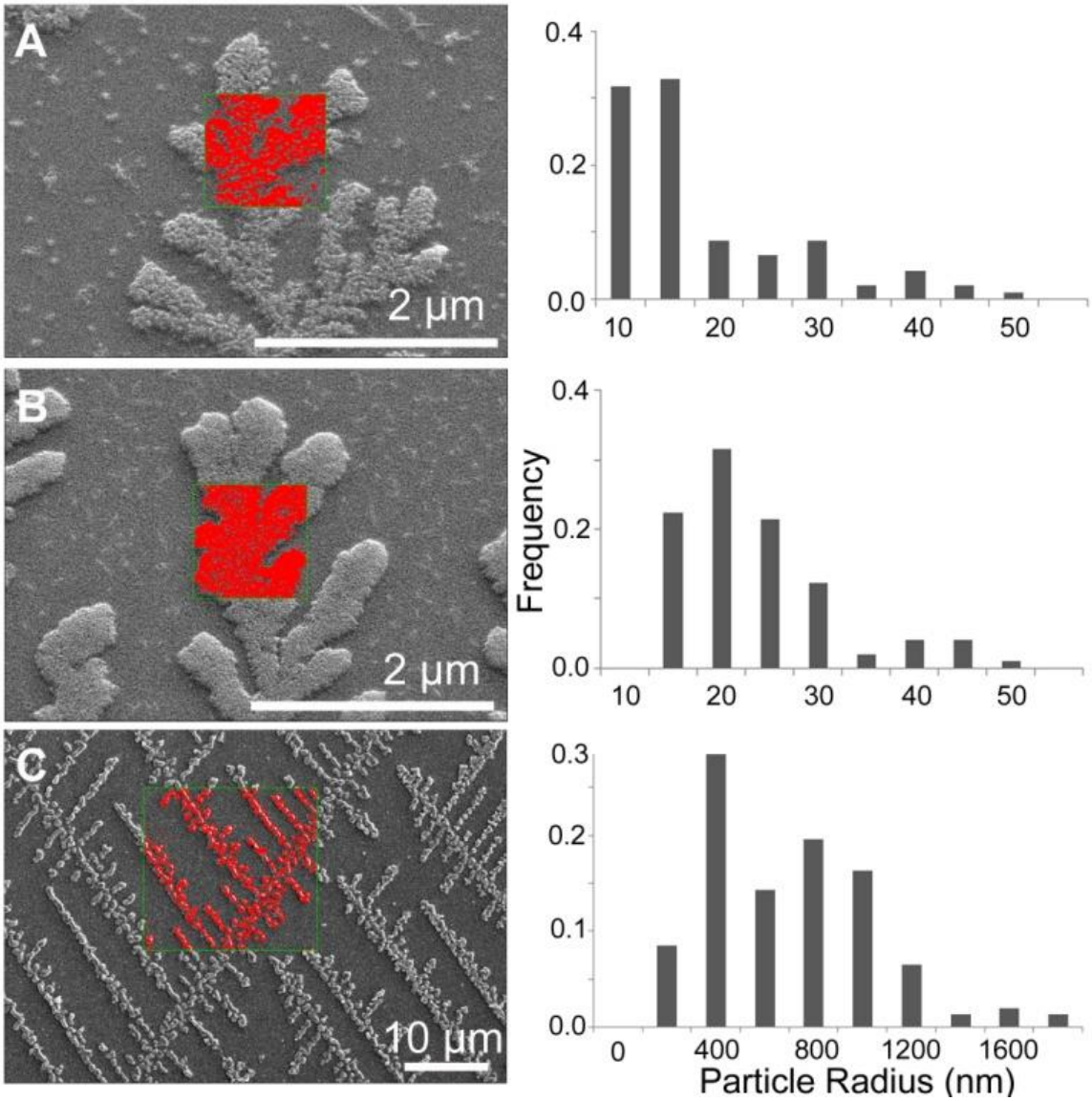

Figure 2.6. Particle size analysis of SEM images: (A) *B. mori*, (B) Wako sericin, (C) *A. mylitta*. Particles of a 25 pixel minimum threshold were located and analyzed.

The small range of *B. mori* and Wako particle radii, respectively at 17.3 ± 11.9 nm, and 22.1 ± 10.1 nm, suggests an initial aqueous aggregation process of the smaller particle fraction observed in DLS data. The significant size difference between particle radius in aggregates observed in SEM images, and DLS data indicating 120 - 130 nm particle size, suggests tight packing and structural rearrangement of particles during the DLA process.

The significance of intermolecular interactions can be observed by considering the probability of approaching sericin particles to adhere to the growing structure. Spherical particles undergoing Brownian motion have some probability to 'stick' to developing branches, irreversibly associating and allowing branch growth.[190] At a stickiness parameter, s = 1, the system possesses perfect absorption, where coalescing particles encounter with protruding branches at the largest current radius of cluster growth. Lower stickiness yields denser (short branches of large width) aggregates as subsequent particles are able to penetrate further into the cluster before irreversible aggregation occurs.[192] Preferential growth also manifests as the addition of particles to outer branches, despite the aggregate's interior being just as accessible, due to peripheral arms having a flux screening effect for approaching particles.[189, 190] A moderately-dense architecture, along with the shielding of particles at smaller radii (a key characteristic of DLA) is seen in these sericin aggregates, displaying a preferential elongation by addition of particles to protruding 'arms' (Figure 2.2 A-B). An intermediate sticking probability likely causes peripheral arms to grow preferentially, allowing flux screening to occur. These observations imply that favorable protein surface charge interactions are a driving force in the emergence of collision probability.[193]

Protein concentration also has a profound influence on the formation of aggregates via DLA. At higher protein concentrations, aggregates of *B. mori* are observed to increase in both size and relative surface coverage (Figure 2.7 A-B). While this phenomenon resembles a higher apparent stickiness parameter, the formation of denser aggregates results from close contact between solubilized aggregates, allowing a larger number of particles to participate in the DLA process per unit area. As protein concentration is decreased (Figure 2.7 C), aggregates become discontinuous in branching and occur over smaller areas—this phenomenon results from the relatively low abundance of particles participating in the DLA process, reaffirming a link between concentration-based effects and aggregate density.

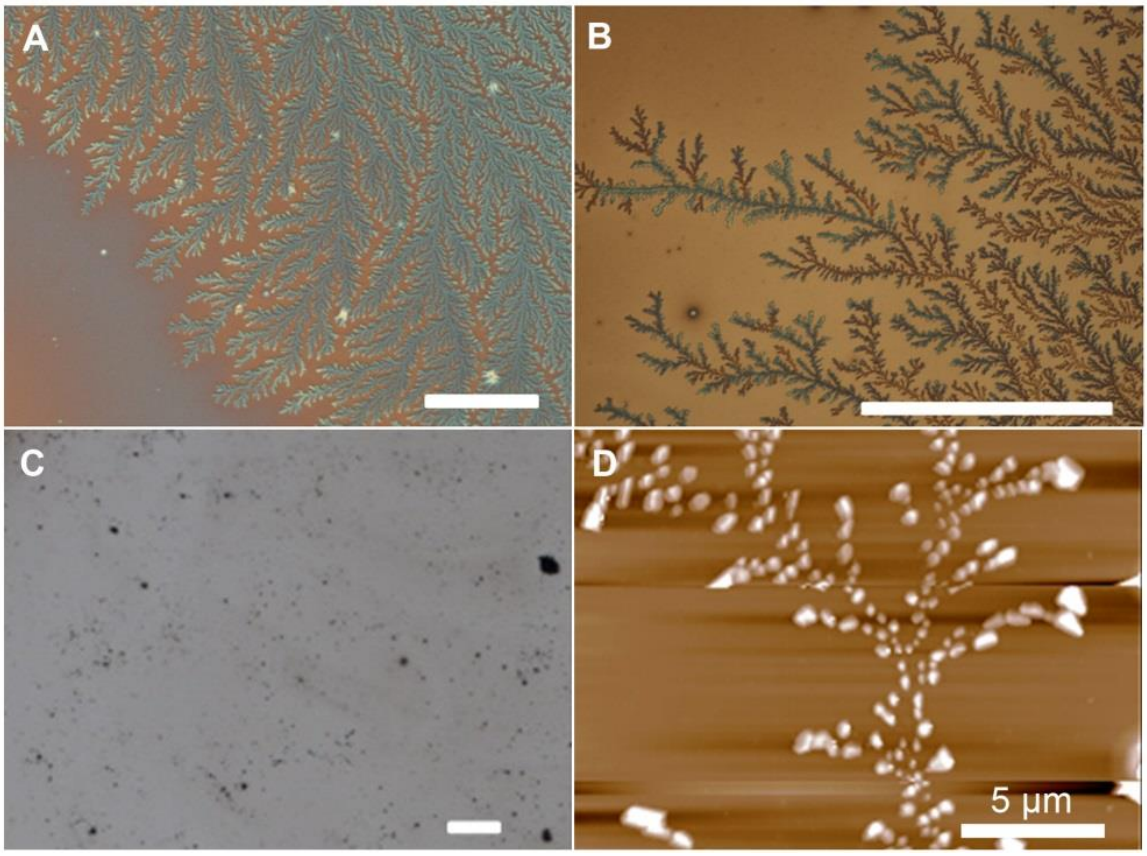

Figure 2.7. Optical micrographs *B. mori* at (A) 2 mg/ml and (B) 1 mg/ml, depicting thinning of branches and increasing void space with diminishing concentration. At a concentration of 0.2 mg/ml, features are no longer visible by (C) optical microscopy, and branches are discontinuous in (D) AFM images. Scale bar = 100 µm.

Similarly, for Wako sericin, these observations hold—in the case of a high concentration, the formation of a thick protein film prevents the observation of individual aggregates (Figure 2.8 A-B). This occurs due to significant surface coverage concealing aggregates under multiple layers of protein particles.

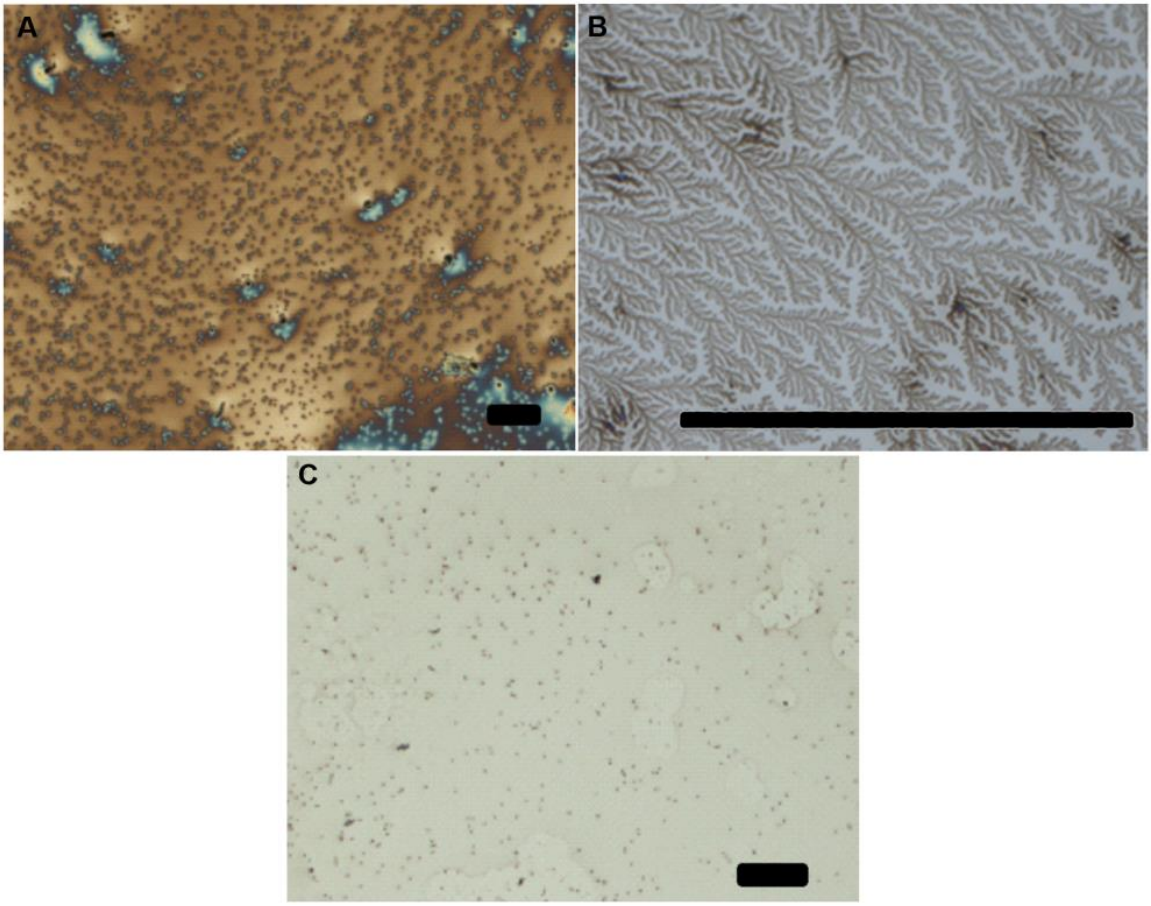

Figure 2.8. Optical micrographs of Wako sericin (A) 2 mg/ml and (B) 1 mg/ml. At high concentrations, Wako forms films of dense aggregates visible in (A). Low concentrations of (C) 0.2 mg/ml lack adequate protein for DLA to occur. Scale bar = 100 µm.

The fractal nature of DLA architectures is determined from the fractal dimension parameter (D_f), which is used for classifying two-dimensional aggregates into aggregation regimes. In terms of architectural properties, fractal dimensionality represents the degree of space-filling of a fractal. The fractal dimension found in modeling off-lattice DLA clusters is commonly 1.715 (DLA without dipolar interactions), though higher values have been reported.[194, 195] For *B. mori* and Wako

sericin, the D_f has been calculated to be 1.75 and 1.78, respectively (Table 2.3).

Table 2.3. DLS data for zeta potential and particle size of sericin protein samples.

Sericin Sample	Mean Particle Size (nm)	Zeta Potential (mV)
B. mori	**132.8 ± 19.8, 10.8 ± 0.8**	**-14.5**
Wako sericin	**123.0 ± 18.5, 8.2 ± 0.6**	**-22.0**
A. mylitta	**207.8 ± 46.0**	**-17.5**
A. assamensis	**200.2 ± 44.1**	**-17.7**

These dimensions, consistent with previously reported scaling models, are explained by the presence of a polydisperse distribution of particles, where multiple particle sizes provides additional nucleation sites for branch growth, increasing D_f (Table 2.4).[170, 191]

Table 2.4. Fractal dimensions (*Df*) of sericin protein microarchitectures.

Sericin	Fractal Dimension D_f
B. mori	**1.75 ± 0.08**
Wako sericin	**1.78 ± 0.02**
A. mylitta	**1.68 ± 0.08**
A. assamensis	**1.72 ± 0.01**

2.3.2 Mechanisms for assembly of non-mulberry silk sericin

Sericins from two non-mulberry silkworms *A. mylitta* and *A. assamensis* were investigated as described above. The *A. mylitta* sericin aggregates into low-density, self-similar architectures with near-constant angle (~ 60°) between successive branches (Figure 1C). This hierarchical, 4-fold semi-symmetric growth process of slanted branches has been previously modeled as a DLA variant, and observed in interfacial solidification.[164, 196] The presence of single particles composing architectures in AFM images (Figure 2.3 C) was investigated at higher resolution in SEM images (Figure 2.4 A). Unlike those architectures observed for mulberry silk sericin, micro-to-millimeter scale aggregates are observed with loosely-packed particles possessing spatial separation between neighbors.

Concentration-dependent morphological effects are observed similarly for both *A. mylitta* (Figure 2.9) and *A. assamensis* (Figure 2.10). As the concentration of *A. mylitta* sericin is decreased, fewer particles are available to participate in DLA, leaving significant voids and incomplete branches (Figure 2.9 A-B). For *A. assamensis*, there exists a clear transition around 1 mg/ml, at which stage the formation of DLA fractal structures is evident. This trend has been previously established, as branched DLA-formed architectures give way to denser aggregates as particle concentration is increased.[197]

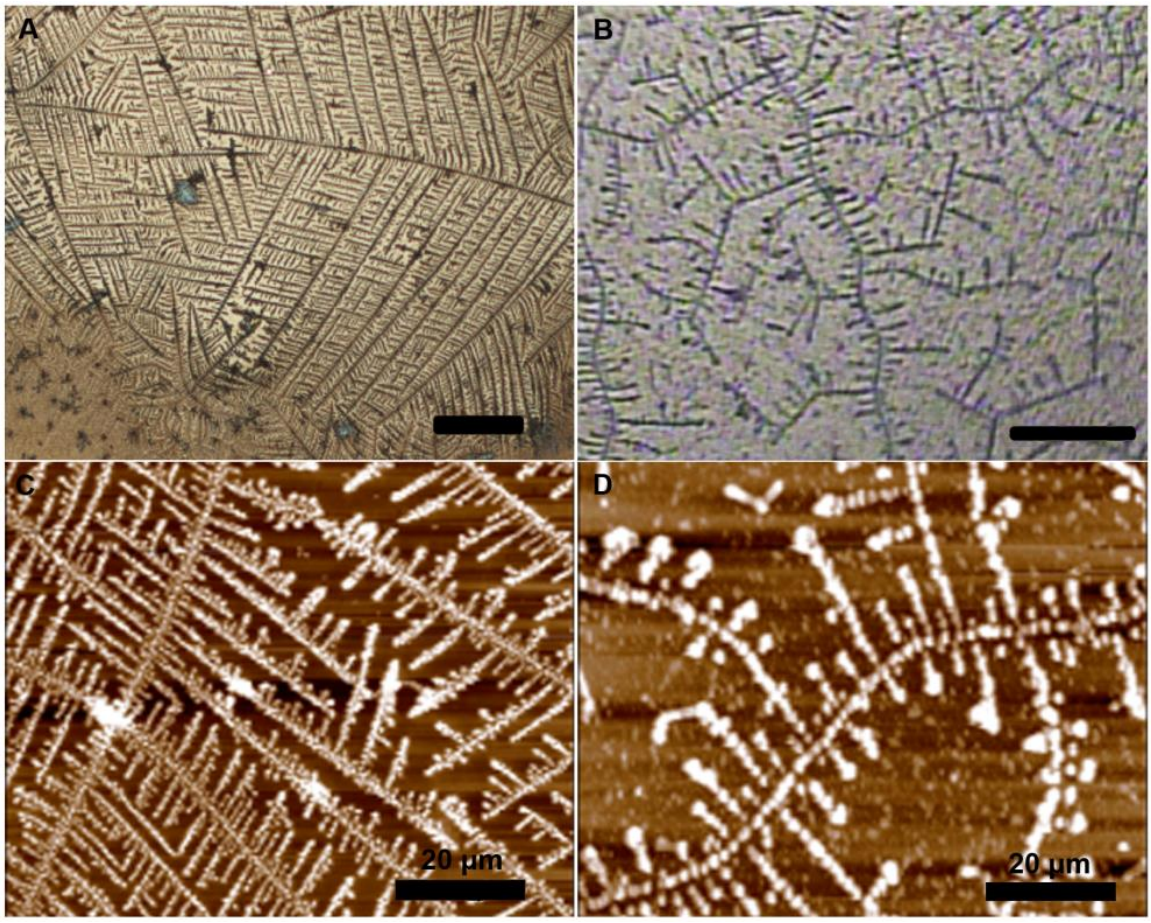

Figure 2.9. Optical micrographs of *A. mylitta* (A) 2 mg/ml and (B) 1 mg/ml, depicting the loss of orthogonal architecture with diminishing concentration. AFM images of (C) 2 mg/ml and (D) 1 mg/ml indicate the extent of branching and surface coverage also decrease with concentration. Scale bar = 100 µm.

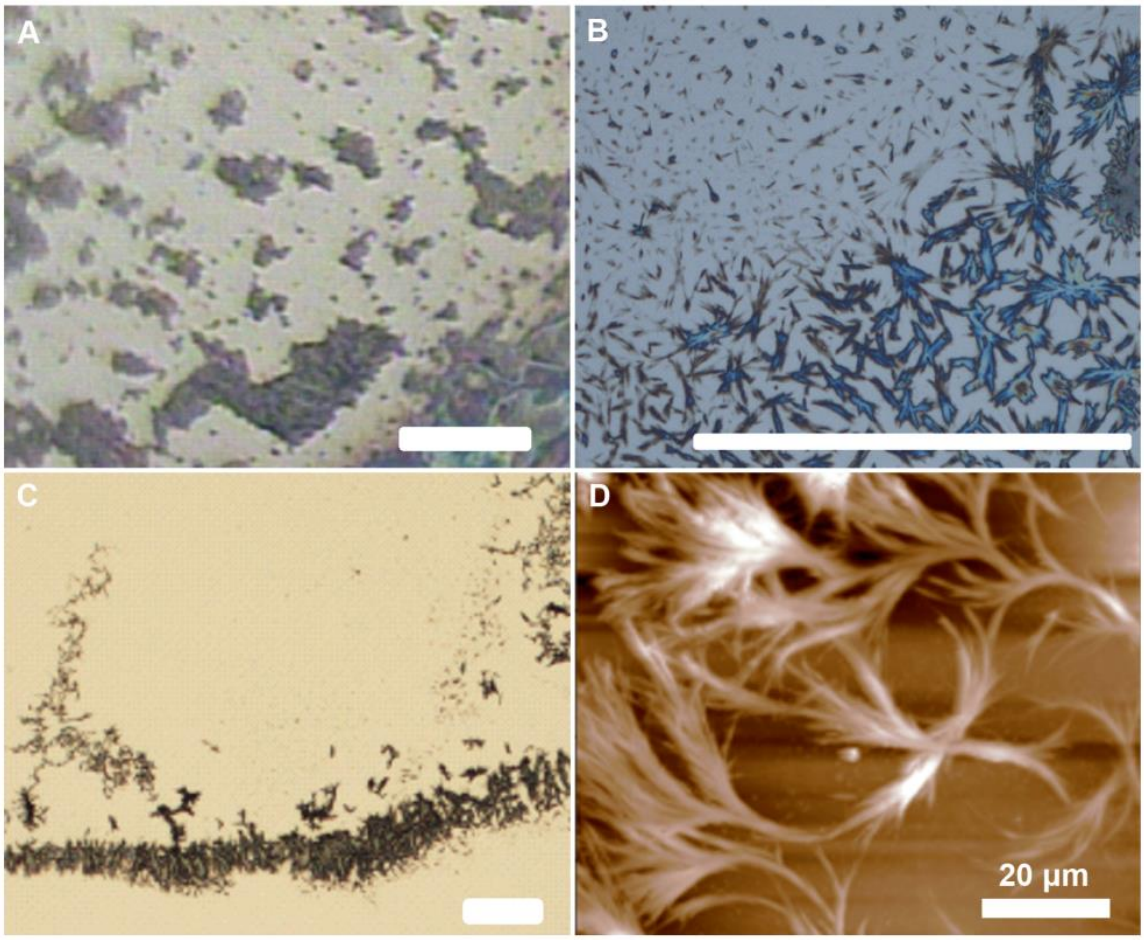

Figure 2.10. Optical micrograph of 2 mg/ml *A. assamensis* (A), showing sericin protein forming clumps, and as concentration is decreased to 1 mg/ml (B), protein begins to form aggregates. At 0.5 mg/ml, these aggregates dissipate (C), and concentrate further towards the contact line of drying, as is seen in AFM images (D). Scale bar = 100 µm.

The colloidal mechanics driving this assembly mechanism are the same as particles undergoing coalescence characterized by DLA. Variations in this 4-fold branched architecture are attributable to a combination of a quasi-static growth process most prominent in snowflake crystals, with tip splitting, and a generally monodisperse

particle size distribution for this species.[198, 199] Tip splitting, or the bifurcation of a single branch into multiple species relates to the consideration of a noise parameter, possessing significant influence in the growth process. Noise may result in irregularities in the growing aggregate—branching periodicity, phase and amplitude, as well as length and position, though this parameter is better defined by resulting fluctuations in the growth process caused by fluid dynamical instability.[199] In classical DLA models, a noise parameter $m = 1$ is considered. With noise reduction ($m > 1$), perimeter sites for particle adhesion are screened for particle collisions. A random walk is evaluated m times before particle addition is successful and the unoccupied perimeter site is then occupied by a new particle. This results in incoming particles approaching the elongating branch at various positions and angles, further leading to a more 'regular' and preferential growth. This effect drives the transition from the branched DLA models observed in mulberry silk species to the snowflake-like architecture seen in *A. mylitta*.

Furthermore, from the particle size analysis (Table 2.3), the absence of smaller particles in *A. mylitta* results in more discrete, separated particles as also confirmed by higher magnification SEM imaging (Figure 2.11).

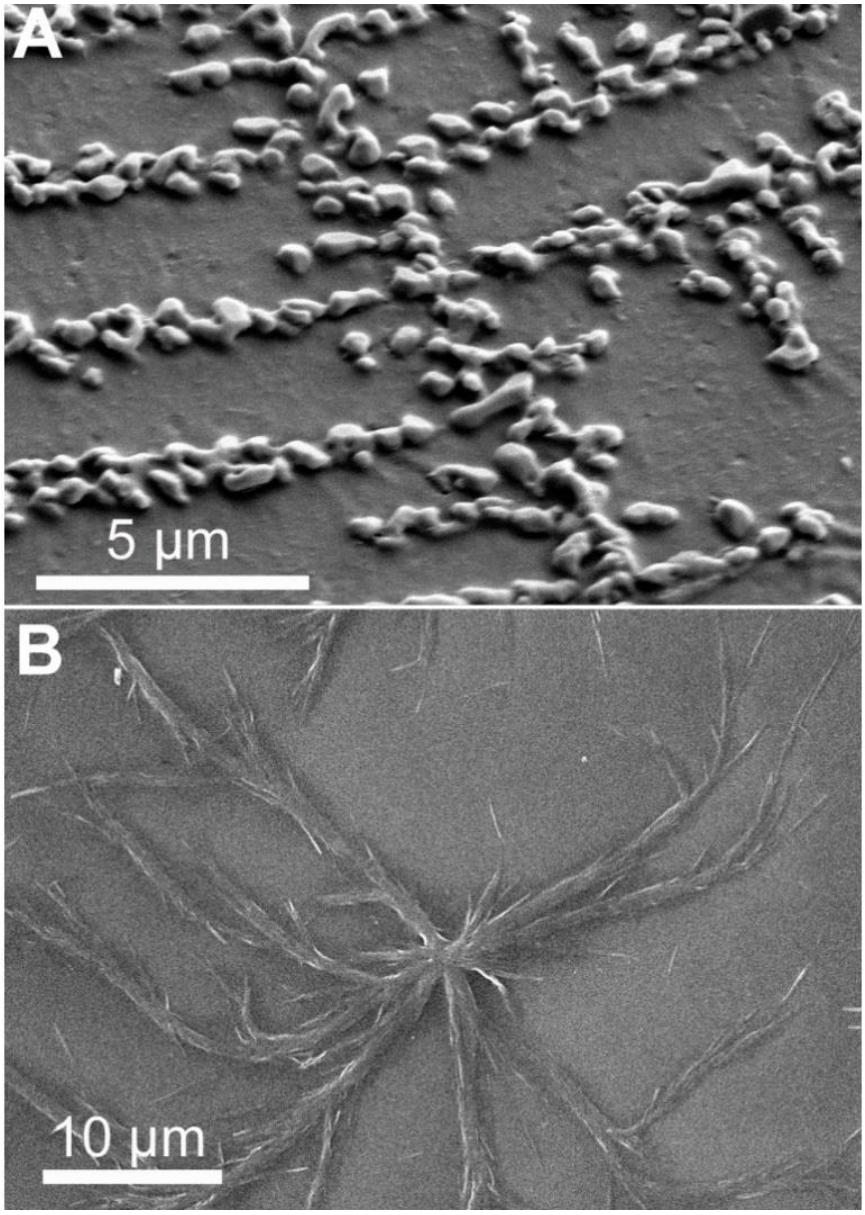

Figure 2.11. Higher magnification SEM images of non-universal DLA assembly of (A) 2 mg/ml Antheraea mylitta and (B) 1 mg/ml Antheraea assamensis.

Conversely, the presence of smaller particles in the mulberry silk sericin (*B. mori*) implies that it is possible for these to occupy the interstitial spaces between the larger particles forming a more homogeneous structure. The appearance of a low density,

stringy structure, is likely due to the inability for these large sericin particles to deeply interpenetrate into a growing cluster, i.e. a low stickiness parameter.[200] Discrete, resolvable particles exist in *A. mylitta* aggregates for comparison to aqueous size data. Particle sizes of 207.8 ± 46.0 nm from DLS show substantially larger particle sizes than branched *B. mori* and Wako sericin. The statistical analysis of particles in SEM images estimates radius to be 591.5 ± 345.6 nm (Figure 2.6 C). Comparison between radii indicates subsequent aggregation of colloidal particles in solution, creating DLA composed of particles 3-fold larger. Importantly, in comparison to *B. mori* sericin, it must be noted that these particles have a distribution about a single peak with only higher molecular weight fractions resulting in these larger particles and hence, a difference in assembly. The low zeta potential of *A. mylitta* supports this additional rapid aggregation through an incipient instability. In two-dimensions, fractal dimension of the classical diffusion-limited aggregation has been determined to be ~ 1.71. Despite the non-ideality of this DLA system, *A. mylitta* architecture is still within range for DLA to occur. The fractal dimension, D_f, for *A. mylitta* of 1.68 is only slightly lower for aggregates in models of noise reduction and quasistatic growth processes.[167]

The compact aggregates observed for the third species of silkworm studied, *A. assamensis,* are not directly comparable to the highly-branched clusters observed in other sericin samples above. Instead, the sericin from this species exhibits a non-universal DLA more similar to spherulitic growth (Figure 2.2 D). The process results from the growth of stacked lamellae from a nucleation site to packed elongated fiber-like aggregates and circular, outward-branched patterns. Similar morphologies have been observed for proteins such as lysozyme and bovine insulin, though generally to a more mature growth

state than that of *A. assamensis* sericin.[201] The formations from *A. assamensis* can be compared to that of polycrystalline polymers, via stacking of protein growth units into sterically-filling structures.

A. assamensis behavior can be approximated to a process of nanorod mediated fractal assembly, forming spherulite-like architectures (Figure 2.12). This process begins with the assembly of nanoparticles into nanorods with a characteristic dimension of around 200 nm, as observed in DLS measurements. The nanorods then come together as the essential diffusion units in this assembly to the spherulite-like and branched formations observed for this species (Figure 2.3 D). The observation of nanorods was further confirmed by high-resolution SEM (Figure 2.11 B). This model of nanorod mediated assembly was proposed earlier for short dipeptide derivatives that first formed rods on the order of around 1 μm prior to fractal assembly on surfaces.[202] In order to explain the formation of nanorods, it is useful to consider the difference in the sericin from *A. assamensis* from the other sericins studied above. This sericin is unique in that it consists only of a *single* polypeptide band at 66 kDa.[185] Comparison to other globular proteins of similar size (e.g. bovine serum albumin) allows us to consider that this sericin consists of particles around 3 – 4 nm.[203] Unlike the larger nanoparticles observed above (typically from a range of molecular weights from 20 - 400 kDa), these particles are incapable of forming fractal structures by themselves. Instead they assemble to form nanorods with characteristic dimensions of around 200 nm (Table 2.3) which then come together to result in the architectures observed.

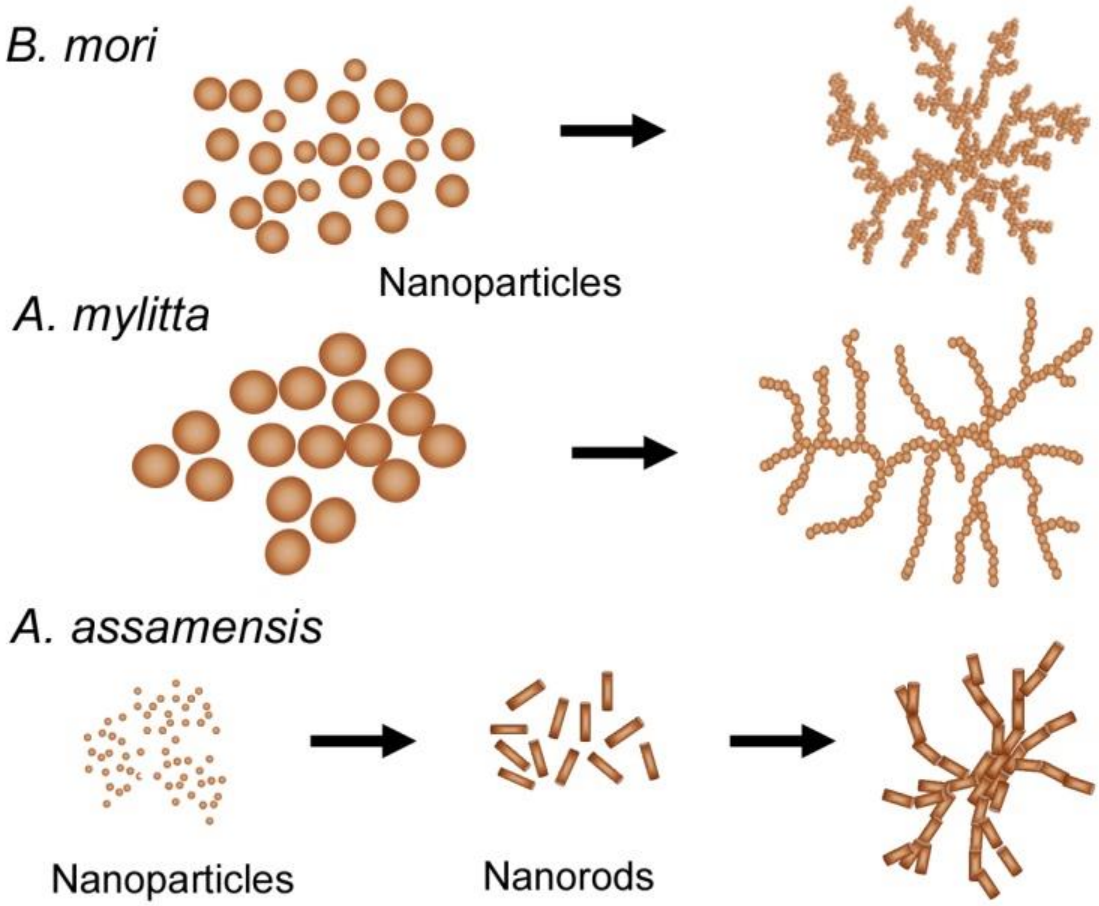

Figure 2.12. Proposed models for diffusion limited self-assembly of different particle distributions. Polydisperse nanoparticles self-assemble to classical DLA. Monodisperse nanoparticles self-assemble to less dense DLA with tip-splitting. Small nanoparticles first form nanorods, which assemble to nanorod-mediated DLA.

The D_f of around 1.69 is similar to that observed earlier for self-assembled peptide nanorods that assembled into similar fractal patterns.[202] This system is also morphologically comparable to the assembly of short DNA fragments into fractal patterns.[204] The central regions of these assemblies are analogous to spherulitic growth

that has a homogenous nucleation from single crystalline needles to form sheaf-like branching pattern. This mechanism may be attributed to a combination of the formation of protein-rich droplets via liquid-liquid phase separation and subsequent crystallization. High resolution SEM imaging (Figure 2.11 B) clearly shows self-assembled nanorods < 5 μm. These short nanostructures are precursors to the non-universal fractal DLA. As observed for β-polyalanine peptides and dipeptide nanorods, these short nanorods are unable to form hydrogels via water immobilization.[204, 205] Instead they are ideally suited to form fractal architectures as observed. As the aspect ratio approaches that of a nanofiber, there is an enhancement of β-sheet content and intrinsically flexible fibers entangle and prevent self-assembly.[205]

Overall it is hypothesized that in protein systems, the process of colloidal diffusion limited aggregation stems from inherently unstable protein nanostructures (nanoparticles, nanorods) in solution. By virtue of sufficiently low repulsive interactions, these self-assemble to form observed fractal structures. Interestingly, these structures are observed to form in the absence of salt. The presence of salt tends to shield particle charges and allow rapid aggregation via diminishing repulsive interactions. However, low zeta potentials indicate an unstable system that may also account for rapid aggregation in the absence of salt. Diversity of architectures is hypothesized to result from the differences in the physical properties of these systems primarily in the form of their sizes in solution (Figure 2.12). In a polydisperse system (*B. mori*), the competition between particles an order of magnitude different in size, allows DLA to proceed to yield denser structures for which single particles cannot be easily differentiated. Smaller particle sizes allow tight packing to occur, filling voids and forming continuous branching. When

considering a monodisperse system (*A. mylitta*), aggregate particles undergo a DLA-like growth mechanism to form linear structures. From these simple linear structures, tip splitting phenomena enable the formation of progressively smaller orders of branches until only branches of single-particle-widths remain. A third mechanism of self-assembly is present in *A. assamensis*, where homogenous nucleation of a single polypeptide fraction enables the formation of nanorods, which in turn assemble to form nanorod-mediated DLA architectures. While the sericin protein is functionally similar across silkworm species, each species possesses differences in protein sequences and molecular weights. The diversity of self-assembly modes is attributed to the significant differences between these physical properties.

2.3.3 Environmental control of sericin self-assembly

In this work, considerable effort has been directed towards the isolation and characterization of sericin protein in the purified state, in the absence of any organic or inorganic contaminants—mostly biomolecules, which were removed during the silk degumming process. Self-assembly and subsequent analyses have largely established a number of possible 2D architectures, available on the basis of the silkworm species from which the sericin protein was extracted. These architectures each possess specific morphological and physical properties, which influence assembly to producing a specific architectural type. Methods for influencing the assembly of sericin, or proteins in general, are not well-represented in literature—thus, it was of interest to evaluate the potential for directing sericin assembly to into defined architectures.

The introduction of salts and/or metals has proven integral to modifying the structure and function of proteins.[206, 207] For example, protein scaffolds have been fabricated by utilizing a physiological buffer in order to induce the formation of macroscopic protein structures.[160, 208] Even in silk fiber assembly, specific physiological parameters, such as pH, ionic strength, and other environmental characteristics, play a key role in inducing specific protein morphologies.[209, 210] Phosphate buffered saline (PBS) was selected to examine the architectural impacts of a physiological buffer on sericin self-assembly. Experiments involved the evaluation of a 1 mg/ml solution of Wako sericin in 1x PBS, and separate sericin and PBS controls, onto planar surfaces of Piranha-treated silicon. This salt-mediated self-assembly was observed to have a significant impact on architectural features of sericin, inducing the formation of a dense, orthogonal network with distinct hierarchy (Figure 2.13).

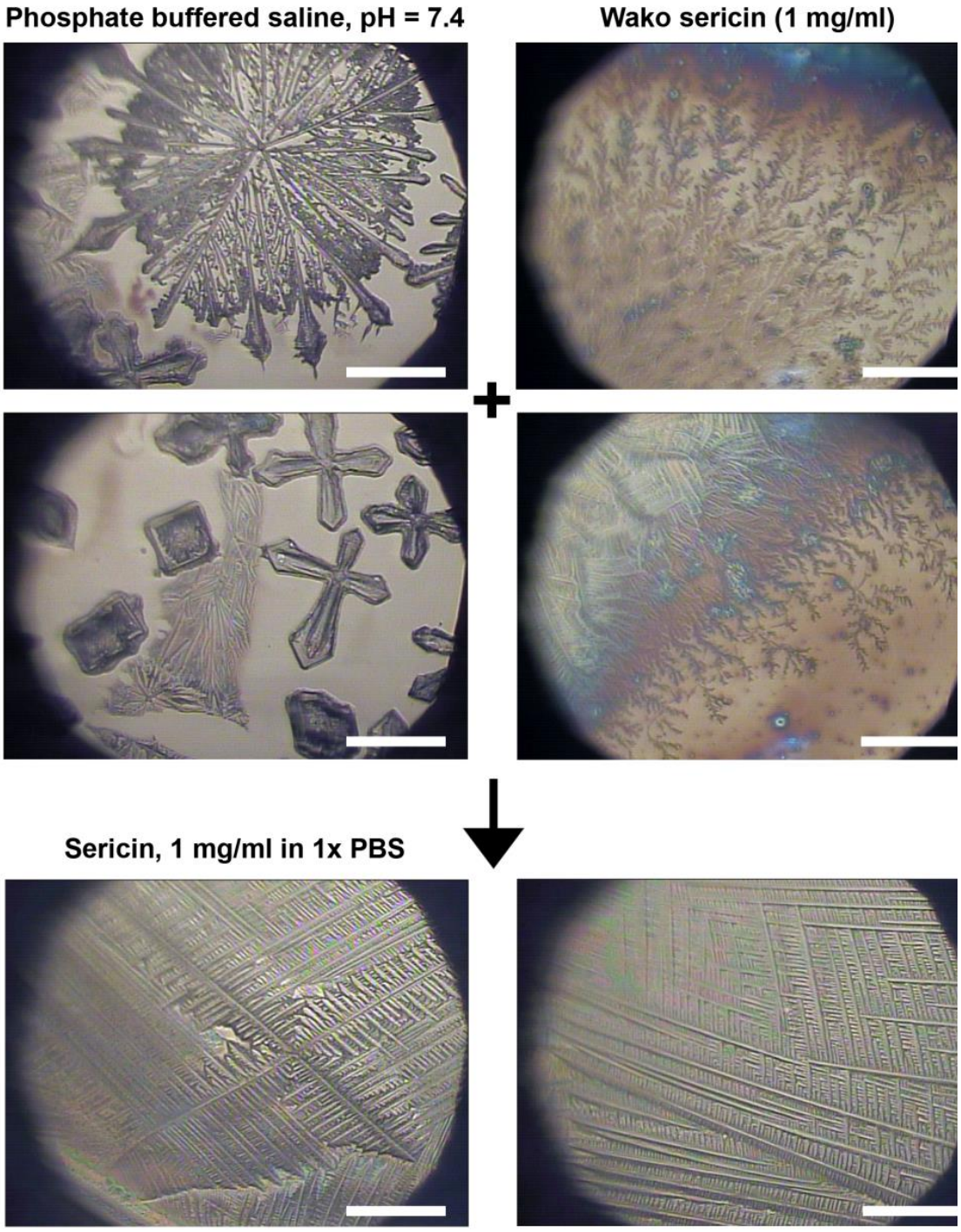

Figure 2.13. The salt-mediated self-assembly of sericin is achieved through reconstituting sericin in a 1x PBS solution, and casting onto a 2D substrate to form well-organized, orthogonal architectures. Scale bar = 200 μm.

By comparison, PBS crystal growth occurs in controls, and Wako sericin forms dendritic structures similar to prior observations. The structurally-distinct architecture is thus a biocomposite of PBS-templated sericin protein, which incorporates the basic 90º crystalline structure of PBS salts into an expansive, well-organized structure. The simple strategy of salt-mediated self-assembly thus provides an effective means for altering sericin morphology—effectively transforming the dendritic Wako architecture into *A. mylitta*-like orthogonal branching patterns—findings which may further be incorporated into fundamental and applied studies on the formation of tunable silk architectures.[211]

2.3.3 Self-Assembly of Engineered Fibroin Microparticles

The self-assembly of silk sericin occurs secondary to the initial *in vivo* aggregation of fibroin polypeptides into nanoscale fibrils. This autonomous assembly occurs with a progression in scale and complexity as fibroin steps through the process from a polypeptide to a mechanically-robust fibrous form, supporting the adhesion of the sericin glue layer. In contrast to sericin, which displays the ability to rapidly self-assemble *ex vivo* into an architecture not exhibited in natural silk formation processes, fibroin is unable to produce similarly ordered architectures in the absence of *in vivo* conditions. In the case of fibroin, a myriad of complex environmental parameters *in vivo* produces the necessary conditions for enabling assembly into meaningful architectures. Further steps are necessary to produce a form of fibroin which can readily undergo self-assembly in the absence of these complex environmental parameters.

In this section, the self-assembly of engineered fibroin is investigated similarly to sericin, in order to demonstrate that the fundamental parameters responsible for silk self-assembly are intrinsic to the peptides themselves. This will support the notion that the formation of complex architectures *in vivo* is a result of a highly controlled environment manipulating the process of self-assembly. Furthermore, these observations effectively demonstrate the limitations of using self-assembly of silk proteins to produce highly-ordered, complex architectures. Particle architectures of fibroin were thus produced using a microsphere fabrication strategy.[176] This strategy utilized ethanol-based microcrystalline induction, where it was found particle size was directly correlated to fibroin concentration, freezing temperature, and inversely correlated with the amount of ethanol added. On this basis, parameters were selected to produce an intermediate size of particles, using a 3.0% (wt/vol) solution of fibroin, compositions of V_{EtOH}/V_{SF} 6:20, 8:20, and 9:20 ethanol to fibroin solution, and incubation at -20 °C.

Shape and Morphology of Microparticles

Analysis of particle shape and morphology was conducted by casting volumes of microparticle solutions onto clean silicon, and drying the substrates overnight. Fibroin particles are observed to be localized in dense aggregates on the surface, and layered in some regions (Figure 2.14). The morphology of fibroin microparticles is spherical and topographically coarse in appearance, without apparent aggregation into distinct architectures. These observations were previously observed for a similar system, and attributed to the structural conformation of fibroin in an aqueous environment.[176]

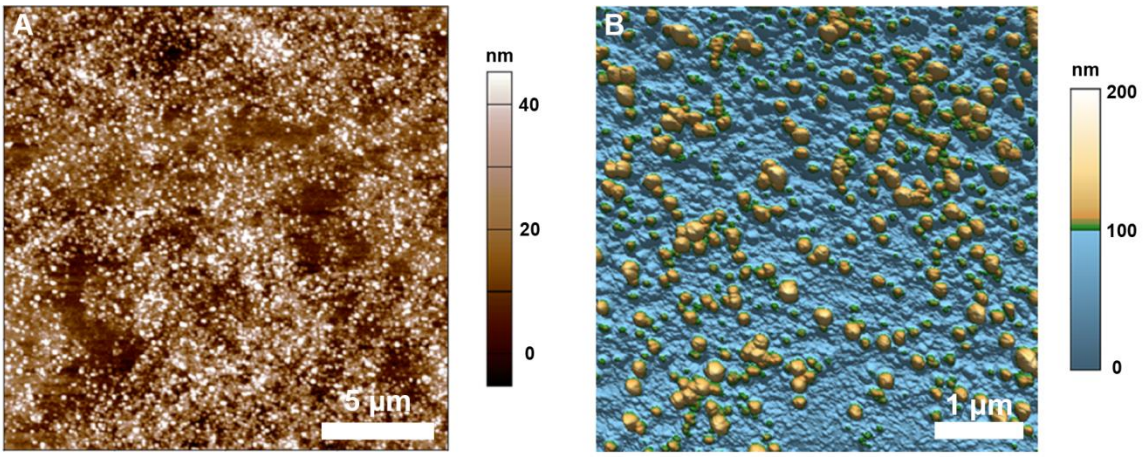

Figure 2.14. Fibroin microparticle shape and morphology investigated via AFM. Microparticles composed from a V_{EtOH}/V_{SF} ratio of 6:20 are depicted here. (A) Expansive distribution of particles is noted, without apparent aggregation into any specific architecture. (B) Microparticles are observed to be rough and distributed in layers on the surface, with a significant variation in size.

Analysis of Microparticle Size and Distribution

Analysis of particle size and polydispersity via has supported observations from fibroin topography, in which particles exhibit a significant variation in size (Table 2.5). From dynamic light scattering, a decreasing trend in particle size is observed with increasing ethanol-fibroin ratio, which supports prior observations. Furthermore, the existence of two discrete particle radii is observed, in which a smaller radii possesses approximately one-third of the size dimension of the larger microparticle. Interestingly, the particle size distributions follow those of *B. mori* sericin, however without apparent dendritic aggregation observed from AFM characterization. As a number of particle sizes

were analyzed with similar results, it was of interest to isolate fractions to evaluate the effects of a single particle size on self-assembly potential.

Table 2.5. Dynamic light scattering on fibroin microparticles (FMP), indicating an inverse correlation between ethanol-fibroin ratio, and particle size.

Fibroin Sample	Large Particle Radius (nm)	Small Particle Radius (nm)
FMP 6:20	619 ± 132	158 ± 21
FMP 8:20	286 ± 81	68 ± 18
FMP 9:20	208 ± 64	64 ± 11

Isolation of Fibroin Fractions

Particular focus on the 6:20 fibroin microparticle composition enables the application of a simple, syringe filtration method, and also allows study of a broader size distribution of particles. Separation was achieved via a facile, 0.22 μm syringe filtration method, in which dilute solutions of fibroin microparticles were slowly pushed through the filter and recovered. After rinsing the filter with excess deionized water, the filter was backwashed with deionized water to recover particles unable to pass through the filter. This technique proved to be effective in separating particles on the basis of size, provided there is sufficient distribution around the porosity of the filter. For example, DLS of the

filtered 6:20 particle fraction indicates the smaller fraction is well-preserved in terms of dimensions: 157 ± 27 nm.

Characterization of Monodisperse Fibroin Microparticle Morphology

Isolation and characterization of single fibroin microparticle fractions via optical microscopy demonstrates dendritic aggregates characteristic of DLA for both the small fraction (filtered), and the larger, recovered fraction (Figure 2.15).

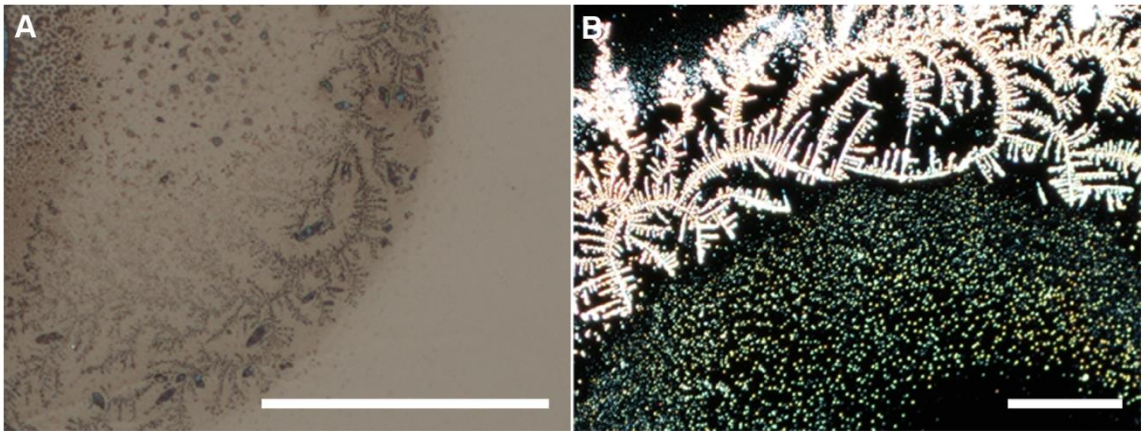

Figure 2.15. Optical microscopy of 6:20 fibroin microparticles, (A) filtered and (B) recovered, demonstrating similar dendritic architectures for both particle sizes. The recovered image is presented in darkfield to enhance visibility of fractal aggregates. Scale bar = 500 µm.

Further analysis via SEM reveals the nature of these architectures, as expansive branching structures composed of discrete spherical particles arranged in a discontinuous,

non-contacting configuration (Figure 2.16). Direct comparison of fibroin self-assembled architecture to that of silkworm sericin proteins is not possible due to the distinct chemistry of fibroin. However, *B. mori* fibroin aggregates are observed to posses the discontinuous branching and non-contacting characteristics of the *A. mylitta* sericin model, while the overall architecture closely resembles that of *B. mori* sericin. This observation strongly suggests the existence of a distinct mechanism for self-assembly, possibly due to the predominantly hydrophobic nature of fibroin.

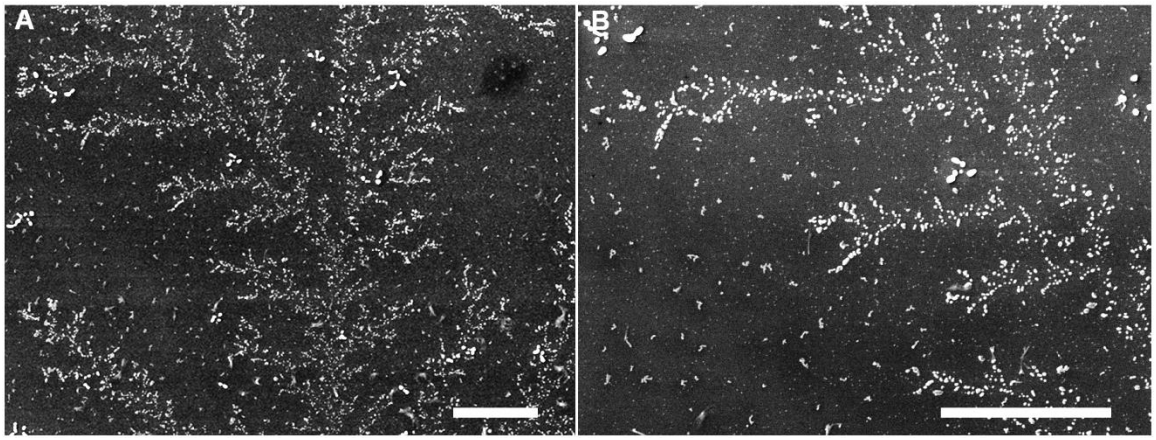

Figure 2.16. SEM characterization of the recovered 6:20 fibroin microparticles reveals a dendritic architecture, composed of discrete, non-contacting particles. Scale bar = 25 μm.

A model has been proposed to explain this phenomenon, which considers the self-assembly of fibroin molecules into microspheres, and finally microscale aggregates. Initially, ethanol induces a conformational change in fibroin from the random coil to a β-sheet-rich structure, creating soluble nucleation sites.[64, 65] These crystalline nucleation sites act as seeds for further crystal growth during stirring, to form microcrystalline, β-sheet-rich subunits.[212] Upon freezing, the shearing forces present enable further

microcrystal self-assembly to produce an ordered particle, with ordered, crystalline core and unordered, amorphous shell.[213] Cao *et al.* (2007) established that this conformation of fibroin, with hydrophobic microcrystalline regions and hydrophilic side chains, contributes to the organization of particles into a sphere, with a hydrophobic core and radially-oriented side chains in an aqueous setting. Topographic characterization (Figure 2.17) supports this observation, and furthermore, particle size analysis reveals an average particle diameter of 565 ± 172 nm, which is in agreement with that of DLS. This theory explains the existence of hydrophobic protein microparticles in solution, however the aggregation behavior into dendritic architectures is largely attributed to sericin-like assembly without further aggregation of particles from the soluble state.

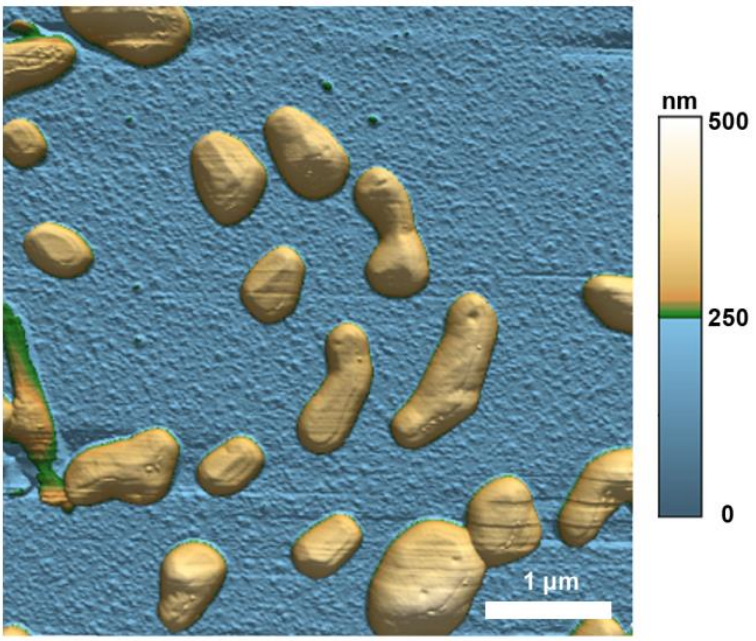

Figure 2.17. AFM of fibroin microparticles recovered post-filtration (500x dilution), via a 6:20 fibroin-ethanol composition, indicates particle aggregation is limited to single particles, or dumbbell-like aggregates. Average particle size: 565 ± 172 nm.

The process of diffusion limited aggregation for fibroin microparticles occurs as an evaporation-induced assembly process in aqueous solutions of single particle fractions. In a manner similar to *A. mylitta* sericin, this particular aggregate growth pattern is described by a quasi-static growth process and tip splitting phenomena. The significant difference in aggregation for engineered fibroin microparticles occurs due to differences in surface chemistry, particle size, and particle abundance. The existence of fibroin as an amphiphile accounts for the lack of aggregation behavior that would otherwise be characteristic of hydrophobic, crystalline particles. The presentation of hydrophilic side chains at the particle surface enables favorable solubility and partial aggregation during solvent evaporation. However, the balance between hydrophilic and hydrophobic character of fibroin enables the ordering of discrete particles into rough patterns while preserving spacing due to the burial of hydrophobic core residues in an aqueous environment. Overall, this strategy of microsphere formation and isolation enables the production of an engineered, relatively monodisperse protein system, which behaves as described by the silk sericin DLA model.

2.4 Conclusions

Sericin silk proteins display the ability to assemble via multiple aggregation mechanisms that allow study of self-assembly processes. When translated to an engineered system of fibroin microparticles, this aggregation behavior is again observed

to occur. The remarkable observation of self-assembly is the occurrence of these mechanisms in the absence of electrolytes that enable repulsive barriers to be effectively shielded. This leaves the issue of aggregation as a purely physical consideration, which highlights DLA processes across organic and inorganic systems, as being a product of simple size and charge properties. These architectures manifest as DLA processes for *B. mori* and Wako sericin, which have been determined to be the same protein, and *A. mylitta*, which possesses some modifications to the classical DLA model. The key differences observed in aggregation mechanisms are the presence of monodispersity vs. polydispersity in colloidal particles, particle sizes both in solution and in the aggregates, and surface charge anisotropy. The presence of polydisperse colloidal particles allows the aggregation mechanism to occur, with a filling in of gaps normally exhibited by DLA models. In a monodisperse system, the absence of smaller size fractions enables single, isolated particles to be resolved. It is these physical differences between colloidal systems that are postulated to yield remarkable changes in branching architectures. In the absence of crystal structures and amino acid sequencing, these physical considerations can illustrate how architectures arise from proteins sharing only function.

[This chapter contains results that have been previously published:

Kurland, N.E., et al., Self-assembly mechanisms of silk protein nanostructures on two-dimensional surfaces. Soft Matter, 2012. 8(18): p. 4952-4959.]

CHAPTER 3

ENHANCING BIOMATERIAL MICRO-ARCHITECTURE AND STIMULI-RESPONSE VIA SILK PROTEIN TEMPLATING

3.1 Introduction

As discussed in the previous chapters, a silk processing waste product, the sericin glycoprotein, has a unique set of attributes, including water-solubility, biocompatibility, and potential bioactivity—all of which support the applicability of sericin in materials fabrication strategies. Longstanding concerns of immunogenicity have lessened the focus on sericin as a useful material, however recent studies have shown these concerns to be unfounded, reigniting interest in the use of sericin as a biofriendly building block with applications in the aqueous setting.[56] In the previous chapter, self-assembly mechanisms of sericin and fibroin were explored, which revealed a hierarchical assembly process from an aggregated protein state in solution, into sub-millimeter scale organized patterns of sericin.[39] As a fundamental study, this research highlighted the step-wise growth in complexity of sericin in particular, and a means of augmenting this architecture, however, potential applications of the fragile two-dimension aggregates were limited. In order to translate the properties of aqueous-based sericin aggregates into a meaningful material, the potential for sericin to integrate into a composite architecture, and the subsequent effects of sericin in composite form, were investigated. Here, the

incorporation of sericin into a composite architecture capable of displaying expanding an enhanced set of structural and functional attributes is of interest. A significant challenge lies in the ability to demonstrate the successful incorporation of sericin into a composite, and to preserve the biocompatibility of the resulting architecture.

Materials capable of altering their properties in response to environmental stimuli have wide ranging applications ranging from aerospace design to tissue engineering and drug delivery.[214, 215] Such "smart" materials are able to actively modify, often in a targeted manner, their physico-chemical properties including structure, optical properties, and permeability in response to changes in temperature, light, ionic strength, irradiation or pH. For materials that interact with biological systems, additional challenging design constraints must be satisfied. For instance, such biomaterials must also possess a low toxicity, high biocompatibility, and often, favorable biodegradation characteristics.[216] A variety of materials, such as crosslinked hydrogels, polypeptides and shape memory polymers and alloys have been proposed in recent years as stimuli responsive materials to be exploited as filaments, membranes, particles and scaffolds.[217-219]

Of specific interest are hydrogel—three-dimensional crosslinked networks capable of absorbing and retaining large quantities of water.[220] These polymers can be structurally designed with discontinuous phase transitions, controlled degradation and responsiveness, making them valuable for various applications, specifically as materials that can induce volume change in response to stimuli such as temperature and pH.[221, 222] As highly biocompatible biomaterials, hydrogels have been widely used in biomedical applications.[223, 224] While traditionally synthetic, new materials such as hybrid hydrogels with synthetic and natural molecules, and poly(amino acid) hydrogels

produced by genetic engineering have greatly expanded the application space of hydrogels.[225, 226] One of the driving forces for developing these classes of materials is the desire to limit products of synthetic polymer degradation. Being comprised of naturally occurring building blocks, upon their degradation, poly(amino acid) hydrogels have the possibility to diminish toxicity typically associated with synthetic materials.

A range of "responsive" hydrogels from polypeptide building blocks, to recombinant natural structural proteins like elastin and silk have been reported.[160, 218, 227] A structurally simpler alternative is poly(aspartic acid) (PASP), a pH-sensitive, water-soluble, biodegradable polymer which can be synthesized through the thermal polycondensation of the amino acid, L-aspartic acid (Figure 3.1).[228] A variety of methods for its synthesis have facilitated the low cost and widespread industrial production of PASP, with a range of physical and chemical characteristics. PASP and its derivatives form excellent stimuli responsive hydrogels as naturally biodegradable, non-toxic, cost efficient and easily prepared materials. PASP hydrogels can be crosslinked using various natural polyamines and retain an elastic modulus consistent with ideal polymer gels.[109] However, thermally-synthesized PASP materials have typically been primarily used in industrial applications to prevent scaling, inhibit dental plaques or as additives for other materials in biological applications.[228, 229]

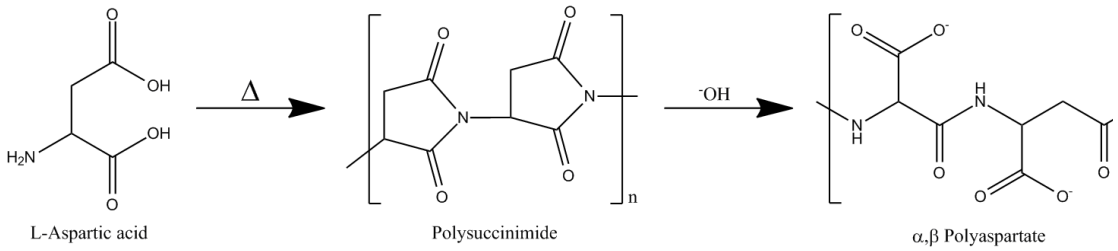

Figure 3.1. The thermal condensation, and subsequent hydrolysis of L-aspartic acid enables a low-cost route to the synthesis of poly(aspartic acid).

To enhance the stimuli responsiveness of PASP and to develop versatile biodegradable amino-acid based hydrogels as cellular scaffolds and biocompatible matrices, a protein-directed templating strategy was developed to augment the microstructural morphology of the network. This technique is partially based on template-directed synthesis, in which a template material acts as a scaffold for the fabrication of porous architectures.[230] To date, template-directed assembly using proteins has been shown as a biomaterial-based equivalent to soft lithography microfabrication.[231] Incorporation of protein-based templating utilizes the aqueous behavior of a protein to create void spaces within a templated species. Here, the water-soluble protein enables the formation of voids within the PASP hydrogel microstructure, effectively increasing porosity, after which the template molecule may be solubilized and removed.

The intrinsically biocompatible and water soluble silk protein, sericin, was selected for use as a template agent in the PASP hydrogel network. In the introduction, sericin was introduced as a macromolecular, water-soluble, glycoprotein produced by the

middle silk gland, which forms the counterpart to the more widely used silk protein, fibroin.[5] Sericin is also rich in β-sheets which lend excellent mechanical integrity, attracting considerable interest in its use in composite biomaterials. Unlike fibroin, sericin has many hydrophilic amino acid chains which lend to its excellent susceptibility to modification and therefore an ideal candidate for hydrogels. Silk proteins have been of recent interest to enhance biocompatibility and decrease cytotoxicity of materials *in vivo*.[20, 232] Indeed, silk proteins have previously been used to fabricate hydrogels but there have been very few studies into their use as templating agents.[90, 233]

In this chapter, the formation of pH-responsive bio-templated poly(amino acid) hydrogel is reported. Using poly(aspartic acid) structurally modified with the silk protein sericin, a biocompatible, protein-based architecture is demonstrated that is highly responsive to changes in external pH and is suitable for cell growth. PASP is classified as a polyelectrolyte which can be swelled after crosslinking due to protonation and deprotonation to different volumes dependent on the pH. Silk sericin is a low cost natural protein obtained from mulberry silkworms that has high mechanical strength but does not in itself possess any pH responsiveness.[234] Sericin is unable to crosslink directly with itself, but being water soluble, provides an avenue to be used with another protein or polymer as a structural modifier to form a hydrogel. Importantly, sericin has been demonstrated to be a biocompatible material when isolated from silk fibroin, and in fact leads to enhanced cellular proliferation.[235] The combination of these materials is therefore highly suited to form a responsive scaffold material. Furthermore, through the formation of a biocomposite, it is possible to expand the range of potential structure and function exhibited by sericin.

Here, a number of parameters are analyzed: the swelling behavior of this composite protein-based biomaterial, the effect of the protein (sericin) templating on the composite, and finally the investigation of their use as cellular substrata. The resulting hydrogels are capable of significant mass swelling, and demonstrate the ability to absorb up to 26x their dry weight in water, while simultaneously displaying a ~25% mass change when transitioned from acidic to basic conditions. These sericin-PASP hydrogels retain structural integrity during this process, and display reversibility in returning to their original mass after pH cycling. Overall, this process provides a low-cost avenue to the production of highly absorbent, pH-responsive protein-based hydrogels. Through the use of the naturally-derived biocompatible protein, sericin, cytocompatibility is effectively maintained during the fabrication process, supporting future applications of sericin as a composite biomaterial.

3.2 Materials and Methods

3.2.1 Materials

L-Aspartic acid (98% reagent-grade, Sigma-Aldrich, St. Louis, MO), sericin silk protein (Wako Chemicals USA, Richmond, VA), 1,4-butanediamine (BD), ethylenediamine (ED, anhydrous), and N,N-dimethylformamide were used as received for synthesis of the hydrogel. Imidazole, boric acid, acetic acid, sodium chloride and citric acid (Sigma-Aldrich, St. Louis, MO), were employed for preparation of buffered

solutions in deionized water (18.2 MΩ•cm, Millipore) across a range of pH values. All chemicals were purchased from Fisher Scientific (Pittsburgh, PA) unless otherwise specified.

3.2.2 Synthesis of Polysuccinimide

The synthesis of polysuccinimide was performed via thermal polycondensation of L-aspartic acid, according to established protocols.[228] Briefly, 10 g (0.075 mol) of L-aspartic acid was added to a 50 mL three-neck round-bottom flask equipped with a thermometer and stir bar. The powder was heated to 260 ºC for 6 hours under a dry N_2 gas purge, to initiate the condensation of aspartic acid monomers. During this process, sufficient gas flow is required through the flask to ensure clearance of water vapor generated as a side product of the condensation reaction. The resulting product was washed thoroughly with deionized water and methanol, and vacuum dried at 85 ºC. A conversion of aspartic acid to polysuccinimide of ~90% was determined directly from the dry weight of the product, as any residual aspartic acid is readily soluble during the post-reaction wash.

3.2.3 Polysuccinimide hydrolysis

Polysuccinimide was hydrolyzed to poly(aspartic acid) using alkaline hydrolysis for the purposes of determining average molecular weight. 1g polysuccinimide was added to a 25 mL beaker, along with 0.4 g sodium hydroxide (added as a molar equivalent per

succinimide repeat). The beaker was cooled on a bed of ice, and 7 mL deionized water was added, prior to stirring the mixture for 1 hour. At the completion of hydrolysis, 1M HCl was added dropwise to the reaction solution, until the solution pH = 7.0. The solution was precipitated in 100 mL methanol, and the precipitate recovered and vacuum-dried at 40ºC.

3.2.4 Static light scattering of poly(aspartic acid)

The molecular weight of the synthesized poly(aspartic acid) was determined by static light scattering on a Malvern Zetasizer Nano ZS90 (Malvern Instruments Ltd., Worcestershire, UK). A range of poly(aspartic acid) concentrations < 1.0 mg/ml were analyzed to generate a Debye plot, and enable determination of molecular weight.

3.2.5 Fabrication of sericin templated-poly(aspartic acid) hydrogels

pH-responsive hydrogels were formed by crosslinking the poly(aspartic acid) precursor, polysuccinimide in the presence of the silk protein, sericin. Hydrogel samples (15 mg) were produced in this fashion, with 0, 25, 50, and 75% sericin, to yield hydrogels of 100, 75, 50, and 25% PSI by mass respectively. The two constituents were dissolved in 100 µL of DMF in a 1.5 mL conical tube and well-mixed prior to crosslinking. The crosslinkers, 1,4-butanediamine (BD) or ethylenediamine (ED), were added over a short time period (30 seconds) to an agitated reaction solution, to ensure homogenous distribution of the crosslinker. To demonstrate the effects of crosslinker length on

hydrogel swelling, crosslinkers were added at a 20 wt% to 50% and 75% PSI hydrogels (3 mg crosslinker). Subsequently, the shorter linker BD was selected due to the superior swelling of hydrogels. Samples were prepared using a 0.5 molar ratio of BD to succinimide subunits (99.09 g/mol). Reaction mixtures were left for 12 hours at ambient temperature to allow the crosslinking reaction to proceed to completion. The resulting hydrogels were then immersed in deionized water (18.2 MΩ-cm) for 24 hours to allow for dilution of DMF, as well as diffusion of free crosslinker and sericin protein. After the crosslinked hydrogel was formed, the imide ring of the polymer backbone was hydrolyzed in 0.1M NaOH solution for 12 hours. The resulting structure is a 3D hydrogel network, consisting of a poly(aspartic acid) backbone with intermittent crosslinks, henceforth referred to as PASP-S in this chapter.

3.2.6 pH response of PASP-S hydrogels

The pH sensitivity of each hydrogel sample was investigated by studying the swelling behavior across a range of pH values, from pH 3.0 to 9.0. As reported before, either the equilibrium swelling based on mass or volume can be reported. In these experiments, the mass swelling degree is utilized as an indicator of hydrogel performance. Buffer solutions (c = 0.1 M, I = 0.25 M) were employed at pH 3 (citrate), pH 5 (acetate), pH 7 (imidazole), and pH 9 (borate). PASP-S hydrogels (n = 3) were immersed in buffer solutions for 30 minutes at each pH value, and incremented to the next buffer at this time interval. To demonstrate reversibility of swelling, hydrogel repeats were immersed initially in different pH buffers, and cycled through the range of

pH values (3 → 5 → 7 → 9) back to their starting pH (for instance, a sample initially swollen in pH 7 is immersed in pH 9 →3 →5 → 7). This simultaneously serves to support a positive trend in swelling with pH as resulting from pH-dependent swelling, rather than from a time-dependent process. Sample mass was determined for the swollen samples, and the swelling ratio of the hydrogels was determined according to the following equation:

$$\text{Equilibrium Swelling Ratio } (Q_m) = [(W_s - W_d) / W_d]$$

where W_s and W_d represent swollen and dry sample weights, respectively.

Following swelling studies, samples were immersed in deionized water to remove any residual salts, then vacuum dried overnight and weighed to determine the final dry mass. Volume changes were also observed by measuring the size of the hydrogel disks at different pH.

3.2.7 Bulk characterization of PASP-S hydrogels

Bulk morphologies of PASP-S hydrogels were characterized using scanning electron microscopy (SEM). To preserve hydrogel porosity and microstructure for morphological analysis, hydrogel samples were cryofixed. Samples were swollen in buffered solutions (citrate at pH 3 – 4 and borate at pH 9 – 10, respectively) for 24 hours. Samples were then rapidly cooled via a 30 second immersion in liquid N2, and immediately fractured to expose bulk interfaces of the hydrogel network. The frozen hydrogel fragments were then lyophilized for 48 hours, mounted on conductive stubs and

sputter-coated with platinum to a thickness of 18 Å. SEM imaging was carried out at a 15 kV accelerating voltage on a Hitachi SU-70 high-resolution field emission microscope and at a 2.0 kV on a JEOL SM-5610 SEM. Bulk morphology of hydrogel fragments was specifically investigated using this technique.

3.2.8 Surface and mechanical characterization

Atomic Force Microscopy (AFM) analysis of surface morphology was performed on an MFP-3D AFM (Asylum Research, Santa Barbara, CA), operating in AC mode. The AFM was further used to determine Young's modulus of the hydrogels in the dry state via AFM-based nanoindentation. Thin hydrogel segments (> 1 μm thickness) were indented with 10 indents at 3 discrete locations under a constant load of 500 nN to a total depth of ~10 nm using an AC240TS tip (nominal k = 2 nN nm^{-1}, Olympus, Japan). Force-distance curves were subsequently analyzed via fitting tip extension data to the Oliver-Pharr model to determine values for Young's moduli.[236, 237]

3.2.9 Cytocompatibility of PASP-S hydrogels

Hydrogel samples with different compositions varying from 25% sericin to 75% sericin were investigated for their absence of cytotoxicity and their ability to function as cell scaffolds. Murine fibroblast (L-929) cells were seeded on the scaffolds (10^5 cells/ml). Cell viability and proliferation was measured by conducting the alamarBlue Cell Viability Assay (Invitrogen, CA) (1:10 in incomplete media) on the samples at day 12.

The supernatant was collected and the optical density (OD) was measured at 570 and 600 nm. Data were plotted in comparison with tissue culture plate (TCP) as a positive control. Cell seeded scaffolds were then washed with incomplete media and 1x PBS followed by staining using Live/Dead stain (Invitrogen). Imaging was performed using confocal laser scanning microscopy (FV1000, Olympus, Center Valley, PA). Statistical analysis of cell viability on PASP-S hydrogel scaffolds and tissue culture polystyrene controls was conducted—the alamarBlue cell viability assays were represented as mean ± S.E. for n = 3. Comparisons between groups were performed using analysis of variance (ANOVA) and differences between means were evaluated via Dunnett's multiple comparison post-hoc test. From this data, p-values < 0.01 (*) and < 0.05 (**) were considered statistically significant. Analysis of live/dead assay data was conducted through the determination of percentage live cells at day 12, via confocal microscopy.

3.3 Results and Discussion

3.3.1 Sericin-templated poly(aspartic acid) (PASP-S) hydrogel fabrication

Poly(aspartic acid) (PASP) and its derivatives are well known as environmentally friendly, biodegradable alternatives to traditional polyanionic materials such as poly(acrylic acid). Poly(aspartic acid) is a very effective surface reactive polymer that has been proposed as a water soluble, biodegradable scale inhibitor against salt scaling in industrial applications and is easily and cheaply obtained in commercial quantities.[229]

Polymeric micelles of poly(ethylene oxide) and PASP as well as pure PASP have been shown as drug-delivery vehicles.[238] Sericin is a glue-like protein that is traditionally discarded in the early stages of silk processing, or from processes for silk degumming to form fabrics.[239] The protein is characterized by the presence of strongly polar side groups such as hydroxyl, carboxyl, and amino groups and in particular, serine (38%), aspartic acid (16%) and glycine (16%).[183] The glue-like property of sericin is attributed to the hydrogen bonding between serine residues of sericin with serine residues in the fibroin components of silk fiber. In this work, the fabrication of pH-sensitive hydrogels is achieved through the use of the largely poly-anionic precursors L-aspartic acid and sericin. Using these commercially viable and available materials represents an opportunity to create low-cost, biodegradable and biocompatible smart hydrogels that are purely amino acid based.

Dry thermal polymerization of poly(aspartic acid) is a relatively simple process adaptable to large scale synthesis with high yields. The thermal polycondensation of aspartic acid yields long-chain amino acid polymers of polysuccinimide (PSI) as an intermediate. This polymerization reaction has the added advantage of a simple conversion process (Figure 3.2A) that produces no other products other than the polymer and the water of condensation. The ring structure of the polyimide is then hydrolyzed to form the polyamide.

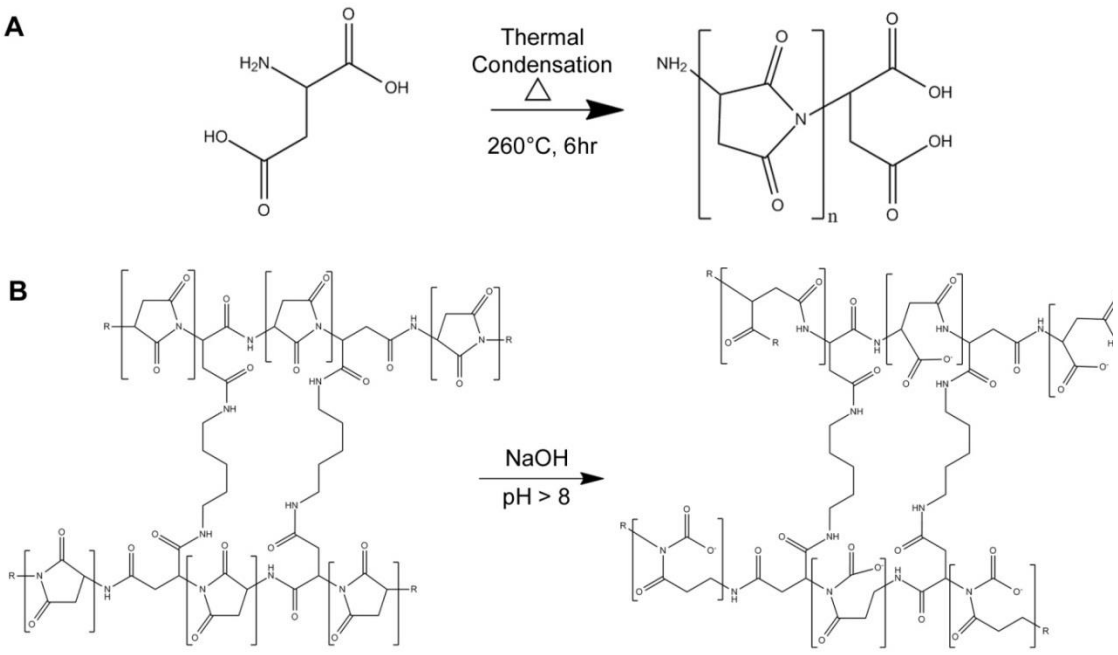

Figure 3.2. Reaction scheme of L-aspartic acid to produce pH-sensitive hydrogels: (A) the thermal polycondensation of L-aspartic acid results in the formation of linear poly(succinimide), which may then be further crosslinked with diamine compounds. (B) Alkaline hydrolysis of diamine-crosslinked polysuccinimide produces the poly(aspartic acid) (PASP) hydrogel network.

Through the hydrolysis of poly(succinimide) into poly(aspartic acid), a water-soluble polypeptide is created. This product enables determination of the average molecular weight through static light scattering (SLS). SLS is an alternative to gel permeation chromatography (GPC) or size exclusion chromatography (SEC) for the facile determination of molecular weight. By measuring the scattering intensity of an incident light source as a function of scattering angle, and correlating this data with

Rayleigh theory, a Debye plot is generated (Figure 3.3).[240-243] From this data, poly(aspartic acid) indicates an average molecular weight of 106,000 Da.

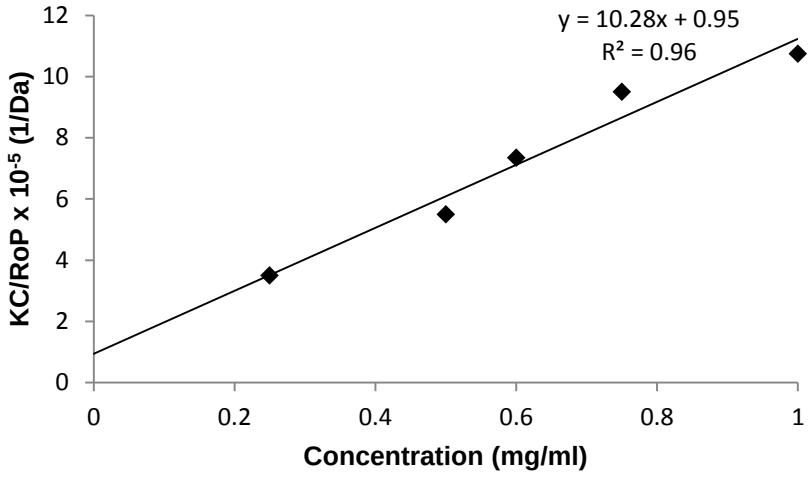

Figure 3.3. The Debye plot of poly(aspartic acid) generated through static light scattering techniques, indicates an average molecular weight of 106 kDa.

In order to achieve a stable hydrogel architecture, linear PSI chains are crosslinked prior to their conversion to poly(aspartic acid). This avoids potential cross-reactions with native carboxylic acid-containing residues in the sericin protein. The succinimide rings of PSI readily react with primary amines at ambient temperature.[244] Crosslinking of PSI is thus possible through bi-functional and multifunctional amine species, of which a number of naturally-derived diamines are available.[109, 245] During this process, sericin provided a template for crosslinking in the resulting hydrogels—sericin effectively occupies volume in the PSI during nascent crosslink formation, while maintaining solubility (Figure 3.4 A). The result is a sericin-templated PASP network

(PASP-S), after which a large fraction of the water-soluble sericin may be diffused out over 24 hours to leave voids, occupied by water. This is observed from SEM, which demonstrates the formation of micrometer-scale voids after the process of hydrolysis (Figure 3.4 B-C). In contrast, a hydrogel consisting of PASP is limited in the complexity and abundance of microstructural voids during the crosslinking process. Since both constituents of the hydrogel, PASP and sericin are naturally biocompatible and biodegradable, crosslinking is achieved using the natural polyamines (ethylenediamine or 1,4-butanediamine) to help preserve compatibility and result in an amino acid-based hydrogel that exhibits pH sensitive behavior. It was noted that the resulting hydrogels may contain small amounts of residual sericin (typically calculated < 10%). However, owing to the biodegradability and biocompatibility of both constituents, the overall composite hydrogel still retains these properties.

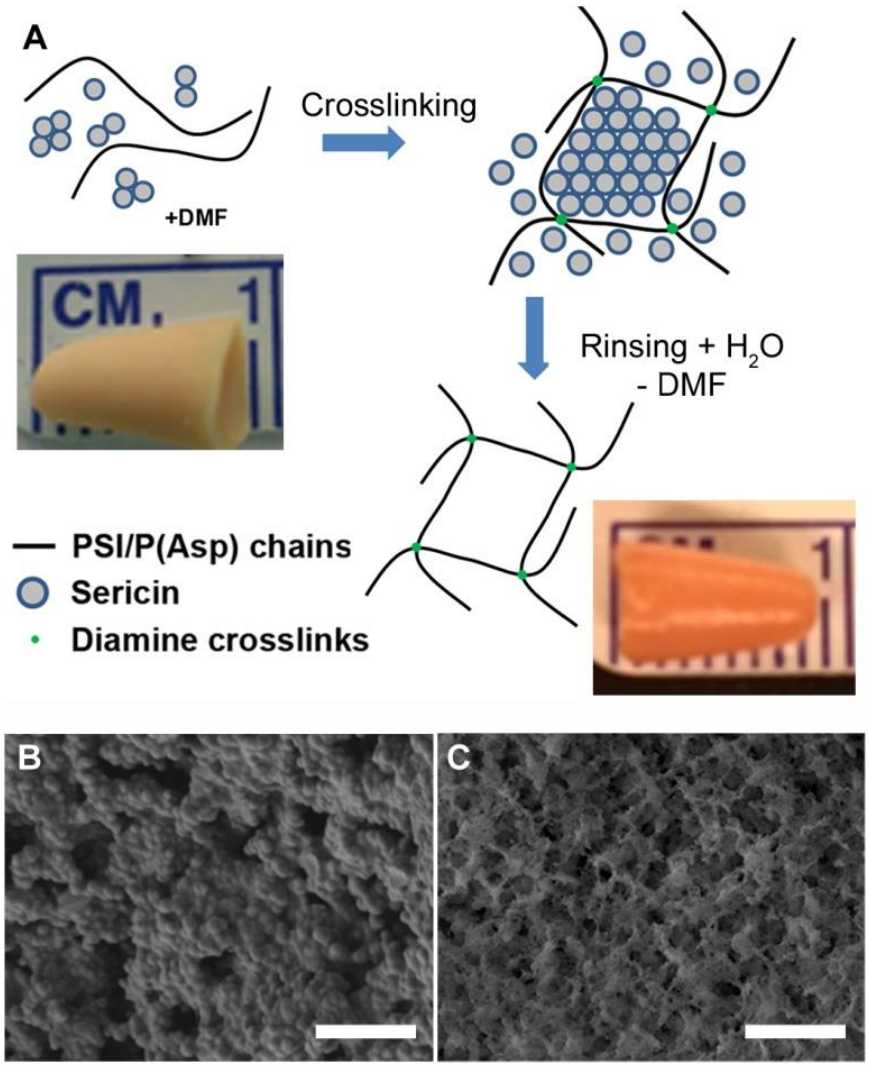

Figure 3.4. The highly absorbent properties of PASP-S hydrogels are a result of the incorporation of sericin into the network, which acts as templating filler increasing void space in the hydrogel network. Following hydrolysis, large hydrogel scaffolds can be formed with a concomitant color change signifying the conversion of PSI to PASP. SEM images of the (B) PSI hydrogel, and the (C) sericin-templated PASP hydrogel, showing the porous microarchitecture of the hydrogel network formed due to the sericin filler. Scale bar = 10 μm.

Hydrolysis of succinimide rings occurs under alkaline conditions, resulting in the production of a racemic mixture of α and β aspartic acid residues.[246] Immersion in buffer (pH > 8) enables hydroxide ions from the alkaline buffer to engage in nucleophilic attack of PSI, yielding ring-opening of succinimide subunits. This step is associated with a significant change in the appearance of hydrogels—opaque orange PSI hydrogels gradually attain a translucent white coloration when hydrolyzed (Figure 3.4 A). Hydrolysis of succinimide is also accompanied by a change in water solubility—water-insoluble imide groups are converted to a highly water-soluble carboxylic acid-terminated form. At this stage, the previously neutral polysuccinimide network is converted into a polyelectrolytic aspartic acid-based hydrogel (Figure 3.2 B). As a result, the hydrogel network possesses a nascent ability to respond to environmental pH changes.

3.3.2 Effects of crosslinker on swelling

PASP-S hydrogels exhibit an increase in swelling degree relative to the pKa values of α- and β-aspartic acid constituents (3.3 and 4.5), yielding a change in morphology from pH 3 to 6.[109, 247] The swelling properties of the PASP-S hydrogel network are expectedly, dependent on the identity and physical properties of the diamine crosslinker.[109, 248] The crosslinkers, ethylenediamine (ED) and 1,4-butanediamine (BD), were initially analyzed for use in pure PASP hydrogels. Samples fabricated from relatively low concentrations (20 wt%) of both crosslinkers yield remarkable swelling properties (Figure 3.5). Ethylenediamine-crosslinked hydrogels indicated significant

swelling at pH 9, Q_m of 14 (50% sericin) and 17 (75% sericin). Analysis of varying sericin content also showed an increase in swelling ratio, in which samples composed of increasing amounts of sericin (75% vs. 50%) displayed enhanced swelling behavior. In comparison, 1,4-butanediamine demonstrated superior swelling over ethylenediamine for both hydrogel compositions. At pH 9, BD-crosslinked hydrogels had swelling ratios of 19 (50% sericin) and 25 (75% sericin). Both crosslinkers enabled swelling of hydrogels to occur, and each was associated with preservation of hydrogel structure and integrity. However, the superior swelling ratio exhibited by BD-crosslinked hydrogels was of interest for a more thorough investigation into the effects of sericin inclusion on swelling. It should be noted, this observation does not preclude further investigation of other multifunctional amines, particularly those of increasing length (e.g., 1,5-pentanediamine and 1,6-hexanediamine). Overall, hydrogels fabricated from a 20% weight ratio of crosslinker display exceptional swelling ratios, however the relatively low structural integrity of such samples precludes study without significant degradation. As a result, BD was next incorporated at an increased quantity into a further set of hydrogel compositions (Table 3.1).

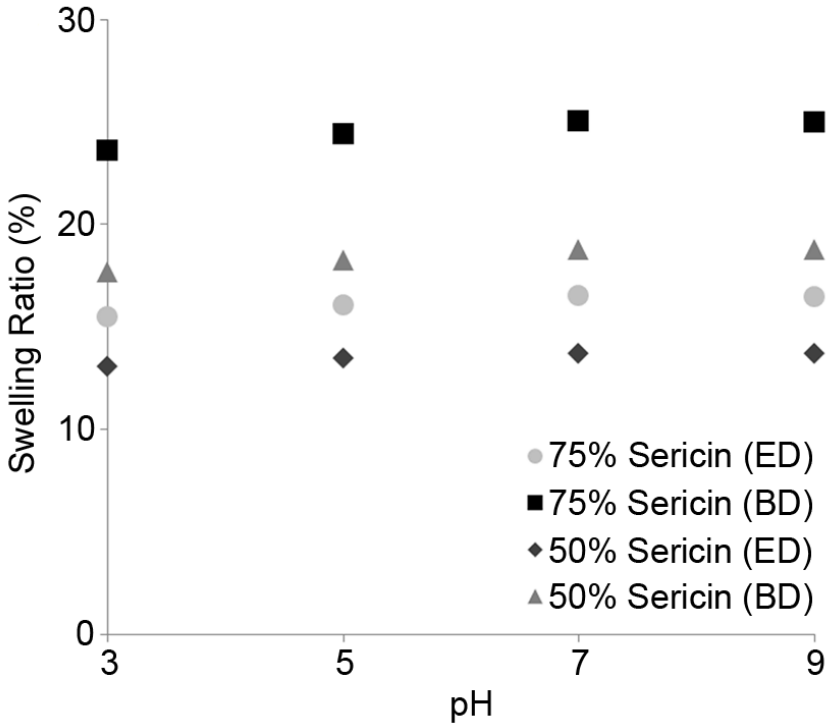

Figure 3.5. Mass swelling data for hydrogels crosslinked with 20 wt% crosslinker, shows a consistent increase in swelling ratio for 1,4-butanediamine (BD) over ethylenediamine (ED). A similar relation between increasing sericin content and swelling ratio is also evident.

3.3.3 pH-sensitivity of sericin-templated poly (aspartic acidAsp) hydrogels

The effects of sericin inclusion on overall swelling of PASP-S networks were then investigated. The crosslinker BD was incorporated into PSI/sericin reaction mixtures at 50 mol% of the total amount of reactive succinimide units (Table 3.1).

Table 3.1. Hydrogel formulations fabricated at varying ratios of PSI and sericin, at a 0.5 (50%) molar ratio of crosslinker BD to succinimide monomer units (SI).

PSI (wt%)	PSI (mg)	Sericin (mg)	PSI (x 10^{-4}) (mol)	BD (x 10^{-4}) (mol)
100	15	0	1.51	0.8
75	11.3	3.7	1.14	0.6
50	7.5	7.5	0.76	0.4
25	3.7	11.3	0.37	0.2

Hydrogels formed at this ratio of BD incorporation were structurally and morphologically indistinct from those formed at a lower crosslinker ratio. It was noted that these hydrogels remained intact, and possessed a greater structural integrity during their preparation and subsequent pH testing. Swelling data for hydrogels is exhibited in Figure 3.6. Swelling data on these BD-crosslinked PASP-S hydrogels established a clear trend, in which swelling ratio at individual pH values increased with increasing sericin content, ranging from Qm of 9 (0% sericin) to 26 (75% sericin) at pH 9. Hydrogels resulting from the inclusion of 75% sericin were shown to possess the greatest water uptake, per weight of dry hydrogel. The significant void space in hydrogels formed via 75% sericin likely enables infiltration of buffers in greater volume and at a faster rate than those composed of 100% PASP, which possess a higher crosslink density. As the overall swelling behavior is directly tied to the amount of sericin present, the protein is established as an effective structural modifier of PASP microstructure.

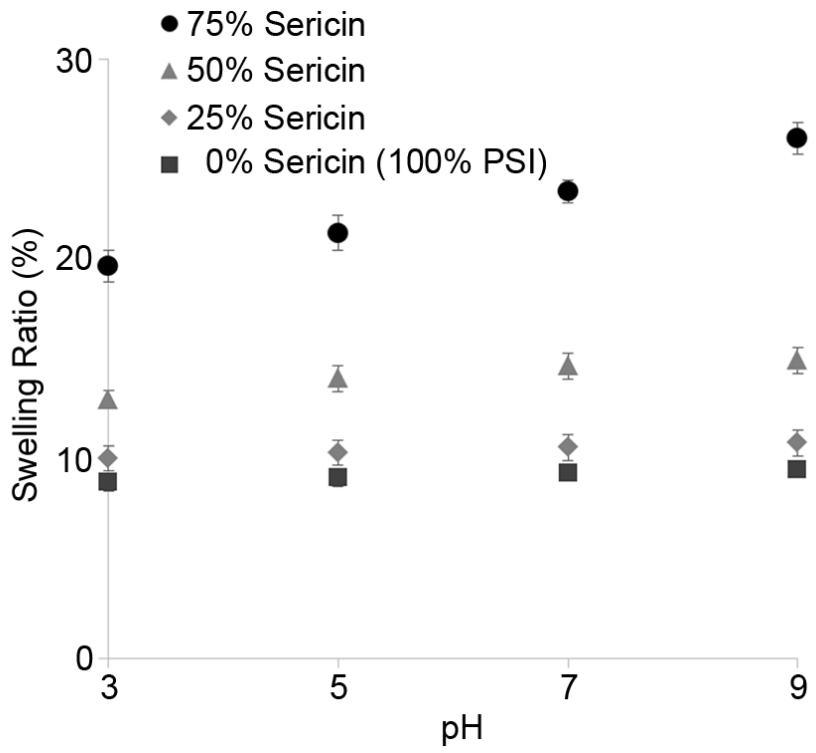

Figure 3.6. Analysis of swelling ratios across an increasing pH gradient yields a clear relation between increasing sericin content and an increase in swelling ratio. PASP-S hydrogels fabricated with 75% sericin content display almost double the swelling of those fabricated from pure PASP.

Reversibility of pH-dependent swelling behavior was also demonstrated for different hydrogel compositions. Through the analysis of hydrogels via a pattern of offset pH testing, described above, it was established that the final mass of samples back in their respective starting buffer was equivalent to initial mass in the starting buffer. Reversibility was established after hydrogels reached a maximum mass gain at pH 9, by subsequently cycling hydrogels to pH 3 buffers. This behavior provides supporting data indicating full crosslinking of the PASP chains—evident through the lack of significant

mass changes after pH-dependent swelling. This step had the added benefit of demonstrating that the significant water uptake at pH 9 exhibited by all hydrogels was not merely a process based on total immersion count or immersion duration. Thus, hydrogel swelling was shown to be a pH-dependent process, instead of a time-based phenomenon, dependent on the total duration of hydration. Additionally, no apparent loss of structural integrity or hydrogel degradation was observed as a result of this cycling, or immersion in acidic or basic buffers (pH 3 or 9). The recovery of swelling behavior is depicted below (Figure 3.7).

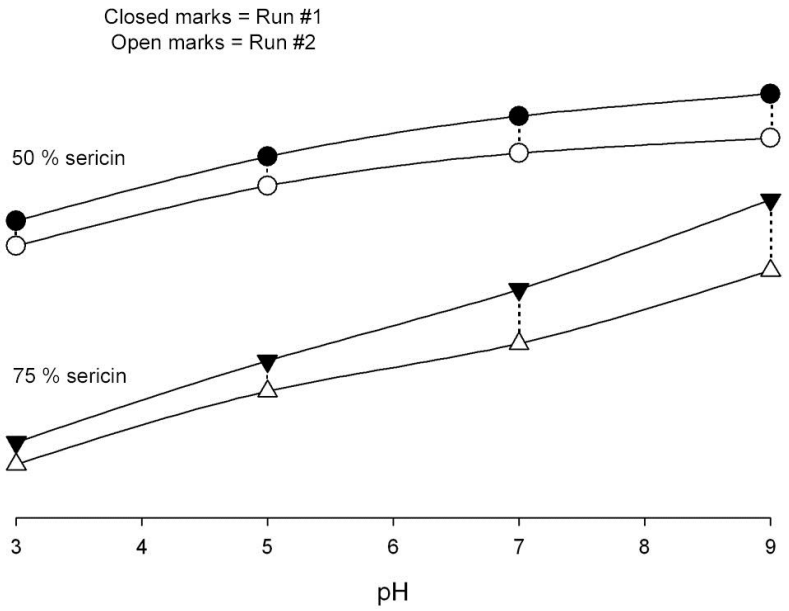

Figure 3.7. Cycling of the hydrogel samples from pH 3 to 9 and back again. The closed tick marks represent Run #1 and the open tick marks show a close correspondence in Run #2.

Overall, the swelling data on these crosslinked PASP-S hydrogels established a clear trend, in which swelling ratio at individual pH values increased with increasing sericin content, ranging from 9 (0% sericin) to 26 (75% sericin) at pH 9. The swelling degree of PASP-S hydrogels demonstrates a remarkable enhancement in swelling capacity over that displayed by 100% PASP hydrogels alone. Overall, hydrogels resulting from the inclusion of 75% sericin were shown to possess the greatest water uptake of all analyzed compositions. In comparison, other reported work on diaminobutane-crosslinked PASP hydrogels, have demonstrated a comparable mass swelling ratio increase from 6 (pH 3) to 17 (pH 9), expressed in percentage of swollen mass to dry mass.[249] The reported hydrogels therefore achieved approximately 50% greater swelling response. When hydrogels are fabricated utilizing a cleavable crosslink in conjunction with diaminobutane, this trend in swelling drops further, to 5 (pH 3) and 15 (pH 9), in terms of the equilibrium mass swelling ratio.[250] As a note, if the volumetric equilibrium swelling degree descriptor is utilized, a 3-fold increase in volumetric capacity of gels is observed when hydrated.[109] Thus, from data collected on PASP-S hydrogels, significant swelling is demonstrated over pure PASP hydrogels, which is observed in this study, and from literature-reported data on PASP hydrogels.

3.3.4 Surface topography, porosity and microstructure of hydrogels

Surface topography of the hydrogels were studied using Atomic Force Microscopy (AFM). Overall, the morphology of sectioned PASP-S segments was

observed to be flat with root mean square (RMS) roughness around 2 - 3 nm, which is comparable to that of a glass slide (Figure 3.8).

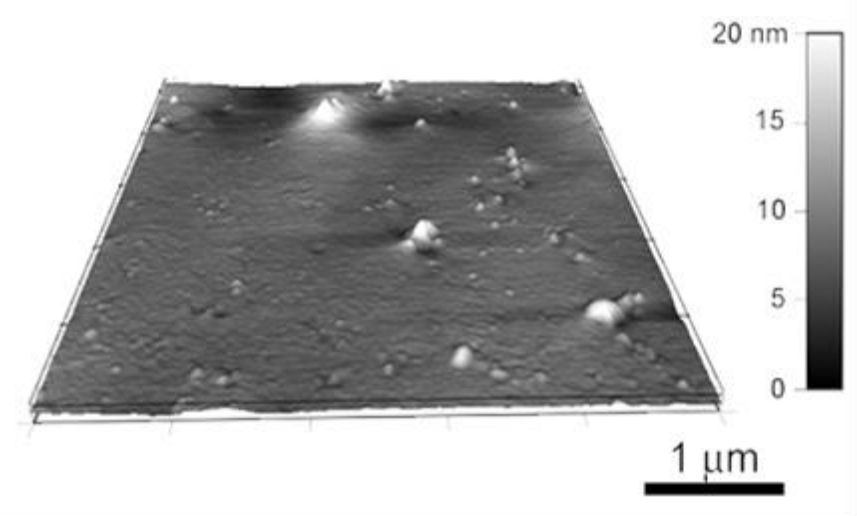

Figure 3.8. AFM image of PASP-S surface. RMS roughness of 2 – 3 nm over 5 µm is comparable to that of a glass slide.

The mechanical properties of the 50% PASP + 50 % sericin hydrogel with an intermediate composition were investigated using AFM-based nanoindentation. Sample triplicates were indented at least 30 different locations to obtain the mechanical properties of the material in the dry state. The Young's modulus of the PASP-S hydrogels was measured to be ~400 MPa (404 ± 148 MPa) (Figure 3.9). In comparison, the Young's modulus of sericin was earlier reported to be ~600 MPa in the dry state, and is known to be a material of high mechanical strength.[251] The protein templating strategy therefore confers some of the mechanical strength of the sericin to the PASP hydrogel which is an added benefit of this process. The mechanical properties were not estimated in the

hydrated state owing to the typical difficulty of obtaining force distance curves of high reliability in liquid.[252] However, it may be anticipated that the modulus values in the fully hydrated state would be around 1/10 the value in the dry state making this material comparable to other polymeric scaffold materials.[237]

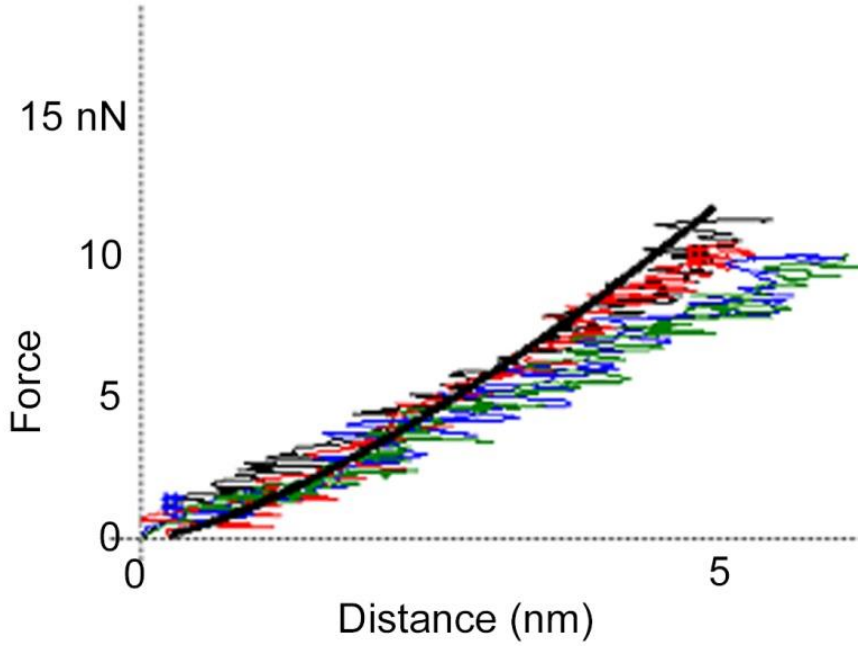

Figure 3.9. Overlay of 5 example nanoindentation curves on the PASP-S hydrogels. Samples were investigated at 50% PASP + 50 % sericin using a Si_3N_4 cantilever with a nominal spring constant of 2 nN nm^{-1}. Values were recorded at constant depth mode at a loading rate of 50 nm/sec. Only the dwell toward curves are presented for clarity.

Swollen hydrogel networks of both PASP and PASP-S hydrogels were studied to provide insight into the effects of buffer pH on their internal microstructure. SEM images of the hydrogels formed by the hydrolysis procedure reveal the difference between

polysuccinimide and sericin-templated poly(aspartic acid) hydrogels (Figure 3.4), illustrating the templating as noted earlier. Typically, hydrogels of 75% sericin and 50% sericin compositions demonstrate highly porous architectures (Figure 3.10). Significant differences in microarchitecture between hydrogels at varying compositions are considered to be an effect of the relative content of sericin—a greater incorporation of sericin within the hydrogel induces a significant change in porosity, leading to an abundance of micrometer-scale pores within the network. The effects of environmental pH are clearly observed in the SEM images. As pH is increased from weakly acidic to weakly basic, the network of small pore size (Figure 3.10 A-B) expands to produce a high porosity matrix with large pore dimensions (Figure 3.10 C-D).

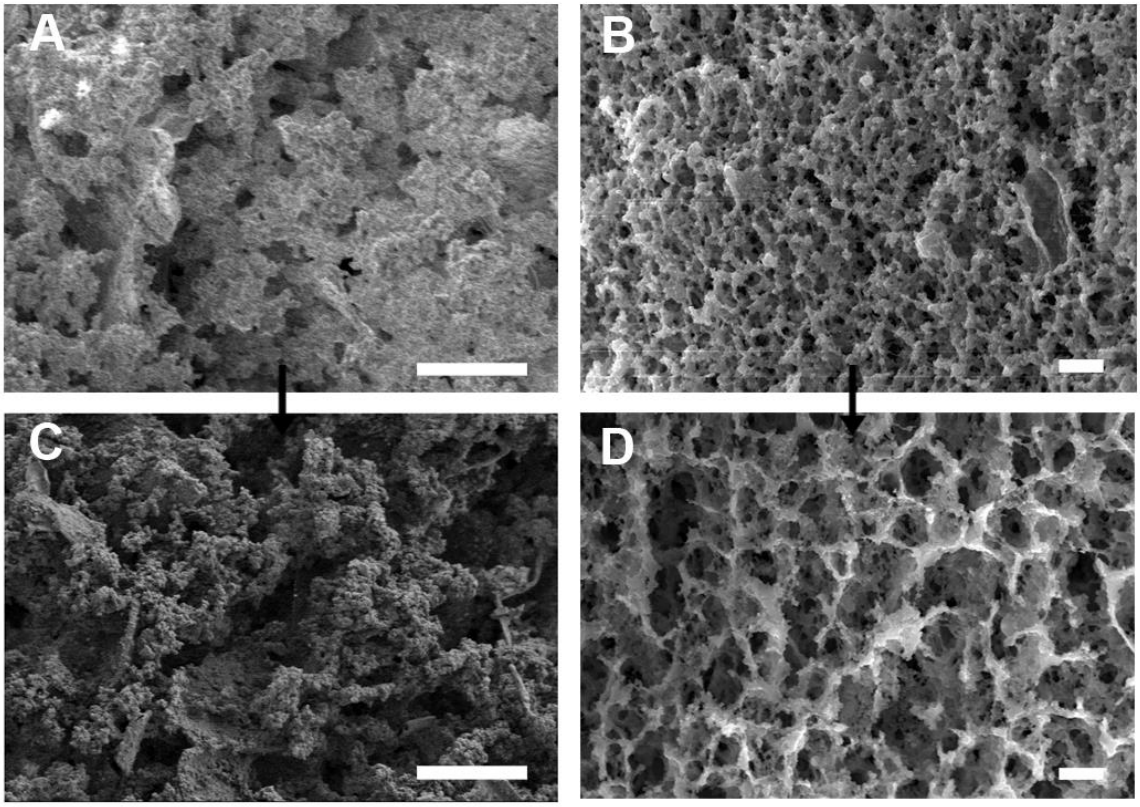

Figure 3.10. SEM of PASP-S hydrogels, demonstrating a change to pore size and structure as pH is increased from an acidic to basic environment. (A) 50% PASP + 50% sericin to (C). (B) 25% PASP + 75% sericin to (D). Images show a change in architecture from a densely-packed morphology at acidic pH to a highly porous, high surface area morphology at basic pH. Scale bar = 10 μm.

For example, in the 75% sericin hydrogels, this change corresponds quantitatively to an enhancement in pore size from r = 1.8 ± 0.5 μm at low pH to 2.4 ± 0.5 μm at high pH, when bulk hydrogel pore dimensions are analyzed (Figure 3.11). This transition is a direct result of the deprotonation of aspartic acid side chains, as pH is increased beyond the pKa of PASP. The deprotonation of carboxylic acid groups produces negatively-

charged carboxylate moieties, which further leads to electrostatic repulsion of neighboring carboxylate residues, and ultimately, expansion of the network as water infiltrates the hydrogel. Thus, SEM images establish the pH-response connecting swelling behavior at the macroscale to morphological changes at the microscale.

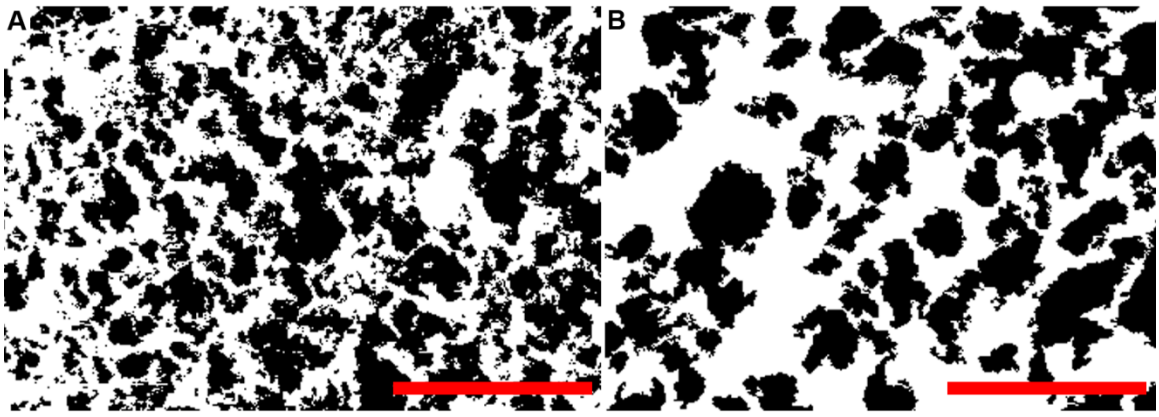

Figure 3.11. SEM analysis of of the 75% PASP-S hydrogels, at low pH (A) and high pH (B), demonstrating characteristic changes to void space and pore dimensions: r = 1.8 ± 0.5 µm (low pH) to 2.4 ± 0.5 µm (high pH). Scale bar = 10 µm.

3.3.5 Cell culture and viability on hydrogel scaffolds

Sericin has long been used to enhance the growth of different cell lines as a cellular substratum. These have included mouse fibroblasts, several human cell lines and mouse hybridoma particularly when added to culture media.[74] The synthetic serine-rich repetitive domain of sericin was shown to replace bovine serum albumin in mouse hybridoma and insect cell culture.[235] Cultured human skin fibroblasts were shown to be enhanced by 250% on sericin in comparison to a sericin-absent control. Similarly, amino acid homopolymers such as poly(aspartic acid) are fully biodegradable polymers

that have interesting biochemical properties. PASP has also been shown in conjunction with other materials to be suitable for cell culture. Poly(D,L-lactic acid) films modified with PASP have enhanced interactions with osteoblasts.[253] PASP used with aqueous-derived silk fibroin scaffolds showed increased osteoconductive outcomes with an increase in initial content of apatite and BMP-2 in the porous matrix.[19] However, studies of PASP as a scaffold material by itself have been limited despite its reported biocompatibility.

In this study, thin, sectioned PASP-S hydrogel scaffolds (25% – 75% sericin) were evaluated for their ability to support healthy adhesion and proliferation of cells. Murine fibroblasts were seeded onto scaffolds and allowed to attach and proliferate for a period of 12 days. The employment of the alamarBlue assay for studying *in vitro* cell growth was selected to monitor populations of fibroblasts on PASP-S scaffolds without inducing cell death (Figure 3.12).[52] Statistical analysis of proliferation over time intervals up to 12 days demonstrated significant differences, (*) and (**), between scaffolds and controls. While viability data indicates the ability of scaffolds to support cell growth, a reduction in cell viability (to 70 – 80% viability) was indicated for all tested PASP-S compositions on day 12 in comparison to tissue culture polystyrene.

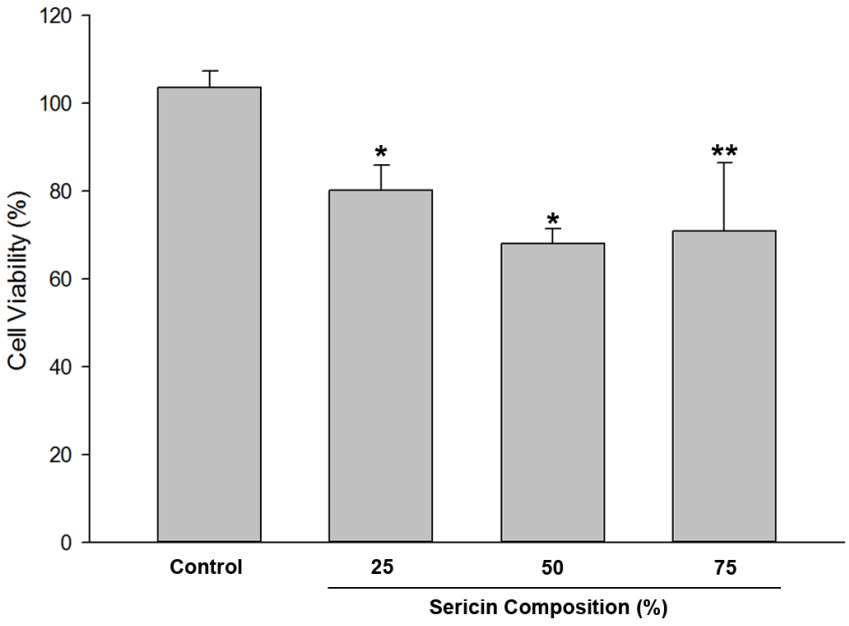

Figure 3.12. The alamarBlue assay provides a quantitative indication of fibroblast viability on PASP-S hydrogel scaffolds versus control surface: p-values < 0.01 (*) and < 0.05 (**) were considered statistically significant. Cell viability was observed to decrease on scaffolds, however still remains at 70 – 80% viability for 25%, 50%, and 75% sericin hydrogels.

To further establish whether this reduction was a function of cytotoxicity resulting from scaffold components or possibly differences in initial cell concentration, the live/dead assay was employed to qualitatively evaluate cytotoxic effects of PASP-S scaffolds (Figure 3.13). Cell death (red) was localized to very small regions of scaffolds, and overall, the cell population exceeds 85% live cells at day 12. This preservation of cell viability over long-term assays suggests that while PASP-S scaffolds do not enhance cell viability in comparison to polystyrene, adverse effects on cell growth and proliferation

are limited, and overall cytotoxicity is low. The ability to act as a suitable cellular scaffold material demonstrates the usefulness of this material, particularly given its pH-responsiveness in comparison to other static materials.

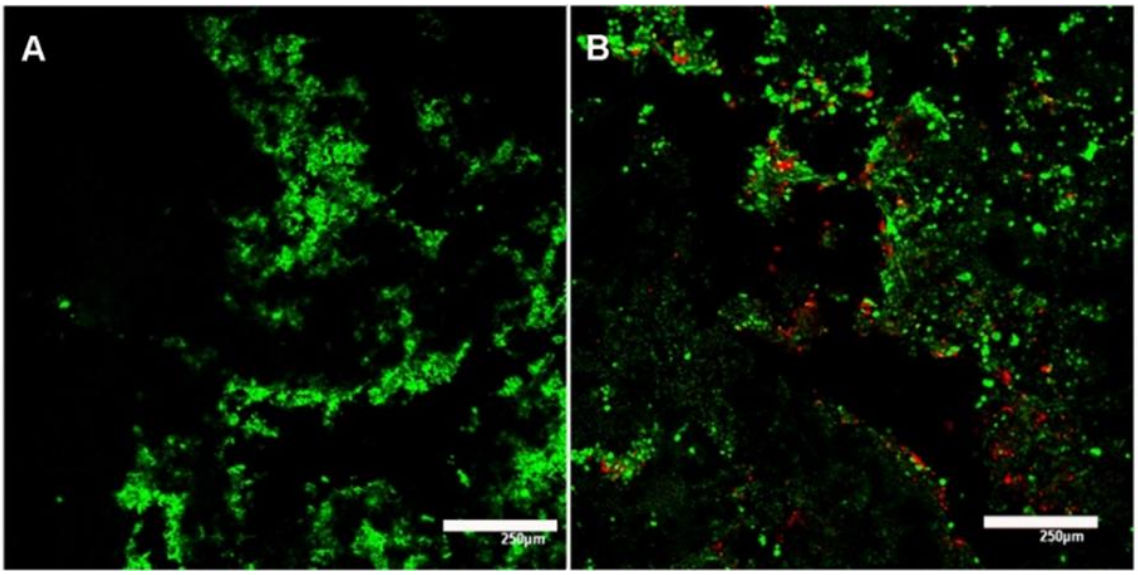

Figure 3.13. L-929 fibroblast proliferation on the 75% sericin PASP-S hydrogel at (A) day 3 (B) day 12, demonstrating limited long-term cytotoxicity of scaffolds. Green denotes live cells and red denotes dead cells. Scale bar = 250 µm.

3.4 Conclusions

An effective method has been demonstrated for producing pH-responsive amino acid-based hydrogels, demonstrating enhanced swelling as a result of sericin incorporation. The hydrogels are formed from the templating of poly(aspartic acid) using

a silk protein sericin that behaves as a 'structural modifier' during the crosslinking of the polysuccinimide precursor. Synergistically utilizing the biocompatibility of both aspartic acid and silk sericin, it is demonstrated that both can be templated into a hydrogel that is an excellent scaffold and will exhibit an enhanced stimuli response to pH changes in comparison to PASP alone. Differences in swelling behavior are demonstrated to occur during a simultaneous transition in pore size and porosity of hydrogels at the micrometer-scale. Overall, this novel protein-protein templating strategy offers the possibility of producing mechanically durable stimuli-responsive amino acid based materials that are also biocompatible and biodegradable. This has numerous potential applications in biomaterials research as base materials for scaffolds or drug delivery systems. By incorporating biocompatible proteins as the bulk of the hydrogel architecture, it is possible to significantly augment existing environmentally-responsive properties without inducing changes to chemistry or biocompatibility. This hydrogel provides a low-cost, high-throughput option for analyzing swelling behavior as well as possible platform for cell proliferation, drug delivery, or as selectively permeable gates for microfluidic devices. Furthermore, these results demonstrate the implications of the unique attributes of sericin on the formation of a biocomposite architecture with high-value applications.

[This chapter contains results that have been submitted for publication in the paper "pH-responsive amino-acid based hydrogels formed via silk sericin templating" in Acta Biomaterialia, 2013.]

CHAPTER 4

DEVELOPMENT OF A PLATFORM FOR SPATIALLY-DIRECTED PATTERNING OF SILK VIA PROTEIN PHOTOLITHOGRAPHY

4.1 Introduction

The research conducted in the previous chapters provided key information on some of the more fundamental assembly properties of silk proteins, and the capacity for silk to structurally augment existing architectures to improve function. Silk proteins have been widely used in biological applications, owing to their ease of processing, biocompatibility, and biodegradation. These proteins have been demonstrated to undergo self-assembly processes to produce complex, ordered architectures in two dimensions. This has the potential for bottom-up nanoscale fabrication as discussed above. However, limited customization of dimensional parameters, combined with a lack of durability of self-assembly necessitates investigating alternate strategies to enable fabrication across length scales. In the previous chapter, the development of stimuli-responsive protein-based materials using the water-soluble sericin protein, enables enhancement of stimuli-response, however this effect occurs at the expense of protein loss. These functional and biologically-relevant architectures together display promise for the use of silk in bio-functional materials such as photonics, implantable bioelectronics, drug delivery and

nanostructured scaffolds.[82, 254, 255] In order to produce stable architectures of silk proteins, it is necessary to investigate biochemical approaches to improve the stability and ease of architectural fabrication for silk proteins. A significant challenge lies in transforming the fundamental properties and attributes of silk proteins—mechanical strength, biocompatibility and ease of processing, from those displayed for intractable processes leading to randomly structured and simple biomaterial architectures, to produce large-scale microarchitectures through facile methods. In this chapter, the development of silk protein conjugates capable of undergoing crosslinking to induce specific microstructural presentations, in addition to improving physical and chemical properties, is considered.

The incorporation of silk into modern biomaterials development has established silk's versatility in addressing diverse applications and improving overall material properties and functionality. Silk protein integration into biomaterial composites has provided an avenue to improving micro- and macrostructural mechanical properties, enhancing biocompatibility, and augmenting existing architectures.[20, 78, 95, 256-258] Conversely, through the formation of composite materials, silk may be indirectly imparted with properties ranging from improved mechanics to electrical conductivity, and fabricated into a range of architectures.[15] Thus, the development of a silk protein photolithography platform is considered in order to translate the unique properties of individual silk proteins into stable, micropatterned architectures via light-based stimuli. In contrast, the use of soft lithography patterning techniques provides limited value in producing complex, yet stable silk microarchitectures.[32, 79, 259, 260] Photolithography provides a route to rapidly and directly fabricating complex features

with high fidelity, however the use of an inherently photoactive species is required.[124, 261, 262] Protein photolithography, and the development of a 'protein photoresist', has been limited in scope when considering the bulk of available literature. As was elaborated upon in the background, studies on developing a comprehensive strategy incorporating protein bioconjugation and high-resolution lithographic processing, are largely non-existent. Instead, past efforts have filled in some gaps in protein photolithography, contributing to expansion into a complete platform. To address this discontinuity in research efforts, investigations to demonstrate tractable and versatile processing systems for creating a system capable of modifying and employing the common biomaterial, silk fibroin protein, were explored.

In the past, recombinant approaches have proven of value to efforts in creating photoactive species, due to their ability to innately modify existing proteins using non-canonical amino acid incorporation *in vivo*. The addition of non-canonical, photocrosslinkable amino acids to the genetic code enables the incorporation of photoactive capacity to proteins.[138, 263] Carrico *et al.* (2000) demonstrated the microbial expression and subsequent photolithography of artificial extracellular matrix proteins utilizing non-canonical incorporation of the photoactive moiety, p-azidophenylalanine.[139] However, development of aryl azide-containing proteins using the denaturant, guanidine hydrochloride, makes these approaches poorly suited to exhibiting conjugated silk proteins that retain their structure and function during photolithography. Combined with the complexity of design, costs of recombinant synthesis, low yield (< 40 mg/L), and inability to modify intact, naturally-available proteins, bioconjugation was selected as a route to producing protein photoresists.

Bioconjugation strategies enable site-specific or promiscuous graft polymerization of chemical moieties, such as fluorescent tags, crosslinkers, and other functional groups, onto proteins.[264] Bioconjugation strategies provide a means for modifying silk fibroin by: a) introducing novel chemical functionalities, b) enhancing mechanical properties and c) improving stability. Carbodiimides (i.e. EDC) have been utilized for fibroin EDC/NHS-based conjugation in the presence of carboxyl-containing residues, however poor stability of EDC-based linkages is noted, ruling out potential use for fibroin.[265] Alternatively, the synthesis of NHS ester-conjugated perfluorophenyl azides enables protein photoactive labeling of amine-containing residue lysine.[266] The underrepresentation of lysine in silk proteins artificially limiting the maximum degree of photoactive incorporation to < 5 mol%.[267] Direct attachment of visible/IR-active (e.g. porphyrin, chlorin, and bacteriochlorin), isocyanate-conjugated reagents to bovine serum albumin has been demonstrated with a high degree of success.[268] However, the use of isocyanates for silk fibroin has not been thoroughly investigated in literature.

Of the available bioconjugation techniques, isocyanate modifications provide an ideal balance in their ease of use and moderate specificity to a range of biologically relevant functional groups, reacting with nucleophilic amine-, hydroxyl-, sulfhydryl-, and carboxylic acid-containing substrates.[269, 270] This has traditionally made them valuable for conjugating fluorescent probes or acting as molecular ‘rulers’ for probing biochemical structural features.[271-273] However, the site-specific reactions of isocyanates often occur in competition with the hydrolysis of the isocyanate group in the presence of water, to produce carbon dioxide, providing a challenge for achieving conjugation of water-soluble silk proteins. Grafting of 2-methacryloyloxyethyl

phosphorylcholine has previously been conducted through isocyanate addition of 2-methacryloyloxyethyl isocyanate on fibroin fabric (i.e. insoluble fibroin) by taking advantage of the large abundance of nucleophilic centers in fibroin.[274] The use of significant molar quantities, exceeding 50-fold excess, makes establishing relative stoichiometric control a goal in the proposed synthesis of photocrosslinkable fibroin. Silk proteins in general possess a number of reactive nucleophilic groups: a) hydroxyl groups are present in serine, threonine, and tyrosine, b) amines are present in lysine and arginine, and c) carboxylic acids are present aspartic and glutamic acid residues, enabling the formation of stable linkages (Figure 4.1). The isocyanate group (-N=C=O) is capable of reacting with alcohols and amides present in polypeptide chains, to form urethane and urea bonds, respectively, in addition to amide linkages with carboxyl-containing residues. Thus, isocyanates allow a wide degree of grafting efficiency to be realized, enabling variable functionalization to preserve key amino acids and allow for the creation of multi-functional materials.

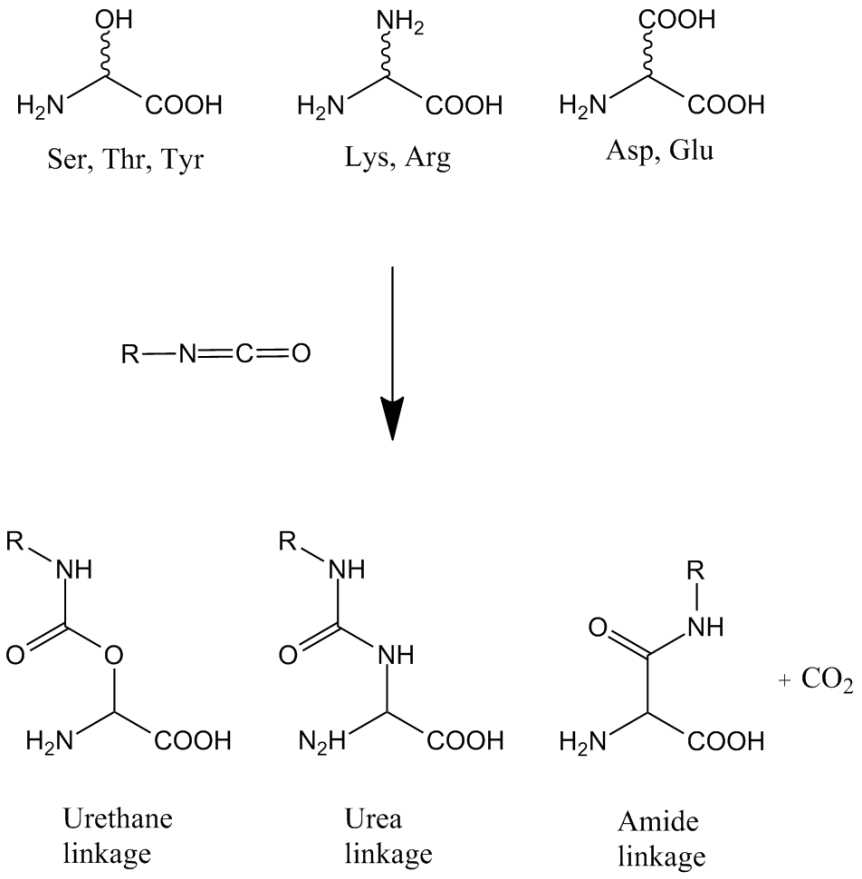

Figure 4.1. The reaction of isocyanates with nucleophilic amino acid side chains enables conjugation with moderate substrate specificity.

Addressing the fundamental limitations of conventional photolithography presented in the introduction is possible through careful selection of key steps of photolithography, and adaptation of the process as necessary. To aid in these efforts, research on photolithography of acrylate-containing species for microstructural fabrication in 2-dimensions, often incorporating water-based processing strategies, is considered for use with photoactive fibroin.[129, 275, 276] Furthermore, simple modifications of substrate surface chemistry promote photoresist adhesion through the

formation of covalent linkages between acrylate-containing photoresist species, and the underlying substrate.[129] This provides a relative simple framework which will be adopted in order to conduct photolithography of the photoactive conjugate.

This research thus employed the isocyanate-containing reagent, 2-isocyanatoethyl methacrylate (IEM, MW = 155.15 Da) in 0.1% butylated hydroxytoluene inhibitor, as a means of producing stable, photoactive silk proteins.[277] IEM possesses a terminal methacrylate, which enables photopolymerization to be conducted at the vinyl end group. In order to expand on the work of Furuzono *et al*. (2000), who demonstrated isocyanate-based functionalization of silk fabric, a non-aqueous environment was considered for dissolution of fibroin. However, the use of DMSO is limited to producing suspensions of fibroin fibers, which are not easily fabricated into architectures for photolithography. Silk sericin has previously been modified through isocyanate addition, in 1M LiCl/DMSO, which is known to interrupt interchain hydrogen bonds, enabling protein dissolution.[278] This solvent system was employed in the following research to enable fibroin solubilization by the same process as sericin.

An approach based on the modular biochemical design of a silk photoresist is reported in the following chapter that can be used in conjunction with optical lithography to form precise patterns and architectures. Silk fibroin from silkworm sources is readily available at low cost, and the facile chemical protocol described provides a versatile material that may be combined with the manufacturing scalability of photolithography. Fibroin provides several modifiable amino acids for site-specific chemical modification without significantly altering protein structure and function.[49] The design of the "protein photoresist" is achieved by the introduction of photo-reactive groups in native

fibroin. Multifunctional acrylate groups are used due to their ease of use, high reactivity, widespread prevalence in existing photolithography techniques, and generation of high-resolution features.[129, 279] These moieties readily react with commercially available photoinitiators, resulting in a material that behaves as a negative photoresist that can be crosslinked using light. Using photolithography, silk protein features can be patterned at sub-microscale resolution (μm) over macroscale areas (cm) (Figure 4.2) in a laboratory environment using a novel technique, termed Silk Protein Photolithography (SPL). It is further demonstrated that these high resolution microstructures can function as bio-friendly cellular substrates for the spatial guidance of cells without use of cell-adhesive ligands. The high mechanical strength and controllable degradation of this material provides opportunities in fabricating sustainable, nanostructured scaffolds and flexible microdevices.

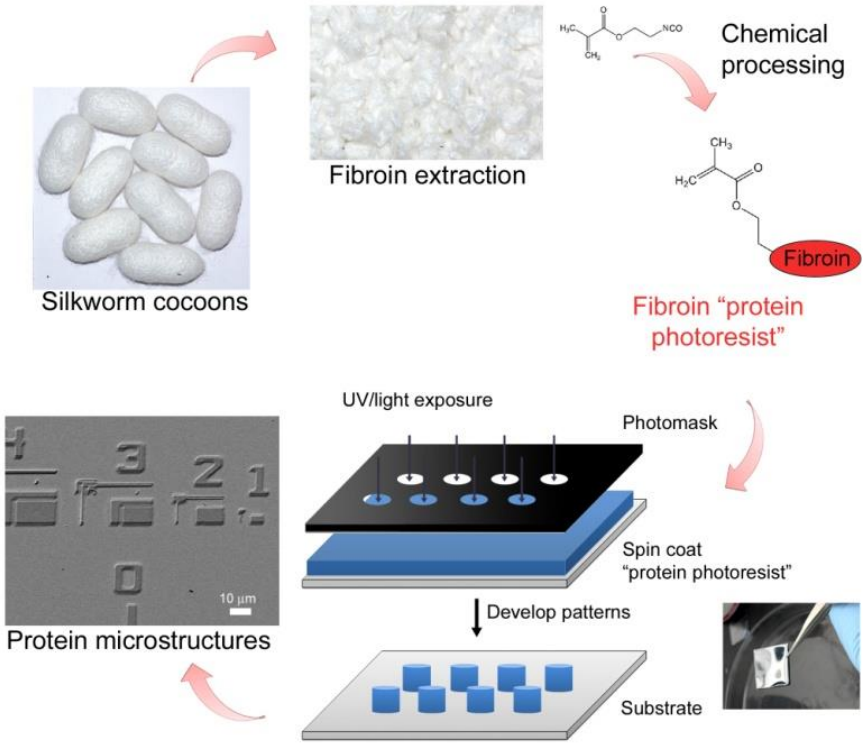

Figure 4.2. The proposed Silk Protein Photolithography (SPL) platform, depicting synthesis of a fibroin-methacrylate photoresist from silkworm cocoons and subsequent photolithography process to form high-resolution silk micropatterns over large areas.

4.2 Experimental Section

4.2.1 Materials

Silk fibroin was extracted and purified from *Bombyx mori* silkworm cocoons using established protocols (Jhargram Tropical Tasar Farms, West Midnapore, West Bengal, India).[21] The reagent 2-isocyanatoethyl methacrylate, 98% with < 0.1% BHT

inhibitor (IEM, MW = 155.15 Da) was utilized for chemical modification of fibroin. Anhydrous dimethyl sulfoxide, anhydrous lithium chloride (LiCl) and dimethyl sulfoxide-d_6 were purchased from Sigma-Aldrich (St. Louis, MO). 1,1,1,3,3,3-Hexafluoro-2-propanol (HFIP) was obtained from Oakwood Chemical (West Columbia, SC). Irgacure 2959 (1-[4-(2-Hydroxyethoxy)-phenyl]-2-hydroxy-2-methyl-1-propane-1-one, Ciba, Tarrytown, NY) was employed as a photoinitiator for photolithography experiments. The fluorescent dyes, fluorescein isothiocyanate-labeled albumin, and Alexa Fluor 555-labeled ovalbumin were obtained from Sigma-Aldrich (St. Louis, MO) and Life Technologies (Grand Island, NY), respectively. All chemicals were used as received without further purification.

4.2.2 Synthesis and purification of photoreactive fibroin

Photoactive silk fibroin conjugates were synthesized in a process adapted from Teramoto *et al.* (2004) and Furuzono *et al.* (2000).[274, 278] Specifically, the solvent system of 1M LiCl in DMSO was adapted for the dissolution of fibroin, and fibroin was reacted with an isocyanate-terminated group. During the reaction, reagents and associated glassware were dried to prevent the moisture-sensitive isocyanate group of IEM from reacting with water and decomposing. Fibroin was initially added to a round-bottom flask and vacuum-dried for 24 hours at 70 °C to remove residual water. LiCl was dried at 120 °C for 24 hours before use. Fibroin was dissolved at a concentration of 1% (w/v) in 1M LiCl/DMSO, while heating at 60 °C for 45 minutes. This mixture was continuously stirred under a dry N_2 purge throughout the dissolution process. A stoichiometric amount

of IEM was added to the round bottom flask, and the reaction was maintained at 60 °C for 5 hours in a dry N_2 atmosphere. Immediately thereafter, the resulting solution was poured into excess cold ethanol and centrifuged to precipitate the product. The product was then twice collected and washed in a mixture of cold ethanol/acetone and centrifuged. The remaining precipitated mass was then frozen at -80 ºC and lyophilized for 48 hours to yield an off-white powder (fibroin). For the purposes of calculating reaction stoichiometry and degree of conjugation, an average molecular weight of 74 Da per residue was used (via fibroin heavy chain: 391,000 Da, 5,263 residues). Reaction recovery was calculated as a ratio of final dry mass to initial fibroin mass, assuming complete recovery of fibroin following the reaction.

4.2.3 IR Spectroscopy

FTIR was conducted on HFIP-cast films of native fibroin and FPP using a Nicolet iS10 FTIR spectrometer. The spectrometer was operated using a Smart iTR ATR (Attenuated Total Reflectance) sampling accessory with a low-penetration depth Ge crystal. Spectral data was collected in the region of 4000 - 800 cm^{-1} at 4 cm^{-1} intervals, and averaged over 32 scans.

4.2.4 Nuclear Magnetic Resonance

Proton nuclear magnetic resonance (^{1}H-NMR) was conducted on a Varian Mercury 300 MHz NMR spectrometer. A system of 1M LiCl in DMSO-d_6 was utilized

for dissolution and analysis of the fibroin-methacrylate conjugates. The figure shows the assigned peaks with the amino acids and the acrylate moieties.

4.2.5 Circular Dichroism (CD)

Secondary structure was measured using an Olis DSM 1000 Circular Dichroism Spectrophotometer (Olis Inc, Bogart, GA). Post-processing was performed using the Olis Spectralworks software containing SELCON3 and CDSSTR reference databases at 178–260 nm. The normalized root mean square deviation (NRMSD) parameter was utilized to quantify differences between experimental and reconstructed data during CD data deconvolution[280]:

$$NRMSD = \left\{ \frac{\sum_{i=1}^{N} [[\theta]^{exp}(\lambda_i) - [\theta]^{cal}(\lambda_i)]^2}{\sum_{i=1}^{N} [[\theta]^{exp}(\lambda_i)]^2} \right\}^{1/2}$$

where λ is wavelength, N is the number of data points collected for a spectrum, and $[\theta]^{exp}(\lambda)$ and $[\theta]^{cal}(\lambda)$ represent the experimental and reconstructed spectra.

4.2.6 Surface Functionalization of Silicon and Glass Substrates

Silicon and glass substrates were incorporated for patterning of silk microstructures. Squares of silicon (1 x 1 cm^2) and glass (2 x 2 cm^2) were initially washed thoroughly with ethanol and deionized water to remove surface contaminants. Substrates were treated with Piranha solution (3:1 98% H_2SO_4:30% H_2O_2) for 30 minutes to remove organic contaminants and to hydroxylate the surface, in order to present silanol surface

groups for further modification (*Caution: Piranha solution reacts violently with organic materials and must be handled with extreme care*). Surfaces were then repeatedly washed with deionized water and ethanol and dried at 150 °C. Functionalization to silanol groups was conducted using 3-(trichlorosilyl)propyl methacrylate (TPM) by means of a chemical vapor deposition (CVD) technique.[281, 282] 100 µL TPM was added to a desiccator containing the substrates. The chamber was then drawn down to 0.4 bar and left for a period of 12 hours for the TPM to react and present covalently bound functional groups. Methacrylate-modified surfaces were extensively washed with hexane and water, and dried before further use.

To enable patterning and subsequent delamination of features, Si surfaces were modified to create a chemically-inert, hydrophobic surface. This was achieved via the modification of Si with a SAM of octadecyltrichlorosilane (OTS). Substrates were then modified using vapor deposition of OTS in a desiccator (0.4 bar for 12 hours). These substrates were washed alternatively with ethanol and water, and dried prior to use.

4.2.7 Silk Protein Photolithography (SPL)

Micropatterns of silk fibroin protein photoresist (FPP) were fabricated using contact photolithography. FPP was dissolved at 2% (w/v) in HFIP with 0.6% (w/v) of Irgacure 2959 photoinitiator and vortexed at low speed for a period of 15 minutes, at which point no solids remain. The FPP solution was cast onto methacrylate-functionalized Si/glass and spread via gentle rotation of the substrate. An ambient ‘pre-bake’ step was then conducted, in which substrates are allowed to sit at ambient

temperature for 5 minutes to allow excess photoresist solvent (HFIP) to evaporate, and decrease photoresist to photomask adhesion. Cast substrates were polymerized via an OmniCure S1000 UV Spot Curing lamp (Lumen Dynamics, Ontario, Canada) equipped with a 320 – 500 nm filter. Substrates were exposed at 150 mW/cm^2, for 4.5 seconds exposure through a chrome photomask. Development of uncrosslinked and unexposed FPP was performed using 1M LiCl in DMSO for 2 hours followed by copious rinsing with deionized water. Substrates with the developed protein patterns were then dried in a gentle stream of N_2.

4.2.8 Protein Microstructure Staining

In order to establish the success of photopolymerization, protein staining of microstructures was accomplished via the Coomassie Blue R-250 dye. A modified rapid stain protocol was employed, in which substrates were stained in a solution of 10% acetic acid in water, containing 60 µg/ml Coomassie Blue R-250.[283] The qualitative appearance of protein-bound dye occurs after 30 minutes, and staining was allowed to proceed for 60 minutes to provide sufficient dye intensity for visualization. Immersion in deionized water for a period of 60 minutes was conducted to remove unbound dye from microstructures and substrates. Analysis of dye localization was subsequently achieved through digital camera imaging and optical microscopy.

4.2.9 Scanning Electron Microscopy (SEM)

SEM imaging was carried out at a 15 kV accelerating voltage on a Hitachi SU-70 high-resolution field emission microscope and at a 2.0 kV on a JEOL SM-5610 SEM. Patterned silicon substrates were sputter coated with 20Å platinum (Denton Vacuum Desk V cold sputtering system, Denton Vacuum, Moorestown, NJ) to enhance conductivity prior to imaging.

4.2.10 Atomic Force Microscopy and Nanomechanical Analysis

Atomic Force Microscopy (AFM) imaging of surface microarchitectures was conducted on an Asylum Research MFP-3D AFM (Santa Barbara, CA), in AC mode (AC240TS probes, Olympus, Japan, k = 1.81 nN nm^{-1}). The AFM was used to determine Young's moduli of the materials. A Tap 190DLC cantilever (k = 48 nN nm^{-1}) was employed for AFM-based nanoindentation. All force constants were measured prior to the experiments using the thermal fluctuation method.[284, 285] Thick films (>10 μm thickness) were indented in air with ~10 indents at 3 different spots in both constant force and constant indent modes. For constant force a load of 1 μN was applied; constant depth indents were performed to a depth of 10 nm. Force-distance curves were analyzed via Hertzian mechanics to determine values for Young's modulus.[286]

4.2.11 *In Vitro* Proteolytic Degradation

Crosslinked films (~ 5 mg) of photoactive sericin prepared via silk protein photolithography, as described above, with a single experimental modification—films were cast from 100 μL of total solvent to limit the spread of the film, and thus maximize film thickness. Photo-crosslinked films were initially weighed in the dry state, and then incubated at 37 °C in a solution of (1 unit/mg protein) Protease XIV (*Streptomyces griseus*, ≥3.5 units/mg, Sigma-Aldrich) in PBS. Films incubated in PBS in the absence of protease acted as negative controls. The Protease XIV and control solutions were changed initially at 3 days, and subsequently every 4 days thereafter to ensure the preservation of protease enzyme activity (Protease XIV activity is > 80% following 3 days of incubation).[66] At designated time points, samples were removed from the buffer, and rinsed with deionized water before drying for analysis—films were first weighed and then cryofractured in liquid N_2 for SEM study.

4.2.12 Fibroblast Cell Culture

A range of fibroblast cell lines was employed for cell culture experiments: human fibroblasts were kindly provided by the laboratory of Dr. Raj Rao (Department of Chemical and Life Science Engineering at Virginia Commonwealth University, Richmond, Virginia) while L-929 murine fibroblasts were provided by the laboratory of Dr. Subhas Kundu (Department of Biotechnology, Indian Institute of Technology, Kharagpur, India). Cells were initially seeded in 75 cm^2 polystyrene tissue culture flasks and incubated at 37 °C in a 5% CO_2 atmosphere in DMEM high glucose media, with

10% FBS and 1% non-essential amino acids. After reaching 70% confluence, fibroblasts were passaged with 0.025% trypsin and incubated at 37 °C for 5 minutes, at which point the cells were observed to attain a spherical morphology and detach from the sidewalls of the tissue culture flask. Additional media was added to dilute the trypsin, and the cell suspension was centrifuged at 1000 rpm for 5 minutes at 4 °C to precipitate the cells. The supernatant was removed, and the cells were washed and resuspended in fresh media. A small aliquot was removed from the homogenized cell solution, and using a haemocytometer, the cell density was determined. Prior to cell seeding, microstructured FPP scaffolds were hydrated in PBS overnight, and UV sterilized for 30 minutes in a laminar flow hood. Cells were seeded onto 1 in^2 scaffolds, consisting of 0.5 mg FPP protein, and controls in a 6-well tissue culture plate at 50,000 cells per well. FPP scaffolds were then incubated at 37ºC for 3 – 4 days to allow for sufficient cell proliferation prior to imaging.

4.2.13 Characterization of cell culture

After reaching approximately 70% confluence (assessed via analysis of glass slide controls), substrates were washed in PBS and fixed with 4% paraformaldehyde. Following permeabilization with wash buffer, actin staining was performed with rhodamine-conjugated phalloidin (1:200 dilution) for L-929 cells, and Alexa Fluor 488 phalloidin for 3T3 cells. Nucleus counterstaining was conducted with Hoechst stain for L-929 cells, and DAPI for 3T3 cells. Focal adhesion was observed by vinculin staining using FITC-conjugated vinculin (Sigma-Aldrich). Imaging was conducted at 405 nm and

488 nm using a confocal laser scanning microscope (Olympus FV1000) with 20 and 60x oil immersion lenses.

4.2.14 Fabrication and Harvesting of Monodisperse Microparticles

The fabrication of free-standing shapes and patterns was achieved through a similar technique to the silk protein photolithography described above, however with a non-wetting substrate capable of allowing facile delamination of features. Surface functionalization was conducted on Piranha-treated silicon substrates using hydrophobic alkylsilanes, octadecyltrichlorosilane (OTS) and trichloro(1H,1H,2H,2H-perfluorooctyl)silane (FOTS), which were then characterized using contact angle analysis to ensure success of chemical vapor deposition. Fabrication of microparticle shapes was conducted using a 2.5% (wt/vol) solution of FPP in HFIP with 0.6% (wt/vol) photoinitiator). This solution contained 1 mg of FPP per 1 cm^2 substrate in a cast volume of 40 µl HFIP. Photoexposure and development were conducted as described in Section 4.2.7 on Silk Protein Photolithography. This procedure was slightly modified through by the removal of rinsing steps to prevent loss of particles from the substrate—instead the developer volume was replaced *in situ* with deionized water three times for 1 hour per immersion to assist in removal of latent developer and unexposed FPP. Fluorescent labeling of specific particle shapes was conducted to enhance localization via loading with a fluorescent dye, either albumin-fluorescein isothiocyanate conjugate, or the ovalbumin-Alexa Fluor 555 conjugate. Fluorescent dyes were added to FPP solutions at 1:10 fluorescent dye:FPP, in terms of total mass. Delamination and harvesting of

microparticles was conducted using a cell scraper to ‘corral’ particles on the substrate. Removal of particles entirely was achieved through collection with a 1 mL micropipette, or brief sonication of the substrate in deionized water to detach all shapes present on the surface. Imaging was conducted on an Asylum Research MFP-3D-BIO Inverted Optical AFM, equipped with fluorescein isothiocyanate (FITC) and tetramethylrhodamine isothiocyanate (TRITC) filter cubes for fluorescent imaging.

4.3 Results and Discussion

4.3.1 Synthesis of Silk Fibroin Conjugates

In order to produce a photoactive silk conjugate, it was necessary to select a modification strategy that could enable grafting under mild conditions, without adversely affecting protein conformation or other fundamental properties. A previously-reported method for incorporating 2-methacryloyloxyethyl phosphorylcholine substituents onto silk fibroin ‘fabric’ through isocyanate addition was considered for fibroin modification.[274] However, this reaction was conducted on suspended and otherwise insoluble fibroin, which greatly limits the ability to process the resulting conjugate into alternative, non-fibrous architectures. Another method for conjugating sericin using isocyanate addition, with the assistance of a DMSO-based solvent system for solubilizing the products has been demonstrated, which enables the reaction to be conducted under mild conditions.[278] The reaction conditions required for this method were observed to

result in minimal degradation of the sericin protein. Using this knowledge, a reaction scheme was designed and implemented for dissolving and conjugating silk fibroin.

The reagent 2-isocyanatoethyl methacrylate (IEM) was incorporated for grafting to the protein.[277] IEM was used for conjugation to fibroin due to the possibility of reaction with hydroxyl terminated amino acids serine, threonine and tyrosine.[277] In the absence of protecting groups, the isocyanate reaction can modify hydroxyl-terminated amino acids serine, threonine, and tyrosine, via an alcoholysis mechanism (Figure 4.3).[287] To a lesser extent, the isocyanate is reactive with carboxyl- and amino-terminated amino acids.[49] In order to achieve successful grafting to fibroin, DMSO was selected as a solvent for the conjugation due to its polar, non-aqueous character. This provides an environment enabling isocyanate dissolution and reaction, while minimizing moisture responsible for premature hydrolysis. However, DMSO alone is not able to achieve dissolution of native fibroin. To induce fibroin dissolution, a solvent system of 1M LiCl in DMSO was selected due to previous observations in which it was able to support silk sericin conjugation.[278] This solvent system is known to interrupt hydrogen bonding of fibroin's β-crystalline structure, enabling dissolution. Ethanol precipitation following IEM conjugation enables selective removal of the methacrylate-conjugated fibroin product from the water-miscible DMSO solvent and soluble IEM monomers.

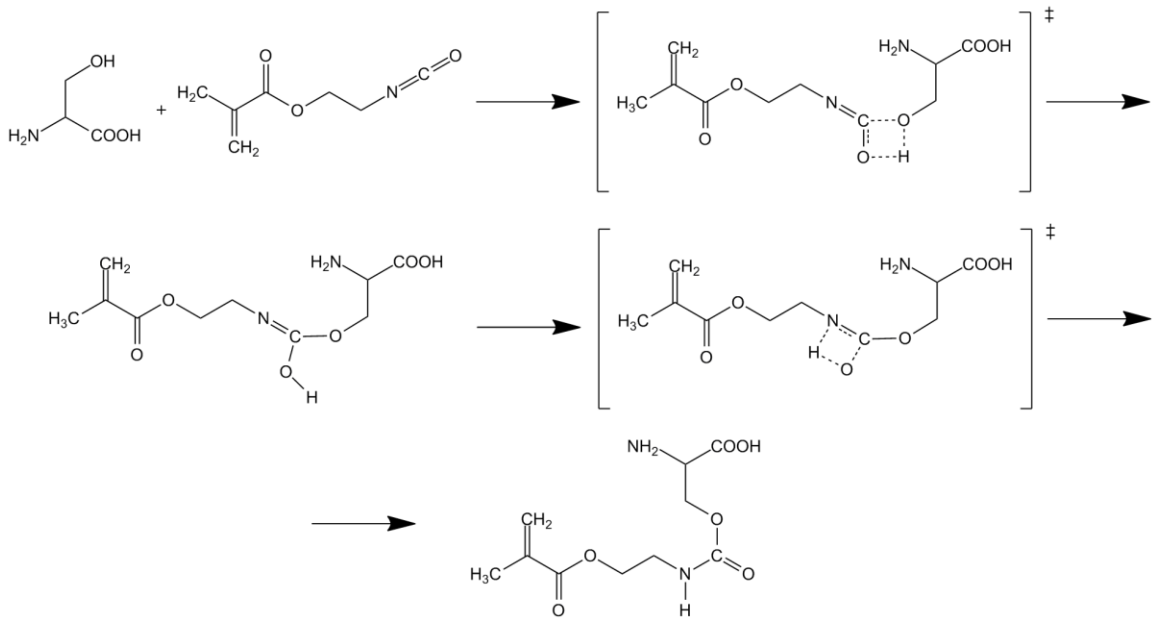

Figure 4.3. Schematic of the isocyanate addition of IEM to serine, with the terminal hydroxyl group attacking the isocyanate carbonyl to yield the initial transition state. Displacement of the hydroxyl proton onto the adjacent nitrogen forms a stable amide linkage, resulting in a vinyl-functionalized serine residue. This mechanism occurs similarly for other hydroxyl-terminated amino acids (e.g. Thr and Tyr, or even water), and primary amines.

Due to the number of side reactions available to subvert IEM from the primary protein-conjugation reaction, IEM does not react with fibroin amino acids in an efficient manner. As a result, it was found to be necessary to add IEM in excess to the number of reactive groups. A 5-fold excess of IEM to the stoichiometric quantity of reactive amino acids was found ideal for conjugation. Purification and recovery of the fibroin-

methacrylate conjugate was achieved at 150.0 mg product for a 129.9 mg starting fibroin mass, or 116% of the protein input if all product is assumed to be efficiently recovered.

The degree of methacrylate substitution can be calculated from the mass gain of fibroin following isocyanate addition. Fibroin contains an abundance of modifiable nucleophilic amino acids: hydroxyl-containing residues (i.e. Ser 12.1 mol%, Thr 0.9 mol% and Tyr 5.2 mol%) account for 18.2 mol% of residues, while amino and carboxyl-containing residues account for only 3.1 mol%. This allows for conversion of up to 21.3 mol% of total residues in fibroin. The mass gain thus indicates that that ~7.8 mol% of all amino acid residues (i.e. both reactive and unreactive amino acids), or 36.6 mol% of reactive nucleophilic residues in fibroin are converted to the methacrylate substituent. After successful conjugation, the product is henceforth referred to as fibroin-methacrylate, or fibroin protein photoresist (FPP).

4.3.2 Characterization of Silk Fibroin Conjugates

Solubility of Fibroin-Methacrylate

Fibroin displays limited solubility when extracted from silk fiber. This necessitates preliminary dissolution in a 9.3M LiBr solution, a process which ‘activates’ the fibroin.[288] Once dissolved, the protein solution may be dialyzed and lyophilized to yield a product which is readily water-soluble, in addition to being soluble in 1,1,1,3,3,3-hexafluoroisopropanol (HFIP). However, with the chemical conjugation described, the solubility characteristics of the FPP change significantly. Following precipitation and recovery, the fibroin-methacrylate conjugate was observed to be water-insoluble, in

addition to being insoluble in most alcohols (methanol, ethanol, isopropanol, and 2,2,2-trifluoroethanol) and other common organic solvents (chloroform and dichloromethane). Solvent systems known to solubilize fibroin, including water and buffers ranging from the 9.3M LiBr used for initial fibroin solubilization, to the 1M LiCl/DMSO system used for the reaction solution, to N-methylmorpholine N-oxide (NMMO), are observed to be ineffective at solubilizing the fibroin-methacrylate conjugates to any extent.[289]

This loss of solubility is attributed to a combination of factors: a) the introduction of a hydrophobic alkene and carbonyl groups onto fibroin via the methacrylate moiety, b) conformational changes induced by 1M LiCl/DMSO dissolution, and c) the process of ethanol precipitation. The 1M LiCl/DMSO solution, which provided a non-aqueous environment for fibroin conjugation, has not been well-characterized for its effects on fibroin. This unique solvent system has been previously utilized for the dissolution of cellulose.[290] This process was mechanistically attributed to the interaction of lithium moieties of the undissociated ion pairs of lithium chloride with hydroxyl-group oxygen molecules in cellulose, effectively disrupting interchain hydrogen bonding. However, no studies are available on structural or conformational effects of this dissolution process. In addition, the treatment of fibroin with ethanol has been previously studied as a method for enhancing β-sheet crystallinity in order to render fibroin water-insoluble.[291]

As a result of these numerous factors, 1,1,1,3,3,3-hexafluorisopropanol (HFIP), a strong hydrogen bond donor, was investigated and found to be an effective solvent for fibroin-methacrylate. This solvation capability is attributed to the highly electronegative structure of HFIP, enabling the disruption of interchain hydrogen bonds, in addition to strong hydrophobic interactions resulting from $–CF_3$ groups. HFIP has been extensively

utilized for the dissolution of 'activated' fibroin (i.e. fibroin which has been previously solubilized using 9.3M LiBr) prior to electrospinning, and its conformational effects are known.[292] As a result, HFIP induces and stabilizes the α-helical conformation of fibroin, while decreasing β-sheet content.[293] HFIP was the only solvent to provide solubility and was thus used as a carrier for characterization as well as deposition of fibroin-methacrylate. Solubility in HFIP was observed up to concentrations of 10% (wt/vol), and solubilization was noted to occur over a period of 15 minutes.

Verification of Conjugation

The conjugation of silk fibroin with the IEM moiety was verified using IR spectroscopy and ^{1}H-NMR spectroscopy, to enable comparison of the fibroin conjugate to the unmodified, native fibroin. ATR-FTIR spectroscopy was conducted on films of fibroin-methacrylate and fibroin cast from HFIP solutions, in addition to the pure IEM reagent (Figure 4.4).

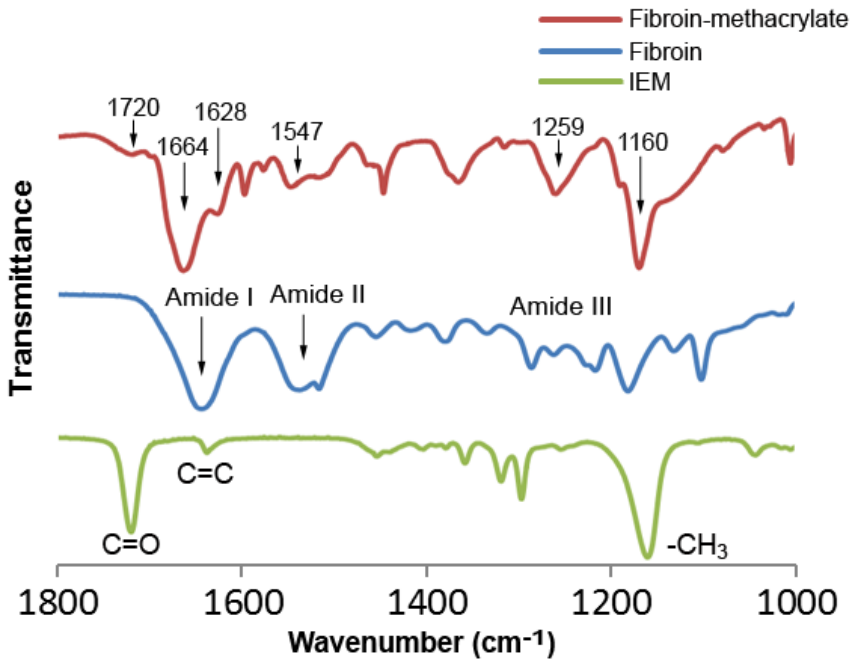

Figure 4.4. FTIR spectra of films of fibroin-methacrylate conjugate, native fibroin films and the modifying reagent IEM. Characteristic amide I-III peaks of fibroin, in addition to stretching vibrations at 1720 cm^{-1} (ester carbonyl C=O) and 1630 cm^{-1} (vinyl C=C), and rocking vibrations at 1160 cm^{-1} (CH_3) are observed on fibroin-methacrylate. The co-existence of these signals in fibroin-methacrylate indicates the successful conjugation of IEM onto native fibroin.

The predominant region of relevance for the native protein and conjugation product, at 1800 – 1000 cm^{-1}, was expanded for peak assignments. Figure 4.4 demonstrates the spectrum of native fibroin (in blue), with clear peaks at 1660, 1550, and 1260 cm^{-1}, assigned to characteristic fibroin amide I, II, and III, respectively. Analysis of the IEM reagent (in green) yields intense stretching vibrations at 1720 cm^{-1}, representing carbonyl ester C=O, and 1640 cm^{-1}, assigned to vinyl C=C (which confers photoreactivity). An

additional intense peak is present at 1160 cm^{-1}, resulting from CH_3 rocking vibrations.[294] The fibroin-methacrylate conjugate (in red) preserves fundamental amide I/II/III signals from native fibroin, while carbonyl C=O (1720 cm^{-1}) and vinyl C=C (1630 cm^{-1}) stretching vibrations are present as moderate-intensity shoulder peaks of amide I. Rocking vibrations, assigned to CH_3, are also present as a strong absorption band at 1160 cm^{-1}. The clear observation of characteristic IEM groups in the fibroin-methacrylate product provides strong proof to support the successful grafting of the IEM monomer onto native fibroin.

In the expanded spectrum, a broad intense peak at 2270 cm^{-1}, resulting from isocyanate (–N=C=O) stretching, is evident. The absence of this isocyanate stretching vibration from the fibroin-methacrylate product indicates the absence of residual isocyanate. The reaction supernatant, consisting of solute left over after precipitation of the FPP product, was separately analyzed for signals from potential IEM side reaction products. From this spectrum a significant amount of IEM is observed to being removed from the fibroin product in the unconjugated state. Amide I/II/III peaks are not evident in this spectrum, indicating the absence of fibroin, and further providing an explanation for the lower than expected degree of methacrylate grafting. Together, these observations indicate the successful precipitation and purification of the fibroin-methacrylate product, from which degraded or oligomerized IEM monomer has been removed, and remains soluble in the DMSO solvent.

Further analysis of the fibroin-methacrylate product was conducted using ^{1}H-NMR. Due to the limited solubility of the conjugate in common deuterated solvents (i.e., D_2O and chloroform-d), the initial solvent system utilized for conjugation of 1M LiCl in

DMSO was tested found to be compatible with NMR. In order to re-solubilize the fibroin-methacrylate in 1M LiCl/DMSO, it was first necessary to dissolve and cast the conjugate from a solution of HFIP. This dynamic solubility behavior of fibroin-methacrylate results from the conformational change induced by HFIP, enabling facile dissolution in the LiCl/DMSO buffer. Thus, samples were analyzed in a solution of 1M LiCl in DMSO-d_6. Annotated ^{1}H-NMR spectra for native fibroin and fibroin-methacrylate are presented in Figure 4.5, and Figure 4.6, respectively.

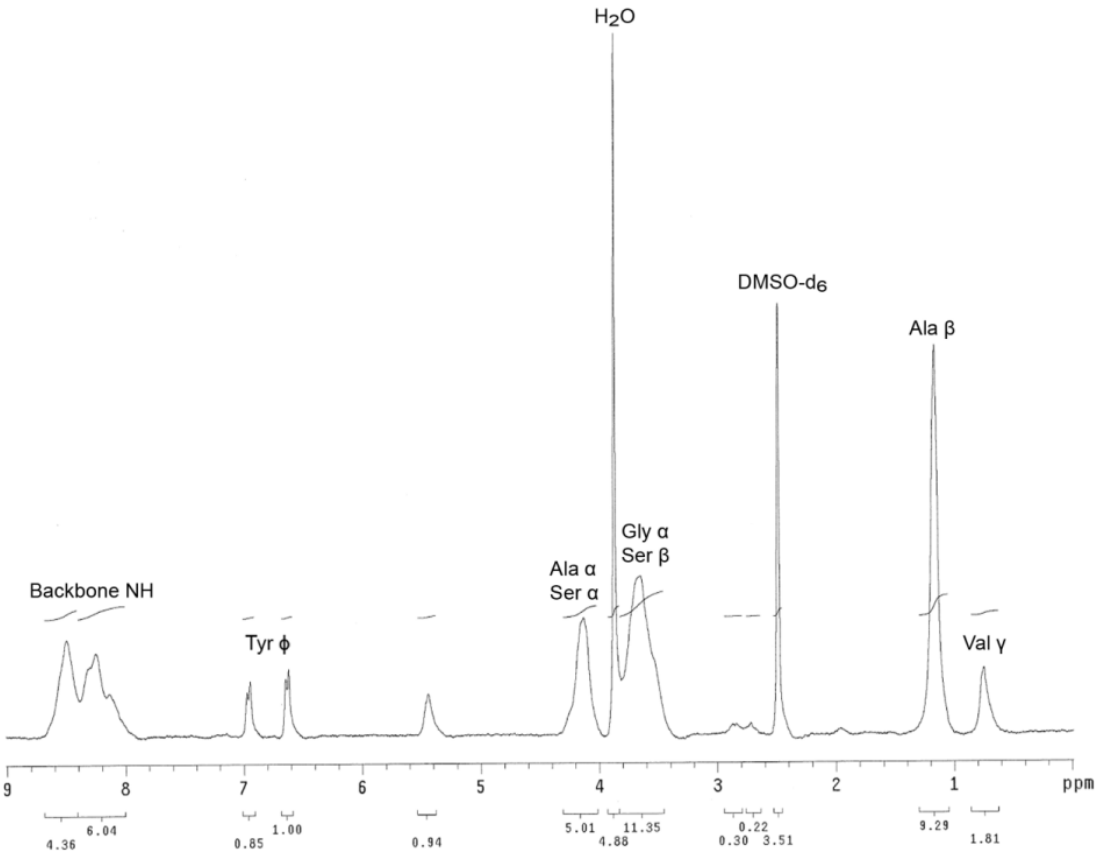

Figure 4.5. Proton NMR of native, unmodified fibroin in a system of 1M LiCl/DMSO. Characteristic signals of the glycine- and alanine-rich protein are assigned to prominent shifts. Doublets belonging to tyrosine Φ are clearly identifiable around 6.6 – 7.0 ppm, in a region where the methacrylate modification would manifest.

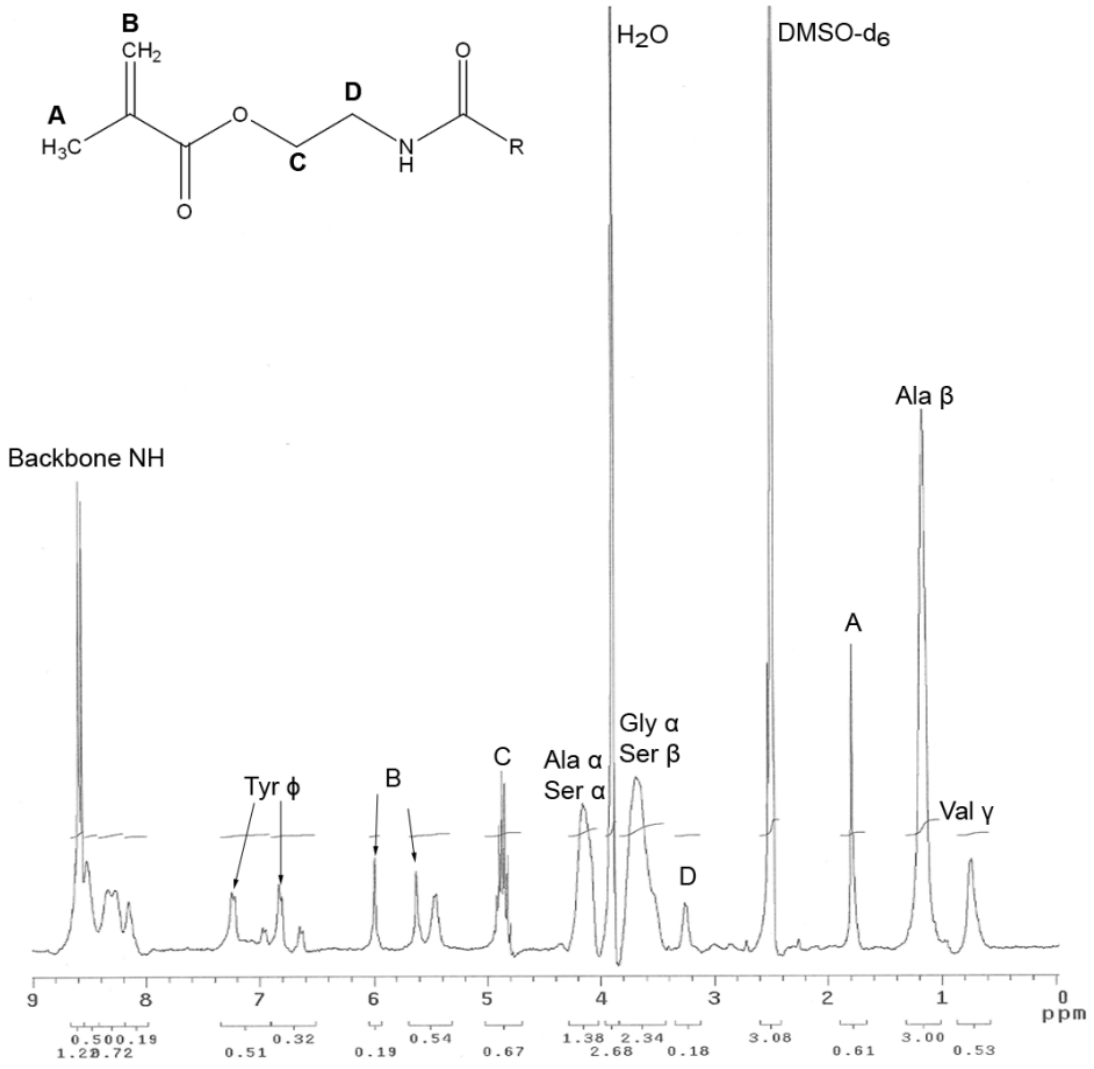

Figure 4.6. Proton NMR of fibroin-methacrylate and native fibroin solution. Groups identified by A, B, C and D on the IEM are assigned on the spectra of FPP.

The successful conjugation of fibroin was verified by comparison of the fibroin-methacrylate conjugate (Figure 4.6), to native fibroin (Figure 4.5). ^{1}H resonances were assigned by examining and comparing NMR data to literature-reported NMR spectra for fibroin.[295] Analysis of native fibroin indicates major shifts from the Gly (H_{α}), Ala

(H_{α}), Ser ($H_{\alpha,\beta}$), from 3.4 – 4.3 ppm, in addition to Val (H_{γ}) and Ala (H_{β}) from 0.6 – 1.4 ppm. These chemical shifts reflect the relatively high abundance of the (GAGAGS) amino acid repeat. Analysis of fibroin-methacrylate reveals vinyl resonance peaks at 5.6 (1H) and 6.0 (1H) ppm, in addition to the occurrence of characteristic chemical shifts of native fibroin. Additional resonance assignments were made by comparing chemical shifts to NMR data for pure IEM, and the spectrum was overall found to be in agreement with literature-reported data for IEM.[296] An approximation as to the methacrylate content can also be quantitatively determined by comparison of methacrylate shifts to prominent amino acid shifts. The abundant amino acids glycine and serine compose 56.7 mol% of the fibroin protein, and share an overlapping chemical shift from NMR data. The degree of methacrylate substitution was calculated from the following equation:

$$Methacrylate\ Substitution\ (\%) = \frac{AUC(H1 + H2)x100x0.567}{AUC(Ser\ \beta CH + Gly\ \alpha CH)/2}$$

Thus, the degree of methacrylate substitution was calculated to be 9.2%, which indicates a conversion of 43.2% of nucleophilic amino acids. This NMR-derived value is in reasonable agreement with calculations made from product mass, indicating 7.8% substitution. Overall, NMR analysis supports the observations made via FTIR, and positively indicates the presence of the methacrylate substituent on the fibroin protein backbone.

Structure and Stability of Fibroin-Methacrylate

Chemical functionalization of proteins is known to have the potential to drastically change secondary structural conformation, as is observed for the PEGylation of fibroin.[297] Considering the nature of the fibroin-methacrylate modification—the replacement of hydrophilic hydroxyl groups with a hydrophobic vinyl moiety, it is expected that some structural effects will manifest. However, significant changes to secondary and tertiary protein structure threaten the fundamental properties of fibroin, which make it such a remarkable material. For example, the significant mechanical capabilities of fibroin, including high strength and toughness, result from the presence of β-sheet-rich nanocrystalline regions.[298] For this reason, secondary structural analysis was carried out on fibroin-methacrylate via circular dichroism spectroscopy, to assess the impact of methacrylate grafting on structural conformation.

Circular dichroism (CD) spectroscopy enables the analysis of differential absorption of circularly polarized components of plane polarized light, which results from intrinsic chirality (i.e. optical activity) in a protein.[280] The determination of 'ellipticity' resulting from this analysis represents the degree of circular polarization, and this parameter thus provides a key insight into the structural configuration of certain biomolecules. When CD is conducted, ellipticity is measured over a range of wavelengths, for which a similarity in ellipticity profiles suggests structural similarity between protein species. Deep UV absorbance of the chloride ion of LiCl necessitated analysis of fibroin samples in HFIP solutions. Superimposed spectra fibroin and FPP indicates structural similarity, despite the methacrylate grafting of FPP (Figure 4.7).

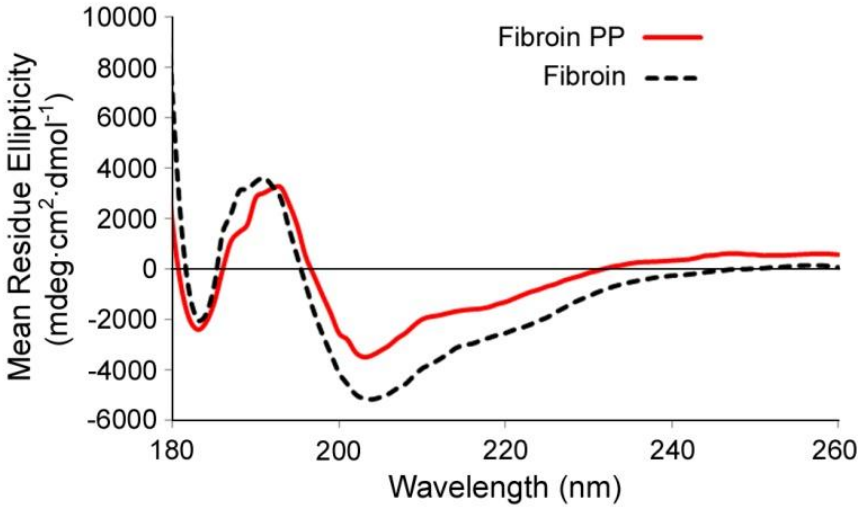

Figure 4.7. Circular Dichroism (CD) of 0.2 mg/ml solutions of fibroin protein photoresist and native fibroin in HFIP.

For silk proteins, signals of interest occur due to the peptide bond (absorption < 240 nm), aromatic amino acids (absorption 260 - 320 nm), and disulfide bonds (weak absorption, ~ 260 nm). The presence of specific secondary structural configurations (i.e. α-helix, β-sheet, β-turns, and random coil) results in characteristic CD signal profiles. With the assistance of reference datasets (i.e. SELCON3, CDSSTR, etc.) for samples of known structural configurations, these proteins may be analyzed to provide a quantitative indicator of the abundance of secondary structural features. The calculation of an NRMSD parameter provides an indication of the "goodness of the fit" of experimental data to reconstructed data (i.e. curves resulting from fitting via the reference program). This parameter ranges from 0 (i.e. perfect fit) to 1 (i.e. no fit). When NRMSD < 0.1, the fit of the experimental data to the reference data is assumed to be sufficient for analysis.

CD spectra were thus fit to multiple databases, SELCON3 and CDSSTR, in order to select the algorithm best fitting experimental data. Via SELCON3 secondary structure reference database at 178–260 nm, fibroin-methacrylate is estimated at 42% α-helical content and 6% β-sheet (in comparison to fibroin: 36% α-helix and 9% β-sheet). However, NMRSD values for the SELCON3 reference database are calculated to be .54 and .84, respectively for fibroin-methacrylate and fibroin. Via CDSSTR, a better fit between experimental and model data is achieved, and fibroin-methacrylate is estimated at 46% α-helical content and 22% β-strands (in comparison to fibroin: 48% α-helix and 21% β-sheet) (Figure 4.8)

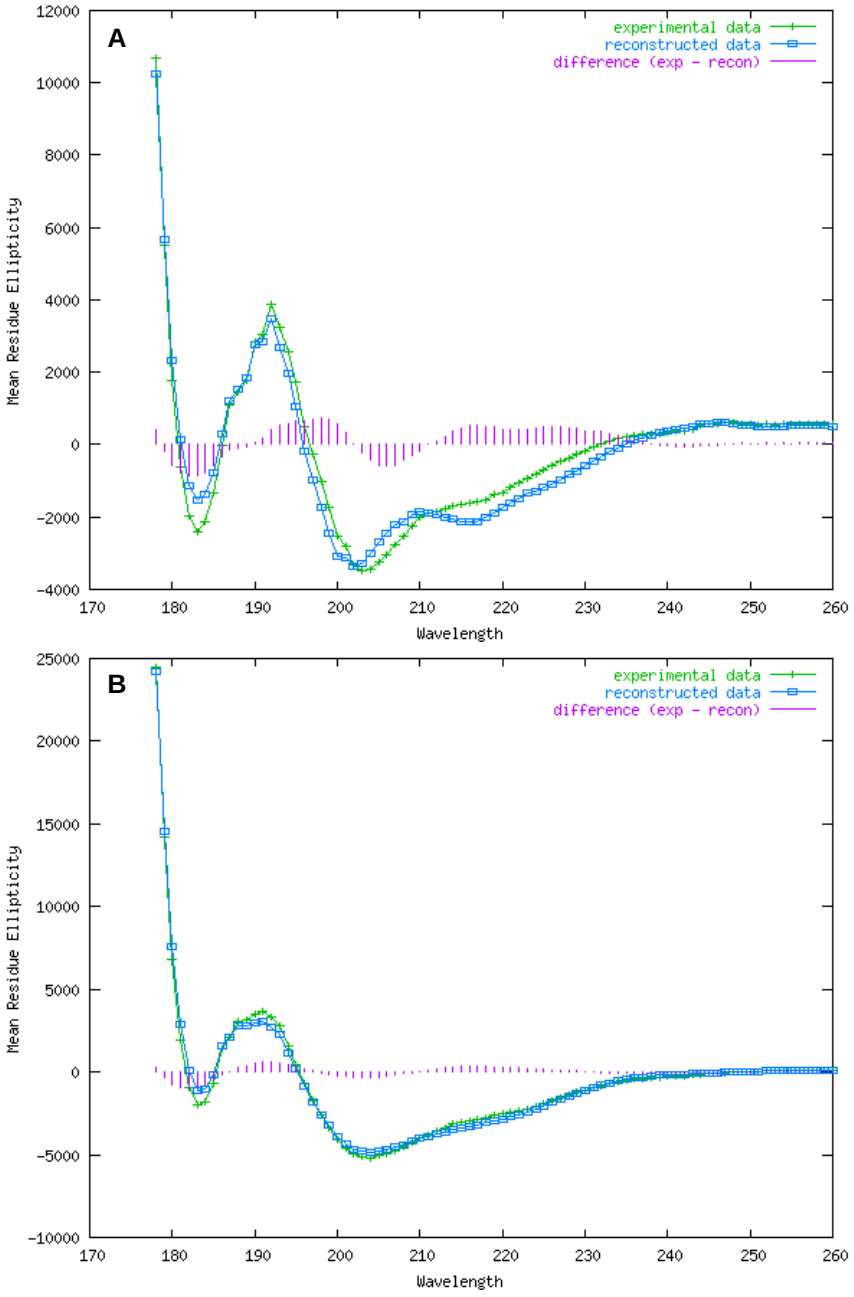

Figure 4.8. Fitting of (A) fibroin-methacrylate and (B) native fibroin CD spectra to the Dichroweb CDSSTR reference database yields agreement between reference and experimental data (purple).[180, 181]

NMRSD values via the CDSSTR database are < 0.1, enabling a direct comparison of data, summarized in Table 4.1.

Table 4.1. CD spectral data was analyzed using the CDSSTR database in Olis SpectralWorks software (dataset 1, 178 – 260 nm) for secondary structure estimation, showing close agreement between fibroin-methacrylate and native fibroin.

Sample	α-Helix	β-Sheet	β-Strand	Random	Total	NRMSD
FMA	0.46	0.22	0.16	0.16	1.00	0.09
Fibroin	0.48	0.21	0.17	0.18	1.04	0.01

The structural composition for unmodified fibroin is in good agreement with prior CD characterization, showing fibroin in HFIP to possess an α-helical-rich structure of 50% α-helix and 24% β-sheet content.[299] The similarity in secondary structural content of FPP to fibroin indicates the presence of a methacrylate substituent does not adversely disrupt the formation of α-helical and β-sheet structure and preserves the fundamental structural characteristics of fibroin.

The impact of these observations on solubility are also noted—once solubilized in HFIP, CD data shows secondary structural content is roughly that of the starting fibroin material, which once again enables solubilization in the LiCl/DMSO system. This reveals how HFIP solubilization is able to alter conformation, fundamentally changing fibroin-

methacrylate solubility. However, it is not possible to fully investigate the structural transition induced by LiCl/DMSO, as the chloride anion absorbs strongly in the far UV range ($\lambda < 195$ nm) during CD studies, preventing deconvolution of protein and salt signals.[300]

Overall, these analyses support the presence of the methacrylate group in the silk fibroin product. In order to conclusively establish the photoactive capability of the fibroin conjugate, it is necessary to conduct studies demonstrating photocrosslinking of fibroin. Further work on processing the fibroin conjugate enables an expansion of this simple photocrosslinking property into the fabrication of complex 2- and 3D architectures.

4.3.3 Silk Protein Photocrosslinking

In an effort to demonstrate the versatility of the fibroin-methacrylate conjugate, a number of processing techniques were initially employed to create stable 2D films and 3D architectures. During these fabrication steps, methacrylate polymerization and the effects on protein stability were investigated. Considerable work has been performed on mechanistic and applied studies using acrylate-based polymers in conjunction with photopolymerization steps to achieve effective crosslinking.[301, 302] Previously, crosslinking agents such as polyethylene glycol diglycidyl ether have been demonstrated to yield simple compliant films of crosslinked silk fibroin.[303] However, in contrast to chemical methods, photopolymerization enables crosslinking of methacrylate in response to a physical stimulus (light) rather than a chemical stimulus, enabling molding or patterning prior to crosslinking.

Photopolymerization of Thin Films

To demonstrate the chemical stability advantages of FPP over native fibroin, the fabrication of simple thin films using photolithography was studied. For photopolymerization trials, Irgacure 2959 (Ciba Specialty Chemicals, Tarrytown, NY) was employed as a free-radical photoinitiator. This solid photoinitiator was selected due to its high solubility in polar organic solvents such as alcohols (ethanol: 10 % (w/w), methanol: 50 % (w/w)), enabling dissolution in HFIP. Maximum absorbance values occur around 220 and 280 nm, however absorbance occurs as high as 380 nm, making exposure in the near-UV region suitable for photo-crosslinking. Highly viscous films of FPP (2.0 % wt/vol with 0.6 % wt/vol Irgacure 2959 in HFIP) and fibroin (2.0 % wt/vol in HFIP) and were cast onto a PDMS substrate, which allowed facile removal and manipulation of films. Exposure to UV light at 200 mW/cm^2 for a duration of 5.0 s was found to be ideal for minimizing exposure duration, while minimizing sample heating—a process which was observed to result a competing polymerization with UV light. Delamination of the films yields a similar appearance between FPP and fibroin (Figure 4.9). As was expected from fundamental fibroin solubility, immersion in water degrades native fibroin films, while the crosslinked FPP remains intact.

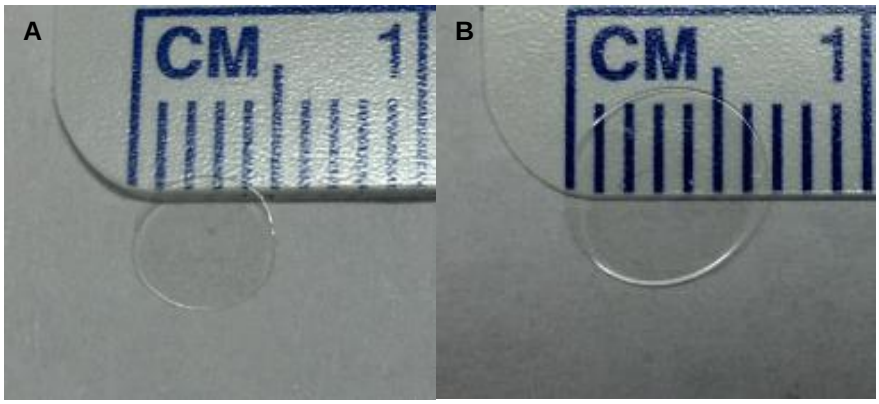

Figure 4.9. UV-exposed films: (A) HFIP-cast fibroin, (B) HFIP-cast fibroin-methacrylate.

Soft Lithography of Silk

FPP is also observed to possess the intrinsic ease of processing of native fibroin, which is capable of micropatterning down to the nanometer scale (> 30 nm) of transverse resolution.[80] Both materials form flexible, free-standing optically transparent films, with little observable structural differences. Previously, the application of soft lithography to photolithography has previously been demonstrated to enable 3D molding of photoactive diazirine-conjugated ELP protein.[143] In this experiment, 3D molding was used to produce free-standing FPP films with micropatterned topography. A concentrated solution of 6% FPP (w/v), containing 2.0% Irgacure 2959 in HFIP was cast onto a photoresist master with embossed micrometer-scale features. Following crosslinking in UV light and evaporation of the HFIP solvent, the formed film was then gently peeled using tweezers. High resolution patterns from the master transfer to the film showing its applicability for soft lithography (Figure 4.10).

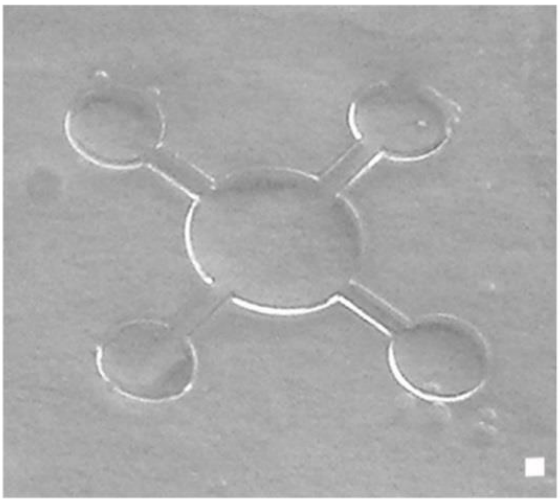

Figure 4.10. Soft lithography of the FPP on a PDMS master showing the formation of high resolution features. Scale bar = 50 μm.

4.3.4 Silk Protein Lithography (SPL) Platform

The potential for employing FPP in conventional photolithography techniques was next investigated by incorporating a micropatterned photomask in order to directly produce selectively crosslinked regions of FPP. In contrast to soft lithography, this technique enables production of binary microscale architectures without a 3D mold. Common steps from conventional photolithography are adapted for use with FPP, however a number of modifications were made to the photolithography steps in order to accommodate a protein photoresist without degradation.

To improve adhesion between the substrate (Si or glass) and FPP, functionalization of substrates via a self-assembled monolayer of 3-(trichlorosilyl)propyl methacrylate (TPM) was considered (Figure 4.11).[129] TPM presents a terminal

methacrylate substituent, capable of participating in covalent bonding of methacrylate-conjugated FPP during the photocrosslinking reaction. Si and glass substrates were initially treated with Piranha solution in order to hydroxylate surfaces, presenting silanol groups for further chemical reaction. Chemical vapor deposition enables the formation of self-assembled monolayer of the TPM. Trichlorosilane groups of TPM react with surface Si-OH groups to form a dense network of Si-O-Si bonds to the substrate, presenting a nascent adhesion-promoting layer of pendant methacrylate groups for enabling FPP conjugation. This surface modification was qualitatively verified by observing an increase in the contact angle of hydrophilic glass/Si (glass: 71 ± 2º, Si: 78 ± 2º), reflecting the presence of the hydrophobic methacrylate alkylsilane monolayer.

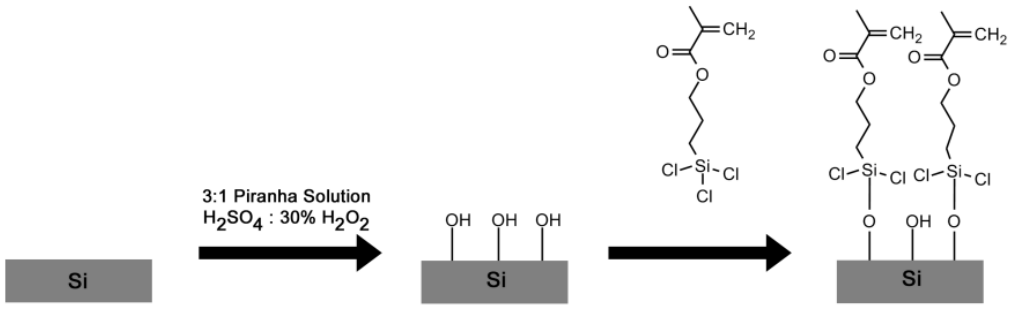

Figure 4.11. Methacrylate functionalization of Si and glass substrates is achieved through treatment with Piranha solution to present a reactive hydroxyl-terminated substrate, followed by chemical vapor deposition of TPM.

The formation of FPP films on methacrylate-functionalized substrates was achieved through use of a HFIP as a carrier for FPP and the Irgacure 2959 photoinitiator. Typically, spin-coating of the photoresist provides a means of achieving a sufficiently

thin film for polymerization. Through careful manipulation of photoresist solution viscosity, angular velocity, acceleration, and spin-coating time, the thickness of the film can be precisely controlled.[304] However, rapid evaporation of HFIP is observed during the spin-coating process due to its high vapor pressure (120 mm Hg at 20 ºC). This leads to an increase in viscosity as the photoresist becomes more concentrated during spin-coating, eventually resulting in FPP precipitating into uneven deposits on the substrate. At significantly low polymer concentrations, HFIP spin-coating is reported to be successful in yielding homogenous thin film deposition; however for FPP in HFIP, the protein is observed to undergo random aggregation on the substrate.[305] In contrast, conventional spin-coating processes incorporate solvents such as γ-butyrolactone and cyclohexanone which possess exceptionally low vapor pressures (1.5 mm Hg, and 2 mm Hg, respectively). Low ambient evaporation rates prevent this rapid evaporation and increase in concentration early in the spin-coating process, which further preserves the solubilized state of the photoresist until sufficient spreading can occur on the substrate. For these reasons, drop casting of FPP onto substrates was incorporated for thin film formation, with precise control of film thickness being achieved through manipulation of FPP concentration and HFIP volume.

For conventional photoresists, such as SU-8, a pre-bake step at 100 ºC after spin-coating helps to drive off excess solvent from the film and harden the photoresist. Due to the significant differences in evaporation rates between the SU-8 solvent, γ-butyrolactone, and HFIP, in addition to concerns of protein degradation at high temperatures, an ambient ‘pre-bake’ step is employed. FPP-coated Si and glass substrates are maintained in darkness at ambient temperature after drop casting of the photoresist,

for a period of 5 minutes. At this point, the FPP films become hard and non-adherent during manipulation (and subsequently, non-adherent to the photomask).

Photoexposure was investigated in both proximity and contact regimes, at a range of UV exposure intensities and durations. In order to properly evaluate the results of photoexposure, a number of developing systems were simultaneously investigated, including 100% HFIP and HFIP/TFE blends. Selective removal via solubilization of uncrosslinked, monomeric photoresist is desired, while crosslinked regions should be resistant to dissolution and/or dimensional loss (i.e. swelling/hydration) when selecting the proper developer.[306] The use of HFIP as a developing agent, while effective in removing unexposed regions of FPP, is less than ideal due to its significant distortion of crosslinked microstructures. Partial solvation occurs as HFIP penetrates the bulk of FPP microstructures, interrupting interchain hydrogen bonds, despite the presence of methacrylate crosslinks. Investigation of TFE as a developer adulterant, intended to diminish the solvation of HFIP (i.e. FPP is insoluble in TFE alone), provided marginal gains in minimizing this distortion (Figure 4.12). For these reasons, 1M LiCl/DMSO was selected as the primary developing agent, which provided slow solvation of unreacted FPP, while preserving microstructural integrity.

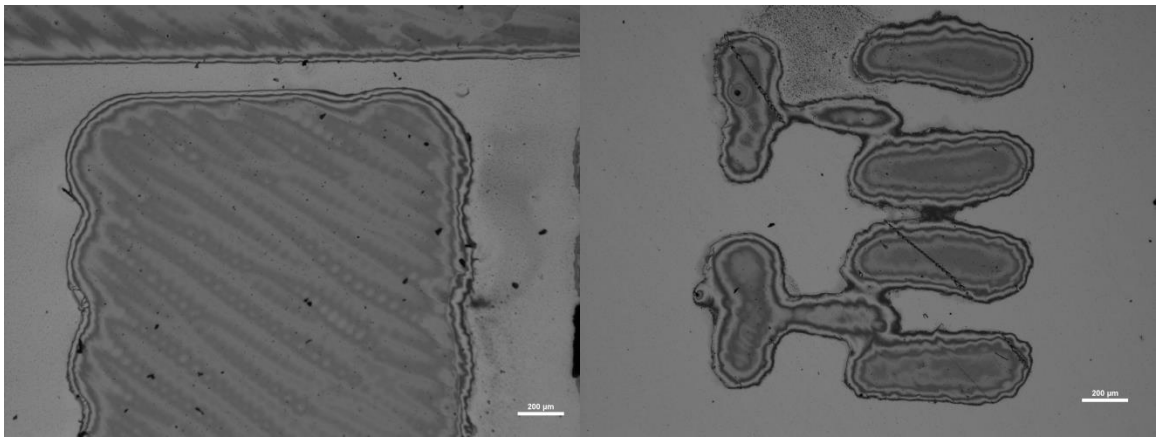

Figure 4.12. Limited reproducibility of microstructures is observed due to proximity photolithography (< 5 mm gap) and lack of substrate pre-bake. (A) Development via a 75/25 HFIP/TFE mixture—significant swelling of crosslinked FPP leads to unrecognizable patterns. (B) Development via 1M LiCl/DMSO—incomplete exposure and rounded feature edges indicates over/under-exposure of pattern. Scale bar = 200 μm.

Initial efforts to accurately reproduce microstructures via proximity photolithography (5 mm gap between photomask and photoresist) demonstrates significant expansion of feature dimensions in the case of both HFIP/TFE and 1M LiCl/DMSO development. In proximity mode, a 10 μm gap offers the minimum distance to minimize defects to the photomask resulting from photoresist contact, at the expense of a reduced resolution limit of 3 μm, however such a gap is not easily achieved without an automated aligner system. Visible exposure artifacts are characteristic of diffractive effects at the edges of opaque features, resulting from resolution limitations intrinsic to proximity photolithography and/or overexposure (Figure 4.12). The minimum feature resolution in this mode of exposure is calculated to be 64 μm, necessitating a significant

reduction in the proximity gap.

Incorporation of proximity photolithography with a 0.5 mm gap is calculated to minimize this resolution limit to 20 µm, which while significant, enables photoexposure to be conducted on adherent FPP films without photomask contact and damage. Development with 1M LiCl/DMSO is demonstrated to be successful in removing protein in unpatterned areas of the substrate. Reproduced features are observed to have a significant increase in size, yielding impinging edges with little separation between structures (Figure 4.13). This is indicative of overexposure and/or limitations of proximity photolithography, which leads to overexposure of photomask features due to the wave-like expansion of light between the photomask-photoresist gap space.

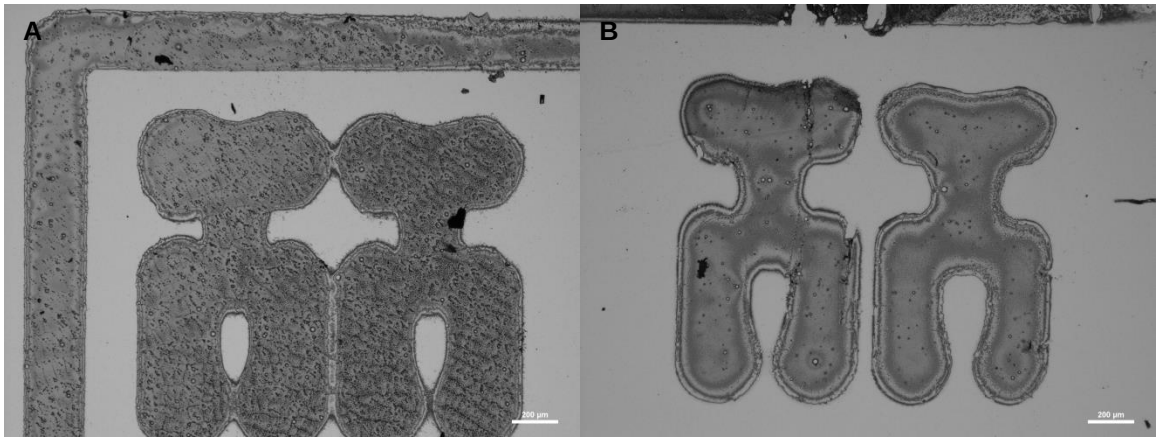

Figure 4.13. Limited reproducibility of microstructures due to proximity photolithography (< 1 mm gap) and lack of substrate pre-bake. However, development strategy via 1M LiCl/DMSO is demonstrated to be successful in removing unexposed areas of photoresist. (A) 1.0s UV exposure at 250 mW/cm^2 (B) 3.0s UV exposure at 250 mW/cm^2 1M LiCl/DMSO for 24 hours. Scale bar = 200 µm.

Contact photolithography was finally investigated, due to fundamental issues in the incorporation of FPP in proximity photolithography. Photolithography in contact with the photoresist providing a minimum feature resolution that is a function of the photoresist thickness (for FPP films < 1 μm). However, the soft surfaces of recently cast FPP films are observed to be deformable under photomask contact, and significant adhesive 'tack' results in unintended photomask adhesion and film destruction during removal. Employing a pre-bake step, by delaying exposure after film casting, provides sufficient time for carrier solvent evaporation, allowing photomask contact without FPP film degradation, and facile substrate removal (Figure 4.14). In addition, development is found to be complete after 2 hours of immersion in the 1M LiCl/DMSO developer. In lower panels, the effects of conducting contact lithography are visible—feature dimensions are valid reproductions from the photomask, however translation of the pattern across the substrate is observed.

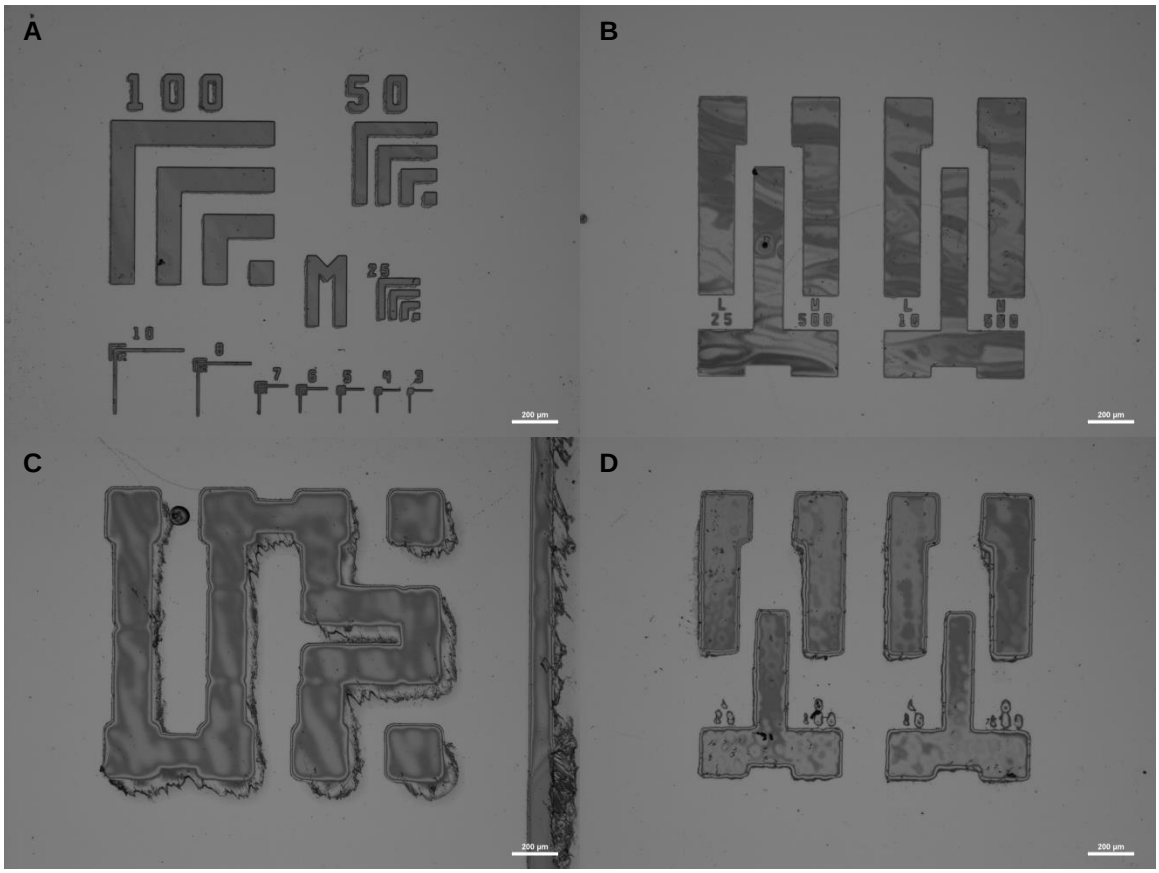

Figure 4.14. FPP photolithography demonstrates successful photolithography at 1.0s UV exposure, with development in 1M LiCl/DMSO for 2 hours. (A)(B) Proper UV exposure and development enables production of architectures down to 3 µm. (C)(D) Photoexposure without a photoresist 'pre-bake' step leads to distortion of features due to the high deformability of the soft FPP film. Scale bar = 200 µm.

In contact mode, a light pressure is applied to minimize any spacing between photomask and photoresist, and thus, for a 1 µm thick photoresist layer at a 365 nm average exposure wavelength, the minimum resolution is 0.6 µm. Despite the presence of 3 µm features in FPP photolithography trials, 'hard' contact between photomask and photoresist may still

allow separation between the photomask and photoresist, producing a gap for which diffraction can occur to effectively limiting minimum resolution.[307]

Using the aforementioned findings, micropatterns of silk fibroin on silicon and glass substrates were able to be fabricated via photolithography using the FPP as a negative photoresist that is crosslinked in the presence of UV light. The protein precursor is cast on a substrate and exposure through a patterned mask results in crosslinking. Photoexposure was found ideal in yielding optimal patterns when employing UV exposure at 150 mW/cm^2 intensity for 4.0s, following removal of residual HFIP. Removal of the unexposed and uncrosslinked protein photoresist (via 2 hour immersion in 1M LiCl/DMSO, followed by rinsing with copious deionized water to remove solvent and traces of photoinitiator and salts) results in clearly defined micro-architectures. Using the above methods, diverse architectures depicting a range of high-resolution (μm) geometries, letters, and numbers, are able to be rapidly fabricated.

Confirmation of protein composition

Protein staining was conducted to conclusively establish the protein-based composition of microstructures. Coomassie Blue R-250 binds to proteins through a number of interactions, including ionic interactions between R-250 sulfonic acid groups and positively-charged protein amine groups, in addition to Van der Waals attractions.[308] These interactions provide a qualitative indicator for the presence of protein, with high sensitivity enabling detection down to 0.1 μg of protein. As such, the dye is easily visualized despite the low levels of protein loading per substrate (0.7 mg per

substrate, pre-development). Figure 4.15 demonstrates the characteristic blue dye binding selectively to protein micropatterns. The scalability of photolithography implies that large areas (several cm) with microstructural topology can be fabricated. This enables translation to large scale production of micropatterned silk substrates or macroscale objects with microscale control, as is seen in the patterned silicon substrate below.

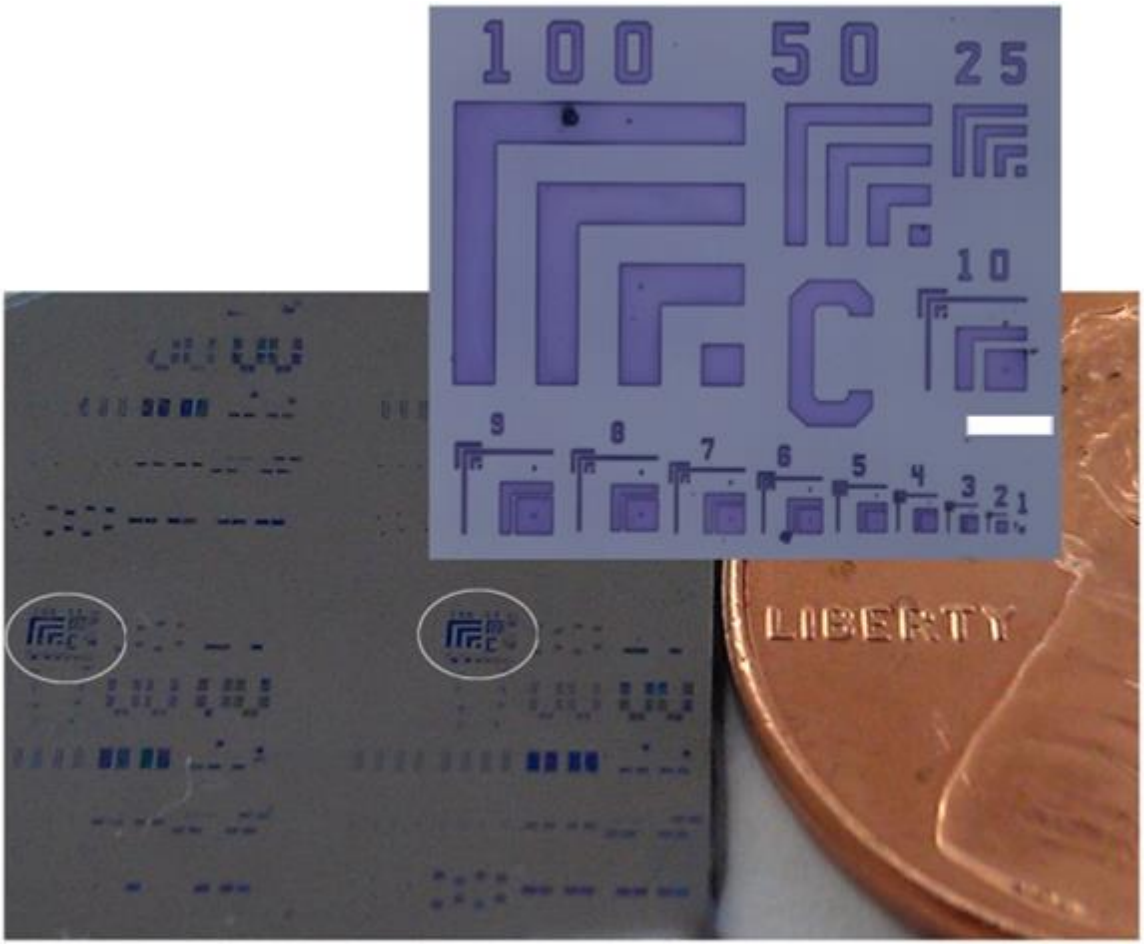

Figure 4.15. Microstructural features down to 1 μm resolution can be patterned over large areas (mm to cm) on Si. Inset shows expanded optical micrographs of a test pattern on glass formed by FPP photolithography. Patterns were stained with Coomassie Blue (R-250) stain to confirm presence of protein. Scale bar = 200 μm.

Analysis of Micropattern Topography

Atomic force microscopy (AFM) and SEM were used to characterize the surface morphology and fidelity of architectures formed. The addition of photoreactive groups makes FPP very versatile owing to its suitability for the formation of complex structures with microstructured morphologies ranging from 1 – 100 μm (Figure 4.16).

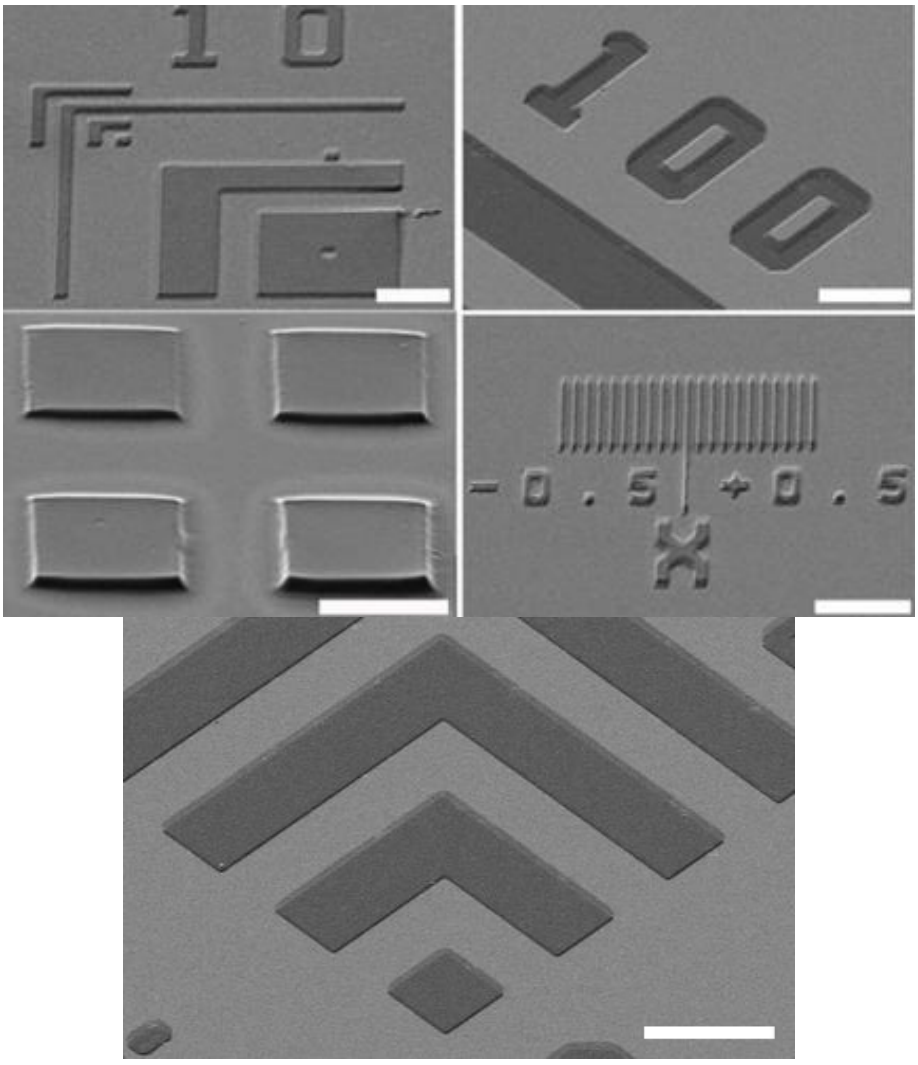

Figure 4.16. Scanning electron microscopy images of high resolution fibroin microstructure formed on silicon surfaces. Line widths of 1 μm and lower can be easily fabricated using the photolithography process described. Scale bars = 50 μm.

By controlling the thickness of the protein layer deposited on the substrate, structures of varying height in 3D can be created. This is achieved either through varying the concentration of photoactive protein (i.e., varying concentration for a volume of HFIP sufficient to cover the substrate, approximately 40 uL for a $1cm^2$ substrate) or limiting the amount of solvent deposited onto the substrate. In the latter case, it is possible to create constrained areas of FPP microstructures that are localized to specific regions of the substrate. In contrast, simply increasing protein concentration has a tendency to produce samples with poor height homogeneity distributions, due to capillary flow effects leading to protein 'pile up' at substrate boundaries.[309] This effect is observed widely in the casting of solvent-rich films, which exhibit a sufficiently rapid evaporation, that leads to insufficient leveling and an inability to 'heal' surface roughness induced by Marangoni instabilities.[310] For this reason, it is preferred to work with smaller solvent volumes for developing features with characteristic height profiles, to effectively limit spread of the protein. Patterns ranging from ~300 nm to several microns in height are easily fabricated in this manner. Figure 4.17 depicts AFM images of a '5' numeral with approximate height of 300 nm, in contrast to an adjacent '7' numeral, at 700 nm. The surface topography of the silk fibroin material is depicted below, which indicates surface roughness roughly comparable to that of a glass slide (RMS roughness of 1.8 nm over a 5 μm x 5 μm area). This low roughness and relative height homogeneity across large microscale areas (50 μm x 50 μm) demonstrates the versatility of controlling solvent parameters in order to establish control of feature height.

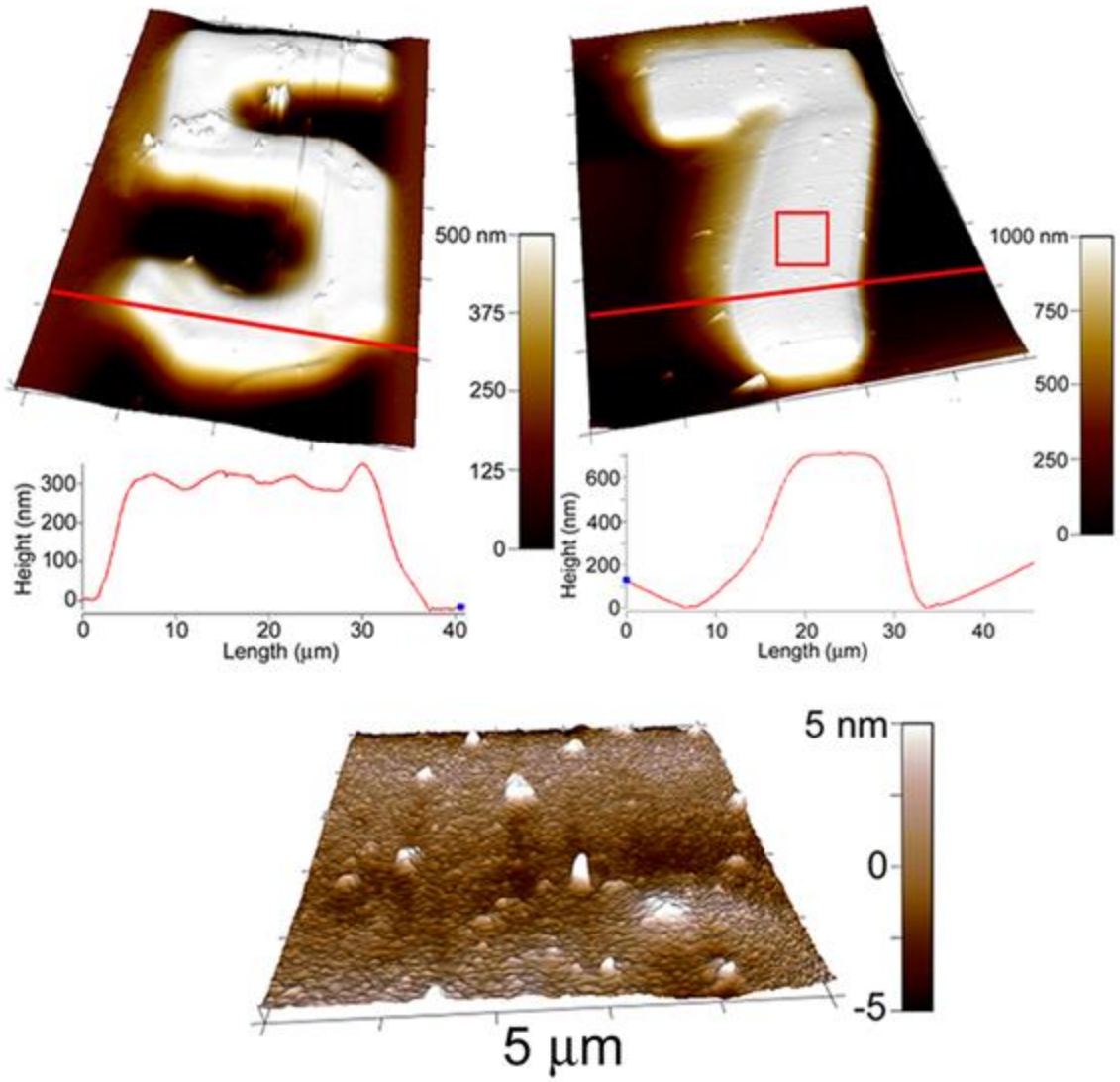

Figure 4.17. AFM topographic analysis showing two microstructures of varying height (300 nm and 700 nm) and surface characterization. Top: both features result from 0.6 mg of FPP cast per substrate: '5' (40 uL HFIP, covering entire surface of Si), and '7' (20 uL HFIP, limiting spreading to 50% of Si surface). Below: a close up of AFM surface morphology: 5 μm^2 surface of a developed feature (red square on "7") shows a surface with a roughness comparable to a glass slide (RMS roughness of the surface ~2 nm).

Fabrication of Free-Standing Microstructures

Smart materials that possess direct programmed responses to external stimuli and biomolecular recognition events are critical to the development of materials capable of binding assays and directing cellular localization.[2, 311, 312] To properly achieve the intended result, it is necessary to engineer particle shape, morphology, and chemistry according to the desired biologically-relevant function. In order to potentially move beyond forming structures on planar substrates, further strategies were thus explored for the formation of isolated shapes and morphologies of fibroin using photolithography. This provides a route towards the application of the silk protein photolithography strategy to creating monodisperse protein shapes that may be harvested for the delivery or presentation of biologically functional agents, among other applications.[313]

To date, general lithographic techniques have been characterized as being incompatible with the use organic materials and/or biomolecules, due to the significant differences between using traditional photoresist materials, and incorporating fragile biomolecules. Previously, an influential method has been demonstrated for the precise control of morphology and structure using top-down assembly for fabricating shaped, organic particles.[314] By embracing the silk photolithography platform described above, direct and rapid fabrication of proteins can be enabled, allowing the creation of biocompatible and biodegradable scaffolds containing functional agents.

Research on the fabrication of monodisperse particle shapes has demonstrated the use of fluorinated substrates for creating non-wetting substrates, allowing facile delamination and harvesting of architectures.[314] This strategy was embraced to explore

the use of various surface treatments and alkylsilanes, preserving adhesion during photoresist application and development, while enabling removal without damage to particles. The effects of silicon surface treatments are summarized in Table 4.2. While the use of FOTS provided similar observed hydrophobicity and higher theoretical hydrophobicity over that of OTS, difficulty in controlling the deposition of single monolayers, in addition to the sufficiently high hydrophobicity leading to loss of particles during development, led to OTS being embraced for surface treatments.

Table 4.2. Contact angle values for various surface treatments of silicon. OTS and FOTS enabled the development of non-adherent, hydrophobic surfaces. OTS was selected due to superior abilities in the ease of chemical vapor deposition, and favorable anti-adhesion properties.

Treatment	**Contact Angle**
Untreated Si	33.4 ± 2.7º
Piranha solution	6.8 ± 1.3º
Octadecyltrichlorosilane (OTS)	> 100º
Trichloro(1H,1H,2H,2H-perfluorooctyl)silane (FOTS)	> 100º

Fabrication of monodisperse shapes is easily achieved using the standard SPL strategy, while using a cell scraper to harvest particles into aggregates while the substrate is still partially hydrated with deionized water (Figure 4.18). Here, water is thought to act

as a ‘collection’ medium, enabling displacement of particles which are observed to aggregate on the surface of water droplets, preventing mechanical damage.

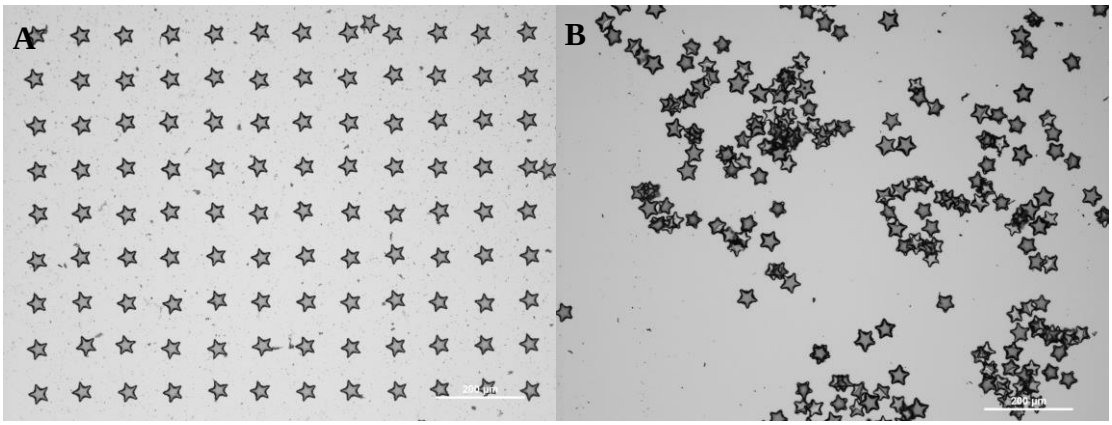

Figure 4.18. Fabrication of independent structures: monodisperse shapes of fibroin in the form of microparticles fabricated through SPL on a non-wetting substrate. (A) Stars after development, however prior to mechanical harvesting. (B) ‘Corralling’ of shapes using a standard cell scraper.

Further strategies were explored, this time using fluorescent dye loading for allowing visualization of particles to effectively demonstrate the ease of incorporation and successful entrapment of functional agents. This strategy also establishes the versatility of the SPL platform in incorporating multiple functional materials as a composite without any changes to structure or noticeable degradation. Initially, fluorescein isothiocyanate-conjugated albumin was loaded into 50 μm stars via a 1:10 mass ratio of fluorescent dye to FPP. UV exposure and development were unremarkable, without any observed leaching of dye (Figure 4.19).

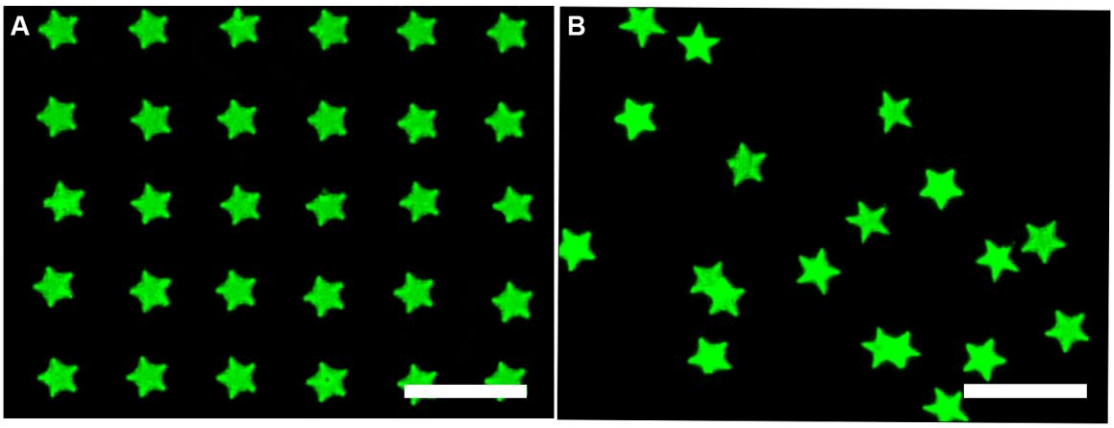

Figure 4.19. Monodisperse FPP stars, 50 μm, loaded with FITC-albumin at 1:10 FITC-albumin:FPP. Lack of detectable fluorescence in background indicates retention of dye throughout the lithography process. Images are false-colored using emission wavelength after image collection via a monochromatic camera. (A) Stars on Piranha-treated silicon surface, displaying adhesion to the underlying susbtrate. (B) Stars on OTS-treated silicon, after development and harvesting. Scale bar = 200 μm.

The combination of functional agents is possible through the blending of FPP particles, where the inclusion of a particular molecule is done so based on shape. Using procedures similar to above, a range of architectures was fabricated using FITC-albumin-loaded triangles, and Alexa Fluor 555-loaded circles (Figure 4.20). Shapes were photoexposed on a shared substrate, by selectively exposing regions coated with a specific dye using desired regions of shapes on the photomask. Development and rinsing is conducted as described for single shape, monodisperse particles, to yield substrates of dispersed particles. Alternatively, harvesting by pipette is possible, through pipette collection and introduction onto a single, shared substrate. This monodisperse shape

fabrication strategy yields a qualitative tool for gauging the cargo of a particle on the basis of shape, enabling the rapid identification of particle contents. Thus, the ability to accurately control size, shape, and particle cargo is of great value in the rapid development of drug delivery and molecular sensing tools, for use in emerging biotechnology applications.

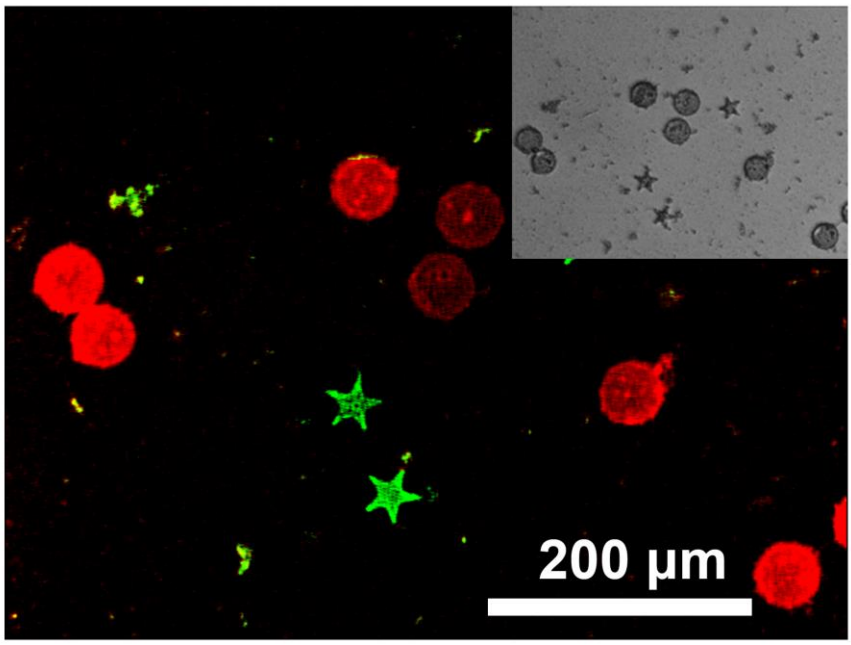

Figure 4.20. Composite of monodisperse stars and circles: FPP stars, 50 µm, loaded with FITC-albumin at 1:10 albumin:FPP, and circles, 50 µm, loaded with Alexa Fluoro 555-ovalbumin at 1:10 albumin:FPP. The emission wavelength of FITC is 520 nm (green), and Alexa Fluor 555 emits at 565 nm (red).

4.3.5 Characterization of the Stability of Crosslinked FPP

Proteolytic Degradation of Crosslinked FPP

Fibroin from silk cocoons exists in a fibrous and intrinsically insoluble form but can be rendered soluble, typically using a solution of 9.3M LiBr.[21] This activated fibroin can dissolve in water and various solvents, facilitating processing into specific architectures. The degree of solubility of architectures cast from soluble fibroin is highly tunable through the use of treatments to increase β-sheet crystallinity, which imparts water insolubility to the fibroin.[64, 113, 315] This solubility is an important consideration for ensuring silk degradation across various applications.[85, 255, 316] In the native state, fibroin has been established to undergo enzymatic biodegradation *in vitro*, exhibiting predictable long-term degradation characteristics.[43, 66] With the assistance of the aforementioned treatments, fibroin is thus able to act across a wide spectrum of solubility, and effectively demonstrate behavior from controllable dissolution and degradation, to high chemical stability and solvent resilience.

In contrast to native fibroin films that readily dissolve in water, the addition of photoactive moieties to fibroin results in a loss of aqueous solubility. Crosslinked films of FPP are observed to remain relatively unchanged and undegraded after immersion in deionized water. This is attributed to the presence of nascent methacrylate substituents and chemical crosslinks in photocrosslinked FPP, which has unknown effects on the long-term degradation properties of FPP. However, conjugated methacrylate crosslinks have been previously associated with decreased degradation rates as the density of crosslinks increases.[317] For this reason, it was of interest to investigate the degradation

behavior of FPP, to evaluate the effects of methacrylate-based crosslinks, and the potential for FPP to act as a bioresorbable material.

The *in vitro* stability of FPP has been evaluated through use of proteolytic degradation. In evaluating fibroin films, as-cast fibroin is observed to rapidly solubilize in PBS buffer. In contrast, FPP films are intact and are relatively stable even after 15 days in PBS. However, in an aqueous solution of protease (Protease XIV from *S. griseus*, ≥3.5 units/mg), FPP films degrade significantly over the same 15 day time period. This was observed quantitatively by measurement of film mass and thickness over time (Figure 4.21). Figure 4.21 (A)-(B) establishes the film mass retention (remaining dried mass as a percentage of starting mass) and thickness over time. SEM images were taken of cross-sections of 3 films on days 0, 7, and 15 (Figure 4.21, C-E).

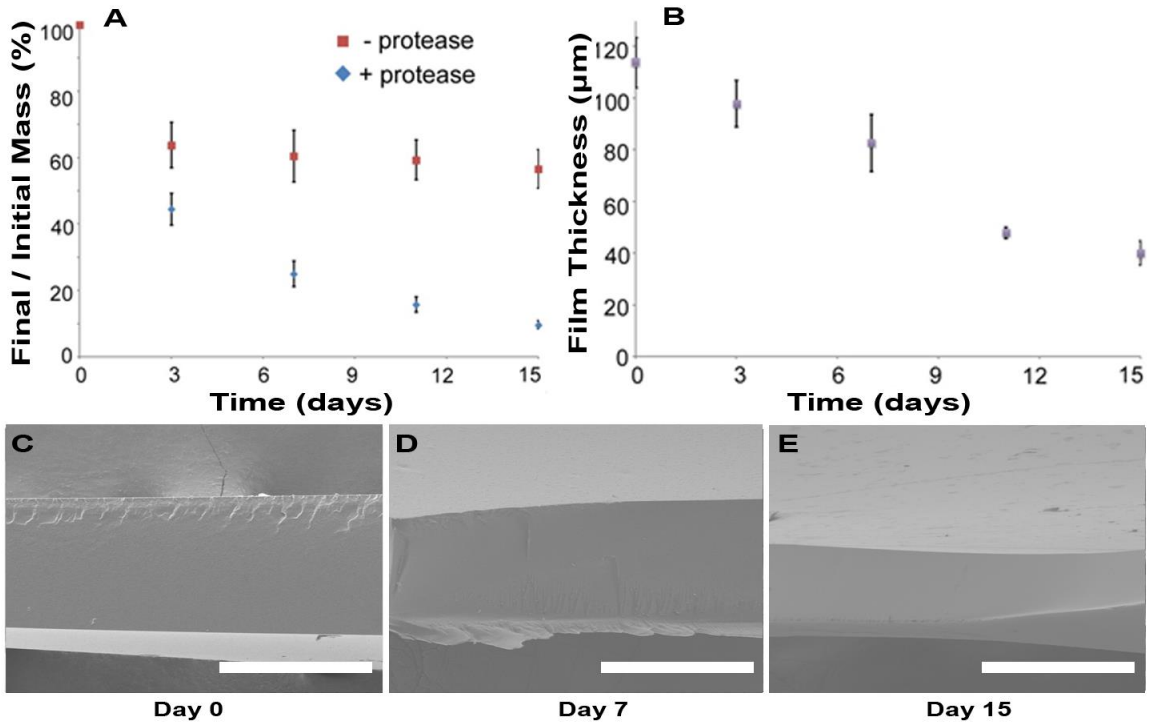

Figure 4.21. Analysis of the degradation profile of the FPP crosslinked films. In the absence of protease the films remain largely intact over a period of two weeks. In the presence of protease (1 unit/mg of FPP), the films degrade as observed by the film thickness and mass loss. The SEM images below show the cross-section of the films. Scale bar = 100 µm.

The initially observed mass loss for FPP controls (absent protease), occurring prior to day 3, is attributed to the efflux of latent photoinitiator from the films, which comprises ~25% of the total mass. After a 15 day time period, film surface morphology is significantly altered, and immediately thereafter, a loss of structural integrity and fragmentation of films is observed as FPP degrades into smaller, soluble polypeptides (Figure 4.22). In the

case of cast fibroin films, since they immediately degraded in water, there was no film to follow over the time of the experiment.

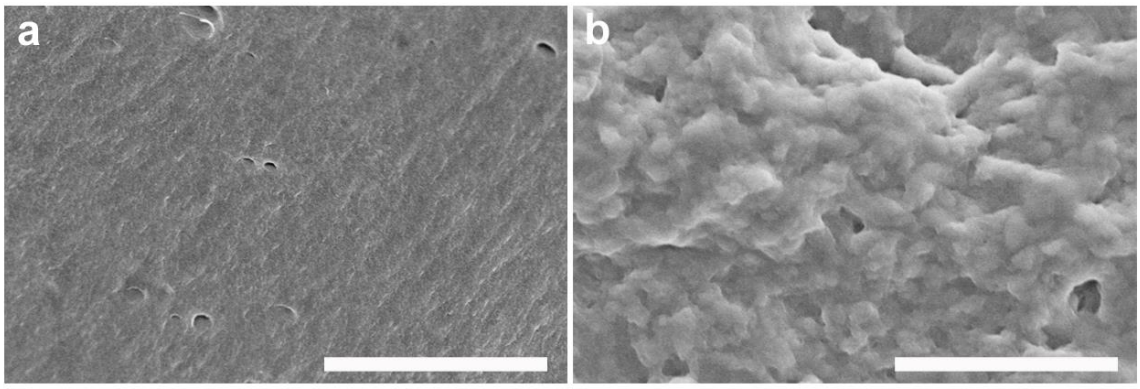

Figure 4.22. FPP undergoes a significant change in surface morphology during a 15 day proteolytic degradation study: (a) 0 day control, (b) 15 days in protease XIV. Scale bar = 5 μm.

The degradation behavior of FPP structures is also tunable. At lower crosslinking of the material, the degradation is much more rapid. For instance, for FPP films with 0.1% initiator (w/v), ~40% of the mass is lost within 3 days and the films are fully fragmented by day 7. The enzymatic degradation of FPP demonstrates its potential to act as a material that can retain its structure prior to bioresorption.

Mechanical analysis of Crosslinked FPP

The crosslinking of the biopolymer also confers a benefit in terms of mechanical strength. The mechanical properties of native fibroin and FPP were compared via AFM-

based nanoindentation studies.[236, 237, 286] A stiff diamond like carbon coated cantilever (*k = 48 N/m*) was used to indent thin films of each material using a constant force of 1 µN, at 1 µN/s. These constant force indents were observed to yield force curves with greater reproducibility and less adhesion than constant indent curves, enabling a more reliable calculation for Young's modulus. The elastic modulus for fibroin was calculated via the Hertz model, and determined to be 11.0 ± 0.9 GPa, a value that is close to its reported values as one of the strongest and toughest natural fibers.[318] Photocrosslinked FPP (0.6 % w/v crosslinker) was measured to have an elastic modulus of 15.6 ± 1.1 GPa (Figure 4.23B). Representative force-distance curves for the nanoindentation of the two materials are presented (Figure 4.23A).

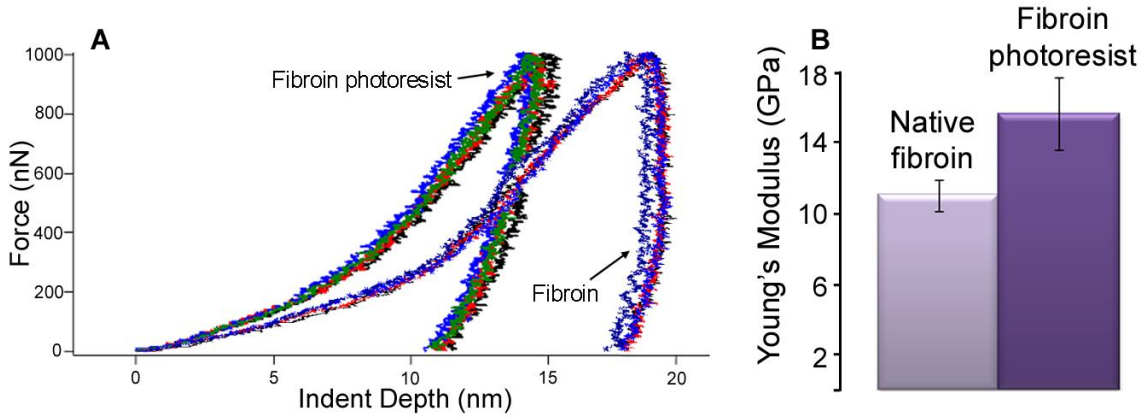

Figure 4.23. (A) Representative AFM nanoindentation curves obtained from indenting surfaces of fibroin (dashed) and FPP (solid) thin films. The force-distance indent curves were fit using the Hertz model to obtain the elastic modulus and stiffness of the material. (B) FPP is observed to have a Young's modulus of 15.6 ± 1.1 GPa, which is significantly higher than that of native fibroin, at 11.0 ± 0.9 GPa.

It is hypothesized that the increased crosslinking between the biopolymer strands can influence the modulus of the material. By controlling the precursors and the photocrosslinking steps, it is possible to tune the mechanical properties of the fibroin photoresist. For instance, an increase in photoinitiator concentration results in an increase in crosslinking density of the FPP as observed via FTIR (Figure 4.24).

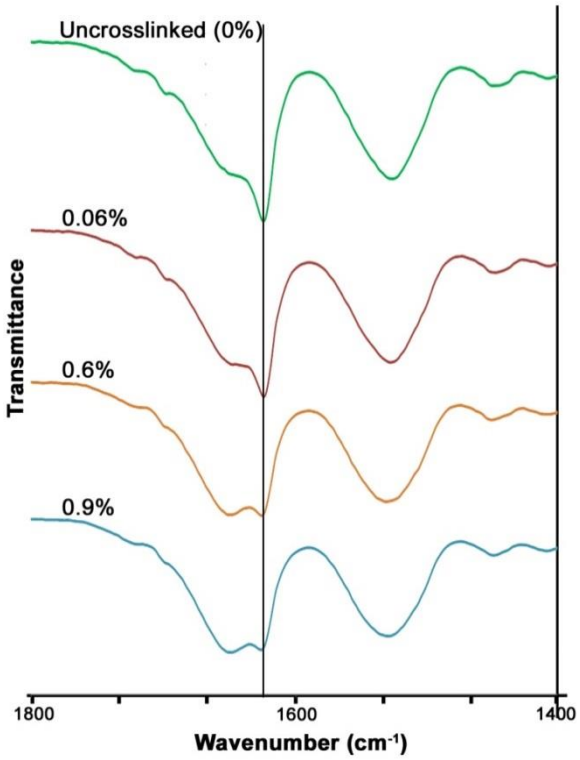

Figure 4.24. FTIR data on films of FPP to investigate extent of crosslinking. The extent of crosslinking was monitored by following the 1630 cm^{-1} (terminal C=C stretch) peak for samples with 0% photoinitiator (uncrosslinked films) to higher concentrations of photoinitiator (0.9%). Due to the photopolymerization reaction, as the concentration of photoinitiator increased, vinyl groups are consumed reflecting an increase in crosslinking.

In the experiments reported, 0.6% (w/v) photoinitiator was used which was found to be optimal for high-fidelity microstructures. This tunability of the mechanical properties of the FPP coupled with direct cellular attachment on a degradable, yet mechanically strong matrix without the use of cell adhesion peptides (e.g. RGD) offers new possibilities in using this material for load bearing applications such as bone tissue engineering.[319]

4.3.6 Cell Culture Studies on Silk Fibroin Scaffolds

Films of native fibroin have been demonstrated to support cellular culture and proliferation.[320] Fibroblasts cultured on these films demonstrate rapid adhesion and elongation, preferring to adhere to stiffer regions of the substrate. However, in the case of FPP, the introduction of hydrophobic methacrylate groups onto fibroin was expected to result in a decrease in the hydrophilicity typically associated with native *B. mori* fibroin.[321] In order to assess the ability of photoactive fibroin to act as a substrate for supporting cell growth, FPP microstructured scaffolds were fabricated with a range of architectures. The micropatterning of FPP on a TPM monolayer creates distinct raised FPP layers with contrasting, unpatterned hydrophobic regions. The relative hydrophobicity of the TPM monolayer is associated with favorable cell adhesion, spreading and proliferation, providing an opportunity to study the influence of FPP on spatial control of cell adhesion.[275] Fibroblast cells were seeded at a density of $7500/cm^2$ on micropatterned surfaces and incubated for 3 – 4 days, with polarized light microscopy being used to assess cell proliferation at specified time intervals.

At 48 hours, human fibroblasts displayed a more significant localization on the fibroin protein patterns in comparison to the surrounding methacrylate-functionalized glass surface (Figure 4.25). The human fibroblasts are observed to elongate on and around the base of FPP structures, effectively maximizing their area of contact with FPP.

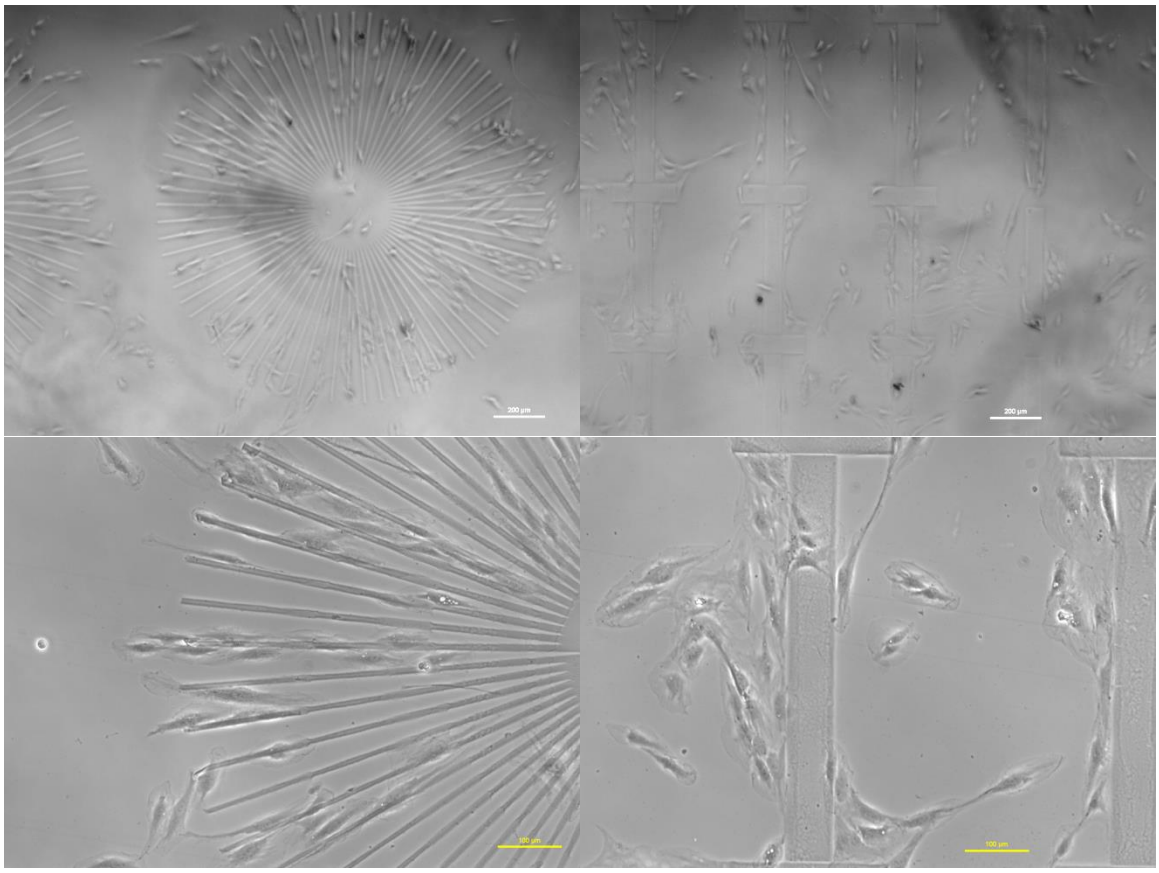

Figure 4.25. Patterning of human fibroblast cells on patterns of FPP. Fibroblast cells display a preferential attachment to pattern surfaces and sidewalls versus attachment to hydrophobic glass. Scale bar = 200 μm (white), 100 um (yellow).

To investigate the influence of the substrate, murine fibroblasts were similarly cultured onto grids of 10 µm lines of FPP, with 200 µm spacing, and onto TPM-functionalized (methacrylate-functionalized) glass controls. In the absence of FPP, fibroblasts are observed to indiscriminately spread and proliferate across the substrate, owing to the hydrophobic surface presented by TPM functionalization (Figure 4.26 B). When FPP patterns are present, fibroblasts migrate to and cluster on the raised FPP material, which is indicative of specific adhesive processes resulting in preferential adhesion to the FPP material (Figure 4.26 A).

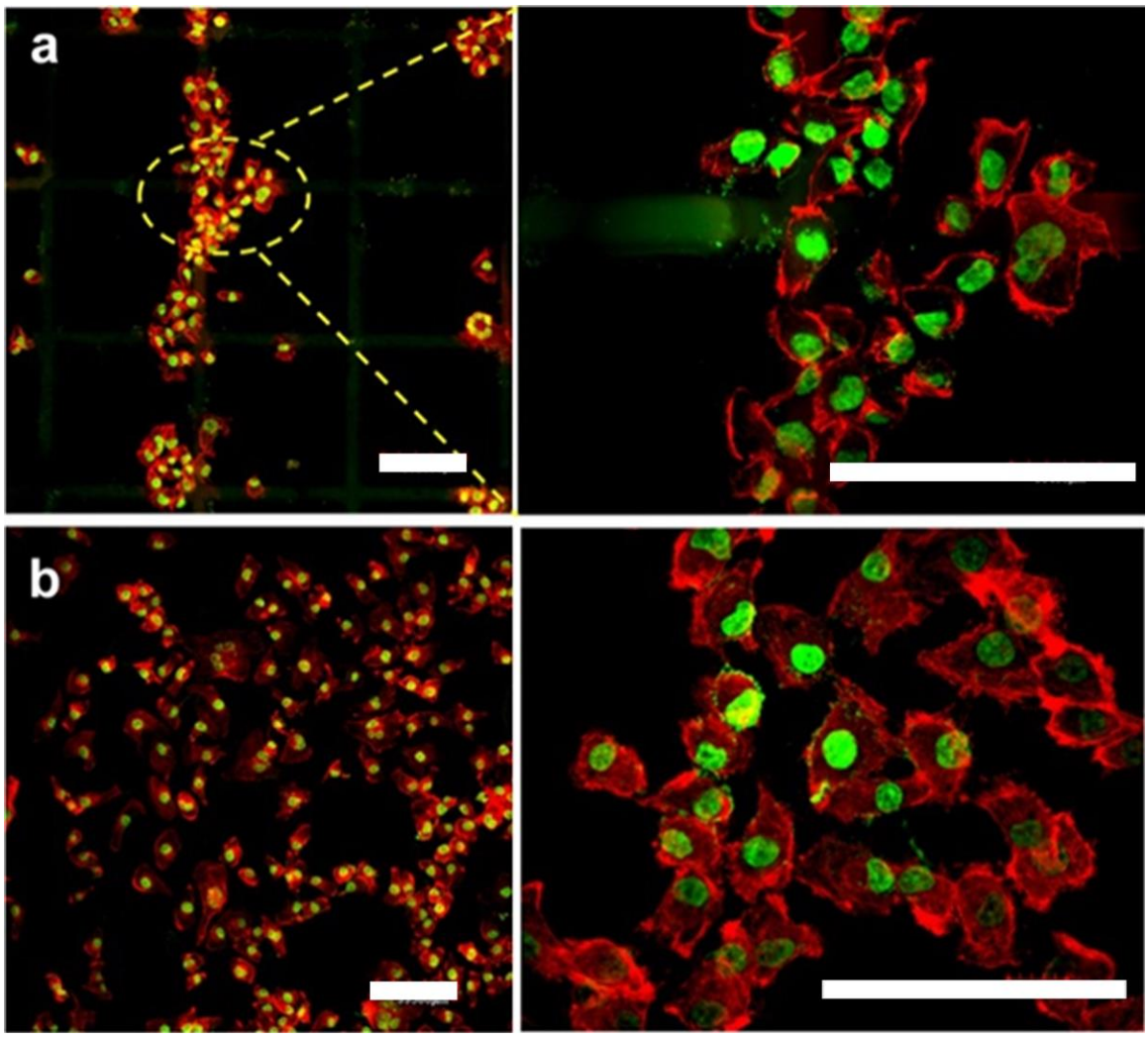

Figure 4.26. (A) Confocal light microscopy of murine fibroblasts grown on fibroin grids. Cells are observed to clearly align along the patterned fibroin lines. (B) In control experiments on silicon surfaces without grids, cells spread non-specifically on the surface. Scale bar = 100 μm.

Focal adhesion of the fibroblasts to the underlying fibroin micropatterns was studied by staining for the presence of focal adhesion complexes using a fluorescent anti-vinculin monoclonal antibody (Figure 4.27). Vinculin is an actin-binding protein, which,

when conjugated to a fluorescent dye, acts as a marker for cell-cell and cell-extracellular matrix adhesion junctions.[322] Here, the presence of focal adhesion complexes is indicated by green fluorescence signal. These structural membrane-associated focal adhesion complexes function as nucleation sites for actin filaments connecting the ECM on the outside to the intracellular actin cytoskeleton. Cells were observed to be well anchored to the patterned fibroin, effectively demonstrating that FPP patterns can be used to spatially micropattern and direct cellular attachment.

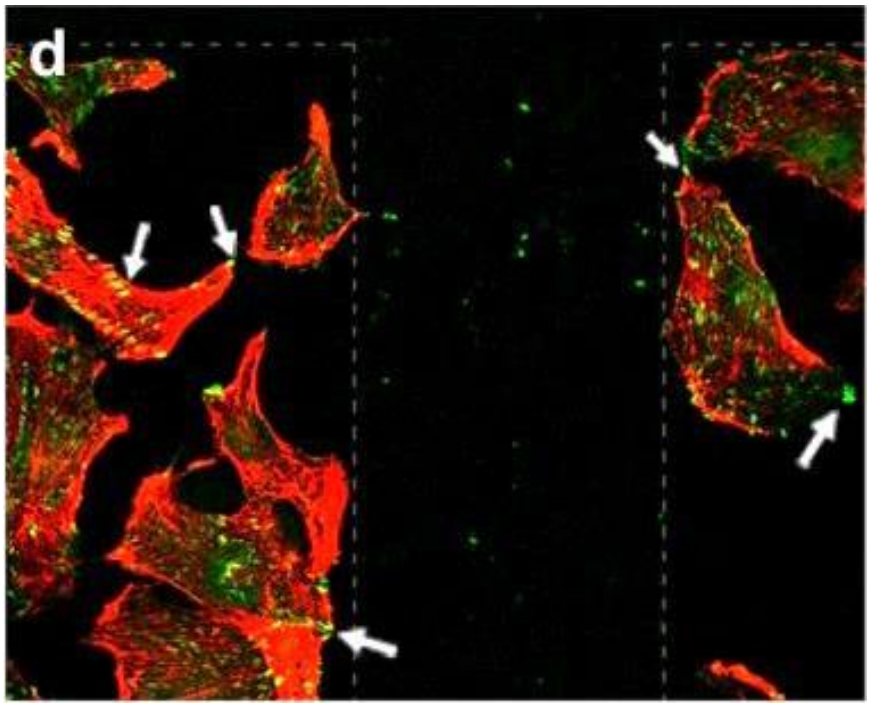

Figure 4.27. Focal adhesion contacts (green) to the underlying fibroin micropatterns (center) are revealed using anti-vinculin monoclonal antibody and FITC-conjugated secondary antibody. White arrows indicate example focal adhesion junctions.

4.4 Conclusions

In summary, in this chapter, a platform termed "Silk Protein Photolithography" (SPL) for the rapid patterning of protein architectures across 4 orders of magnitude (1 μm to cm) is demonstrated via a novel photoreactive silk fibroin. While optical lithography has been used to indirectly pattern proteins in prior works, *direct* patterning of proteins to form high fidelity and high-resolution structures still remains a challenge. The inherent simplicity of the process described coupled with mature photolithographic techniques from the microelectronics industry allows formation of complex structures that can be precisely tailored in terms of shape, size (nm to μm). Furthermore, the high degree of reproducibility, indicated by the observation of similar results across multiple batches of silk, helps to alleviate concerns of the potential variability in naturally sourced materials.[117] The tunable mechanical strength and degradation of FPP presents opportunities for the fabrication of sustainable, silk-based microdevices. FPP can be used for further synthesis of functional nanomaterials through bio-templating or in prototyping tools such as multiphoton lithography—areas which have typically been the purview of synthetic polymers.[323-325] The use of a developing agent with established effects on protein structure, potentially enables recovery and reuse of the fibroin-methacrylate conjugate, providing an avenue to a renewable means of protein photo-processing. "Photoresist-like" natural silk with light-activated direct-write processes can be adapted for wide ranging applications in biological arrays, tissue engineering and drug delivery. Independent, flexible and optically transparent silk protein shapes can be fabricated and harvested for drug delivery applications. Organic and inorganic molecules can be coupled

to enhance fibroin applications for cell guidance on micro and nanostructured wires and scaffolds.[42] Furthermore, these results establish a potentially versatile method for conducting protein photolithography on structurally and chemically distinct protein species.

[This chapter contains results that have been previously published: Kurland, N.E., et al., Precise Patterning of Silk Microstructures Using Photolithography. Advanced Materials, 2013. 25(43): p. 6207-6212.]

CHAPTER 5

APPLICATION OF SILK PROTEIN PHOTOLITHOGRAPHY TO THE PHOTOPATTERNING OF SILK SERICIN

5.1 Introduction

As a natural, renewable silk protein, sericin provides an excellent building block for producing tailorable, biocompatible materials to address a wide range of biotechnological needs. The cytocompatibility and water-soluble nature of sericin makes it ideal for cellular culture, enhancing cell attachment, improving cellular growth, and accelerating proliferation when added to culture media.[45, 74, 235] Despite these unique physicochemical properties, the limited ability to form sericin into complex patterns necessitates implementing a novel approach for its development into biologically-relevant architectures.[73, 75] In comparison, the plethora of knowledge available for silk fibroin has enabled it to engage in a variety of physical and chemical modification strategies, to yield a range of biofunctional silk materials.[16, 21] Furthermore, despite reports on its intrinsic biocompatibility and that the perceived inflammatory behavior of silk sericin is often when it is present in conjunction with fibroin, sericin has had an uphill climb in its overall acceptance in the biomaterials field. As a natural silk biopolymer, sericin provides an equivalent green chemistry alternative to the use of

fibroin and synthetic materials for applications in bioelectronics, tissue engineering and photonics.[32, 254] A key challenge lies in the development of chemical processing strategies which take into account environmental factors, particularly in the use of other benign chemical species.

Increasing the use of biologically-derived materials and enabling sustainable manufacturing have emerged as important considerations in the development of the next generation of biologically-integrated devices. Integrating high-resolution fabrication platforms using materials from biological precursors to form rationally designed and engineered structures have been proposed as feasible routes not only for viable bionanomanufacturing, but also to form organic devices that can interface and interact with biological systems.[32, 326, 327] Silk sericin demonstrates an important intermediate bridging this evolution of sustainable manufacturing with the limitations in silk manufacturing strategies. Some of the key challenges in this process lie in the development of techniques to fashion sericin, and biomaterials in general, into the structural components of an electronic or photonic device with desired spatial resolution, complexity or mechanical properties. This problem extends to the fabrication of intricate microstructured scaffolds for directing cellular growth in two and three dimensions, which have not been demonstrated using existing sericin processing strategies.[313, 328-330] One potential solution to this lies in the applying photolithographic processing to sericin as a means of enhancing stability and allowing sustainable processing using a natural, water-soluble biomolecule.[278, 331]

In the previous chapters, sericin was investigated for development into functional protein architectures by taking advantage of intrinsic properties and engineered assembly

techniques. This work highlighted the ability of sericin to self-aggregate into highly-ordered architectures, and further took advantage of its water-soluble state to demonstrate the implications in improving stimuli-response of silk-based materials. These studies noted the lack of durability of sericin architectures in aqueous environments—sericin was not prevented from re-solubilizing, leading to partial loss of structural features. Aside from common de-solvation methods using alcohols to improve β-sheet crystallinity, limited options exist for improving this stability.[77, 90] Furthermore, the loss of native protein structure associated with inducing a crystalline secondary structural conformation, has the potential to negatively impact mechanics and biological interactions.[23, 332] On the basis of the silk protein photolithography (SPL) platform described in the previous chapter, by taking advantage of similar reactive amino acids, the process of fibroin photolithography can be adapted for sericin processing. This expands the flexibility of the silk protein photolithography platform, allowing the incorporation of environmentally favorable water-based processing strategies.

In this chapter, translation of the silk protein photolithography (SPL) platform to the patterning of silk sericin is considered, effectively demonstrating the applicability of SPL to a chemically and structurally-distinct silk protein. In contrast to fibroin, which supports cellular adhesion and proliferation, sericin demonstrates far greater bioactivity and specificity to use for tissue engineering applications. The absence of cell-recognition integrin-binding sequences in *B. mori* fibroin imply that cellular interactions observed in the previous chapter are attributable to the morphology of fibroin, as specific biological interactions have not been conclusively established.[333, 334] On the other hand, sericin has well-documented bioactive properties, promoting cellular adhesion and proliferation

across multiple cell lines.[76, 235] To date, this activity has been extensively investigated, and is hypothesized to be a result of serine-rich repeats facilitating specific cellular adhesion.[70, 74] This observation allows sericin to potentially serve as cell-guiding material, inducing specific adhesive properties as a biomaterial. Thus, the preservation of serine-rich regions of sericin is considered critical to maintaining bioactivity. In the previous chapter, partial conversion of nucleophilic centers, such as serine residues, was noted through the isocyanate bioconjugation step of SPL. In exchange for demonstrating the versatility of the SPL platform to species other than fibroin, this platform opens further applications to sericin owing to its ability to produce tailorable, stable microarchitectures.

The modular biochemical modification of sericin may therefore be used to create a photoactive hydrophilic protein species—sericin protein photoresist (SPP). This material can be combined with photolithography to generate micro and nano-scale architectures over large areas in a strategy that parallels the one discussed in the previous chapter. Silk sericin thus provides a structurally- and chemically-distinct renewable protein that provides a route to the "green synthesis" of engineered structures. Due to the site-specific modification strategy, the resulting silk sericin conjugate is demonstrated to retain fundamental properties of the protein, while possessing nascent photoreactive capacity. Photoactive sericin conjugates are combined with optical lithography to create high-resolution patterned architectures (μm) across macroscale areas (cm) conducive to cellular attachment and proliferation. The application of these microstructured substrates as cellular scaffolds for the directed culture of osteoblasts is further demonstrated. The facile processing of this photoactive sericin into complex architectures, while preserving

intrinsic protein properties, provides diverse opportunities for this protein in the formation of scaffolds for tissue engineering, and further advances in biomedical engineering (Figure 5.1).

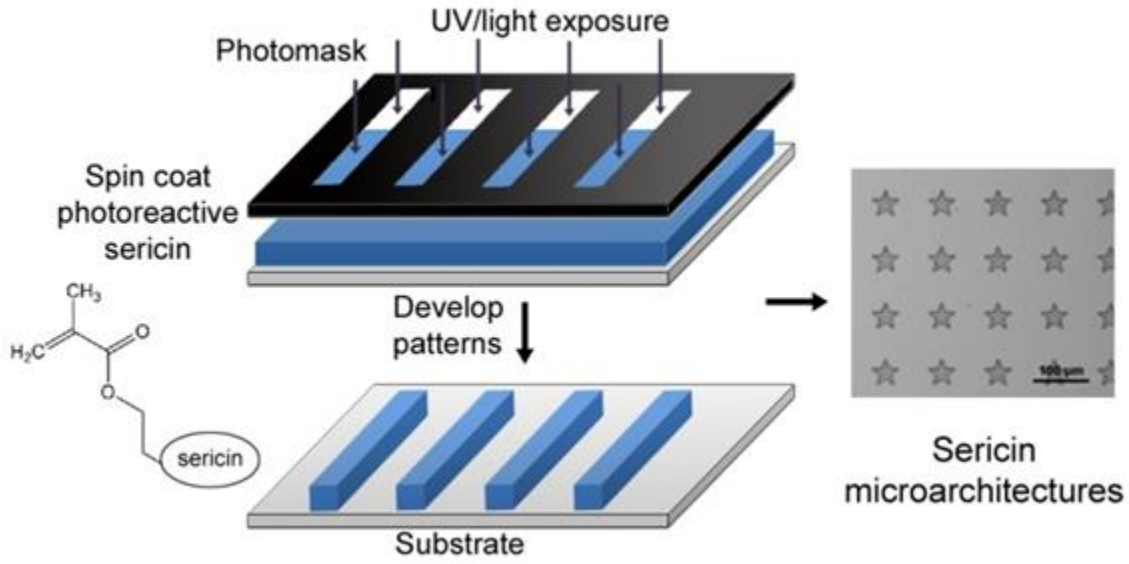

Figure 5.1. Schematic of fabrication of sericin microstructures using silk protein lithography.

5.2 Experimental Section

5.2.1 Materials

Pure sericin protein (Wako Chemicals USA, Richmond, VA) and 2-isocyanatoethyl methacrylate (IEM, Sigma-Aldrich, St. Louis, MO) reagents were utilized for chemical conjugation. Anhydrous dimethyl sulfoxide (DMSO) and anhydrous

lithium chloride (LiCl) were utilized as a solvent for the reagents. 2,2,2-Trifluoroethanol (TFE, 99.8%, Sigma-Aldrich, St. Louis, MO) was used as a solvent for the sericin-methacrylate conjugate. Irgacure 2959 photoinitiator (1-[4-(2-Hydroxyethoxy)-phenyl]-2-hydroxy-2-methyl-1-propane-1-one, Ciba Specialty Chemicals, Tarrytown, NY) was employed as a free-radical photoinitiator. Standard 75 x 25 cm glass slides (Fisher Scientific, Fair Lawn, NJ) and P-type <111> silicon (Si) wafers were utilized as substrates. Hydrogen peroxide (30%, H_2O_2) and sulfuric acid (95 - 98%, H_2SO_4, Sigma-Aldrich, St. Louis, MO) were employed for substrate cleaning and hydroxylation. 3-(trichlorosilyl)propyl methacrylate (TPM, Sigma-Aldrich, St. Louis, MO) was used for functionalizing substrates to allow photoresist adhesion. Nanopure, deionized water (18.2 MΩ•cm, Millipore, Billerica, MA) was used as a developing agent. Protein staining was conducted using Coomassie Brilliant Blue R-250 (Sigma-Aldrich, St. Louis, MO) and glacial acetic acid (Fisher Scientific, Fair Lawn, NJ). Osteoblast mineralization media was prepared using Dulbecco's Modified Eagle's Medium (DMEM) powder, ascorbic acid, gentamicin, calcium chloride ($CaCl_2$), sodium bicarbonate ($NaHCO_3$), HEPES buffer, antibiotic antimycotic solution (10,000 units penicillin, 10 mg streptomycin and 25 μg amphotericin B per mL), and fetal bovine serum (FBS), all of which were obtained from Sigma-Aldrich (St. Louis, MO).

5.2.2 Synthesis and purification of photoreactive sericin

Photoactive silk sericin conjugates were synthesized in a similar fashion to the process shown in the previous chapter, for silk fibroin conjugation. Methacrylate grafting

was conducted via chemical conjugation between sericin and the reactive isocyanate group of IEM. The conjugation was conducted in an anhydrous solvent system of 1M LiCl in DMSO, to prevent premature isocyanate reaction.[278] Lithium chloride and all related glassware was thoroughly dried at 150 ºC for 24 hours prior to use, while silk sericin was dried at 70ºC to remove residual moisture prior to reaction. Sericin (100.0 mg) was suspended at 1% (w/v) in a solution of 1M LiCl/DMSO in a 25 mL round bottom flask. To enable dissolution of sericin, the flask was stirred at 60 ºC in a dry N_2 atmosphere for 45 minutes, at which point no solids remained suspended in solution. A stoichiometric amount of IEM was added to the round bottom flask, which was continuously purged with dry N_2. The reaction was allowed to proceed to completion at 60 ºC for 5 hours, after which the product was precipitated out into cold ethanol, and centrifuged. The protein pellet was then washed with a mixture of cold ethanol/acetone and centrifuged, and this process was repeated three times. The remaining precipitated mass was then frozen at -80 ºC and lyophilized for 48 hours to yield a brilliant white powder of sericin-methacrylate.

For the purposes of calculating reaction stoichiometry and degree of conjugation, an average molecular weight of 100 Da per residue was used.[278] In comparison, by using the core repeat sequence of sericin, the average molecular weight per residue is 95 Da (via 38-mer core sequence composition, SSTGSSSNTDSNSNSVGSSTSGGSSTYGYSSNSRDGSV), which is increased by larger amino acids at chain termini.[70] Reaction recovery was calculated as a ratio of final dry mass to initial sericin mass, assuming complete recovery of sericin following the reaction. Henceforth, this photoreactive version of sericin that behaves as a negative

photoresist will be referred to as a sericin protein photoresist (SPP).

5.2.3 IR Spectroscopy

To confirm the presence of the methacrylate moiety on sericin, Fourier transform infrared spectroscopy (FTIR) was conducted on unmodified sericin and sericin-methacrylate films cast from TFE solvent, using a Nicolet iS10 FTIR spectrometer. The spectrometer was operated using a Smart iTR ATR (Attenuated Total Reflectance) sampling accessory with a low-penetration depth Ge crystal. Spectral data was collected in the region of 4000 - 1000 cm^{-1} at 4 cm^{-1} intervals, and averaged over 32 scans.

5.2.4 Surface Functionalization of Silicon and Glass Substrates

Silicon wafers were cut into 1 x 1 cm^2 squares for use with micropatterning experiments. Glass slides for sericin-methacrylate scaffold fabrication were segmented into 0.75 x 0.75 $in.^2$ pieces to facilitate use in tissue culture plates. Surfaces were initially treated with Piranha solution (3:1 98% H_2SO_4:30% H_2O_2) to hydroxylate the surface for further chemical modification (*Caution: Piranha solution reacts violently with organic materials and must be handled with extreme care*). Following treatment, surfaces were washed with copious deionized water and ethanol and dried at 150 °C on a hot plate. Functionalization to silanol groups was conducted using 3-(trichlorosilyl)propyl methacrylate (TPM) by means of a chemical vapor deposition (CVD) technique.[281, 282] 100 µL TPM was added to a desiccator containing the substrates. The chamber was

then drawn down to 0.4 bar and left for a period of 12 hours for the TPM to react and present covalently bound functional groups. Methacrylate-modified surfaces were extensively washed with hexane and water, and dried before further use.

5.2.5 Silk Protein Photolithography (SPL) of Sericin

Micropatterns of silk sericin protein photoresist (SPP) were fabricated using contact photolithography. SPP was dissolved at 2% (w/v) in TFE with 0.5% (w/v) of Irgacure 2959 photoinitiator and mixed at low speed for 12 hours, at which point the SPP is observed to be fully dissolved. The SPP solution was cast onto methacrylate-functionalized glass at 0.3 mg sericin-methacrylate per substrate, and spread via gentle rotation of the substrate. An ambient 'pre-bake' step was then conducted, in which substrates are allowed to sit at ambient temperature for 10 minutes to allow excess photoresist solvent (TFE) to evaporate, and decrease photoresist to photomask adhesion. Contact photolithography was performed in direct contact with SPP films, via an OmniCure S1000 UV Spot Curing lamp (Lumen Dynamics, Ontario, Canada) equipped with a 320 – 500 nm filter. Substrates were exposed at 150 mW/cm^2, for 3.0 seconds exposure through a chrome mask. Development of uncrosslinked and unexposed protein photoresist was performed using deionized water (18.2 MΩ·cm) for 2 hours followed by copious rinsing with deionized water and ethanol. Substrates with the developed protein patterns were then dried in a gentle stream of dry N_2.

5.2.6 Protein Microstructure Staining

To establish the success of the photopolymerization steps and to verify that the structures formed were indeed protein, staining of the microstructures was performed via the Coomassie Blue R-250 dye. A modified rapid stain protocol was employed, in which substrates were stained in a solution of 10% acetic acid in water, containing 60 μg/ml Coomassie Blue R-250.[283] The qualitative appearance of protein-bound dye occurs after 30 minutes, and staining was allowed to proceed for 60 minutes to provide sufficient dye intensity for visualization. Immersion in deionized water for a period of 60 minutes was conducted to remove unbound dye from microstructures and substrates. Analysis of dye localization was subsequently conducted through digital imaging and optical microscopy.

5.2.7 Scanning Electron Microscopy (SEM)

Scanning electron microscopy (SEM) was conducted using a JEOL high-resolution field emission microscope, at a 2.0 kV accelerating voltage. Prior to SEM, patterned substrates were sputter coated with 15Å platinum to enhance conductivity prior to imaging (Denton Vacuum Desk V cold sputtering system, Denton Vacuum, Moorestown, NJ).

5.2.8 Atomic Force Microscopy and Nanomechanical Analysis

Atomic Force Microscopy (AFM) analysis of surface morphology was performed on an Asylum Research MFP-3D AFM (Santa Barbara, CA), operating in AC mode. The AFM was further used to determine Young's modulus of the sericin-methacrylate conjugate, through AFM-based nanoindentation, with an AC240TS tip (nominal k = 2 nN nm^{-1}, Olympus, Japan).[236, 237, 286] All force constants were measured prior to the experiments using the thermal fluctuation method. Films (>1 μm thickness) were indented in air with 10 indents at 3 discrete locations under a constant load of 500 nN, to a total depth of ~10 nm. Force-distance curves were subsequently analyzed via fitting tip extension data to the Hertz model to determine values for Young's moduli.

5.2.9 *In Vitro* Proteolytic Degradation

Crosslinked films (~ 5 mg) of crosslinked sericin prepared via silk protein photolithography, as described above, with a single experimental modification—films were cast from 100 μL of total solvent to limit the spread of the film, and thus maximize film thickness. Crosslinked films were initially weighed in the dry state, and then incubated at 37 °C in a solution of (1 unit/mg protein) Protease XIV (*Streptomyces griseus*, ≥3.5 units/mg, Sigma-Aldrich) in PBS. Films incubated in PBS in the absence of protease acted as negative controls. The Protease XIV and control solutions were changed initially at 3 days, and subsequently every 4 days thereafter to ensure the preservation of protease enzyme activity (Protease XIV activity is > 80% following 3 days of incubation).[66] At designated time points, samples were removed from the

buffer, and rinsed with deionized water before drying for analysis—films were first weighed and then cryofractured in liquid N_2 for SEM study.

5.2.10 Human Osteoblast Cell Culture

Normal human osteoblasts were kindly provided by the laboratory of Dr. Xuejun Wen (Department of Chemical and Life Science Engineering, Virginia Commonwealth University, Richmond, Virginia). Cells were seeded in 75 cm^2 culture flasks and incubated at 37 °C in a 5% CO_2 atmosphere in osteoblast media. Osteoblast mineralization media was prepared via reconstitution of 13.5 g DMEM high glucose powder with 1L distilled water, and supplemented with 2.54 g $NaHCO_3$, in addition to 0.0588 g ascorbic acid, 0.588 g gentamicin, 0.0783 g $CaCl_2$, 3.905 g HEPES buffer, and 20 mL antibiotic antimyotic solution. The pH was then adjusted to 7.35 – 7.37, and the solution was filtered before finally adding 88 mL FBS per 500 mL volume of resulting media. After reaching 70% confluence, osteoblasts were passaged with 0.025% trypsin, and washed with osteoblast media. Cells were seeded onto 0.75 x 0.75 in^2 scaffolds, consisting of 0.3 mg SPP protein, and controls in a 6-well tissue culture plate at 50,000 cells per well. Cell adhesion and proliferation was monitored via polarized light microscopy every 24 hours post-seeding.

5.2.11 Murine Fibroblast Cell Culture

A range of cell lines was employed for cell culture 3T3 murine fibroblasts and isolated human fibroblasts were provided by the laboratory of Dr. Xuejun Wen (Department of Chemical and Life Science Engineering, Virginia Commonwealth University, Richmond, Virginia), while L-929 murine fibroblasts were provided by the laboratory of Dr. Subhas Kundu (Department of Biotechnology, Indian Institute of Technology, Kharagpur, India). Cells were initially seeded in 75 cm^2 culture flasks and incubated at 37 °C in a 5% CO_2 atmosphere in DMEM high glucose media, with 10% FBS and 1% non-essential amino acids. After reaching 70% confluence, fibroblasts were passaged with 0.025% trypsin and incubated at 37 °C for 5 minutes, at which point the cells were observed to attain a spherical morphology and detach from the sidewalls of the tissue culture flask. Additional media was added to dilute the trypsin, and the cell suspension was centrifuged at 1000 rpm for 5 minutes at 4 °C to precipitate the cells. The supernatant was removed, and the cells were washed and resuspended in fresh media. A small aliquot was removed from the homogenized cell solution, and using a haemocytometer, the cell density was determined. Prior to cell seeding, microstructured SPP scaffolds were hydrated in PBS overnight, and UV sterilized for 30 minutes in a laminar flow hood. Cells were seeded onto 0.75 x 0.75 in^2 scaffolds, consisting of 0.3 mg SPP protein, and controls in a 6-well tissue culture plate at 50,000 cells per well. Cell adhesion and proliferation was monitored via polarized light microscopy every 24 hours post-seeding.

5.2.12 Characterization of cell culture

After reaching approximately 70% confluence (assessed via analysis of glass slide controls), substrates were washed in PBS and fixed with 4% paraformaldehyde to prepare for staining and fluorescence imaging. Following permeabilization with wash buffer, actin staining was performed with rhodamine-conjugated phalloidin (1:200 dilution) for L-929 cells, and Alexa Fluor 488 phalloidin for 3T3 and human osteoblast cells. Nucleus counterstaining was conducted with Hoechst stain for L-929 cells, and DAPI for 3T3 and human osteoblast cells. Imaging was conducted at 405 nm and 488 nm using a confocal laser scanning microscope (Olympus FV1000) with 20 and 60x oil immersion lenses.

5.3 Results and Discussion

5.3.1 Synthesis of Silk Sericin Conjugates

Photoactive sericin (also referred to as SPP) was produced through the biochemical modification of the silk sericin protein, using a synthesis method thoroughly characterized in the previous chapter on silk protein photolithography. The processes depicted in the previous chapter were initially derived from isocyanate-based modification of silk sericin in the LiCl/DMSO solvent. In the reported study, the process of sericin dissolution in LiCl/DMSO and heating at 60 ºC for 5 hours was associated with negligible degradation of high molecular weight sericin chains.[278] Silk sericin has demonstrated dissolution in this solvent system, up to high concentrations of 30%

(w/v).[335] When conducted at elevated temperature, this modification is associated with the preservation of cellular interactions of interest for sericin—low cellular toxicity to fibroblasts and the activation of extensive type I collagen production.[155] Direct conjugation of the protein with a photoactive-capable isocyanate is achieved due to the hydroxyl-rich nature of sericin (~36 mol% Ser, 9 mol% Thr, 3 mol% Tyr), providing a composition of ~50% reactive hydroxyl groups.[71] The methacrylate was selected due to the extensive employment and characterization of acrylate biocompatibility in biomaterials techniques.[336, 337] Facile processing of acrylates also ensures the novel photoactive sericin conjugate is able to be inserted into existing fabrication steps to produce stable protein-based scaffolds.[129] The sericin protein was modified to impart 25% of hydroxyl-containing amino acids with photoreactive methacrylate groups, leaving the bulk of serine groups untouched to preserve these regions associated in favorable cellular interactions.[74, 75] Upon exposure to UV light, these pendant methacrylate groups rapidly crosslink in the presence of a photoinitiator to form long chain polymers, which enables the fabrication of stable networks of sericin-methacrylate.

The degree of substitution of methacrylate was established from the weight increase of sericin-methacrylate recovered following the IEM reaction, which corresponds to a conversion of ~11% of amino acids to methacrylate moieties. From this observation, a stoichiometry of 2.3 moles of IEM to moles of primary hydroxyl-containing amino acids is required in order to achieve a desired degree of substitution. This substitution degree was maintained at a low population of amino acids converted in order to preserve the fundamental bioactive properties of sericin, and to minimize widespread modification of serine-rich repeats. However, controlling the degree of

substitution provides a means of producing architectures of variable crosslinking densities. Alternatively, the presence of unmodified amino acids also enables the production of multifunctional biomaterial architectures via concurrent or subsequent modification strategies.[121]

5.3.2 Characterization of Silk Sericin Conjugates

Solubility and Stability of Sericin-Methacrylate

Sericin-methacrylate solubility was initially investigated to facilitate analysis and processing of the conjugate. Native sericin is highly water-soluble, owing to its secondary structural content—sericin is structurally dominated by amorphous random coil regions, with additional β-sheet content, and little or no α-helical content.[72] From the results on fibroin modification observed in the previous chapter, it was expected that the addition of a hydrophobic methacrylate in addition to masking of hydrophilic serine groups, would induce a significant change in solubility characteristics for sericin conjugates. Furthermore, efforts to modify sericin with a hydrophobic cyanophenyl substituent have demonstrated a rapid loss of solubility.[278] However, despite the introduction of a hydrophobic substituent, the resulting sericin conjugate is observed to retain the characteristic solubility properties of unmodified sericin, dissolving in water to form solutions up to 10% (w/v). In contrast to fibroin-methacrylate, this water-solubility offers the opportunity to replace key steps of the photolithography process with aqueous-based processing, at considerable environmental and safety benefits.

To enable rapid processing of sericin-methacrylate, the solubility of sericin in a range of high-volatility solvents was investigated. In the previous chapter, methacrylate-conjugated fibroin was observed to readily solubilize in HFIP. However, in an effort to demonstrate an alternative to this high-toxicity processing method, a substitute for HFIP was sought. Alcohols are known to follow a trend of protein solubilization: HFIP > TFE > isopropanol > ethanol > methanol, where the fluorinated alcohols HFIP and TFE are specifically known to enhance solubility thorough stabilization of the α-helical conformation.[338] Isopropanol, ethanol, and methanol do not yield any detectable solvation of sericin-methacrylate, however, over a period of 12 hours, the conjugate dissolves completely in TFE. This is attributed to the ability of TFE to act as a hydrogen bond donor, disrupting interchain bonding in a similar fashion to HFIP. TFE has demonstrated wide utilization as a peptide solvent, and is significantly less toxic than HFIP.[339] Furthermore, solubility of sericin, and by corollary sericin-methacrylate, in non-aqueous solvents DMSO, N,N-dimethylacetamide (DMAc), and N,N-dimethylformamide (DMF) is negligible without use of salts to disrupt hydrogen bonding.[278] Thus, TFE was embraced as the primary carrier of sericin-methacrylate for incorporation into later photolithography steps.

Verification of Conjugation

This successful conversion of native sericin to sericin-methacrylate was verified via ATR-FTIR spectroscopy on TFE-casted protein films (Figure 5.2). Here, comparison of spectra to that of the reagent, IEM, demonstrates functionalization of IEM to sericin.

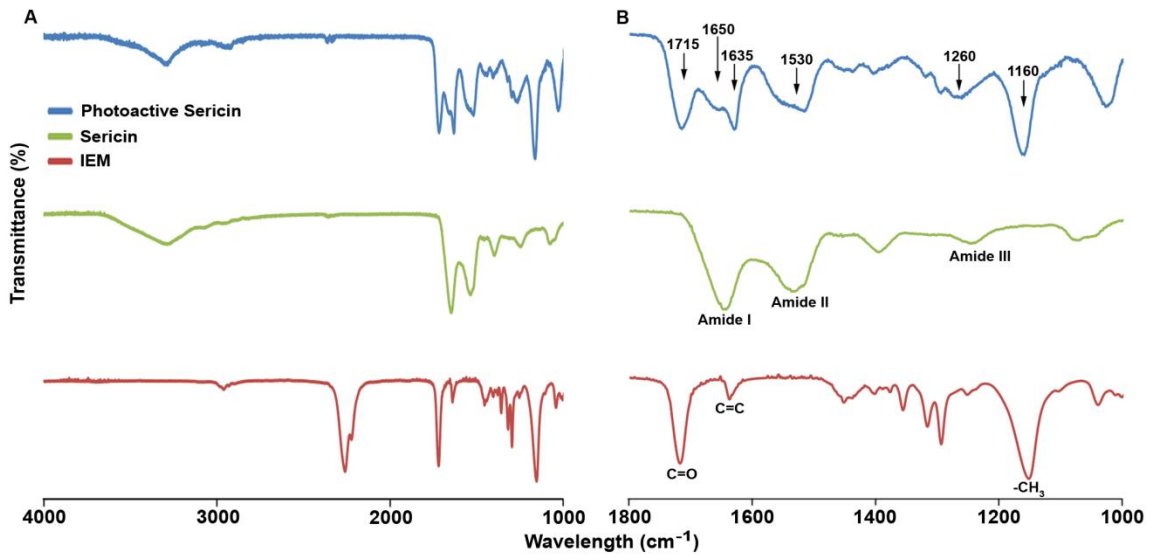

Figure 5.2. ATR-FTIR spectroscopy on the sericin conjugate confirms the presence of both amide I/II/III peaks from native sericin, in addition to stretching vibrations at 1720 cm^{-1} (ester carbonyl C=O) and 1630 cm^{-1} (vinyl C=C), and rocking vibrations at 1160 cm^{-1} (CH_3) from the methacrylate substituent.

Native sericin (green) displays intrinsic amide I/II/III signals, which are simultaneously observed for the sericin-methacrylate product (blue). Analysis of the IEM reagent (red) yields intense stretching vibrations at- 1720 cm^{-1}, representing carbonyl ester C=O, and 1640 cm^{-1}, assigned to vinyl C=C (which confers photoreactivity), and an additional intense peak is present at 1160 cm^{-1}, resulting from CH_3 rocking vibrations.[294] The modified sericin-methacrylate product also indicates peaks representing an ester carbonyl, terminal C=C stretching vibrations as broad shoulder peaks of amide I, and CH_3 rocking vibrations, all provided by the methacrylate group. In the expanded spectrum, a broad intense peak at 2270 cm^{-1}, resulting from isocyanate (–N=C=O)

stretching, is evident. The absence of this isocyanate stretching vibration from the sericin-methacrylate product indicates the absence of residual isocyanate. The clear observation of characteristic IEM groups in the sericin-methacrylate product provides evidence to support the successful grafting of IEM onto the sericin protein. From prior efforts on this modification strategy, depicted for silk fibroin in the previous chapter, the secondary structural content of the polypeptide backbone remains relatively unchanged with this methacrylate bioconjugation reaction. This establishes that, while the conjugation is successful, the biochemical addition of methacrylate does not adversely affect the core structure of sericin.

5.3.3 Application of the Silk Protein Lithography (SPL) Platform to Sericin

When sericin-methacrylate monomers are exposed to UV light in the presence of the Irgacure 2959 photoinitiator, the conjugate becomes insoluble in water—a transition which is attributed to chemical crosslinking of methacrylate vinyl groups between large constituent polypeptide chains of the sericin protein. Biomaterials fabricated from pure sericin are readily water-soluble unless chemically treated to modify secondary structure, however complexity of architectures using this method are limited.[90] The crosslinking of sericin-methacrylate provides significant benefits in terms of aqueous solubility, enabling the production of water-insoluble biomaterial architectures.

Sericin-methacrylate was investigated for the production of microscale architectures through photolithography. In the previous chapter, the Silk Protein Photolithography (SPL) platform was introduced. Silk fibroin was incorporated into this

initial attempt and thoroughly characterized, due to its standing as one of the more difficult silk proteins to process. Despite being sourced from the same *B. mori* silk fibers, the sericin glycoprotein is structurally-distinct from fibroin in amino acid constituents, displaying differences in physical and chemical properties, structure and function, and overall solubility.[73] The water solubility of sericin-methacrylate greatly aids in the process of photolithography using innocuous solvents in contrast to fibroin-methacrylate, allowing casting and development with water as the only solvent. This offers the opportunity to embrace water-based processing strategies, such as those utilized for biocompatible, poly(ethylene glycol) diacrylate (PEGDA) microfabrication processes.[129] However, the solvent 2,2,2-trifluoroethanol (TFE) is associated with a greater evaporation rate in comparison to water, allowing rapid casting of thick homogenous films for photolithography. By avoiding repeated solvation/de-solvation events in multiple solvent systems, significant conformational change can be avoided.

Using the findings in the previous chapter, micropatterns of silk sericin on silicon and glass substrates were able to be fabricated via photolithography using the sericin-methacrylate as a negative photoresist that is crosslinked in the presence of UV light. Irgacure 2959 is employed as a photoinitiator, dissolved in TFE at a ratio of 1:4 to the total mass of sericin-methacrylate, to yield films of variable thickness. Here, the total volume of TFE and mass of sericin-methacrylate will determine the substrate surface coverage and film thickness, respectively. The sericin-methacrylate solution is drop cast onto methacrylate-treated substrates and exposure through a selectively patterned mask results in crosslinking between adjacent methacrylate moieties. Prior to photoexposure, substrates are covered for a period of 10 minutes to allow residual TFE to evaporate (i.e.

'pre-bake'), preserving film integrity and preventing film adhesion to the photomask. Photoexposure was found ideal in yielding optimal patterns when employing UV exposure at 150 mW/cm^2 intensity for 4.0s. The development step consists of immersion in deionized water for 2 hours, followed by rinsing with copious deionized water to remove unexposed and uncrosslinked sericin-methacrylate. The formation of a methacrylate self-assembled monolayer on glass substrates promotes covalent bonding between crosslinked protein features, allowing the emergence of insoluble protein microstructures with a range of architectural features after development (Figure 5.3). The process of photolithography using sericin-methacrylate is capable of producing a diversity of micro-architectures, similar to what is achieved by the application of soft lithography to materials patterning. Coomassie Blue R-250 staining of 1.0 mg sericin-methacrylate on a 1 x 1 in^2 glass substrate establishes the composition of protein microstructures. A linear array of 10 μm lines is depicted in Figure 5.3 (B), which is to be used for cellular culture studies. Furthermore, large-scale patterning of micro-scale features is possible via silk protein lithography (Figure 5.3 C).

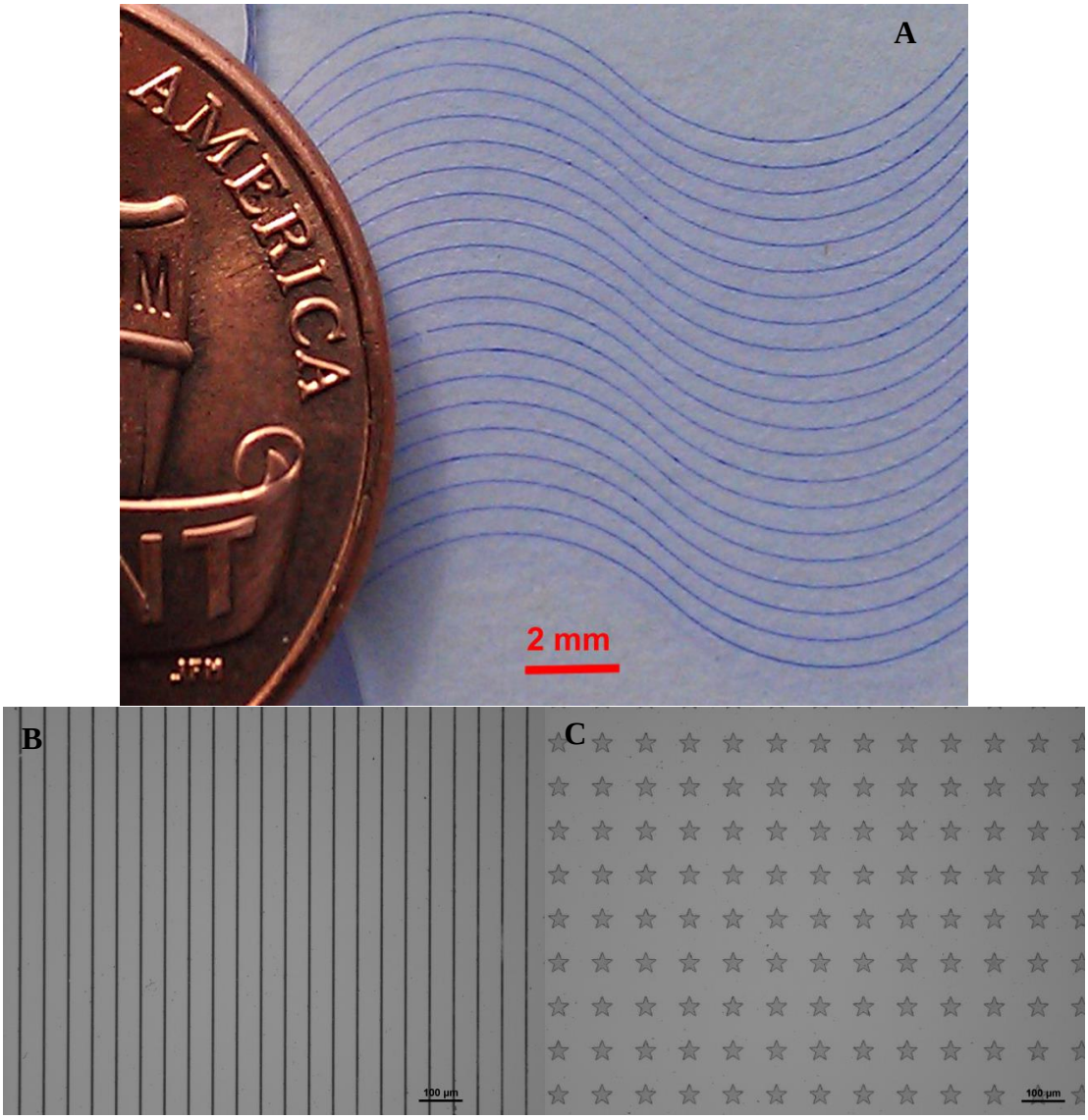

Figure 5.3. (A) Optical image of 100 µm, Coomassie Blue R-250 stained lines patterned over 1 cm. Scale bar = 100 µm. (B)(C) Optical micrographs of 10 µm and 50 µm stars, demonstrating reproducible patterning over 1 cm areas. Scale bar = 100 µm.

AFM and SEM were employed for the analysis of surface topography and to ensure the fidelity of high-resolution features. The versatility of this rapid, large-scale fabrication process is depicted—this technique is applied to micrometer-features existing in millimeter-scale arrays, enabling fabrication of thousands of similar structures (Figure 5.4). Importantly, in features produced at the single-micrometer regime, the underlying hydrophobic monolayer of methacrylate remains present in unexposed regions after development, ensuring compatibility of the substrate in cell culture applications.[276]

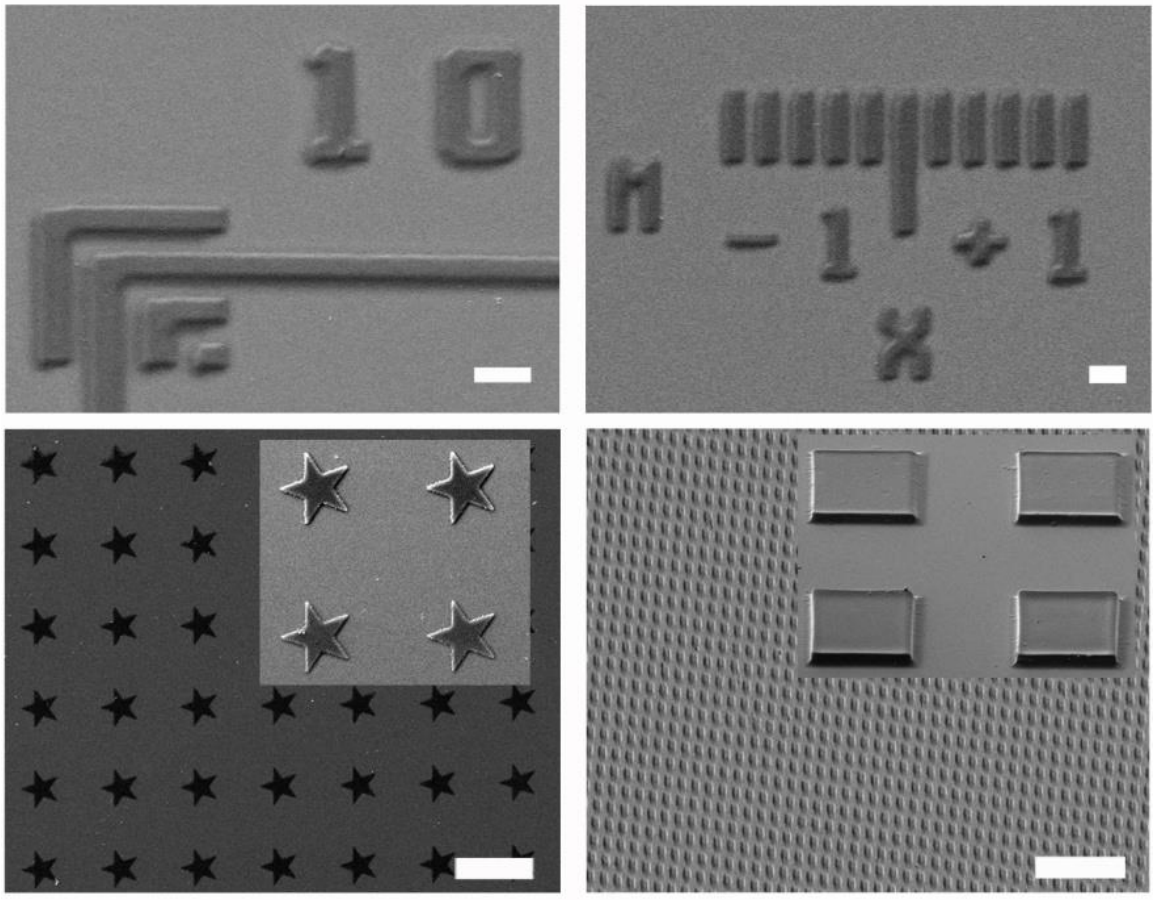

Figure 5.4. Microscopy of SPP microarchitectures. SEM images depict various patterns formed by photolithography. Features with observable height and lateral dimensions down to a few microns are easily created over large areas. Scale bar = 100 μm.

Varying the protein loading per substrate (1 cm^2) is associated with the ability to create features of well-defined height profiles, producing features ranging from sub-micrometer height upwards to tens of micrometers. Via AFM, a ~2 μm height profile (1.0 mg sericin-methacrylate) is clearly highlighted, with corresponding surface roughness of 2.8 ± 1.9 over a 5 μm area (Figure 5.5). This scalability in height and feature aspect allows the fabrication of thin microstructures, appropriate for cellular adhesion, up to thick-walled microwells. Furthermore, the ability to vary feature height and spatial resolution of sericin-methacrylate allows fabrication of cellular scaffolds over a large range of aspect ratios.

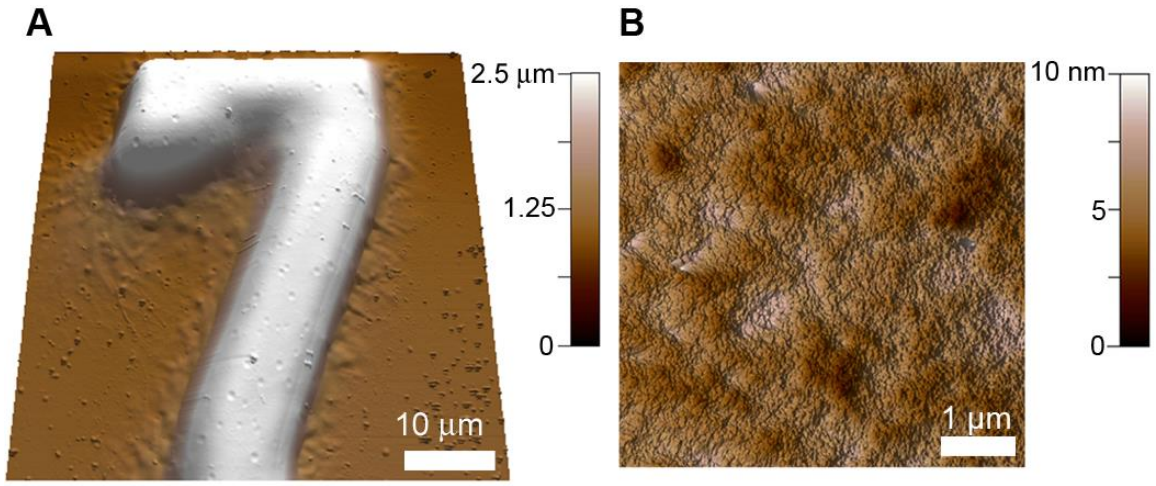

Figure 5.5. Surface characterization of the photopatterned sericin: (A) AFM image of a patterned "7" on a silicon surface. The feature is around 2 μm in height (B) 5 μm surface scan of the photopolymerized product, demonstrating RMS surface roughness < 5 nm.

5.3.4 Characterization of the Stability of Crosslinked SPP

Mechanical analysis of Crosslinked Sericin-Methacrylate

Photocrosslinking was expected to yield an improvement in mechanical properties in comparison to native sericin, due to the presence of a flexible crosslink between polypeptide chains. To understand the mechanical implications of crosslinking, AFM nanoindentation studies were conducted to yield elastic modulus values for sericin-methacrylate, in comparison to native sericin. Adherent films (> 1 μm) of sericin-methacrylate (1.0 mg) were fabricated on Si-methacrylate substrates, in a process identical to those depicted in the previous section. To date, mechanical properties of sericin films have not been thoroughly investigated, and data consists of studies on complex architecture, indicating a relatively low modulus (0.5 MPa).[340] Crosslinked sericin-methacrylate presents an elastic modulus of 8.6 ± 1.0 GPa, which provides a 72% increase over that of native sericin, at 5.0 ± 0.4 GPa (Figure 5.6). This is attributed to nascent crosslinks between adjacent protein chains, which enhance network elasticity, indicated by an enhancement of Young's modulus. This improvement in mechanical stability of the crosslinked protein, in addition to the ability to 'tune' the degree of crosslinking, enables sericin-methacrylate to satisfy a range of load-bearing requirements in diverse tissue engineering applications.[319]

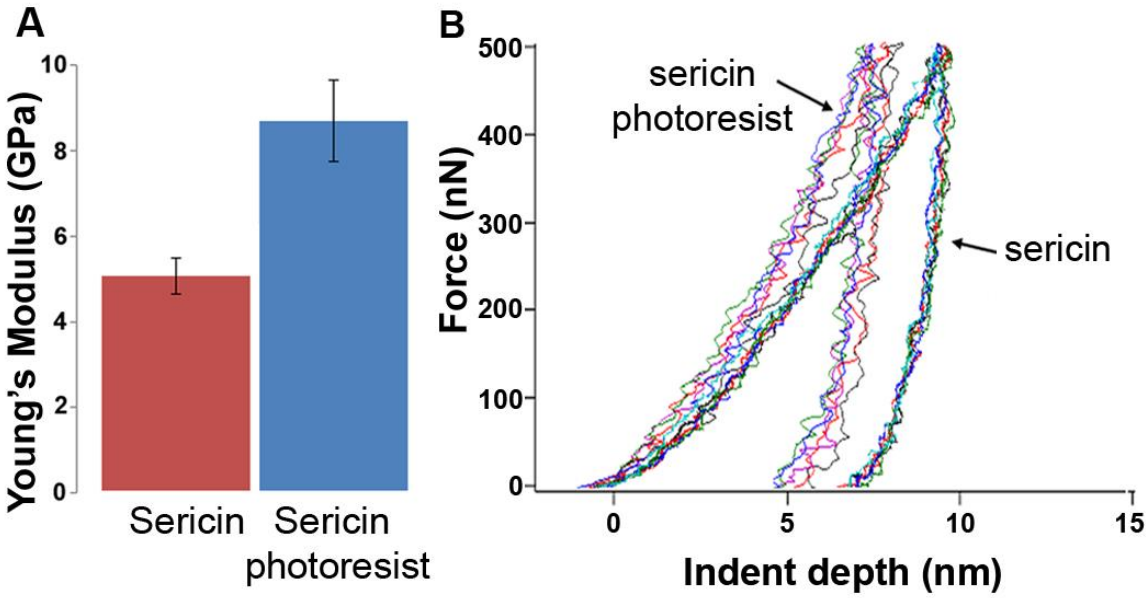

Figure 5.6. (A) AFM nanoindentation of sericin-methacrylate demonstrates improvement of elasticity (Young's modulus), increasing from 5.0 ± 0.4 GPa (native sericin), to 8.6 ± 1.0 GPa (sericin-photoresist material). (B) Nanoindentation curves overlaid, from which the Hertz mechanics model is fit to determine elasticity.

Proteolytic Degradation of Crosslinked Sericin-Methacrylate

Stability of the resulting protein network has been analyzed through incubation studies in PBS buffer, in addition to Protease XIV (*S. griseus*, ≥3.5 units/mg) in PBS buffer, to assess proteolytic degradation. As-cast sericin-methacrylate films exhibit water-solubility, dissolving over short time periods (< 4 hours). Photocrosslinked sericin-methacrylate films in PBS buffer alone demonstrate an initial rapid decrease in mass, corresponding to the loss of residual photoinitiator from the network (Figure 5.7). In the presence of the protease XIV is added to the buffer, sericin-methacrylate shows a

significant reduction in mass, and loss of the film's structural integrity over a 3-day period. Films initially swell in the aqueous environment, and slowly fragment during incubation, gradually losing peripheral aspects of the film. The relatively hydrophilic nature of sericin-methacrylate network is implicated in this rapid loss of structural integrity—swelling of the sericin-methacrylate 'hydrogel' allows influx of the protease enzyme, which then digests the polypeptide backbone, eroding the bulk of the film. This gradual *in vitro* degradation establishes the ability of crosslinked sericin-methacrylate architectures to undergo controlled biodegradation and bioresorption. Both of these properties are important considerations for cellular culture and tissue engineering applications, in which the rate of scaffold degradation must ideally match that of tissue regeneration.[319, 341] Thus, by controlling the crosslinking degree of the sericin-methacrylate network, it may be possible to create architectures of tailored physical (biodegradation and bioresorption) and mechanical (Young's modulus) properties.

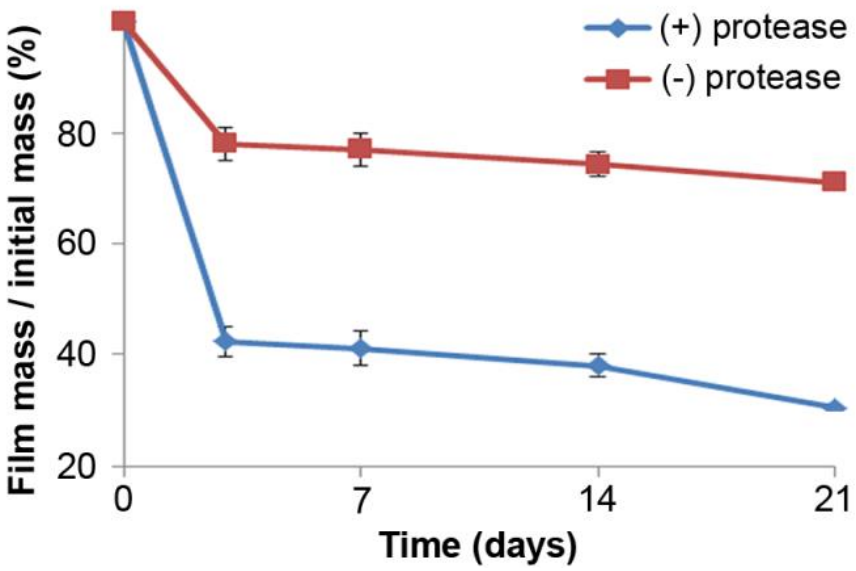

Figure 5.7. Proteolytic degradation of sericin-methacrylate indicates a rapid initial degradation of crosslinked films in the presence of Protease XIV. In the first 3 days of analysis, films swell in PBS buffer and gradually lose fragments up to day 21. In comparison, control films indicate an initial loss of mass, without significant mass loss over time.

5.3.5 Cell Culture Studies on Silk Sericin Scaffolds

To effectively translate sericin-methacrylate into biologically-relevant tissue scaffolds, the conjugate was patterned into pre-defined microstructures on glass substrates. Scaffolds tested included parallel 10 μm lines, and a grid of 10 μm lines arranged at intersecting 90º angles with 200 μm separation (Figure 5.8). Protein loading per substrate was 0.3 mg, corresponding to a height of < 1 μm, in order to establish the role of sericin-methacrylate in directing/promoting cellular attachment and proliferation.

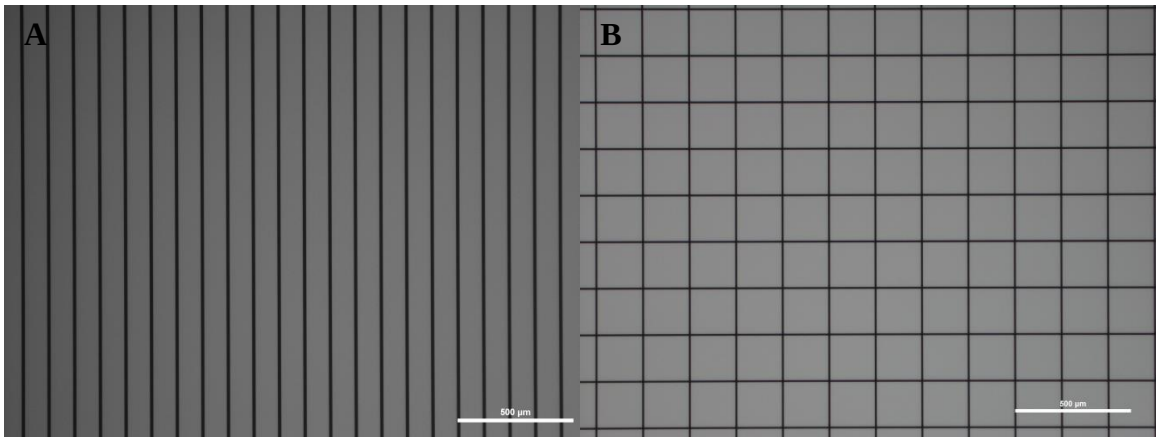

Figure 5.8. Photopatterns utilized in cell culture experiments: (A) array of parallel µm lines with ~100 micrometer spacing, (B) grid of 10 µm lines with 200 µm spacing. Scale bar = 500 µm.

Osteoblasts were selected for cell culture experiments in an effort to explore the potential use for 2D scaffolds to address tissue engineering applications in fundamental and applied studies involving bone formation and regeneration. Human osteoblasts were seeded onto patterned glass substrates and incubated over 96 hours in the presence of osteoblast mineralization media. The process of seeding yields nonspecific adhesion and subsequent spreading, as evident in initial optical images—cells are located at the site of initial seeding, in regions on the scaffold and in between features. Osteoblasts display preferential migration and adhesion of osteoblast cells to micropatterned sericin architectures, effectively demonstrating the ability of sericin to selectively promote adhesion in a desired pattern. At 96 hours, osteoblasts tended to specifically follow elevated protein patterns, producing a mimicking architecture localized on the existing sericin scaffold (Figure 5.9 A). More specifically, non-specific adhesion is not evident in

such scaffolds, and cellular adhesion outside of patterns is only observed when significant osteoblast clustering is present. Close-up images very clearly demonstrate this pattern-following behavior of osteoblasts (Figure 5.9 B).

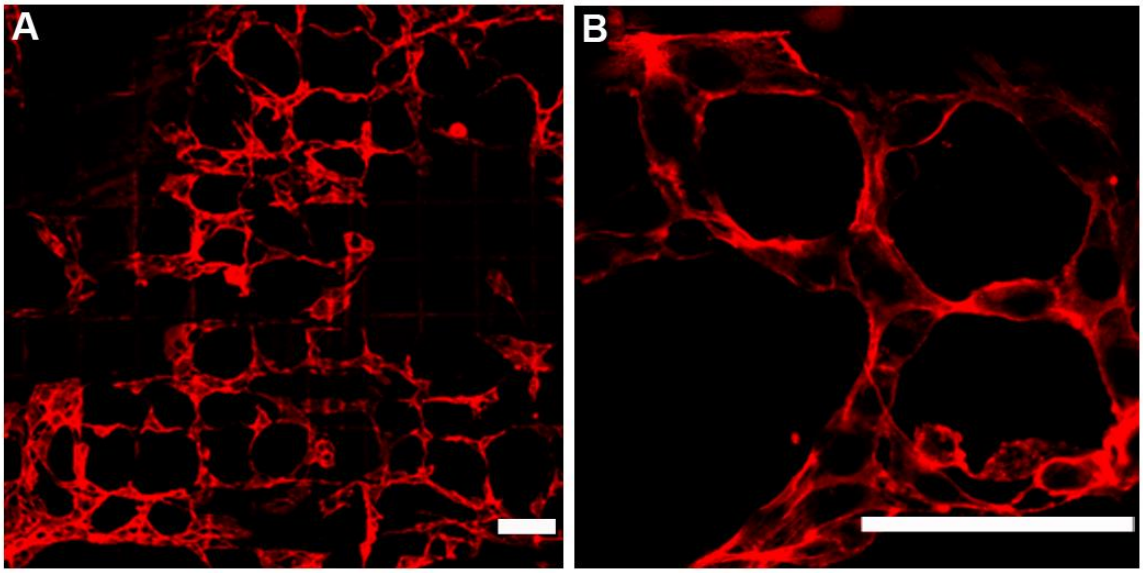

Figure 5.9. Fluorescence micrographs of osteoblast proliferation on SPP scaffolds demonstrate selective growth on microstructures. (A) Rhodamine-conjugated phalloidin staining of osteoblasts on a dense grid (A) displays cellular adhesion over a widespread area, with (B) clear deficiency of osteoblasts in the grid void space. Scale bar = 100 µm.

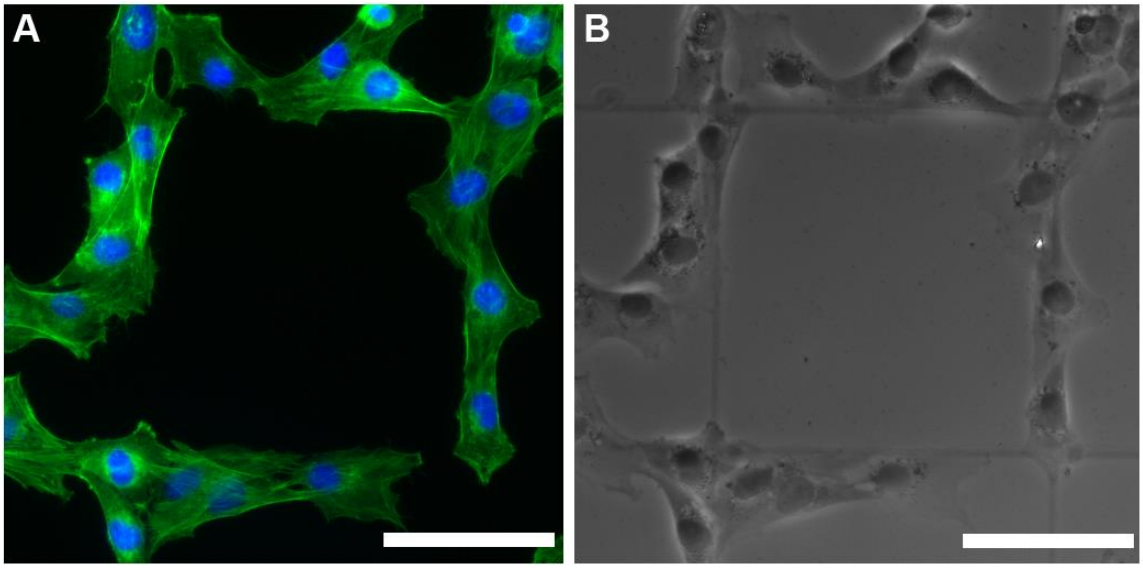

Figure 5.10. Fluorescence micrographs of human osteoblast proliferation on SPP scaffolds demonstrate selective growth on microstructures. (A) FITC-phalloidin and DAPI stained osteoblasts are displayed with the ability to selectively follow SPP patterns (B), avoiding growth on unpatterned regions. Scale bar = 100 μm.

The absence of osteoblasts from growth and spreading on methacrylate-functionalized Si is unexpected, given the high degree of hydrophobicity of this substrate in comparison to the relatively hydrophilic sericin-methacrylate. In addition, numerous studies exist that utilize methacrylate-presenting TPM monolayers for selective cellular adhesion.[276] Poly(methacrylic acid) is associated with an inhibition of cellular adhesion, which implies that the observed osteoblast adhesion and proliferation on crosslinked sericin-methacrylate features is due to the sericin component alone.[75] Furthermore, sericin-methacrylate is relatively hydrophilic in comparison to the hydrophobic Si-methacrylate substrate. Thus, the selective adhesion and proliferation of

osteoblasts on sericin-methacrylate surfaces is attributed to the chemical properties of silk sericin, rather than surface wetting phenomena. The preservation of serine-rich repeats in sericin, implicated as critical regions for cellular interactions, enables sericin-methacrylate to actively promote adhesion and proliferation, while existing in the bound, patterned configuration.[74] The low surface roughness (~ 3 nm) of sericin-methacrylate is additionally implicated in this preferential adhesion of osteoblasts, which are known to display a marked improvement in adhesion on low-roughness surfaces.[342] As a result, the primary cause of pattern-specific adhesion is considered to be the serine-rich regions of sericin protein, followed by favorable nanotopography, promoting integrin adhesion.

5.3.6 Formation of Sericin-Methacrylate/Fibroin-Methacrylate Biocomposites

As discussed above, the fabrication of micropatterned silk architectures has been limited to the use of covalently-functionalized two-dimensional silicon or glass substrates. The incorporation of a rigid Si-based substrate has been a necessary requirement for the retention of silk microstructures and their stability. This approach follows the traditional use of an inert, non-degradable substrate for the purposes of 2D, *in vitro* tissue culture, in contrast to biodegradable 3D substrates for implantable, *in vivo* use.[343, 344] To expand the scope and applications of the structures developed in this work, we investigated the idea of combining these two photoreactive materials into one platform that could form a flexible substrate. To fabricate 3D, biodegradable silk architectures, a multilayer process is necessary for allowing patterning of sequential layers.[345] However, the utilization of multilayer photolithography is not a viable

strategy for sericin-methacrylate, or even fibroin-methacrylate, due to the high swelling potential exhibited by carrier solvents. This results in significant swelling and loss of fidelity of the underlying layer when a subsequent layer of silk protein photoresist is cast.

While soft lithography offers an alternative strategy to multilayer lithography, it was desired to establish the capacity for silk to undergo patterning by photolithography alone.[346] Noting the decrease in protein solubilization exhibited from HFIP to TFE, a strategy was devised by using the stronger hydrogen bond donor, HFIP, to cast and photopolymerize a planer substrate of fibroin-methacrylate. Here, the low solubility of fibroin-methacrylate in TFE enables casting of a subsequent layer of sericin-methacrylate without distortion of the underlying layer. This strategy was utilized for the fabrication of stable sericin-methacrylate micropatterns on a thick film of fibroin-methacrylate (Figure 5.11).

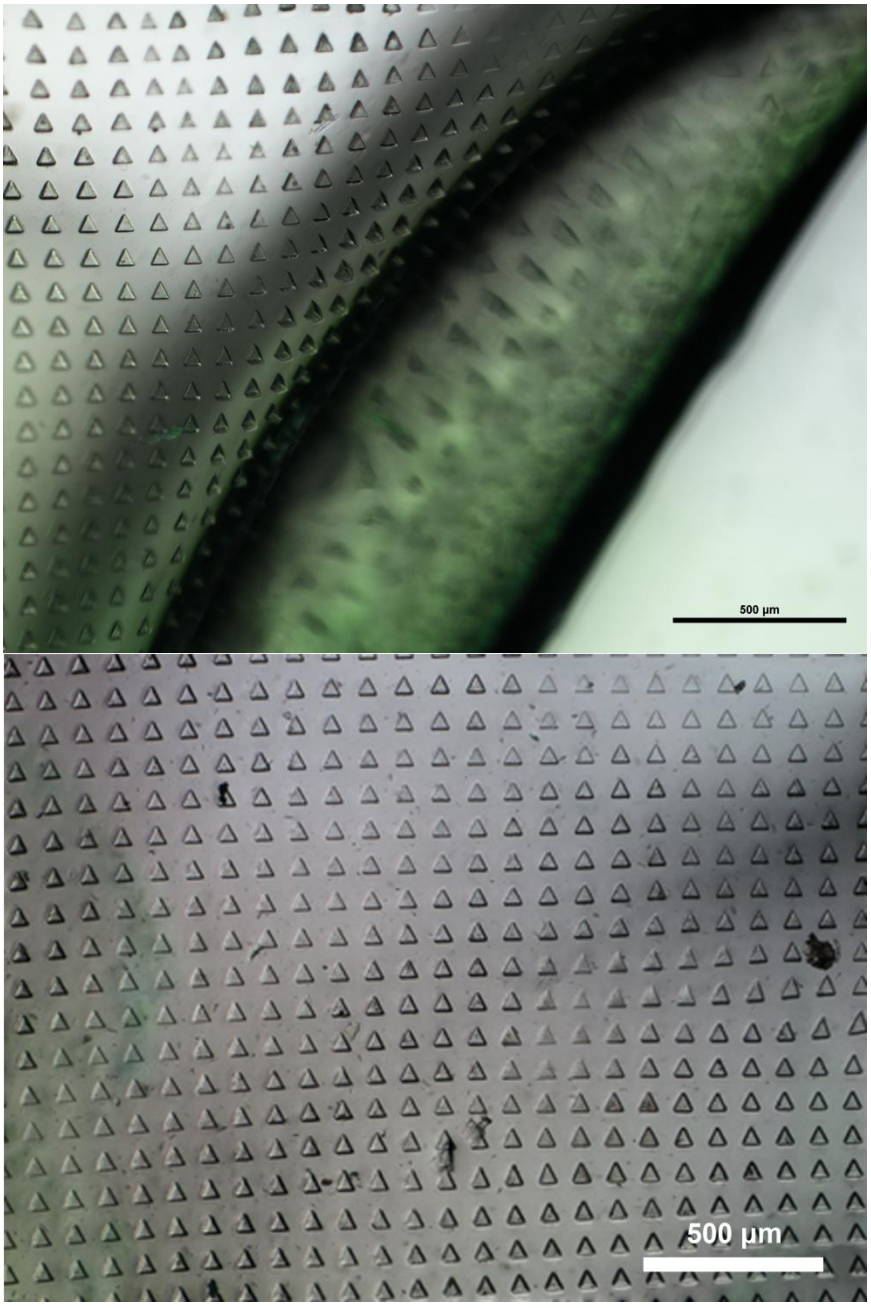

Figure 5.11. Optical microscopy of a sericin-fibroin biocomposite, (A) composed of 50 µm triangles of sericin-methacrylate on a flexible layer of fibroin-methacrylate. (B) The contoured biocomposite, flattened into a two-dimensional representation of film topography via a z-series capture.

The multilayer silk biocomposite strategy enables the integration of two mechanically-robust, biodegradable materials into a free-standing architecture. This demonstrates the ability to isolate fibroin and sericin components of a silk fiber, and recombine functionalized proteins into a novel three-dimensional architecture with tailored surface topography. Multilayered silk fabrication therefore offers exciting possibilities in the use of silk protein photolithography for fabrication of flexible materials exhibiting diverse functionalities—this effectively provides a novel, tractable processing strategy for the incorporation of a naturally-derived, renewable material into fields of degradable bioelectronics and biologically-integrated optics.[85, 347, 348]

5.4 Conclusions

In conclusion, in this chapter, the application of a biochemical modification strategy of sericin to produce a photoactive conjugate, capable of rapid photopatterning into 2D scaffolds is demonstrated. Sericin microstructures resulting from photocrosslinking of the conjugate are observed to act as ideal 2D substrates for the spatial guidance of osteoblast adhesion and proliferation. Sericin scaffolds simultaneously exhibit a high degree of cytocompatibility to cultured human osteoblasts. Sericin-specific patterning of osteoblasts is attributed to the presence of specific serine-rich cell-binding sequences within the sericin polypeptide chain, in addition to a low, 3

nm nanotopography of scaffolds. Despite the impartation of a nascent photoactive potential, sericin was demonstrated to remain mechanically stable during the fabrication process, and exhibited controlled proteolytic degradation *in vitro*. The ease of biomaterials fabrication using modified sericin, combined with a stable, highly cytocompatible configuration, provides an incredibly versatile material for future biomaterials fabrication. The incorporation of silk sericin into the SPL platform further provides a powerful foundation for fabrication strategies incorporating structurally- or environmentally-unstable biomolecules in general. By incorporating this technology for silk sericin, this offers the ability to overcome limited materials processing strategies, providing an avenue to the formation of highly complex, multifunctional nanomaterials, which possess significant potential in tissue engineering applications. Furthermore, through the use of a multilayer modification to the SPL platform, biocomposites formed via photoactive silk proteins enable the creation of flexible and free-standing architectures, opening a host of applications to this modification strategy.

[This chapter contains results that have been submitted for publication in the paper "Fabrication of sericin microstructures via silk protein lithography" in Advanced Functional Materials, November 2013.]

CHAPTER 6

CONCLUSIONS AND FUTURE WORK

6.1 Conclusions

The research described in this dissertation is focused on the investigation of silkworm silk proteins (sericin and fibroin), their self-assembly and the development of new fabrication strategies that can enable the control of complex architecture and functionality across multiple length scales—from the nanoscale to the macroscale. These studies on the impact of physical and chemical modification strategies and their role in forming complex silk biomaterial architectures involved the following:

1. Fundamental investigations of protein self-assembly of chemically-distinct silk sericins sourced from a range of silkworm species. A mechanism describing the resulting two-dimensional aggregations was developed, showing the influence of various physical and biochemical factors in inducing protein self-assembly. These include electrokinetic potential, globular particle size, particle size dispersity and abundance, and amino acid composition. This model was demonstrated to be broadly applicable to general protein systems via investigations involving the other silk protein fibroin. Fibroin nanoparticles prepared in accordance with the self-assembly model similarly exhibited a tendency to self-organize into dendritic

architectures. These results help to understand the unstudied role of self-assembly in the formation of silk fibers, and further provide an insight into potential roles in bottom-up nanoscale fabrication strategies for biomaterials.

2. The unique characteristics of sericin as a water-soluble silk protein were harnessed for incorporation into a pH-responsive hydrogel composite. A poly(aspartic acid)-sericin hydrogel was formed using a novel protein-based templating strategy. Sericin provides a biocompatible material for controlling pore structure and enhances the pH-based stimuli-response of the composite hydrogel, which was observed to support cell growth. This fabrication approach helps to demonstrate the use of sericin as a class of protein-based composite materials capable of *in vitro* incorporation and cell-friendly usage.

3. To overcome limitations in fabricating complex architectures using conventional platforms, a novel protein-based photolithography technique was subsequently developed. This involved biochemical modification of the silk fibroin and sericin to enable photoreactivity and thereby, microfabrication of silk proteins. The “Silk Protein Photolithography” platform is capable of preserving the structure and unique functions of the silk proteins, while offering a renewable, biologically-active and biodegradable material as a viable replacement in conventional synthetic-reagent-based photolithography platforms. Effective cell adhesion and proliferation behavior is demonstrated on the microstructures formed, which further possess the ability to actively guide the spreading of various cell types. These results open new avenues to harness silk proteins in hitherto unavailable methods and form complex macroscale architectures in two- and three-

dimensions, with applications in flexible bioelectronics and tissue engineering scaffolds with micro- and nanoscale resolution.

The implications for this work go beyond the scope of the tested applications, via the formation of hitherto uncharacterized, stable structures and functionalities from silk proteins. Fundamental insights into self-assembly help to elucidate the mysteries of biological systems, while providing the opportunity to harness natural organization processes to build a new class of materials. The fabrication of stimuli-responsive biocomposites provides a new purpose for silk sericin in particular, enabling the use of biologically-integrated materials responsive to microenvironmental conditions, in biosensing, protein arrays, and cellular scaffolds. Importantly, the versatility demonstrated for the SPL platform allows facile production of biocompatible and biodegradable building blocks with precisely engineered structure, function and mechanics, appropriate for use in biomedical applications demanding specific physical and chemical attributes. Overall, the high abundance, low cost, and sustainable ('green chemistry') approaches by which a new class of silk biomaterials may be fabricated creates significant potential in the use of silk proteins as inert, non-toxic replacements for future engineering opportunities.

6.2 Future Work

Synthesis of Hybrid pH-Responsive-Silk Protein Hydrogel Networks

In general, silk proteins and their composites demonstrate remarkable potential as biocompatible, renewable building blocks for biomedical applications—sericin-modified poly(aspartic acid), for example, was fabricated into pH responsive architectures. The potential for incorporating these materials into planar, or particle-based architectures (nano- and microparticles, or even fibers) is highly advantageous to catering overall structure to intended function—such as in stimuli-responsive cellular substrates, drug delivery devices, and biosensors. Effective applications may be realized through the coupling an environmentally-dependent stimuli response with a stable surface-immobilized, or pre-patterned, free-standing architecture, exhibiting intrinsic bioactivity.

Photoactive "Green Chemistry" Bioconjugation Via Aqueous-based Modification

Efforts on bioconjugation of silk proteins demonstrate a reproducible and scalable strategy for effective conversion of these structurally and chemically distinct proteins to a versatile "photoreactive" form. The evolution of this approach can extend to proteins outside the realm of silk, exhibiting a vast combination of specific functionalities, for which microfabrication strategies are valuable. Further work is necessary to evaluate a generalized approach to enabling photoactive conversion on diverse chemical species. For example, N-hydroxysuccinimide ester (NHS) coupling provides an amine-specific means of modification in mild, aqueous-based reaction conditions and furthermore

reduces the time required by isocyanate conjugation through non-aqueous solvents. This method offers the potential to rapidly produce a variety of photo-reactive proteins in high yield, and through facile synthesis under ambient conditions, in contrast to more complex, expensive strategies such as recombinant synthesis.

Active Induction of Cellular Adhesion in Silk Scaffolds

Fibroin, with hitherto unknown bioactivity, was demonstrated to promote selective cell patterning. Conjugation of the RGD peptide sequence was demonstrated to promote adhesion and proliferation of fibroblasts through favorable interactions with cell adhesive proteins.[349] The incorporation of RGD offers the ability to enable specific cellular adhesion through the induction of focal adhesion complexes in specific cell types in the case of fibroin, or enhance existing cellular adhesion for sericin. This provides a route to inducing cellular adhesion in silk and non-bioactive materials, creating opportunities for unrelated proteins with unique properties to undergo both micropatterning, and participate as cell-friendly materials. Specifically, the fabrication of complex cellular scaffolds in 2 and 3 dimensions can be coupled with bioactive agents and growth factors to achieve enhanced growth for tissue repair and replacements.

Flexible Bioelectronics and Optics

Photoactive silk conjugates were demonstrated to be capable of photopatterning on rigid two-dimensional substrates, specifically glass and silicon—while subsequent

work demonstrated the potential for fibroin-methacrylate to act as a substrate for sericin-methacrylate patterning, effectively forming a structurally-compliant composite material. The fabrication of photo-crosslinked films of fibroin thus offers the potential for creating flexible and degradable micropatterned films pure protein origin. The use of silk as a scaffold has previously demonstrated expansive applications in biologically-integrated fields, ranging from bioelectronics, optical applications, and biosensing.[85, 347, 350] The development of composites incorporating fibroin-methacrylate and sericin-methacrylate, provides the possibility to fabricate flexible, silk-based materials exhibiting tailorable mechanics, degradation, and bioactivity while enhancing functionality to address specific electronic and optical requirements.

Expansion of Protein Photolithography into the Three-Dimensional Constructs

Photolithography, as demonstrated in this work, is fundamentally limited in single-step processes to two-dimensional, bottom-up fabrication. Structures are capable of possessing a height aspect, however spatial patterning does not vary in the spatial xy-dimension with an increase in the z-dimension. The rapid evolution of microfabrication strategies has demonstrated additive manufacturing strategies, such as extrusion molding and stereolithography, as influential approaches to forming intricate, three-dimensional structures.[351] The implications of stereolithography in the biomedical setting are vast, encompassing the rapid fabrication of cellular and tissue scaffolds, bioprinting, and the printing of cells, tissues and whole organs.[352-354] Furthermore, the potential to spatially incorporate multiple chemical species at the nanoscale provides immense benefit

in producing complex, 3D hydrogel architectures with applications in spinal cord regeneration and vascular grafts. The ability to incorporate modified silk proteins in this setting, using optical photolithography and modified photoinitiators is within grasp in the very near future. After decades in the commercial setting, affordable digital microcontrollers have advanced this field to enable the design and construct low-cost computer-controlled stereolithography systems using off-the-shelf components. An example of such a project is shown in Figure 6.1 showing how technologies such as 3D printing may be combined with novel biomaterial technologies to enable low cost manufacture of biomedically relevant architectures.

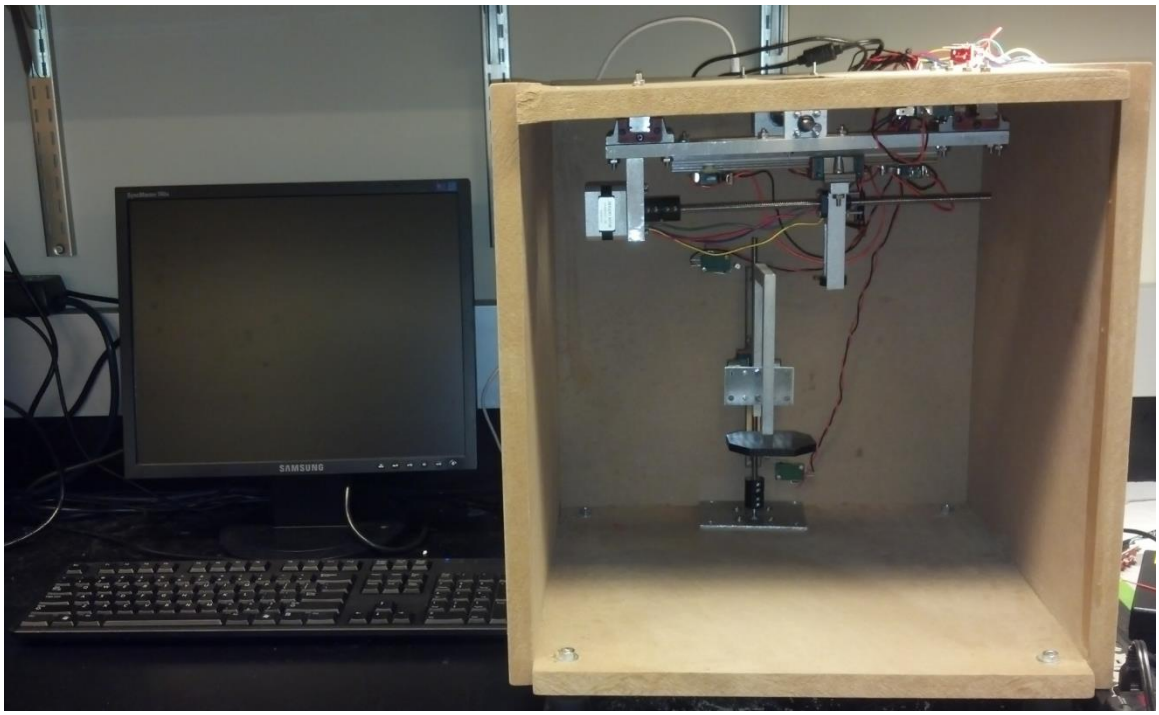

Figure 6.1. A 3-axis optical laser stereolithography system constructed from machined aluminum, and operated using an Arduino microcontroller.

References

1. Ratner, B.D., *Biomaterials science : an introduction to materials in medicine*. 2nd ed. 2004, Amsterdam ; Boston: Elsevier Academic Press. xii, 851 p.
2. Langer, R. and D.A. Tirrell, *Designing materials for biology and medicine.* Nature, 2004. **428**(6982): p. 487-492.
3. Mitragotri, S. and J. Lahann, *Physical approaches to biomaterial design.* Nature Materials, 2009. **8**(1): p. 15-23.
4. Pérez, R.A., et al., *Naturally and synthetic smart composite biomaterials for tissue regeneration.* Advanced Drug Delivery Reviews, 2013. **65**(4): p. 471-496.
5. Altman, G.H., et al., *Silk-based biomaterials.* Biomaterials, 2003. **24**(3): p. 401-416.
6. Parenteau-Bareil, R., R. Gauvin, and F. Berthod, *Collagen-Based Biomaterials for Tissue Engineering Applications.* Materials, 2010. **3**(3): p. 1863-1887.
7. Tziampazis, E., J. Kohn, and P.V. Moghe, *PEG-variant biomaterials as selectively adhesive protein templates: model surfaces for controlled cell adhesion and migration.* Biomaterials, 2000. **21**(5): p. 511-520.
8. Hubbell, J.A., *Biomaterials in Tissue Engineering.* Bio-Technology, 1995. **13**(6): p. 565-576.
9. Hodde, J., *Naturally occurring scaffolds for soft tissue repair and regeneration.* Tissue Engineering, 2002. **8**(2): p. 295-308.
10. Place, E.S., N.D. Evans, and M.M. Stevens, *Complexity in biomaterials for tissue engineering.* Nature Materials, 2009. **8**(6): p. 457-470.

11. Ahuja, T., et al., *Biomolecular immobilization on conducting polymers for biosensing applications.* Biomaterials, 2007. **28**(5): p. 791-805.

12. Sofia, S., et al., *Functionalized silk-based biomaterials for bone formation.* Journal of Biomedical Materials Research, 2001. **54**(1): p. 139-148.

13. Schmidt, C.E. and J.M. Baier, *Acellular vascular tissues: natural biomaterials for tissue repair and tissue engineering.* Biomaterials, 2000. **21**(22): p. 2215-2231.

14. Ratner, B.D. and S.J. Bryant, *Biomaterials: Where we have been and where we are going.* Annual Review of Biomedical Engineering, 2004. **6**: p. 41-75.

15. Hardy, J.G. and T.R. Scheibel, *Composite materials based on silk proteins.* Progress in Polymer Science, 2010. **35**(9): p. 1093-1115.

16. Murphy, A.R. and D.L. Kaplan, *Biomedical applications of chemically-modified silk fibroin.* Journal of Materials Chemistry, 2009. **19**(36): p. 6443-6450.

17. Ayutsede, J., et al., *Carbon nanotube reinforced Bombyx mori silk nanofibers by the electrospinning process.* Biomacromolecules, 2006. **7**(1): p. 208-214.

18. Feng, X.-X., et al., *Preparation and characterization of novel nanocomposite films formed from silk fibroin and nano-TiO2.* International journal of biological macromolecules, 2007. **40**(2): p. 105-111.

19. Kim, H.J., et al., *Bone tissue engineering with premineralized silk scaffolds.* Bone, 2008. **42**(6): p. 1226-1234.

20. Chen, G., et al., *Silk fibroin modified porous poly(E-caprolactone) scaffold for human fibroblast culture in vitro.* Journal of Materials Science-Materials in Medicine, 2004. **15**(6): p. 671-677.

21. Rockwood, D.N., et al., *Materials fabrication from Bombyx mori silk fibroin.* Nat. Protocols, 2011. **6**(10): p. 1612-1631.

22. Gobin, A.S., V.E. Froude, and A.B. Mathur, *Structural and mechanical characteristics of silk fibroin and chitosan blend scaffolds for tissue regeneration.* Journal of Biomedical Materials Research Part a, 2005. **74A**(3): p. 465-473.

23. Jin, H.J., et al., *Water-Stable Silk Films with Reduced β-Sheet Content.* Advanced Functional Materials, 2005. **15**(8): p. 1241-1247.

24. Oh, S.J., et al., *Surface modification for DNA and protein microarrays.* Omics-a Journal of Integrative Biology, 2006. **10**(3): p. 327-343.

25. Chalker, J.M., et al., *Chemical Modification of Proteins at Cysteine: Opportunities in Chemistry and Biology.* Chemistry-an Asian Journal, 2009. **4**(5): p. 630-640.

26. Lundblad, R.L., *Chemical reagents for protein modification*. 3rd ed. 2005, Boca Raton: CRC Press. 339 p.

27. Cai, K., et al., *Poly(d,l-lactic acid) surfaces modified by silk fibroin: effects on the culture of osteoblast in vitro.* Biomaterials, 2002. **23**(4): p. 1153-1160.

28. Ma, X.L., C.B. Cao, and H.S. Zhu, *The biocompatibility of silk fibroin films containing sulfonated silk fibroin.* Journal of Biomedical Materials Research Part B-Applied Biomaterials, 2006. **78B**(1): p. 89-96.

29. Williams, C.K., *Synthesis of functionalized biodegradable polyesters.* Chemical Society Reviews, 2007. **36**(10): p. 1573-1580.

30. Ragauskas, A.J., et al., *The path forward for biofuels and biomaterials.* Science, 2006. **311**(5760): p. 484-489.

31. Hansen, N.M.L. and D. Plackett, *Sustainable films and coatings from hemicelluloses: A review.* Biomacromolecules, 2008. **9**(6): p. 1493-1505.

32. Tao, H., D.L. Kaplan, and F.G. Omenetto, *Silk Materials - A Road to Sustainable High Technology.* Advanced Materials, 2012. **24**(21): p. 2824-2837.

33. Whitesides, G.M. and B. Grzybowski, *Self-assembly at all scales.* Science, 2002. **295**(5564): p. 2418-2421.

34. Israelachvili, J.N., D.J. Mitchell, and B.W. Ninham, *Theory of self-assembly of lipid bilayers and vesicles.* Biochimica et biophysica acta, 1977. **470**(2): p. 185-201.

35. Winfree, E., et al., *Design and self-assembly of two-dimensional DNA crystals.* Nature, 1998. **394**(6693): p. 539-544.

36. Jin, H.-J. and D.L. Kaplan, *Mechanism of silk processing in insects and spiders.* Nature, 2003. **424**(6952): p. 1057-1061.

37. Khire, T.S., et al., *The fractal self-assembly of the silk protein sericin.* Soft Matter, 2010. **6**(9): p. 2066-2071.

38. Lu, Q., et al., *Silk Self-Assembly Mechanisms and Control From Thermodynamics to Kinetics.* Biomacromolecules, 2012. **13**(3): p. 826-832.

39. Kurland, N.E., et al., *Self-assembly mechanisms of silk protein nanostructures on two-dimensional surfaces.* Soft Matter, 2012. **8**(18): p. 4952-4959.

40. Scott, P., *The book of silk.* 1993, London: Thames and Hudson. 256 p.

41. Mackenzie, D., *The History of Sutures.* Medical History, 1973. **17**(02): p. 158-168.

42. Vepari, C. and D.L. Kaplan, *Silk as a biomaterial.* Progress in Polymer Science, 2007. **32**(8-9): p. 991-1007.

43. Horan, R.L., et al., *In vitro degradation of silk fibroin.* Biomaterials, 2005. **26**(17): p. 3385-3393.

44. Suzuki, Y., D.D. Brown, and L.P. Gage, *Genes for Silk Fibroin in Bombyx-Mori.* Journal of Molecular Biology, 1972. **70**(3): p. 637-&.

45. Minoura, N., et al., *Attachment and growth of cultured fibroblast cells on silk protein matrices.* J Biomed Mater Res, 1995. **29**(10): p. 1215-21.

46. Pérez-Rigueiro, J., et al., *Silkworm silk as an engineering material.* Journal of Applied Polymer Science, 1998. **70**(12): p. 2439-2447.

47. Heim, M., D. Keerl, and T. Scheibel, *Spider Silk: From Soluble Protein to Extraordinary Fiber.* Angewandte Chemie-International Edition, 2009. **48**(20): p. 3584-3596.

48. Gamo, T., T. Inokuchi, and H. Laufer, *Polypeptides of fibroin and sericin secreted from the different sections of the silk gland in Bombyx mori.* Insect Biochemistry, 1977. **7**(3): p. 285-295.

49. Lotz, B. and F. Colonna Cesari, *The chemical structure and the crystalline structures of Bombyx mori silk fibroin.* Biochimie, 1979. **61**(2): p. 205-214.

50. Pérez-Rigueiro, J., et al., *Mechanical properties of single-brin silkworm silk.* Journal of Applied Polymer Science, 2000. **75**(10): p. 1270-1277.

51. Valluzzi, R., et al., *Silk: molecular organization and control of assembly.* Philosophical Transactions of the Royal Society of London. Series B: Biological Sciences, 2002. **357**(1418): p. 165-167.

52. Klok, H.-A., et al., *Cholesteryl-(l-Lactic Acid)n̄ Building Blocks for Self-Assembling Biomaterials.* Macromolecules, 2002. **35**(3): p. 746-759.

53. Kyle, S., et al., *Production of self-assembling biomaterials for tissue engineering.* Trends in Biotechnology, 2009. **27**(7): p. 423-433.

54. Dewair, M., X. Baur, and K. Ziegler, *Use of Immunoblot Technique for Detection of Human Ige and Igg Antibodies to Individual Silk Proteins.* Journal of Allergy and Clinical Immunology, 1985. **76**(4): p. 537-542.

55. Soong, H.K. and K.R. Kenyon, *Adverse reactions to virgin silk sutures in cataract surgery.* Ophthalmology, 1984. **91**(5): p. 479-483.

56. Panilaitis, B., et al., *Macrophage responses to silk.* Biomaterials, 2003. **24**(18): p. 3079-3085.

57. Zhou, C.Z., et al., *Fine organization of Bombyx mori fibroin heavy chain gene.* Nucleic acids research, 2000. **28**(12): p. 2413-2419.

58. Zhou, C.-Z., et al., *Silk fibroin: Structural implications of a remarkable amino acid sequence.* Proteins: Structure, Function, and Bioinformatics, 2001. **44**(2): p. 119-122.

59. Nakamae, K., T. Nishino, and H. Ohkubo, *Elastic-Modulus of the Crystalline Regions of Silk Fibroin.* Polymer, 1989. **30**(7): p. 1243-1246.

60. Shao, Z.Z. and F. Vollrath, *Materials: Surprising strength of silkworm silk.* Nature, 2002. **418**(6899): p. 741-741.

61. Pins, G.D., et al., *Self-assembly of collagen fibers. Influence of fibrillar alignment and decorin on mechanical properties.* Biophysical journal, 1997. **73**(4): p. 2164-2172.

62. Engelberg, I. and J. Kohn, *Physicomechanical Properties of Degradable Polymers Used in Medical Applications - a Comparative-Study.* Biomaterials, 1991. **12**(3): p. 292-304.

63. Pérez-Rigueiro, J., et al., *Effect of degumming on the tensile properties of silkworm (Bombyx mori) silk fiber.* Journal of Applied Polymer Science, 2002. **84**(7): p. 1431-1437.

64. Tsukada, M., et al., *Structural changes of silk fibroin membranes induced by immersion in methanol aqueous solutions.* Journal of Polymer Science Part B: Polymer Physics, 1994. **32**(5): p. 961-968.

65. Minoura, N., M. Tsukada, and M. Nagura, *Fine-Structure and Oxygen Permeability of Silk Fibroin Membrane Treated with Methanol.* Polymer, 1990. **31**(2): p. 265-269.

66. Taddei, P., et al., *In vitro study of the proteolytic degradation of Antheraea pernyi silk fibroin.* Biomacromolecules, 2006. **7**(1): p. 259-267.

67. Park, S.H., et al., *Relationships between degradability of silk scaffolds and osteogenesis.* Biomaterials, 2010. **31**(24): p. 6162-6172.

68. Santin, M., et al., *In vitro evaluation of the inflammatory potential of the silk fibroin.* Journal of Biomedical Materials Research, 1999. **46**(3): p. 382-389.

69. Meinel, L., et al., *The inflammatory responses to silk films in vitro and in vivo.* Biomaterials, 2005. **26**(2): p. 147-155.

70. Tsujimoto, K., et al., *Cryoprotective effect of the serine-rich repetitive sequence in silk protein sericin.* Journal of Biochemistry, 2001. **129**(6): p. 979-986.

71. Takasu, Y., H. Yamada, and K. Tsubouchi, *Isolation of three main sericin components from the cocoon of the silkworm, Bombyx mori.* Bioscience Biotechnology and Biochemistry, 2002. **66**(12): p. 2715-2718.

72. Teramoto, H. and M. Miyazawa, *Molecular orientation behavior of silk sericin film as revealed by ATR infrared spectroscopy.* Biomacromolecules, 2005. **6**(4): p. 2049-2057.

73. Padamwar, M.N. and A.P. Pawar, *Silk sericin and its applications: A review.* Journal of Scientific & Industrial Research, 2004. **63**(4): p. 323-329.

74. Tsubouchi, K., et al., *Sericin enhances attachment of cultured human skin fibroblasts.* Bioscience Biotechnology and Biochemistry, 2005. **69**(2): p. 403-405.

75. Zhang, F., et al., *Silk-functionalized titanium surfaces for enhancing osteoblast functions and reducing bacterial adhesion.* Biomaterials, 2008. **29**(36): p. 4751-4759.

76. Terada, S., et al., *Preparation of silk protein sericin as mitogenic factor for better mammalian cell culture.* Journal of Bioscience and Bioengineering, 2005. **100**(6): p. 667-671.

77. Teramoto, H., T. Kameda, and Y. Tamada, *Preparation of Gel Film from Bombyx mori Silk Sericin and Its Characterization as a Wound Dressing.* Bioscience Biotechnology and Biochemistry, 2008. **72**(12): p. 3189-3196.

78. Zhang, Y.-Q., *Applications of natural silk protein sericin in biomaterials.* Biotechnology Advances, 2002. **20**(2): p. 91-100.

79. Galeotti, F., et al., *Precise surface patterning of silk fibroin films by breath figures.* Soft Matter, 2012. **8**(17): p. 4815-4821.

80. Perry, H., et al., *Nano- and Micropatterning of Optically Transparent, Mechanically Robust, Biocompatible Silk Fibroin Films.* Advanced Materials, 2008. **20**(16): p. 3070-3072.

81. Nazarov, R., H.J. Jin, and D.L. Kaplan, *Porous 3-D scaffolds from regenerated silk fibroin.* Biomacromolecules, 2004. **5**(3): p. 718-726.

82. Kim, S., et al., *Silk inverse opals.* Nature Photonics, 2012. **6**(12): p. 817-822.

83. Bettinger, C.J., et al., *Silk Fibroin Microfluidic Devices.* Advanced Materials, 2007. **19**(19): p. 2847-2850.

84. Amsden, J.J., et al., *Rapid Nanoimprinting of Silk Fibroin Films for Biophotonic Applications.* Advanced Materials, 2010. **22**(15): p. 1746-1749.

85. Kim, D.-H., et al., *Dissolvable films of silk fibroin for ultrathin conformal bio-integrated electronics.* Nat Mater, 2010. **9**(6): p. 511-517.

86. Wang, C.H., C.Y. Hsieh, and J.C. Hwang, *Flexible Organic Thin-Film Transistors with Silk Fibroin as the Gate Dielectric.* Advanced Materials, 2011. **23**(14): p. 1630-+.

87. Hota, M.K., et al., *A Natural Silk Fibroin Protein-Based Transparent Bio-Memristor.* Advanced Functional Materials, 2012. **22**(21): p. 4493-4499.

88. Ohgo, K., et al., *Preparation of non-woven nanofibers of Bombyx mori silk, Samia cynthia ricini silk and recombinant hybrid silk with electrospinning method.* Polymer, 2003. **44**(3): p. 841-846.

89. Wang, M., et al., *Mechanical properties of electrospun silk fibers.* Macromolecules, 2004. **37**(18): p. 6856-6864.

90. Teramoto, H., K. Nakajima, and C. Takabayashi, *Preparation of elastic silk sericin hydrogel.* Bioscience Biotechnology and Biochemistry, 2005. **69**(4): p. 845-847.

91. Aznar-Cervantes, S., et al., *Fabrication of conductive electrospun silk fibroin scaffolds by coating with polypyrrole for biomedical applications.* Bioelectrochemistry, 2012. **85**: p. 36-43.

92. Sashina, E.S., et al., *Preparation and properties of films of fibroin-polyvinyl alcohol blends from solutions in hexafluoroisopropanol.* Russian Journal of Applied Chemistry, 2007. **80**(3): p. 466-471.

93. Liu, X.Y., et al., *Controlled release of heparin from blended polyurethane and silk fibroin film.* Materials Letters, 2009. **63**(2): p. 263-265.

94. Roohani-Esfahani, S.I., et al., *Effect of self-assembled nanofibrous silk/polycaprolactone layer on the osteoconductivity and mechanical properties of biphasic calcium phosphate scaffolds.* Acta Biomaterialia, 2012. **8**(1): p. 302-312.

95. Cai, Z.X., et al., *Fabrication of Chitosan/Silk Fibroin Composite Nanofibers for Wound-dressing Applications.* International Journal of Molecular Sciences, 2010. **11**(9): p. 3529-3539.

96. She, Z., et al., *Silk fibroin/chitosan scaffold: preparation, characterization, and culture with HepG2 cell.* Journal of Materials Science: Materials in Medicine, 2008. **19**(12): p. 3545-3553.

97. Xia, Y. and L. Yun, *Fabrication and properties of conductive conjugated polymers/silk fibroin composite fibers.* Composites Science and Technology, 2008. **68**(6): p. 1471-1479.

98. Lv, Q., et al., *Fibroin/collagen hybrid hydrogels with crosslinking method: Preparation, properties, and cytocompatibility.* Journal of Biomedical Materials Research Part a, 2008. **84A**(1): p. 198-207.

99. Choi, Y., et al., *Enhanced mechanical properties of silk fibroin-based composite plates for fractured bone healing.* Fibers and Polymers, 2013. **14**(2): p. 266-270.

100. Lv, Q., et al., *Preparation and characterization of PLA/fibroin composite and culture of HepG2 (human hepatocellular liver carcinoma cell line) cells.* Composites Science and Technology, 2007. **67**(14): p. 3023-3030.

101. Wang, L. and C. Li, *Preparation and physicochemical properties of a novel hydroxyapatite/chitosan–silk fibroin composite.* Carbohydrate Polymers, 2007. **68**(4): p. 740-745.

102. Nair, L.S. and C.T. Laurencin, *Biodegradable polymers as biomaterials.* Progress in Polymer Science, 2007. **32**(8–9): p. 762-798.

103. Chen, X., et al., *Studies on chitosan-fibroin blend membranes .2. The pH and ion sensitivities of semi-IPN membranes.* Chemical Journal of Chinese Universities-Chinese, 1996. **17**(6): p. 968-972.

104. Roweton, S., S.J. Huang, and G. Swift, *Poly(aspartic acid): Synthesis, biodegradation, and current applications.* Journal of Environmental Polymer Degradation, 1997. **5**(3): p. 175-181.

105. Zhao, J., et al., *Apatite-coated silk fibroin scaffolds to healing mandibular border defects in canines.* Bone, 2009. **45**(3): p. 517-527.

106. Jiang, X.Q., et al., *Mandibular repair in rats with premineralized silk scaffolds and BMP-2-modified bMSCs.* Biomaterials, 2009. **30**(27): p. 4522-4532.

107. Shimokuri, T., T. Kaneko, and M. Akashi, *Specific thermosensitive volume change of biopolymer gels derived from propylated poly(gamma-glutamate)s.* Journal of Polymer Science Part a-Polymer Chemistry, 2004. **42**(18): p. 4492-4501.

108. Yerushalmi, R., et al., *Stimuli responsive materials: new avenues toward smart organic devices.* Journal of Materials Chemistry, 2005. **15**(42): p. 4480-4487.

109. Gyenes, T., et al., *Synthesis and swelling properties of novel pH-sensitive poly(aspartic acid) gels.* Acta Biomaterialia, 2008. **4**(3): p. 733-744.

110. Yuk, S.H., S.H. Cho, and S.H. Lee, *pH/Temperature-Responsive Polymer Composed of Poly((N,N-dimethylamino)ethyl methacrylate-co-ethylacrylamide).* Macromolecules, 1997. **30**(22): p. 6856-6859.

111. Ehrick, J.D., et al., *Genetically engineered protein in hydrogels tailors stimuli-responsive characteristics.* Nat Mater, 2005. **4**(4): p. 298-302.

112. Motta, A., et al., *Stabilization of Bombyx mori silk fibroin/sericin films by crosslinking with PEG-DE 600 and genipin.* Journal of Bioactive and Compatible Polymers, 2011. **26**(2): p. 130-143.

113. Lawrence, B., et al., *Processing methods to control silk fibroin film biomaterial features.* Journal of Materials Science, 2008. **43**(21): p. 6967-6985.

114. Kane, R.S., et al., *Patterning proteins and cells using soft lithography.* Biomaterials, 1999. **20**(23–24): p. 2363-2376.

115. Veiseh, M., M.H. Zareie, and M.Q. Zhang, *Highly selective protein patterning on gold-silicon substrates for biosensor applications.* Langmuir, 2002. **18**(17): p. 6671-6678.

116. Nelson, C.M. and J. Tien, *Microstructured extracellular matrices in tissue engineering and development.* Current Opinion in Biotechnology, 2006. **17**(5): p. 518-523.

117. Blawas, A.S. and W.M. Reichert, *Protein patterning.* Biomaterials, 1998. **19**(7–9): p. 595-609.

118. Wang, Y., et al., *Stem cell-based tissue engineering with silk biomaterials.* Biomaterials, 2006. **27**(36): p. 6064-6082.

119. Hardy, J.G., L.M. Römer, and T.R. Scheibel, *Polymeric materials based on silk proteins.* Polymer, 2008. **49**(20): p. 4309-4327.

120. Grabarek, Z. and J. Gergely, *Zero-length crosslinking procedure with the use of active esters.* Analytical Biochemistry, 1990. **185**(1): p. 131-135.

121. Wong, S.S. and D.M. Jameson, *Chemistry of protein and nucleic acid cross-linking and conjugation*. 2nd ed. 2012, Boca Raton: Taylor & Francis/CRC Press. xvii, 602 p.

122. Sung, H.-W., et al., *Crosslinking of biological tissues using genipin and/or carbodiimide.* Journal of Biomedical Materials Research Part a, 2003. **64A**(3): p. 427-438.

123. Mandal, B.B., B. Ghosh, and S.C. Kundu, *Non-mulberry silk sericin/poly (vinyl alcohol) hydrogel matrices for potential biotechnological applications.* International journal of biological macromolecules, 2011. **49**(2): p. 125-133.

124. Nie, Z.H. and E. Kumacheva, *Patterning surfaces with functional polymers.* Nature Materials, 2008. **7**(4): p. 277-290.

125. Decker, C., *Kinetic study and new applications of UV radiation curing.* Macromolecular Rapid Communications, 2002. **23**(18): p. 1067-1093.

126. Grinstaff, M.W., et al., *Photocrosslinkable polymers for biomedical applications.* Abstracts of Papers of the American Chemical Society, 2001. **222**: p. U249-U249.

127. Anderson, D.G., et al., *A combinatorial library of photocrosslinkable and degradable materials.* Advanced Materials, 2006. **18**(19): p. 2614-+.

128. Fodor, S., et al., *Light-directed, spatially addressable parallel chemical synthesis.* Science, 1991. **251**(4995): p. 767-773.

129. Revzin, A., et al., *Fabrication of Poly(ethylene glycol) Hydrogel Microstructures using Photolithography.* Langmuir, 2001. **17**(18): p. 5440-5447.

130. Cuchiara, M.P., et al., *Multilayer microfluidic PEGDA hydrogels.* Biomaterials, 2010. **31**(21): p. 5491-5497.

131. Zhong, C., et al., *Synthesis, characterization and cytotoxicity of photo-crosslinked maleic chitosan–polyethylene glycol diacrylate hybrid hydrogels.* Acta Biomaterialia, 2010. **6**(10): p. 3908-3918.

132. Williams, C.G., et al., *Variable cytocompatibility of six cell lines with photoinitiators used for polymerizing hydrogels and cell encapsulation.* Biomaterials, 2005. **26**(11): p. 1211-1218.

133. Mooney, J.F., et al., *Patterning of functional antibodies and other proteins by photolithography of silane monolayers.* Proceedings of the National Academy of Sciences of the United States of America, 1996. **93**(22): p. 12287-12291.

134. Douvas, A., et al., *Biocompatible photolithographic process for the patterning of biomolecules.* Biosensors and Bioelectronics, 2002. **17**(4): p. 269-278.

135. Mir, M., et al., *Electrochemical biosensor microarray functionalized by means of biomolecule friendly photolithography.* Biosensors and Bioelectronics, 2010. **25**(9): p. 2115-2121.

136. Griffin, B.A., S.R. Adams, and R.Y. Tsien, *Specific Covalent Labeling of Recombinant Protein Molecules Inside Live Cells.* Science, 1998. **281**(5374): p. 269-272.

137. Kalia, J. and R.T. Raines, *Advances in Bioconjugation.* Current Organic Chemistry, 2010. **14**(2): p. 138-147.

138. Chin, J.W., et al., *Addition of a photocrosslinking amino acid to the genetic code of Escherichia coli.* Proceedings of the National Academy of Sciences of the United States of America, 2002. **99**(17): p. 11020-11024.

139. Carrico, I.S., et al., *Lithographic Patterning of Photoreactive Cell-Adhesive Proteins.* Journal of the American Chemical Society, 2007. **129**(16): p. 4874-4875.

140. Hino, N., et al., *Protein photo-cross-linking in mammalian cells by site-specific incorporation of a photoreactive amino acid.* Nat Meth, 2005. **2**(3): p. 201-206.

141. Carlsson, J., H. Drevin, and R. Axén, *Protein thiolation and reversible protein-protein conjugation. N-Succinimidyl 3-(2-pyridyldithio)propionate, a new heterobifunctional reagent.* Biochem. J., 1978. **173**(3): p. 723-737.

142. Nowatzki, P.J. and D.A. Tirrell, *Physical properties of artificial extracellular matrix protein films prepared by isocyanate crosslinking.* Biomaterials, 2004. **25**(7–8): p. 1261-1267.

143. Raphel, J., A. Parisi-Amon, and S.C. Heilshorn, *Photoreactive elastin-like proteins for use as versatile bioactive materials and surface coatings.* Journal of Materials Chemistry, 2012. **22**(37): p. 19429-19437.

144. Wang, W. and S.A. Soper, *Bio-MEMS : technologies and applications*. 2007, Boca Raton: CRC/Taylor & Francis. 477 p.

145. Rabarot, M., et al. *Thick SU-8 photolithography for BioMEMS*. 2003.

146. Yuli, W., et al., *Surface graft polymerization of SU-8 for bio-MEMS applications.* Journal of Micromechanics and Microengineering, 2007. **17**(7): p. 1371.

147. Pease, R.F. and S.Y. Chou, *Lithography and other patterning techniques for future electronics.* Proceedings of the Ieee, 2008. **96**(2): p. 248-270.

148. Mansuripur, M. and R. Liang, *Projection Photolithography.* Optics and Photonics News, 2000. **11**(2): p. 36-40.

149. Levinson, H.J., *Principles of lithography*. 3rd ed. Press monograph. 2010, Bellingham, Wash.: SPIE Press. xiv, 503 p.

150. Madou, M.J., *Fundamentals of microfabrication : the science of miniaturization*. 2nd ed. 2002, Boca Raton: CRC Press. 723 p.

151. Huang, J., et al., *Cloning, expression, and assembly of sericin-like protein.* Journal of Biological Chemistry, 2003. **278**(46): p. 46117-46123.

152. Arnold, W. and H.V. Mayersbach, *Changes in the solubility of immunoglobulins after fluorescent labeling and its influence on immunofluorescent techniques.* Journal of Histochemistry & Cytochemistry, 1972. **20**(12): p. 975-985.

153. Wagner, J.R., D.A. Sorgentini, and M.C. Anon, *Relation between Solubility and Surface Hydrophobicity as an Indicator of Modifications during Preparation*

Processes of Commercial and Laboratory-Prepared Soy Protein Isolates. Journal of Agricultural and Food Chemistry, 2000. **48**(8): p. 3159-3165.

154. Brahim, S., D. Narinesingh, and A. Guiseppi-Elie, *Synthesis and Hydration Properties of pH-Sensitive p(HEMA)-Based Hydrogels Containing 3-(Trimethoxysilyl)propyl Methacrylate.* Biomacromolecules, 2003. **4**(3): p. 497-503.

155. Aramwit, P., et al., *The Effect of Sericin from Various Extraction Methods on Cell Viability and Collagen Production.* International Journal of Molecular Sciences, 2010. **11**(5): p. 2200-2211.

156. Aznar-Cervantes, S.D., et al., *Influence of the protocol used for fibroin extraction on the mechanical properties and fiber sizes of electrospun silk mats.* Materials Science & Engineering C-Materials for Biological Applications, 2013. **33**(4): p. 1945-1950.

157. Gleason, N.J., et al., *Patterning proteins and cells using two-dimensional arrays of colloids.* Langmuir, 2003. **19**(3): p. 513-518.

158. Philp, D. and J.F. Stoddart, *Self-assembly in natural and unnatural systems.* Angewandte Chemie-International Edition in English, 1996. **35**(11): p. 1155-1196.

159. Rochet, J.C. and P.T. Lansbury, *Amyloid fibrillogenesis: themes and variations.* Current Opinion in Structural Biology, 2000. **10**(1): p. 60-68.

160. Zhang, S.G., *Fabrication of novel biomaterials through molecular self-assembly.* Nature Biotechnology, 2003. **21**(10): p. 1171-1178.

161. Lin, M.Y., et al., *Universal reaction-limited colloid aggregation.* Physical Review A, 1990. **41**(4): p. 2005.

162. Ramanlal, P. and L.M. Sander, *Theory of Ballistic Aggregation.* Physical Review Letters, 1985. **54**(16): p. 1828.

163. Bohr, H., et al., *Hierarchical organization in aggregates of protein molecules.* Zeitschrift für Physik D Atoms, Molecules and Clusters, 1997. **40**(1): p. 513-515.

164. Meakin, P., *Models for Colloidal Aggregation.* Annual Review of Physical Chemistry, 1988. **39**: p. 237-267.

165. Choi, J., D. Crowdy, and M.Z. Bazant, *Diffusion-limited aggregation on curved surfaces.* EPL (Europhysics Letters), 2010. **91**(4): p. 46005.

166. Tokuyama, M. and K. Kawasaki, *Fractal Dimensions For Diffusion-Limited Aggregation.* Physics Letters A, 1984. **100**(7): p. 337-340.

167. Chiu, K.C., et al., *A Study in Monte-Carlo Simulation of Modified Dla.* Chinese Journal of Physics, 1992. **30**(1): p. 143-155.

168. Lin, M.Y., et al., *Universality in Colloid Aggregation.* Nature, 1989. **339**(6223): p. 360-362.

169. Weitz, D.A., et al., *Limits of the Fractal Dimension for Irreversible Kinetic Aggregation of Gold Colloids.* Physical Review Letters, 1985. **54**(13): p. 1416-1419.

170. Ossadnik, P., C.H. Lam, and L.M. Sander, *Nonuniversal Diffusion-Limited Aggregation and Exact Fractal Dimensions.* Physical Review E, 1994. **49**(3): p. R1788-R1791.

171. Zhao, Q., et al., *Interfacial self-assembly of cellulose-based polyelectrolyte complexes: pattern formation of fractal "trees".* Soft Matter, 2010. **6**(6): p. 1129-1137.

172. Lomander, A., W.M. Hwang, and S.G. Zhang, *Hierarchical self-assembly of a coiled-coil peptide into fractal structure.* Nano Letters, 2005. **5**(7): p. 1255-1260.

173. Gupta, A.N. and H.B. Bohidar, *Temporal evolution of self-organization of gelatin molecules and clusters on quartz surface.* Physical Review E, 2007. **76**(5).

174. Lin, D.C., B. Yurke, and N.A. Langrana, *Mechanical Properties of a Reversible, DNA-Crosslinked Polyacrylamide Hydrogel.* Journal of Biomechanical Engineering, 2004. **126**(1): p. 104-110.

175. Jia, H., C.W.P. Foo, and D.L. Kaplan, *Biosynthesis and Applications of Silk-like and Collagen-like Proteins.* Polymer Reviews, 2007. **47**(1): p. 29-62.

176. Cao, Z.B., et al., *The preparation of regenerated silk fibroin microspheres.* Soft Matter, 2007. **3**(7): p. 910-915.

177. Akiyama, D., M. Okazaki, and K. Hirabayashi, *Method for the preparation of a polymer with a high water absorption capacity containing sericin.* The Journal of Sericultural Science of Japan, 1993. **62**(5): p. 392-396.

178. Abramoff, M.D.M., P.J. and S.J. Ram, *Image Processing with ImageJ.* Biophotonics International, 2004. **11**(7): p. 36-42.

179. Smith, T.G., G.D. Lange, and W.B. Marks, *Fractal methods and results in cellular morphology - Dimensions, lacunarity and multifractals.* Journal of Neuroscience Methods, 1996. **69**(2): p. 123-136.

180. Whitmore, L. and B.A. Wallace, *DICHROWEB, an online server for protein secondary structure analyses from circular dichroism spectroscopic data.* Nucleic acids research, 2004. **32**: p. W668-W673.

181. Whitmore, L. and B.A. Wallace, *Protein secondary structure analyses from circular dichroism spectroscopy: Methods and reference databases.* Biopolymers, 2008. **89**(5): p. 392-400.

182. Hu, Y., et al., *Self-assembly and Fractal Feature of Chitosan and Its Conjugate with Metal Ions: Cu (II) / Ag (I).* International Journal of Molecular Sciences, 2007. **8**(1): p. 1-12.

183. Dash, R., S. Mukherjee, and S.C. Kundu, *Isolation, purification and characterization of silk protein sericin from cocoon peduncles of tropical tasar silkworm, Antheraea mylitta.* International journal of biological macromolecules, 2006. **38**(3-5): p. 255-258.

184. Dash, R., et al., *Purification and biochemical characterization of a 70 kDa sericin from tropical tasar silkworm, Antheraea mylitta.* Comparative Biochemistry and Physiology B-Biochemistry & Molecular Biology, 2007. **147**(1): p. 129-134.

185. Ahmad, R., A. Kamra, and S.E. Hasnain, *Fibroin silk proteins from the nonmulberry silkworm Philosamia ricini are biochemically and immunochemically distinct from those of the mulberry silkworm Bombyx mori.* DNA and Cell Biology, 2004. **23**(3): p. 149-154.

186. Viswanath, B., et al., *Nanoporous Pt with High Surface Area by Reaction-Limited Aggregation of Nanoparticles.* Langmuir, 2009. **25**(5): p. 3115-3121.

187. Alkorta, J., J.M. Martinez-Esnaola, and J.G. Sevillano, *Critical examination of strain-rate sensitivity measurement by nanoindentation methods: Application to severely deformed niobium.* Acta Materialia, 2008. **56**(4): p. 884-893.

188. Song, X., *Role of anisotropic interactions in protein crystallization.* Physical Review E, 2002. **66**(1): p. 011909.

189. Witten, T.A. and L.M. Sander, *Diffusion-Limited Aggregation, a Kinetic Critical Phenomenon.* Physical Review Letters, 1981. **47**(19): p. 1400.

190. Witten, T.A. and L.M. Sander, *Diffusion-limited aggregation.* Physical Review B, 1983. **27**(9): p. 5686-5697.

191. Tan, Z.J., et al., *Influence of particle size on diffusion-limited aggregation.* Physical Review E, 1999. **60**(5): p. 6202-6205.

192. Paul, B., *Constrained diffusion-limited aggregation in 3 dimensions.* Computers & Graphics, 2006. **30**(4): p. 646-649.

193. Majhi, P.R., et al., *Electrostatically driven protein aggregation: beta-lactoglobulin at low ionic strength.* Langmuir, 2006. **22**(22): p. 9150-9159.

194. Pastor-Satorras, R. and J.M. Rubí, *Particle-cluster aggregation with dipolar interactions.* Physical Review E, 1995. **51**(6): p. 5994.

195. Tolman, S. and P. Meakin, *Off-lattice and hypercubic-lattice models for diffusion-limited aggregation in dimensionalities 2–8.* Physical Review A, 1989. **40**(1): p. 428-437.

196. Trivedi, R. and K. Somboonsuk, *Pattern formation during the directional solidification of binary systems.* Acta Metallurgica, 1985. **33**(6): p. 1061-1068.

197. Nagatani, T. and Y. Usami, *Pattern-Formation in Nonlinear Diffusion-Limited Aggregation.* Physical Review A, 1989. **39**(4): p. 2169-2174.

198. Kessler, D.A., J. Koplik, and H. Levine, *Numerical simulation of two-dimensional snowflake growth.* Physical Review A, 1984. **30**(5): p. 2820-2823.

199. Nittmann, J. and H.E. Stanley, *Tip splitting without interfacial tension and dendritic growth patterns arising from molecular anisotropy.* Nature, 1986. **321**(6071): p. 663-668.

200. Hurd, A.J. and D.W. Schaefer, *Diffusion-Limited Aggregation in Two Dimensions.* Physical Review Letters, 1985. **54**(10): p. 1043-1046.

201. Krebs, M.R.H., et al., *The formation of spherulites by amyloid fibrils of bovine insulin.* Proceedings of the National Academy of Sciences of the United States of America, 2004. **101**(40): p. 14420-14424.

202. Wang, W.P. and Y. Chau, *Self-assembled peptide nanorods as building blocks of fractal patterns.* Soft Matter, 2009. **5**(24): p. 4893-4898.

203. Jachimska, B., M. Wasilewska, and Z. Adamczyk, *Characterization of globular protein solutions by dynamic light scattering, electrophoretic mobility, and viscosity measurements.* Langmuir, 2008. **24**(13): p. 6866-6872.

204. Chandra, A., et al., *Fractal Growth in Uv-Irradiated DNA - Evidence of Nonuniversal Diffusion-Limited Aggregation.* Physical Review E, 1995. **51**(4): p. R2767-R2768.

205. Giri, K., N.P. Bhattacharyya, and S. Basak, *pH-dependent self-assembly of polyalanine peptides.* Biophysical Journal, 2007. **92**(1): p. 293-302.

206. Holm, R.H., P. Kennepohl, and E.I. Solomon, *Structural and functional aspects of metal sites in biology.* Chemical Reviews, 1996. **96**(7): p. 2239-2314.

207. Eggers, D.K. and J.S. Valentine, *Molecular confinement influences protein structure and enhances thermal protein stability.* Protein Science, 2001. **10**(2): p. 250-261.

208. Zhang, S.G., et al., *Spontaneous Assembly of a Self-Complementary Oligopeptide to Form a Stable Macroscopic Membrane.* Proceedings of the National Academy of Sciences of the United States of America, 1993. **90**(8): p. 3334-3338.

209. Askarieh, G., et al., *Self-assembly of spider silk proteins is controlled by a pH-sensitive relay.* Nature, 2010. **465**(7295): p. 236-U125.

210. Zong, X.H., et al., *Effect of pH and copper(II) on the conformation transitions of silk fibroin based on EPR, NMR, and Raman spectroscopy.* Biochemistry, 2004. **43**(38): p. 11932-11941.

211. Ozbas, B., et al., *Salt-triggered peptide folding and consequent self-assembly into hydrogels with tunable modulus.* Macromolecules, 2004. **37**(19): p. 7331-7337.

212. Li, G.Y., et al., *The natural silk spinning process - A nucleation-dependent aggregation mechanism?* European Journal of Biochemistry, 2001. **268**(24): p. 6600-6606.

213. Li, M., et al., *Structure and properties of silk fibroin–poly(vinyl alcohol) gel.* International journal of biological macromolecules, 2002. **30**(2): p. 89-94.

214. Strelec, J.K., et al., *Design and implementation of a shape memory alloy actuated reconfigurable airfoil.* Journal of Intelligent Material Systems and Structures, 2003. **14**(4-5): p. 257-273.

215. Guimard, N.K., N. Gomez, and C.E. Schmidt, *Conducting polymers in biomedical engineering.* Progress in Polymer Science, 2007. **32**(8-9): p. 876-921.

216. Peppas, N.A., et al., *Hydrogels in biology and medicine: From molecular principles to bionanotechnology.* Advanced Materials, 2006. **18**(11): p. 1345-1360.

217. Mano, J.F., *Stimuli-responsive polymeric systems for biomedical applications.* Advanced Engineering Materials, 2008. **10**(6): p. 515-527.

218. Fairman, R. and K.S. Akerfeldt, *Peptides as novel smart materials.* Current Opinion in Structural Biology, 2005. **15**(4): p. 453-463.

219. Wornyo, E., et al., *Nanoindentation of shape memory polymer networks.* Polymer, 2007. **48**(11): p. 3213-3225.

220. Cai, W. and R.B. Gupta, *Hydrogels*, in *Kirk-Othmer Encyclopedia of Chemical Technology*. 2000, John Wiley & Sons, Inc.

221. Tachibana, Y., et al., *Thermoresponsive hydrogels based on biodegradable poly(amino acid)s.* Chemistry Letters, 2003. **32**(4): p. 374-375.

222. Park, T.G. and A.S. Hoffman, *Synthesis and Characterization of Ph- and or Temperature-Sensitive Hydrogels.* Journal of Applied Polymer Science, 1992. **46**(4): p. 659-671.

223. Khademhosseini, A. and R. Langer, *Microengineered hydrogels for tissue engineering.* Biomaterials, 2007. **28**(34): p. 5087-5092.

224. Kopecek, J., *Hydrogel biomaterials: A smart future?* Biomaterials, 2007. **28**(34): p. 5185-5192.

225. Kopecek, J. and J.Y. Yang, *Hydrogels as smart biomaterials.* Polymer International, 2007. **56**(9): p. 1078-1098.

226. Khan, W., et al., *Biodegradable Polymers Derived From Amino Acids.* Macromolecular Bioscience, 2011. **11**(12): p. 1625-1636.

227. Annabi, N., et al., *Synthesis of highly porous crosslinked elastin hydrogels and their interaction with fibroblasts in vitro.* Biomaterials, 2009. **30**(27): p. 4550-4557.

228. Nakato, T., et al., *Relationships between structure and properties of poly(aspartic acid)s.* Macromolecules, 1998. **31**(7): p. 2107-2113.

229. Alford, D.D.,Wheeler, A.P., Pettigrew, C.A., *Biodegradation of Thermally Synthesized Polyaspartate.* Journal of Environmental Polymer Degradation, 1994. **2**(4): p. 225-236.

230. Xia, Y., et al., *Monodispersed Colloidal Spheres: Old Materials with New Applications.* Advanced Materials, 2000. **12**(10): p. 693-713.

231. Khripin, C.Y., et al., *Protein-Directed Assembly of Arbitrary Three-Dimensional Nanoporous Silica Architectures.* ACS Nano, 2011. **5**(2): p. 1401-1409.

232. Nathwani, B.B., et al., *Fabrication and Characterization of Silk-Fibroin-Coated Quantum Dots.* Ieee Transactions on Nanobioscience, 2009. **8**(1): p. 72-77.

233. Kundu, B. and S.C. Kundu, *Silk sericin/polyacrylamide in situ forming hydrogels for dermal reconstruction.* Biomaterials, 2012. **33**(30): p. 7456-7467.

234. Wenk, E., H.P. Merkle, and L. Meinel, *Silk fibroin as a vehicle for drug delivery applications.* Journal of Controlled Release, 2011. **150**(2): p. 128-141.

235. Terada, S., et al., *Sericin, a protein derived from silkworms, accelerates the proliferation of several mammalian cell lines including a hybridoma.* Cytotechnology, 2002. **40**(1-3): p. 3-12.

236. Kovalev, A., et al., *Nanomechanical probing of layered nanoscale polymer films with atomic force microscopy.* Journal of Materials Research, 2004. **19**(3): p. 716-728.

237. Kurland, N.E., Z. Drira, and V.K. Yadavalli, *Measurement of nanomechanical properties of biomolecules using atomic force microscopy.* Micron, 2012. **43**(2–3): p. 116-128.

238. Kwon, G.S., et al., *Biodistribution of Micelle-Forming Polymer Drug Conjugates.* Pharmaceutical Research, 1993. **10**(7): p. 970-974.

239. Capar, G., S.S. Aygun, and M.R. Gecit, *Treatment of silk production wastewaters by membrane processes for sericin recovery.* Journal of Membrane Science, 2008. **325**(2): p. 920-931.

240. Einstein, A., *Theorie der Opaleszenz von homogenen Flüssigkeiten und Flüssigkeitsgemischen in der Nähe des kritischen Zustandes.* Annalen der Physik, 1910. **338**(16): p. 1275-1298.

241. Debye, P., *Light Scattering in Solutions.* Journal of Applied Physics, 1944. **15**(4): p. 338-342.

242. Burchard, W., *Static and dynamic light scattering from branched polymers and biopolymers*, in *Light Scattering from Polymers*. 1983, Springer Berlin Heidelberg. p. 1-124.

243. Zimm, B.H., *Molecular Theory of the Scattering of Light in Fluids.* The Journal of Chemical Physics, 1945. **13**(4): p. 141-145.

244. Katritzky, A.R., et al., *Ring opening reactions of succinimides.* Heterocycles, 1998. **48**(12): p. 2677-2691.

245. Zhao, Y., et al., *Superabsorbent hydrogels from poly(aspartic acid) with salt-, temperature- and pH-responsiveness properties.* Polymer, 2005. **46**(14): p. 5368-5376.

246. Mosig, J., C.H. Gooding, and A.P. Wheeler, *Kinetic and Thermal Characterization of the Hydrolysis of Polysuccinimide.* Industrial & Engineering Chemistry Research, 1997. **36**(6): p. 2163-2170.

247. Jiang, H.L. and K.J. Zhu, *Comparison of poly(aspartic acid) hydrogel and poly(aspartic acid)/gelatin complex for entrapment and pH-sensitive release of protein drugs.* Journal of Applied Polymer Science, 2006. **99**(5): p. 2320-2329.

248. Cao, H., et al., *Preparation A Novel pH-Sensitive Blend Hydrogel Based on Polyaspartic Acid and Ethylcellulose for Controlled Release of Naproxen Sodium.* Journal of Applied Polymer Science, 2009. **113**(1): p. 327-336.

249. Varga, Z., et al., *Kinetics of volume change of poly(succinimide) gels during hydrolysis and swelling.* Physical Chemistry Chemical Physics, 2010. **12**(39): p. 12670-12675.

250. Zrinyi, M., et al., *Volume change of double cross-linked poly(aspartic acid) hydrogels induced by cleavage of one of the crosslinks.* Acta Biomaterialia, 2013. **9**(2): p. 5122-5131.

251. Zhang, H.P., et al., *Enhancing Effect of Glycerol on the Tensile Properties of Bombyx mori Cocoon Sericin Films.* International Journal of Molecular Sciences, 2011. **12**(5): p. 3170-3181.

252. Drira, Z. and V.K. Yadavalli, *Nanomechanical measurements of polyethylene glycol hydrogels using atomic force microscopy.* Journal of the Mechanical Behavior of Biomedical Materials, 2013. **18**: p. 20-8.

253. Cai, K.Y., et al., *Improvement of the functions of osteoblasts seeded on modified poly(D,L-lactic acid) with poly(aspartic acid).* Journal of Biomedical Materials Research, 2002. **62**(2): p. 283-291.

254. Omenetto, F.G. and D.L. Kaplan, *New Opportunities for an Ancient Material.* Science, 2010. **329**(5991): p. 528-531.

255. Tao, H., et al., *Implantable, multifunctional, bioresorbable optics.* Proceedings of the National Academy of Sciences, 2012. **109**(48): p. 19584-19589.

256. Miroiu, F.M., et al., *Composite biocompatible hydroxyapatite–silk fibroin coatings for medical implants obtained by Matrix Assisted Pulsed Laser Evaporation.* Materials Science and Engineering: B, 2010. **169**(1–3): p. 151-158.

257. Wang, L., R. Nemoto, and M. Senna, *Changes in microstructure and physico-chemical properties of hydroxyapatite–silk fibroin nanocomposite with varying silk fibroin content.* Journal of the European Ceramic Society, 2004. **24**(9): p. 2707-2715.

258. Lee, S.M., et al., *Novel silk/poly(butylene succinate) biocomposites: the effect of short fibre content on their mechanical and thermal properties.* Composites Science and Technology, 2005. **65**(3–4): p. 647-657.

259. Brenckle, M.A., et al., *Protein-protein nanoimprinting of silk fibroin films.* Adv Mater, 2013. **25**(17): p. 2409-14.

260. Young, S.L., et al., *Utilizing Conformational Changes for Patterning Thin Films of Recombinant Spider Silk Proteins.* Biomacromolecules, 2012. **13**(10): p. 3189-3199.

261. Geissler, M. and Y.N. Xia, *Patterning: Principles and some new developments.* Advanced Materials, 2004. **16**(15): p. 1249-1269.

262. Gates, B.D., et al., *New approaches to nanofabrication: Molding, printing, and other techniques.* Chemical Reviews, 2005. **105**(4): p. 1171-1196.

263. Chin, J.W. and P.G. Schultz, *In vivo photocrosslinking with unnatural amino Acid mutagenesis.* Chembiochem, 2002. **3**(11): p. 1135-7.

264. Stephanopoulos, N. and M.B. Francis, *Choosing an effective protein bioconjugation strategy.* Nat Chem Biol, 2011. **7**(12): p. 876-84.

265. Karageorgiou, V., et al., *Bone morphogenetic protein-2 decorated silk fibroin films induce osteogenic differentiation of human bone marrow stromal cells.* Journal of Biomedical Materials Research Part a, 2004. **71A**(3): p. 528-537.

266. Yan, M.D., et al., *N-Hydroxysuccinimide Ester Functionalized Perfluorophenyl Azides as Novel Photoactive Heterobifunctional Cross-Linking Reagents - the Covalent Immobilization of Biomolecules to Polymer Surfaces.* Bioconjugate chemistry, 1994. **5**(2): p. 151-157.

267. Nakajima, N. and Y. Ikada, *Mechanism of Amide Formation by Carbodiimide for Bioconjugation in Aqueous-Media.* Bioconjugate chemistry, 1995. **6**(1): p. 123-130.

268. Sutton, J.M., et al., *Porphyrin, chlorin, and bacteriochlorin isothiocyanates: useful reagents for the synthesis of photoactive bioconjugates.* Bioconjugate chemistry, 2002. **13**(2): p. 249-63.

269. Sabbioni, G., et al., *Reactions of 4 methylphenyl isocyanate with amino acids.* Biomarkers, 1997. **2**(4): p. 223-232.

270. Fleischel, O., E. Giménez-Arnau, and J.-P. Lepoittevin, *Nuclear Magnetic Resonance Studies on Covalent Modification of Amino Acids Thiol and Amino Residues by Monofunctional Aryl 13C-Isocyanates, Models of Skin and Respiratory Sensitizers: Transformation of Thiocarbamates into Urea Adducts.* Chemical Research in Toxicology, 2009. **22**(6): p. 1106-1115.

271. Brown, W.E., et al., *Biochemistry of Protein-Isocyanate Interactions: A Comparison of the Effects of Aryl vs. Alkyl Isocyanates.* Environmental health perspectives, 1987. **72**(ArticleType: research-article / Full publication date: Jun., 1987 / Copyright © 1987 The National Institute of Environmental Health Sciences (NIEHS)): p. 5-11.

272. Tse, C.S.T. and A.J. Pesce, *Chemical characterization of isocyanate-protein conjugates.* Toxicology and Applied Pharmacology, 1979. **51**(1): p. 39-46.

273. Chadwick, C.S., E.M. Mc, and R.C. Nairn, *Fluorescent protein tracers; a simple alternative to fluorescein.* Lancet, 1958. **1**(7017): p. 412-4.

274. Furuzono, T., et al., *Chemical modification of silk fibroin with 2-methacryloyloxyethyl phosphorylcholine. II. Graft-polymerization onto fabric through 2-methacryloyloxyethyl isocyanate and interaction between fabric and platelets.* Biomaterials, 2000. **21**(4): p. 327-333.

275. Koh, W.G., et al., *Control of mammalian cell and bacteria adhesion on substrates micropatterned with poly(ethylene glycol) hydrogels.* Biomedical Microdevices, 2003. **5**(1): p. 11-19.

276. Revzin, A., R.G. Tompkins, and M. Toner, *Surface engineering with poly(ethylene glycol) photolithography to create high-density cell arrays on glass.* Langmuir, 2003. **19**(23): p. 9855-9862.

277. Cranley, P.E., *Isocyanatoethyl Methacrylate - a Latent Crosslinker for Coating and Adhesive Resins.* Journal of Coatings Technology, 1984. **56**(716): p. 57-57.

278. Teramoto, H., K.-i. Nakajima, and C. Takabayashi, *Chemical Modification of Silk Sericin in Lithium Chloride/Dimethyl Sulfoxide Solvent with 4-Cyanophenyl Isocyanate.* Biomacromolecules, 2004. **5**(4): p. 1392-1398.

279. Decker, C., *Photoinitiated crosslinking polymerization.* Progress in Polymer Science, 1996. **21**(4): p. 593-650.

280. Kelly, S.M., T.J. Jess, and N.C. Price, *How to study proteins by circular dichroism.* Biochimica Et Biophysica Acta-Proteins and Proteomics, 2005. **1751**(2): p. 119-139.

281. Brzoska, J.B., I. Benazouz, and F. Rondelez, *Silanization of Solid Substrates - a Step toward Reproducibility.* Langmuir, 1994. **10**(11): p. 4367-4373.

282. Janczewski, D., et al., *Fabrication and responsive behaviour of Quantum Dot/PNIPAM micropatterns obtained by template copolymerization in water.* Journal of Materials Chemistry, 2011. **21**(18): p. 6487-6490.

283. *Rapid Coomassie blue reagent B.* Cold Spring Harbor Protocols, 2010. **2010**(4): p. pdb.rec12190.

284. Cappella, B. and G. Dietler, *Force-distance curves by atomic force microscopy.* Surface Science Reports, 1999. **34**(1-3): p. 1-+.

285. Butt, H.J., B. Cappella, and M. Kappl, *Force measurements with the atomic force microscope: Technique, interpretation and applications.* Surface Science Reports, 2005. **59**(1-6): p. 1-152.

286. Akhremitchev, B.B. and G.C. Walker, *Finite sample thickness effects on elasticity determination using atomic force microscopy.* Langmuir, 1999. **15**(17): p. 5630-5634.

287. Raspoet, G., et al., *The Alcoholysis Reaction of Isocyanates Giving Urethanes: Evidence for a Multimolecular Mechanism.* The Journal of Organic Chemistry, 1998. **63**(20): p. 6878-6885.

288. Sashina, E., et al., *Structure and solubility of natural silk fibroin.* Russian Journal of Applied Chemistry, 2006. **79**(6): p. 869-876.

289. Sashina, E.S., N.P. Novoselov, and K. Heinemann, *Dissolution of silk fibroin in N-methylmorpholine-N-oxide and its mixtures with organic solvents.* Russian Journal of Applied Chemistry, 2003. **76**(1): p. 128-131.

290. Petrus, L., D.G. Gray, and J.N. Bemiller, *Homogeneous Alkylation of Cellulose in Lithium-Chloride Dimethyl-Sulfoxide Solvent with Dimsyl Sodium Activation - a Proposal for the Mechanism of Cellulose Dissolution in Licl/Me(2)So.* Carbohydrate Research, 1995. **268**(2): p. 319-323.

291. Nogueira, G.M., et al., *Preparation and characterization of ethanol-treated silk fibroin dense membranes for biomaterials application using waste silk fibers as raw material.* Bioresource Technology, 2010. **101**(21): p. 8446-8451.

292. Jin, H.-J., et al., *Electrospinning Bombyx mori Silk with Poly(ethylene oxide).* Biomacromolecules, 2002. **3**(6): p. 1233-1239.

293. Sashina, E.S., et al., *Conformational changes in fibroin upon its dissolution in hexafluoroisopropanol.* Polymer Science Series A, 2005. **47**(10): p. 1096-1103.

294. Kaczmarczyk, B., B. Morejko-Buz, and A. Stolarzewicz, *Investigation of infrared calibration methods for application to the study of methyl methacrylate polymerization.* Fresenius J Anal Chem, 2001. **370**(7): p. 899-903.

295. Zainuddin, et al., *The behavior of aged regenerated Bombyx mori silk fibroin solutions studied by H-1 NMR and rheology.* Biomaterials, 2008. **29**(32): p. 4268-4274.

296. Hensarling, R.M., et al., *Thiol-isocyanate "click" reactions: rapid development of functional polymeric surfaces.* Polymer Chemistry, 2011. **2**(1): p. 88-90.

297. Gotoh, Y., et al., *Physical properties and structure of poly(ethylene glycol)-silk fibroin conjugate films.* Polymer, 1997. **38**(2): p. 487-490.

298. Keten, S., et al., *Nanoconfinement controls stiffness, strength and mechanical toughness of beta-sheet crystals in silk.* Nat Mater, 2010. **9**(4): p. 359-67.

299. Trabbic, K.A. and P. Yager, *Comparative Structural Characterization of Naturally- and Synthetically-Spun Fibers of Bombyx mori Fibroin.* Macromolecules, 1998. **31**(2): p. 462-471.

300. Kelly, S.M. and N.C. Price, *The Use of Circular Dichroism in the Investigation of Protein Structure and Function.* Current protein & peptide science, 2000. **1**(4): p. 349-384.

301. Lee, T.Y., et al., *The kinetics of vinyl acrylate photopolymerization.* Polymer, 2003. **44**(10): p. 2859-2865.

302. Priola, A., et al., *Properties of polymeric films obtained from u.v. cured poly(ethylene glycol) diacrylates.* Polymer, 1993. **34**(17): p. 3653-3657.

303. Li, M., et al., *Compliant film of regenerated Antheraea pernyi silk fibroin by chemical crosslinking.* International journal of biological macromolecules, 2003. **32**(3–5): p. 159-163.

304. Ghandhi, S.K., *VLSI fabrication principles : silicon and gallium arsenide*. 2nd ed. 1994, New York: Wiley. xxiv, 834 p.

305. Song, J.L., et al., *CELL 67-Adsorption of nonionic and amphoteric polymers on organic thin films.* Abstracts of Papers of the American Chemical Society, 2007. **233**: p. 700-700.

306. Zhou, Z., et al., *The swelling effects during the development processes of deep UV lithography of SU-8 photoresists: Theoretical study, simulation and verification.* 2007 Ieee Sensors, Vols 1-3, 2007: p. 325-328.

307. Novotny, D.B., *Measurement of the Separation Distance in Contact and Proximity Lithography.* Journal of The Electrochemical Society, 1986. **133**(12): p. 2600-2605.

308. Tal, M., A. Silberstein, and E. Nusser, *Why does Coomassie Brilliant Blue R interact differently with different proteins? A partial answer.* Journal of Biological Chemistry, 1985. **260**(18): p. 9976-80.

309. Deegan, R.D., et al., *Capillary flow as the cause of ring stains from dried liquid drops.* Nature, 1997. **389**(6653): p. 827-829.

310. Strawhecker, K.E., et al., *The critical role of solvent evaporation on the roughness of spin-cast polymer films.* Macromolecules, 2001. **34**(14): p. 4669-4672.

311. Roy, I. and M.N. Gupta, *Smart polymeric materials: Emerging biochemical applications.* Chemistry & Biology, 2003. **10**(12): p. 1161-1171.

312. Rosso, F., et al., *Smart materials as scaffolds for tissue engineering.* Journal of Cellular Physiology, 2005. **203**(3): p. 465-470.

313. Petros, R.A. and J.M. DeSimone, *Strategies in the design of nanoparticles for therapeutic applications.* Nature Reviews Drug Discovery, 2010. **9**(8): p. 615-627.

314. Rolland, J.P., et al., *Direct fabrication and harvesting of monodisperse, shape-specific nanobiomaterials.* Journal of the American Chemical Society, 2005. **127**(28): p. 10096-10100.

315. Lv, Q., et al., *Preparation of insoluble fibroin films without methanol treatment.* Journal of Applied Polymer Science, 2005. **96**(6): p. 2168-2173.

316. Hwang, S.-W., et al., *A Physically Transient Form of Silicon Electronics.* Science, 2012. **337**(6102): p. 1640-1644.

317. Baier Leach, J., et al., *Photocrosslinked hyaluronic acid hydrogels: Natural, biodegradable tissue engineering scaffolds.* Biotechnology and Bioengineering, 2003. **82**(5): p. 578-589.

318. Jiang, C., et al., *Mechanical Properties of Robust Ultrathin Silk Fibroin Films.* Advanced Functional Materials, 2007. **17**(13): p. 2229-2237.

319. Mandal, B.B., et al., *High-strength silk protein scaffolds for bone repair.* Proceedings of the National Academy of Sciences of the United States of America, 2012. **109**(20): p. 7699-7704.

320. Servoli, E., et al., *Surface Properties of Silk Fibroin Films and Their Interaction with Fibroblasts.* Macromolecular Bioscience, 2005. **5**(12): p. 1175-1183.

321. Acharya, C., S.K. Ghosh, and S.C. Kundu, *Silk fibroin film from non-mulberry tropical tasar silkworms: A novel substrate for in vitro fibroblast culture.* Acta Biomaterialia, 2009. **5**(1): p. 429-437.

322. Ziegler, W.H., R.C. Liddington, and D.R. Critchley, *The structure and regulation of vinculin.* Trends in Cell Biology, 2006. **16**(9): p. 453-460.

323. Sotiropoulou, S., et al., *Biotemplated nanostructured materials.* Chemistry of Materials, 2008. **20**(3): p. 821-834.

324. Spivey, E.C., et al., *Multiphoton Lithography of Unconstrained Three-Dimensional Protein Microstructures.* Advanced Functional Materials, 2013. **23**(3): p. 333-339.

325. Ostendorf, A. and B.N. Chichkov, *Two-photon polymerization: A new approach to micromachining.* Photonics Spectra, 2006. **40**(10): p. 72-+.

326. Macleod, J. and F. Rosei, *Photonic crystals: Sustainable sensors from silk.* Nature Materials, 2013. **12**(2): p. 98-100.

327. Wu, L.Q. and G.F. Payne, *Biofabrication: using biological materials and biocatalysts to construct nanostructured assemblies.* Trends in Biotechnology, 2004. **22**(11): p. 593-599.

328. Weibel, D.B., W.R. DiLuzio, and G.M. Whitesides, *Microfabrication meets microbiology.* Nature Reviews Microbiology, 2007. **5**(3): p. 209-218.

329. Goldberg, M., R. Langer, and X.Q. Jia, *Nanostructured materials for applications in drug delivery and tissue engineering.* Journal of Biomaterials Science-Polymer Edition, 2007. **18**(3): p. 241-268.

330. Park, T.H. and M.L. Shuler, *Integration of cell culture and microfabrication technology.* Biotechnology Progress, 2003. **19**(2): p. 243-253.

331. Kurland, N.E., et al., *Precise Patterning of Silk Microstructures Using Photolithography.* Advanced Materials, 2013. **25**(43): p. 6207-6212.

332. Park, A. and L.G. Cima, *In vitro cell response to differences in poly-L-lactide crystallinity.* Journal of Biomedical Materials Research, 1996. **31**(1): p. 117-130.

333. Jin, H.J., et al., *Human bone marrow stromal cell responses on electrospun silk fibroin mats.* Biomaterials, 2004. **25**(6): p. 1039-1047.

334. Minoura, N., et al., *Attachment and Growth of Fibroblast Cells on Silk Fibroin.* Biochemical and biophysical research communications, 1995. **208**(2): p. 511-516.

335. Oh, H., et al., *Preparation of silk sericin beads using LiCl/DMSO solvent and their potential as a drug carrier for oral administration.* Fibers and Polymers, 2007. **8**(5): p. 470-476.

336. Belkas, J.S., et al., *Long-term in vivo biomechanical properties and biocompatibility of poly(2-hydroxyethyl methacrylate-co-methyl methacrylate) nerve conduits.* Biomaterials, 2005. **26**(14): p. 1741-1749.

337. Baudis, S., et al., *(Meth)acrylate-based photoelastomers as tailored biomaterials for artificial vascular grafts.* Journal of Polymer Science Part A: Polymer Chemistry, 2009. **47**(10): p. 2664-2676.

338. Hirota, N., K. Mizuno, and Y. Goto, *Cooperative alpha-helix formation of beta-lactoglobulin and melittin induced by hexafluoroisopropanol.* Protein Science, 1997. **6**(2): p. 416-421.

339. Blake, D.A., et al., *Animal Toxicity of 2,2,2-Trifluoroethanol.* Toxicology and Applied Pharmacology, 1969. **15**(1): p. 83-&.

340. Siritientong, T., T. Srichana, and P. Aramwit, *The Effect of Sterilization Methods on the Physical Properties of Silk Sericin Scaffolds.* Aaps Pharmscitech, 2011. **12**(2): p. 771-781.

341. Drury, J.L. and D.J. Mooney, *Hydrogels for tissue engineering: scaffold design variables and applications.* Biomaterials, 2003. **24**(24): p. 4337-4351.

342. Goreham, R.V., et al., *Small surface nanotopography encourages fibroblast and osteoblast cell adhesion.* RSC Advances, 2013. **3**(26): p. 10309-10317.

343. Jones, J.R., L.M. Ehrenfried, and L.L. Hench, *Optimising bioactive glass scaffolds for bone tissue engineering.* Biomaterials, 2006. **27**(7): p. 964-973.

344. Freed, L.E., et al., *Biodegradable Polymer Scaffolds for Tissue Engineering.* Bio-Technology, 1994. **12**(7): p. 689-693.

345. Yao, P., et al. *Fabrication of three-dimensional photonic crystals with multilayer photolithography*. 2005.

346. Unger, M.A., et al., *Monolithic microfabricated valves and pumps by multilayer soft lithography.* Science, 2000. **288**(5463): p. 113-116.

347. Lawrence, B.D., et al., *Bioactive silk protein biomaterial systems for optical devices.* Biomacromolecules, 2008. **9**(4): p. 1214-1220.

348. Parker, S.T., et al., *Biocompatible Silk Printed Optical Waveguides.* Advanced Materials, 2009. **21**(23): p. 2411-+.

349. Li, B., J. Chen, and J.H.C. Wang, *RGD peptide-conjugated poly(dimethylsiloxane) promotes adhesion, proliferation, and collagen secretion of human fibroblasts.* Journal of Biomedical Materials Research Part a, 2006. **79A**(4): p. 989-998.

350. Omenetto, F.G. and D.L. Kaplan, *A new route for silk.* Nature Photonics, 2008. **2**(11): p. 641-643.

351. Gibson, I., D.W. Rosen, and B. Stucker, *Additive manufacturing technologies : rapid prototyping to direct digital manufacturing*. 2010, London ; New York: Springer. xxii, 459 p.

352. Melchels, F.P.W., et al., *Additive manufacturing of tissues and organs.* Progress in Polymer Science, 2012. **37**(8): p. 1079-1104.

353. Mironov, V., N. Reis, and B. Derby, *Bioprinting: A beginning.* Tissue Engineering, 2006. **12**(4): p. 631-634.

354. Melchels, F.P.W., J. Feijen, and D.W. Grijpma, *A review on stereolithography and its applications in biomedical engineering.* Biomaterials, 2010. **31**(24): p. 6121-6130.

Vita

Nicholas Kurland was born on 27 April 1987 in Roanoke, Virginia and is an American Citizen. He grew up in Virginia Beach, Virginia and graduated from Kellam High School in 2004. He received a Bachelor of Science in 2009 from Virginia Commonwealth University, with a major in Chemical Engineering and a minor in Chemistry. In 2011, he earned a Master of Science in Chemical and Life Science Engineering. Doctoral work was concurrently carried out under the supervision of Dr. Vamsi Yadavalli at Virginia Commonwealth University.